frontiers | Research Topics

Helminthosis: immuno-pathology and anthelmintic vaccines

Edited by
Anisuzzaman Anisuzzaman, Muhammad Tofazzal Hossain, Md. Aminul Islam and Joydeep Paul

Published in
Frontiers in Immunology

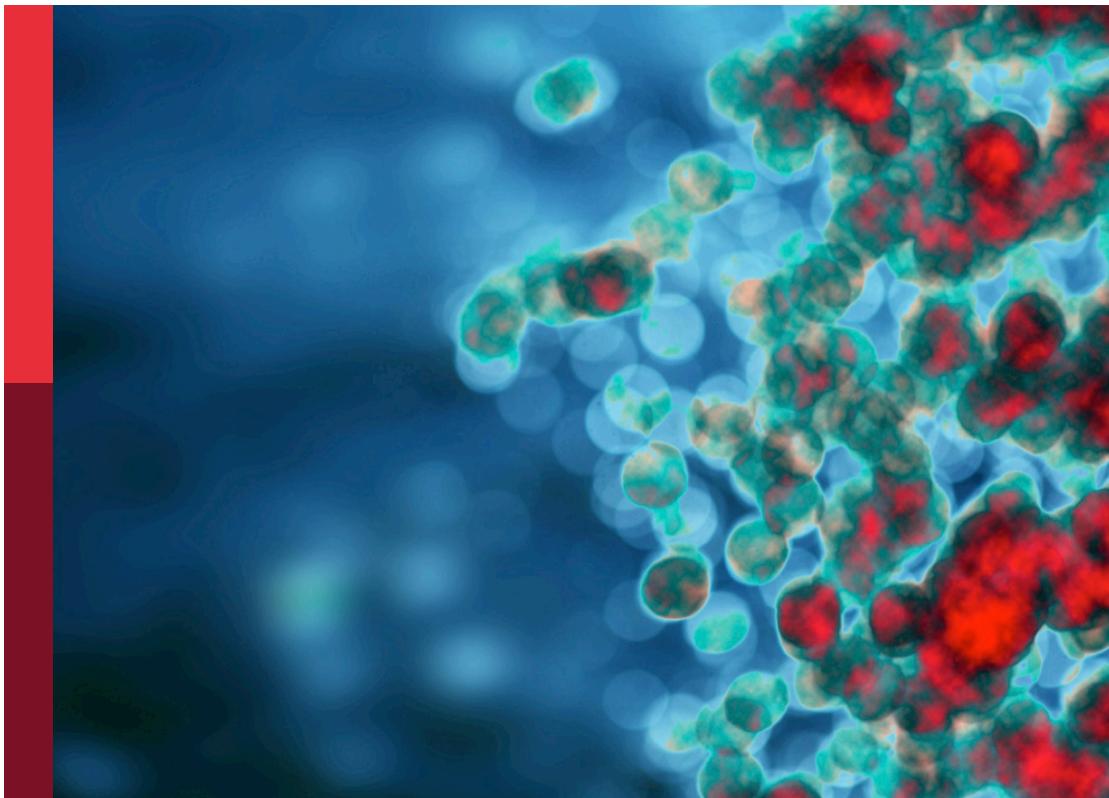

ISSN 1664-8714
ISBN 978-2-8325-7210-8
DOI 10.3389/978-2-8325-7210-8

Generative AI statement
Any alternative text (Alt text) provided alongside figures in the articles in this ebook has been generated by Frontiers with the support of artificial intelligence and reasonable efforts have been made to ensure accuracy, including review by the authors wherever possible. If you identify any issues, please contact us.

About Frontiers

Frontiers is more than just an open access publisher of scholarly articles: it is a pioneering approach to the world of academia, radically improving the way scholarly research is managed. The grand vision of Frontiers is a world where all people have an equal opportunity to seek, share and generate knowledge. Frontiers provides immediate and permanent online open access to all its publications, but this alone is not enough to realize our grand goals.

Frontiers journal series

The Frontiers journal series is a multi-tier and interdisciplinary set of open-access, online journals, promising a paradigm shift from the current review, selection and dissemination processes in academic publishing. All Frontiers journals are driven by researchers for researchers; therefore, they constitute a service to the scholarly community. At the same time, the *Frontiers journal series* operates on a revolutionary invention, the tiered publishing system, initially addressing specific communities of scholars, and gradually climbing up to broader public understanding, thus serving the interests of the lay society, too.

Dedication to quality

Each Frontiers article is a landmark of the highest quality, thanks to genuinely collaborative interactions between authors and review editors, who include some of the world's best academicians. Research must be certified by peers before entering a stream of knowledge that may eventually reach the public - and shape society; therefore, Frontiers only applies the most rigorous and unbiased reviews. Frontiers revolutionizes research publishing by freely delivering the most outstanding research, evaluated with no bias from both the academic and social point of view. By applying the most advanced information technologies, Frontiers is catapulting scholarly publishing into a new generation.

What are Frontiers Research Topics?

Frontiers Research Topics are very popular trademarks of the *Frontiers journals series*: they are collections of at least ten articles, all centered on a particular subject. With their unique mix of varied contributions from Original Research to Review Articles, Frontiers Research Topics unify the most influential researchers, the latest key findings and historical advances in a hot research area.

Find out more on how to host your own Frontiers Research Topic or contribute to one as an author by contacting the Frontiers editorial office: frontiersin.org/about/contact

Helminthosis: immuno-pathology and anthelmintic vaccines

Topic editors

Anisuzzaman Anisuzzaman — Bangladesh Agricultural University, Bangladesh
Muhammad Tofazzal Hossain — Bangladesh Agricultural University, Bangladesh
Md. Aminul Islam — Bangladesh Agricultural University, Bangladesh
Joydeep Paul — Adamas University, India

Citation

Anisuzzaman, A., Hossain, M. T., Islam, M. A., Paul, J., eds. (2025). *Helminthosis: immuno-pathology and anthelmintic vaccines*. Lausanne: Frontiers Media SA. doi: 10.3389/978-2-8325-7210-8

Table of contents

frontiers | Frontiers in Immunology

TYPE Editorial
PUBLISHED 17 November 2025
DOI 10.3389/fimmu.2025.1727852

OPEN ACCESS

EDITED AND REVIEWED BY
Dario S. Zamboni,
University of São Paulo, Brazil

*CORRESPONDENCE
Joydeep Paul
joydeep.paul@adamasuniversity.ac.in
Anisuzzaman Anisuzzaman
zaman.a@bau.edu.bd

RECEIVED 18 October 2025
REVISED 05 November 2025
ACCEPTED 06 November 2025
PUBLISHED 17 November 2025

CITATION
Paul J, Hossain MT, Islam MA and Anisuzzaman (2025) Editorial: Helminthosis: immuno-pathology and anthelmintic vaccines.
Front. Immunol. 16:1727852.
doi: 10.3389/fimmu.2025.1727852

Editorial: Helminthosis: immuno-pathology and anthelmintic vaccines

Joydeep Paul[1]*, Muhammad Tofazzal Hossain[2], Md. Aminul Islam[3] and Anisuzzaman[4]*

[1]Department of Biotechnology, School of Life Science and Biotechnology, Adamas University, Kolkata, India, [2]Department of Microbiology and Hygiene, Bangladesh Agricultural University, Mymensingh, Bangladesh, [3]Department of Medicine, Bangladesh Agricultural University, Mymensingh, Bangladesh, [4]Department of Parasitology, Bangladesh Agricultural University, Mymensingh, Bangladesh

KEYWORDS

helminthosis, immunopathology, anthelmintic vaccines, extracellular vesicles (EVs), host–parasite interaction, immune modulation

Editorial on the Research Topic
Helminthosis: immuno-pathology and anthelmintic vaccines

Helminth infections remain a major global challenge, especially in the tropics and the sub-tropics. While they rarely receive the attention accorded to tuberculosis or malaria, their burden is considerable, resulting in growth impairment, infertility, chronic disability, and premature mortality (1–3). Co-evolution of these helminths along with their respective hosts is the key to their survival and persistence, even in the modern world (4). Initially, helminth infections induce a Th1 immune response, accompanied by increased IgE and T cell activation. Later in the chronic illness, polarization of the host immune response towards Th2 helps the parasites to survive in a more favourable environment (5). The immune response to the helminths is inherently paradoxical. Protective in some contexts, yet can be manipulated by the parasites to ensure survival (Figure 1). This duality is central to the immunopathology examined in this Research Topic. Helminths also actively induce Treg cells, which helps the helminth's survival by suppressing the host's immune response. Helminth-induced Treg ameliorates "bystander" immune responses, protecting against allergies and autoimmune diseases (6). The pursuit of vaccines is equally important, which, despite decades of work, lags behind efforts against bacterial and viral diseases (7). This study offered fresh perspectives on these intertwined challenges. This Research Topic will also help us to understand the host-parasite interactions more intricately by highlighting the underlying molecular mechanisms, particularly in the field of vaccine development.

The issue discussed many newer and evolving problems related to helminthosis. Ten different articles range from giving intricate highlights in understanding the modulation of immune responses and other host inflammatory responses in helminthosis to the development of protective responses against different helminths, either through regular physical exercises or with the advancement of new prophylactic and therapeutic modules. Sternkopf et al. showed that the vesicular fluid derived from the *Taenia solium* cyst (CVF) induces Caspase 3 and 9 mediated apoptosis in human neurocysticercosis patients by significantly inhibiting mitochondrial function. This article also identifies that elevated FasL levels act as a key mediator to induce brain inflammation by primarily targeting

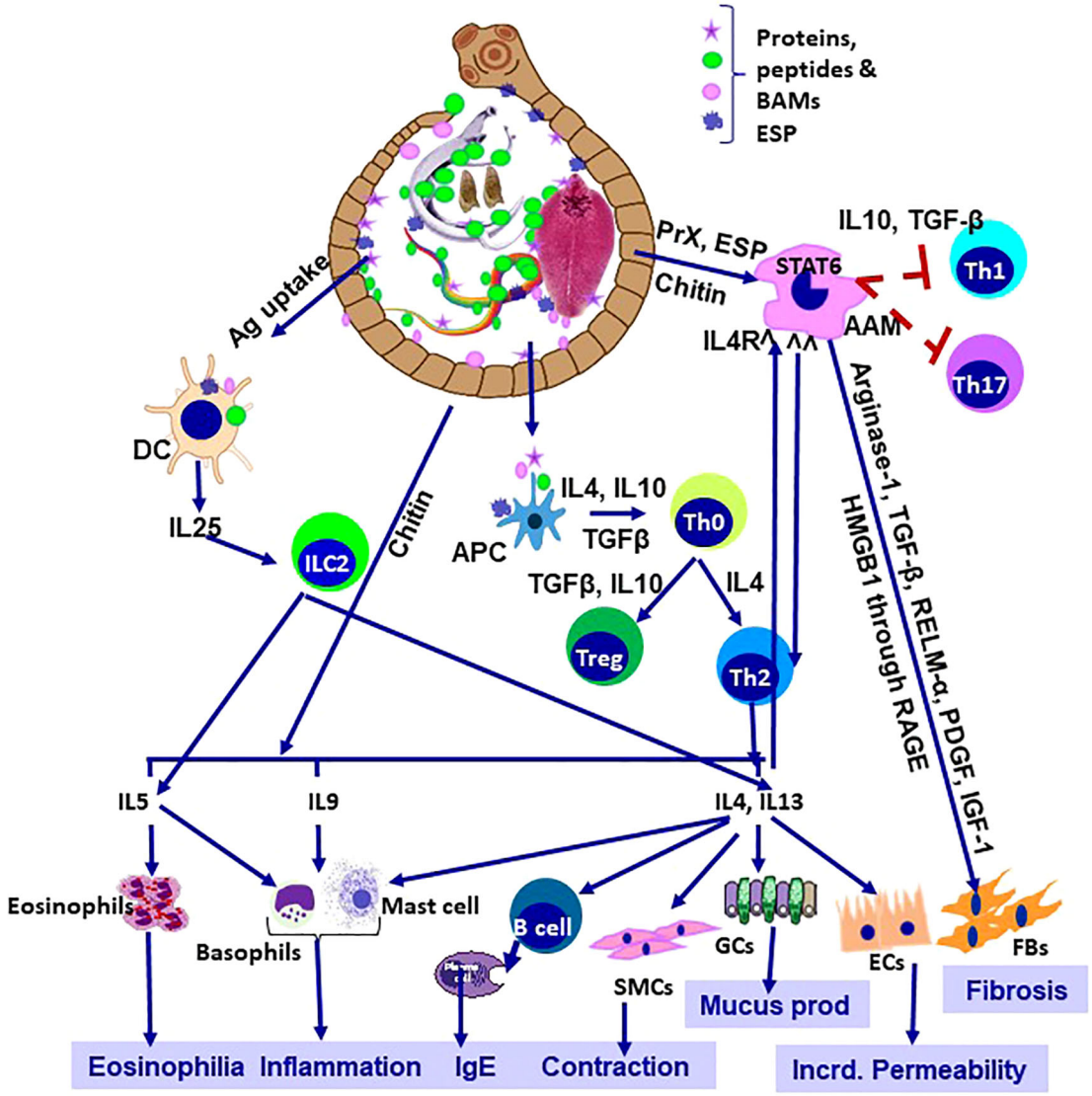

FIGURE 1
Helminthiosis: Immunological orchestra and patho-biology. AAM, alternatively activated macrophage; APC, antigen presenting cell; DC, dendritic cell; SMCs, smooth muscle cells, GCs, goblet cells; Ecs, epithelial cells; FBs, fibroblasts; Incrd, increased; Ag, antigens; BAMs, bioactive molecules, PrX, 2-Cys peroxiredoxin; RELM-α, Resistin-like Molecule- α; PDGF, platelet-derived growth factor; IGF-1, insulin-like growth factor 1; HMGB1, High-Mobility Group Box 1, RAGE, receptor for advanced gycation end-products; ESP, excretory-secretory products.

monocytes, microglia, and in CD3+ expressing T cells. Yuan et al. demonstrated how *Nippostrongylus brasiliensis*-derived uridine alleviates colitis in mice via apical sodium-dependent bile acid transporter (ASBT). Their findings suggest novel molecular targets for treating inflammatory bowel diseases and also suggest how helminth biology can reform wider field of medicine. Schulze et al. characterize the immune remodelling in *Schistosoma mansoni* infection by documenting granulocyte expansion, cytokine dynamics and the interplay between Th1 and Th2 responses. They contribute significantly to understanding the late-stage disease and its systemic immunological impact. Adjah et al. broaden our knowledge on compartmentalized immunity by showing that portal lymph nodes, along with the mesenteric nodes, generate parasite-specific follicular helper T and B cells during *Heligmosomoides bakeri* infection. Lema et al. analyze immune responses in HIV-positive individuals with *Taenia solium* cysticercosis. Their observations show cytokine patterns and CD4 variations in a sex-biased manner, having stronger responses in males. This study also underscores the complexity of co-infections and the need for tailored management strategies. Lopez et al. reviewed how ILC2 activity correlates with egg burden, IgE production and tryptase levels in *Ascaris lumbricoides* infection, thus linking innate immune responses with allergic and inflammatory consequences. While Sanku et al. emphasized the impaired APC activity and the suppression of the T cell responses by a filarial nematode (*Brugia malayi*) derived EVs. Their work also illustrates the inhibitory role of parasite-derived EVs in cytokine production and may extend to several dissimilar antigens, such as SARS-CoV-2.

Addressing the prophylactic and therapeutic challenges against helminthosis, Liu et al. identified various glycoprotein components

of the H11 antigen and also demonstrated that combinations of recombinant cocktails can reproduce a significant amount of protection as seen with native H11 antigen. With barbervax still being considered as the sole commercial helminth vaccine, such advances mark critical progress towards recombinant platforms. Addressing co-endemicity, Zhong et al. reviewed the role of EV-derived *let*-7 microRNAs in shaping host-parasite interactions. Their synthesis highlights both conserved pathways and translational challenges, pointing toward diagnostic and therapeutic opportunities. Lastly, Berkiks et al. contributed in a novel way by showing that moderate exercise reduces neuroinflammation and improves memory in mice infected with schistosomiasis. By linking lifestyle interventions to disease outcomes, this study broadens the scope of the helminth research beyond parasite clearance.

In summary, all ten articles not only provided insights into how helminths use different strategies for their survival in the host, but also suggested diverse approaches that could be used to combat infection. From cellular pathways and EV microRNAs to vaccine antigens and exercise-based interventions, the breadth of inquiry represented here is striking. Importantly, modern understanding unmasked that helminths are not only pathogens but also sources of therapeutic insights, resulting a twist whether helminths are 'friends or foe'. This Research Topic also highlights the ongoing need for increased visibility in helminth research. Despite their enormous global burden, particularly in low and middle-income countries, these diseases risk neglect amid shifting public health priorities. By bringing together diverse work, this Research Topic highlights both the scientific vibrancy of helminthology and its translational relevance for wider immunological and inflammatory conditions.

In conclusion, this Research Topic is more than a compilation of papers. The studies here remind us that advancing vaccines and therapies against these parasites requires scientific rigor but also collaborative persistence. May it inspire further inquiry and innovation in tackling helminthiosis and its far-reaching consequences.

Author contributions

JP: Conceptualization, Investigation, Methodology, Software, Supervision, Validation, Writing – original draft, Writing – review & editing. MH: Conceptualization, Investigation, Supervision, Writing – original draft, Writing – review & editing. MI: Conceptualization, Investigation, Supervision, Writing – original draft, Writing – review & editing. AA: Conceptualization, Investigation, Project administration, Software, Supervision, Validation, Writing – original draft, Writing – review & editing.

Funding

The author(s) declare financial support was received for the research and/or publication of this article. This study was partially funded by the internal seed grant by Adamas University (No. AU/R&D/SEED/28/03-2020-21) granted to JP-lab, Krishi Gobeshana Foundation (KGF, TF-102-L/21), Bangladesh, Bangladesh Agricultural University Research System (2024/30/BAU) and Ministry of Science and Technology (MoST), Bangladesh (SRG-244380/2025/MoST).

Acknowledgments

We want to thank all the authors who have contributed to the Research Topic.

Conflict of interest

The authors declare that the research was conducted in the absence of any commercial or financial relationships that could be construed as a potential conflict of interest.

Generative AI statement

The author(s) declare that Generative AI was used in the creation of this manuscript. Line rephrasing and reconstruction.

Any alternative text (alt text) provided alongside figures in this article has been generated by Frontiers with the support of artificial intelligence and reasonable efforts have been made to ensure accuracy, including review by the authors wherever possible. If you identify any issues, please contact us.

Publisher's note

References

1. Anisuzzaman, Tsuji N. Schistosomiasis and hookworm infection in humans: Disease burden, pathobiology and anthelmintic vaccines. *Parasitol Int*. (2020) 75:102051. doi: 10.1016/j.parint.2020.102051

2. Frahm S, Anisuzzaman A, Prodjinotho UF, Vejzagić N, Verschoor A, Prazeres da Costa C. A novel cell-free method to culture Schistosoma mansoni from cercariae to juvenile worm stages for *in vitro* drug testing. *PloS Negl Trop Dis*. (2019) 13:e0006590. doi: 10.1371/journal.pntd.0006590

3. Anisuzzaman FS, Prodjinotho UF, Bhattacharjee S, Verschoor A, da Costa CP. Host-specific serum factors control the development and survival of Schistosoma mansoni. *Front Immunol*. (2021) 12:635622. doi: 10.3389/fimmu.2021.635622

4. Yasmin H, Datta P, Deb A, Willingham AL, Kishore U. Innate immune response to helminth infections. *Adv Exp Med Biol*. (2025) 1476:251–73. doi: 10.1007/978-3-031-85340-1_10

5. Gazzinelli-Guimaraes PH, Jones SM, Voehringer D, Mayer-Barber KD, Samarasinghe AE. Eosinophils as modulators of host defense during parasitic, fungal, bacterial, and viral infections. *J Leukoc Biol*. (2024) 116:1301–23. doi: 10.1093/jleuko/qiae173

6. Ohnmacht C, Park JH, Cording S, Wing JB, Atarashi K, Obata Y, et al. The microbiota regulates type 2 immunity through RORγt^+ T cells. *Science*. (2015) 349:989–93. doi: 10.1126/science.aac4263

7. García-Bernalt Diego J, Desai P, Yeung ST, Damani-Yokota P, Khanna KM, Diamond MS, et al. Helminth infections affect host immune responses to viral infections and vaccines. *FEMS Microbiol Rev*. (2025) 49:fuaf036. doi: 10.1093/femsre/fuaf036

frontiers | Frontiers in Immunology

TYPE Original Research
PUBLISHED 07 October 2024
DOI 10.3389/fimmu.2024.1436818

OPEN ACCESS

EDITED BY
Anisuzzaman Anisuzzaman,
Bangladesh Agricultural University,
Bangladesh

REVIEWED BY
Jayaraman Tharmalingam,
University of Wisconsin-Madison,
United States
Fela Mendlovic,
National Autonomous University
of Mexico, Mexico

*CORRESPONDENCE
Gayatri Sanku
gayatrisanku@gmail.com
Thomas B. Nutman
tnutman@niaid.nih.gov

RECEIVED 22 May 2024
ACCEPTED 08 August 2024
PUBLISHED 07 October 2024

CITATION
Sanku G, Ricciardi A, Redekar NR, Schaughency P, Lack J, Gazzinelli-Guimaraes PH and Nutman TB (2024) *Brugia malayi* filarial helminth-derived extracellular vesicles suppress antigen presenting cell function and antigen-specific CD4+ T cell responses.
Front. Immunol. 15:1436818.
doi: 10.3389/fimmu.2024.1436818

Brugia malayi filarial helminth-derived extracellular vesicles suppress antigen presenting cell function and antigen-specific CD4+ T cell responses

Gayatri Sanku[1*], Alessandra Ricciardi[1], Neelam R. Redekar[2], Paul Schaughency[2], Justin Lack[2], Pedro H. Gazzinelli-Guimaraes[1] and Thomas B. Nutman[1*]

[1]Laboratory of Parasitic Diseases, National Institute of Allergy and Infectious Diseases, National Institutes of Health (NIH), Bethesda, MD, United States, [2]Integrated Data Science Section (IDSS), National Institute of Allergy and Infectious Diseases (NIAID), National Institutes of Health (NIH), Bethesda, MD, United States

Introduction: Live microfilariae (mf) and mf-derived extracellular vesicles (EVs) have been shown to modulate human antigen presenting cell (APC) function, most notably by suppressing the induction of IL-12 (and other pro-inflammatory cytokines) following activation with LPS and interferon-γ.

Methods: To explore further how EVs alter human APC function, we studied the effect of mf and EVs on human elutriated monocyte-derived dendritic cells (DC) following exposure to Mf, mf-derived excretory/secretory (E/S) products, E/S depleted of EVs through ultracentrifugation and purified EVs. After demonstrating that the measurable responses induced by live mf could be recapitulated by EVs and EV-containing E/S, we next performed RNAseq analysis of human DC following exposure to live mf, EVs, E/S, or EV-depleted E/S.

Results: In our analyses of the data for the DC, using a false discovery rate (FDR) <0.05, EV-exposed DC had induced the expression of 212 differentially expressed genes (DEGs) when compared to unexposed DC and 157 when compared to E/S-depleted EVs. These genes were enriched in GO biological processes associated with neutrophil degranulation and 15 DEGs associated with KEGG Lysosome pathways. IPA analysis point to immune dysregulation. We next aimed to understand the intracellular processes altered by EVs and the effect these have on effector T cells. When SARS CoV-2 Membrane-specific CD4+ TCLs were assessed following EV conditioning of autologous DC and activation with the SARS CoV-2-Membrane peptide pool, we found conditioning reduced the frequency of SARS CoV-2 Membrane-specific CD3+ CD4+ CD154+ cells (p=.015). Similarly, EV-conditioning of SARS CoV-2 Membrane-specific CD3+ CD4+ cells induced fewer cell capable of producing IFN-γ (p=.045).

Discussion: Taken together, our data suggest a modulatory role of EVs on APC function that likely leads to defects in T cell effector function.

KEYWORDS

***Brugia malayi*, extracellular vesicle (EV), microfilariae excretory-secretory protein, T cell, helminth**

1 Introduction

Among the various filarial infections that together infect >200 million people worldwide, those with lymphatic filariasis, caused by *Brugia* spp. and *W. bancrofti* infection, are the most severely affected. A common immunologic feature of all the filarial infections (and most notably those that are bloodborne) is the expansion of parasite antigen-specific Th2 cells well as the expansion of IL-10-producing CD4+ T cells (1), processes largely associated with the presence of circulating microfilariae (Mf), the parasite stage that provides the most significant source of excreted/secreted (E/S) parasite antigen. Additionally, parasite antigen-specific Th1 responses are muted leading to what has been termed antigen-specific T cell hypo-responsiveness; this suppressed parasite-specific memory response spills over to non-parasite bystander antigens with persistent, longstanding infection (2, 3).

A number of hypotheses have been put forth to explain the T cell alterations seen in chronic filarial infections including: 1) TGF-β receptor engagement (4); 2) induction of Tregs (5); and 3) APC dysfunction (6), mostly triggered by E/S products. Previous studies have shown that E/S antigens can drive CD14+ monocytes to become capable of modulating both T cell and lymphatic endothelial functions (7). Moreover, E/S products have been shown to modulate dendritic cell (DC) maturation, leading to altered immune responses (8). Studies have demonstrated that exposure of DC to helminth E/S products can inhibit the upregulation of costimulatory molecules, such as CD80 and CD86 and promote the downregulation of antigen uptake receptors, such as DEC-205 and mannose receptor, thereby preventing full maturation of DC (9). This immature DC phenotype is associated with the induction of regulatory T cell (Treg) responses (10) which may contribute to immune suppression and parasite persistence. Filarial helminth infections have also been shown to interfere with the Toll-like receptor (TLR) signaling pathway in DC, again resulting in impaired DC maturation and cytokine production (11).

Because extracellular vesicles (EVs) are part of E/S products (12–14), it has been suggested that EVs can interact with a range of host cells and may be mediators or central drivers of immune modulation. These interactions could suppress APC functions and alter the generation of antigen-specific T cells (15). Interestingly, EVs produced by intestinal nematodes have also been associated with immunoregulation (12). *Heligmosomoides polygyrus*-derived EVs can suppress the activation of type 2 innate lymphoid cells (ILC2s) (16) by inhibiting the expression of IL-33 receptor, which is essential for the activation of ILC2s.

Notwithstanding, Mf-derived EVs, known to be released in large quantities and being capable of modifying intracellular functions and cellular signaling in APCs (12), have previously been shown to alter some intracellular processes including mTOR signaling (17). Thus, EVs have emerged as attractive carriers of proteins, lipids, and nucleic acids that may penetrate host defensive barriers and increase cellular susceptibility to immune suppression (18). Having previously shown that these Mf-derived EVs are heterogenous in size with both exosome and microvesicle-like particles that contain protein cargo with mammalian exosome markers (elongation factor 1- α, histones, heat shock proteins and ATP synthase) (17), we have previously demonstrated EVs to be readily internalized within human monocytes, where they affect key intracellular functions (17). However, the underlying mechanisms on how Mf-derived EVs alter the molecular program of APCs and its subsequent effect on antigen-specific T cell effector responses are less studied.

Therefore, we sought to understand the role played by these Mf-derived EVs in modulating APC function. In this paper we characterize the role played by Mf-derived EVs, their impact on antigen presenting cell function, and how this affects antigen-specific T-cell effector responses, particularly those responses driven by viral antigens. Our data suggest that EVs are central drivers of diminished cytokine production from APCs following activation that in turn downregulates antigen-driven T cell effector function.

2 Methods

2.1 Preparation of microfilariae, E/S products and EVs

Live *B. malayi* Mf were provided by the University of Georgia, Athens, GA by peritoneal lavage of infected jirds and were purified as previously described (8). To prepare Mf E/S products (supernatant), live Mf were thoroughly washed with culture media (RPMI 1640, 1% D-glucose, 1% L-glutamine, 1% penicillin/streptomycin) and maintained in culture media at a concentration of $1x10^6$ Mf/mL at 37°C for 24h. Mf were then pelleted, and the supernatant was collected. EVs were collected as previously described (17). Briefly, the ExoQuick-TC ULTRA kit (System Biosciences, Palo Alto, CA) was used, according to the manufacturer's instructions, to isolate Mf-derived EVs after 24 hours of incubation. To perform the depletion of EVs from Mf E/S, E/S was collected and subjected to ultracentrifugation at 100,000 X g for 1 hour. The EV-depleted supernatant was collected and the pelleted EVs were discarded.

2.2 Cell culture

Human monocytes used for this study were isolated from leukopaks from healthy donors by counterflow centrifugal elutriation. This work was performed under Institutional Review Board (IRB)-approved protocols (99-CC-0168) from the Department of Transfusion Medicine (Clinical Center, National Institutes of Health, Bethesda, MD. All donors provided informed written consent. Human monocyte cells were isolated from 4 donors using magnetic beads (Pan Monocyte Isolation Kit, human, Miltenyi). 12x10^6 human monocyte cells were cultured for 6 days with addition of GMCSF and IL-4 to differentiate monocyte-derived DC.

Human DC were resuspended in complete culture media [RPMI 1640 medium (Gibco) supplemented with 10% heat-inactivated AB serum (Pan Biotech), 1% nonessential amino

acids, 1% HEPES, 1 mM sodium pyruvate, 2 mM fresh L-glutamine, 100 µg/ml streptomycin, 100 units/ml penicillin (all from Life Technologies, USA)] and cultured in 6-well tissue culture plates at a concentration of $1x10^6$/mL. DC were activated with a final concentration of 100ng/mL IFN-y and 100ng/mL of LPS or incubated in media alone overnight. Lastly, DC were either left unconditioned (media), or conditioned with 50,000 live Mf, Mf-derived EVs (normalized using 10ug of protein content), 10uL of Mf E/S, or 10uL of Mf supernatant depleted of EVs for 48hrs at 37° C in 5% CO2.

Due to inherent limitations in sample availability and experimental design constraints, donor cells and cell lines were not uniformly accessible across all analyses. RNA sequencing experiments were conducted on a subset of 4 donors, while cytokine profiling encompassed 6 donors, with an additional cohort of 6 donors utilized for supplementary extracellular vesicle-dependent cytokine analyses. In a related investigation exploring T cell lineage dynamics in the context of COVID-19, a more extensive donor pool of 11 individuals was employed, as elucidated in the referenced study (19).

2.3 Cytokine and chemokine measurements

Supernatant from DC cultures was collected and assessed using a customized assay (Millipore HCYTOMAG-60K) for 10 human analytes: IL-10, IL-1a, IL-1b, IL-8, IL-12p70, RANTES, TNF-α, and IL-12p40. The assay was performed according to the manufacturer's instructions, and samples were analyzed using a Bio-Plex 200 (Bio-Rad).

2.4 Preparation and analysis of samples for mRNA-Seq

RNA was extracted from 1x10^6 DC exposed to media (unconditioned), Mf, EV, E/S and EV-depleted E/S, from 4 different donors, using the Total RNA and Protein Isolation Kit (Thermo Fisher Scientific) following the manufacturer's instructions. 1ul of total RNA from each sample was used to assess its concentration using a Qubit 4 (Invitrogen). 2ul of a normalized concentration of RNA from each sample was loaded into an Agilent RNA 6000 Nano LabChip using manufacturer recommendations and assessed through an Agilent 2100 bioanalyzer. The Agilent 2100 bioanalyzer calculated and reported RNA Integrity Numbers (ratio of 28S:18S ribosomal RNA) to determine total RNA sample quality. Next, mRNA was purified from total RNA using the RNeasy Pure mRNA Bead Kit (Qiagen) according to manufacturer instructions. Sample concentrations were normalized identically to total RNA normalization. 1ul of a normalized concentration of mRNA from each sample was loaded into an Agilent RNA 6000 Pico LabChip (Agilent Technologies) using manufacturer recommendations and assessed through an Agilent 2100 bioanalyzer. Samples with RIN values above 8.0 were prepared for mRNA-Seq analysis.

Bulk mRNA-Seq was performed by the Frederick National Laboratory for Cancer Research Sequencing Facility. Indexed RNA sequencing (RNA-seq) libraries were constructed from 1 µg total RNA using a TruSeq Stranded mRNA Library Prep (Illumina). 20 pooled mRNA-Seq samples were sequenced in paired-end mode using 1 lane of Illumina HiSeq3000/4000 flowcell, generating 2 × 151 bp reads. The mapping statistics are calculated using Picard software. Basecalling was performed using RTA (v.2.11.3). Samples were demultiplexed using Bcl2fastq v217) and aligned using STAR 2.7.0f. Library complexity is measured by unique fragments in the mapped reads using Picard's MarkDuplicate utility.

2.5 Sequencing data analysis

The mRNA sequencing data was processed using default parameter with RNA-seek workflow (https://github.com/OpenOmics/RNA-seek). This included preprocessing of the raw sequencing reads to remove low quality bases, adapters, and shorter reads using Cutadapt v1.18, followed by alignment to human hg38 reference genome (GRCh38, Gencode Release 30) using STAR (v.2.7.6a) aligner in two-pass mapping mode. The gene expression counts estimated from number of reads mapping to each annotated gene using RSEM (v.1.3.0). The expression data were transformed to log2-counts per million (logCPM) and then filtered to remove genes with <1 CPM that are expressed in less than 4 samples. The filtered gene expression count was normalized using TMM (Trimmed Mean of M-values) method (20). Normalized data was then used for differential expression analyses using limma. The variation in gene expression data originating from cell-line donor patients was blocked for this analysis. EV-Media differential expression genes (FDR=0.05) were assessed using canonical pathway enrichment profiles generated using Ingenuity Pathway Analysis (IPA, Qiagen, Redwood City, CA, US). Information on these files may be found in an online repository (GEO: GSE263690 and GEE263693- see Supplementary Tables 1, 2 for associated metadata).

2.6 RNA isolation for RT-PCR

$10x10^6$ monocyte-derived DC were cultured in complete media and exposed to purified EVs for 48hrs. RNA was extracted from EV-conditioned and unconditioned (media) DC using the Total RNA and Protein Isolation Kit (Thermo Fisher Scientific) following the manufacturer's instructions. Using the Taqman Advanced RNA cDNA Synthesis Kit (Thermo Fisher Scientific) cDNA was made. 1–10 ng of RNA extracted from cells was used to perform polyadenylation tailing reaction at 37°C for 45 minutes and then 65° C for 15 minutes. This was followed by adenylation ligation reaction that was performed at 16°C for 60 minutes. The reverse transcriptase reaction was performed at 42°C for 15 minutes followed by 85°C for 5 minutes. An amplification step was performed at 95°C for 5 minutes for 1 cycle, 95°C for 3 seconds for 14 cycles, 60°C for 30 seconds for 14 cycles, and 99°C for 10 minutes for 1 cycle. RT-PCR was performed to detect mRNA expression of genes identified within the RNASeq

analysis. The reaction mix contained 18ul of cDNA, 2 ul of each respective primer and 20ul of Taqman Advanced Mastermix. Cycling parameters were 95°C for 20 seconds for 1 cycle, 95°C for 40 cycles and 60°C for 40 cycles. A Ct value of 40 is negative. All of the primers used were purchased commercially from Bio-Rad: (PrimePCR™ SYBR® Green Assay: TNC, Human (#10025636), PrimePCR™ SYBR® Green Assay: MT1F, Human (#10025636), PrimePCRSYBR® Green Assay: SLC7A11, Human (#10025636), PrimePCR™ SYBR® Green Assay: PAPPA2, Human (#10025636), PrimePCR™ SYBR® Green Assay: JAK3, Human (#10025636), PrimePCR™ SYBR® Green Assay: SLC39A10, Human (#10025636), PrimePCR™ SYBR® Green Assay: TLR7, Human (#10025636), PrimePCR™ SYBR® Green Assay: S100A4, Human (#10025636), PrimePCR™ SYBR® Green Assay: SLAMF1, Human (#10025636), PrimePCR™ SYBR® Green Assay: mTOR, Human (#10025636)).

2.7 RT-PCR data handling

The 2^DeltaDelta (Ct) formula was used to calculate fold change in gene expression. The average Ct of EV-treated DC, untreated (media) DC, and 18s (housekeeping gene) were calculated for each gene. Average 18s Ct values were subtracted from all genes to calculate the Delta Ct values for EV-treated DC and untreated DC replicates. Next, the Media delta Ct values were subtracted from the EV-treated delta Ct values to calculate delta delta Ct values. Lastly, to calculate fold change, 2^ (delta delta Ct values) were calculated for EV-treated cells.

2.8 Conditions for filarial helminth exposed DC and SARS CoV-2-membrane specific T- cell lines

As previously described, we generated SARS-CoV-2 Membrane protein-specific CD4+ T cell lines (TCLs) from 6 donors (19) who provided PBMCs under a NIAID IRB approved protocol (88-I-0083) (19). For *in vitro* expansion of these $CD4^+$ TCLs, cryopreserved Membrane specific-TCLs were thawed and incubated for 12 days in the presence of the respective antigens, irradiated autologous feeder PBMCs, and 60U of rIL-2, as previously described (REF). Separately, autologous monocytes were purified from cryopreserved PBMCs from whom the TCLs were generated using negative depletion magnetic cell sorting (MACS Miltenyi Biotec, USA). 12x10^6 purified monocytes were seeded in 6-well plates and placed in R10 media culture [RPMI 1640 medium (Gibco) supplemented with 10% heat-inactivated AB serum (Pan Biotech), 1% nonessential amino acids, 1% Hepes 1M, 1 mM sodium pyruvate, 2 mM fresh L-glutamine, 100 µg/ml streptomycin, 100 units/ml penicillin (all from Life Technologies, USA)] at 37°C, 5% CO2 for 6 days to be differentiated into DC with addition of 10uL of IL-4 (1mg/mL) and 10uL of GM-CSF (1mg/mL) at days 1,3, and 5. 1x10^5 DC were seeded into 6-well plates and exposed to 50,000 live Mf, EVs or media alone for 48hours in 37C with 5% CO2. After treatment conditioning, DC were washed and loaded for 4hrs with 1µg/mL of SARS-CoV-2 peptide megapools (MPs).

Next, all DC conditions were counted and seeded in 96-well round bottom culture plates by condition (Mf-conditioned, EV-conditioned, media/unconditioned). SARS-CoV-2 Membrane-specific T-cells from autologous donors were added in a ratio of 1 DC:10 CD4+ T-cells in each plate. DC: TCL co-cultures were unstimulated (media) or stimulated with 1ug/mL Membrane protein, or 1ug/mL SEB for 17hrs in 37C. BFA was added after 6hrs of stimulation.

2.9 Flow cytometry conditions for filarial helminth exposed DC and CD4+ SARS CoV-2- membrane specific T- cell lines

The activation and intracellular cytokine profiles of the SARS-CoV-2-Membrane specific CD4+ TCLs incubated with their autologous Mf and EV-conditioned DC were analyzed using flow cytometry immunophenotypic and functional assays. Briefly, TCLs were stimulated overnight in 5% CO2 at 37°C with autologous donor SARS-CoV-2 antigen-loaded monocyte-derived DC conditioned with Mf and EV or unconditioned (media). Cells were stained for viability (Live/Dead fixable blue, UV450, Molecular Probes) and then incubated with anti-CD3 (BUV805, UCHT1, BD), anti-CD4 (cFluor YG584, SK3, BD) for 30 min in the dark at room temperature. The cells were then washed twice with FACS buffer and fixed using a Fix/Perm buffer kit (BioLegend) for 30 min at 4°C. The cells were washed twice with Perm buffer (BioLegend) and resuspended with the intracellular antibody mix containing anti-CD69 (BV711, FN50, Biolegend), anti-CD154 (PE, TRAP-1, BD), anti-IFN-γ (PE-Cy7, B27, BD) for 30 min at 4°C. Finally, the cells were washed twice with Perm buffer and acquired using the Cytek Aurora flow cytometer (Cytek Bio) and Spectroflo software (Cytek Bio) for acquisition. FCS files were analyzed using OMIQ software (Dotmatics) and cell frequencies and ratios were exported to GraphPad Prism 7 for analysis.

2.10 Statistical analysis

For Luminex assay and flow cytometry cell frequencies/MfI results, paired samples were analyzed using the Wilcoxon test, and the Mann-Whitney test (nonparametric test) was used to compare among different groups. The geometric mean was used as a measure of central tendency. GraphPad Prism 7 was used for all statistical analysis. *P* values less than.05 were considered significant.

3 Results

3.1 Microfilaria-derived EVs downregulate activated DC cytokine production

Having previously shown that live Mf and Mf-derived E/S products alter APC function [34 (21)] EVs may downregulate APC mTOR phosphorylation (8, 17), we chose initially to corroborate some of these data and to assess the role of Mf-derived EVs in altering DC cytokine production both before and following activation. To this end,

DC derived from monocytes from 11 healthy donors were stimulated with live Mf or with EVs for 2 days. As has been shown previously (22), compared to their respective baseline levels, both live Mf and Mf-derived EVs were capable of inducing significantly higher amounts of ($p<.05$ for all cytokines) IL-10, IL-8, RANTES and TNF-α (Supplementary Figure 1) compared to unexposed DC. IL-12p40 and IL-12p70 were not induced following exposure to live Mf or Mf-derived EVs. We next assessed differences in cytokine induction by Mf- or EV-conditioned DC following activation with LPS and IFN-γ. As can be seen in Figure 1, IL-1b ($p=.019$), IL-12p40 ($p=.014$), RANTES ($p=.005$), and IL-12p70 ($p=.032$) levels were statistically significantly lower in EV-treated human DC than in those left unexposed; RANTES ($p=.027$) and IL-12p40 ($p=.0068$) induction was also statistically significantly lower in Mf-treated DC when compared to Mf-unexposed DC. There were no statistically significant differences seen between Mf- or EV-exposed IL-10, IL-1α or TNF-α production compared to unexposed DC. The percentage of inhibition of cytokine production was calculated by comparing the average cytokine pg/mL production per treatment condition (EV-conditioned DC vs. Media). All cytokines assessed, except for IL-8, demonstrated inhibition in cytokine production as a consequence of EV-conditioning: IL10 (52.85%), IL12p40 (60.58%), IL8 (-33.63%), 12p70 (40.52%), RANTES (56.54%), TNF (71.17%), IL1 (60.1%), and IL1b (22.23%). These data indicate EVs diminish DC cytokine production following activation to the same degree as live Mf.

3.2 EVs downregulate IL-10 and IL-12p40 cytokine induction in DC

Having found that EV exposure downregulates cytokine production from DC following activation, we next assessed the role of EVs in driving alterations in DC function. By comparing E/S and E/S depleted of EV (Figure 2), we could show that DC, when conditioned with E/S and activated with LPS/IFN-γ, markedly downregulated the production of IL-10 (Figure 2A) and IL-12p40 (Figure 2E) when compared to DC conditioned with media alone. When exposed to E/S depleted of EVs, the IL-10, IL-1a, IL-1b, IL-1c, IL-12p70 and IL-12p40 levels were no different than DC conditioned by media alone ($p>.05$ for all comparisons) following activation (Figures 2A–F). These data indicates that EVs contained within the E/S are likely responsible for the alteration of DC cytokine production following activation with LPS/IFN-γ.

3.3 EVs are central drivers of gene function alterations in human DC

Next, we assessed the impact of Mf-derived EV exposure on the function of DC through RNASeq analysis. Human DC were treated with Mf-derived EVs, E/S, or EV-depleted-E/S. Following exposure, cells were harvested, RNA prepared and sequenced. Using a false discovery rate (FDR)<0.05, we found EV-exposed DC had 212 differentially expressed genes (DEGs) when compared to EV-unexposed DC (147 upregulated/65 downregulated). Most interestingly, there was essentially no difference in DEGs between DC exposed to EVs and those exposed to E/S (only 10 [7 upregulated, 3 downregulated] DEGs. Like the comparison between EV-exposed and media-exposed DC, EV-depleted E/S looked similar to media when compared to EVs (157 DEGs [56 downregulated/101 upregulated (Figure 3A). Clustering of the DEGs across all conditions showing all 4 donor DC, demonstrate that EVs contained within the E/S were responsible for the effects

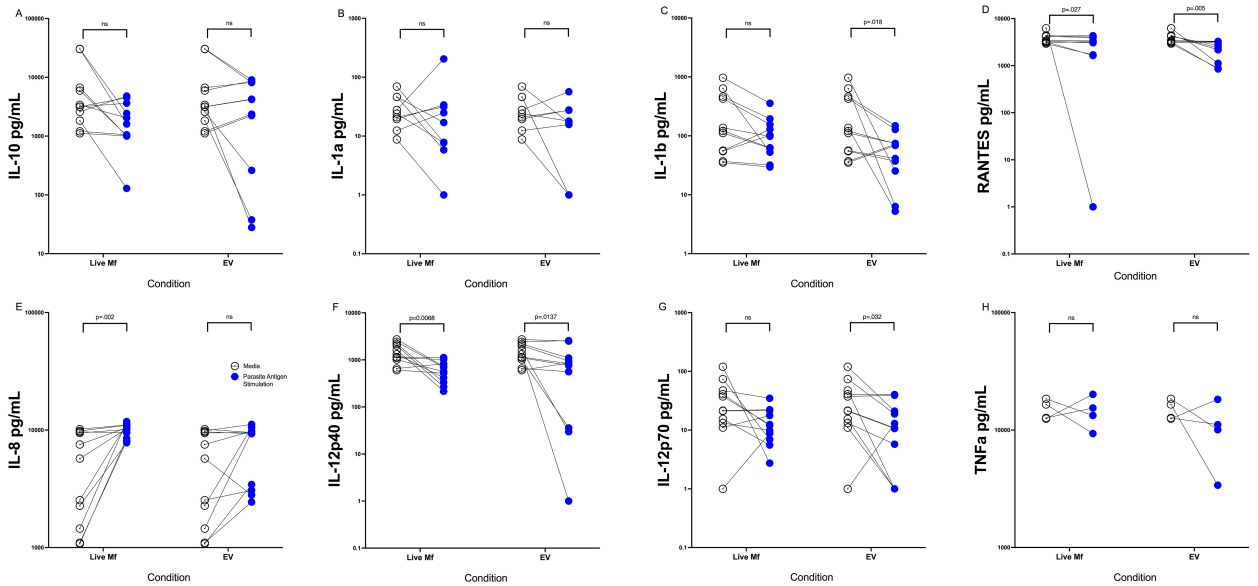

FIGURE 1
EVs downregulate cytokine production in activated DC Human DC (n=10-11) after exposure to media alone (open circles), live Mf (closed circles) or EV (closed circles) were activated with LPS and IFN-γ and supernatants assessed for production of IL-10 **(A)**, IL-1a **(B)**, IL-1b **(C)**, RANTES **(D)**, IL-8 **(E)**, IL-12p40) **(F)**, IL-12p70 **(G)**, TNF-α **(H)**. NS, non-significant.

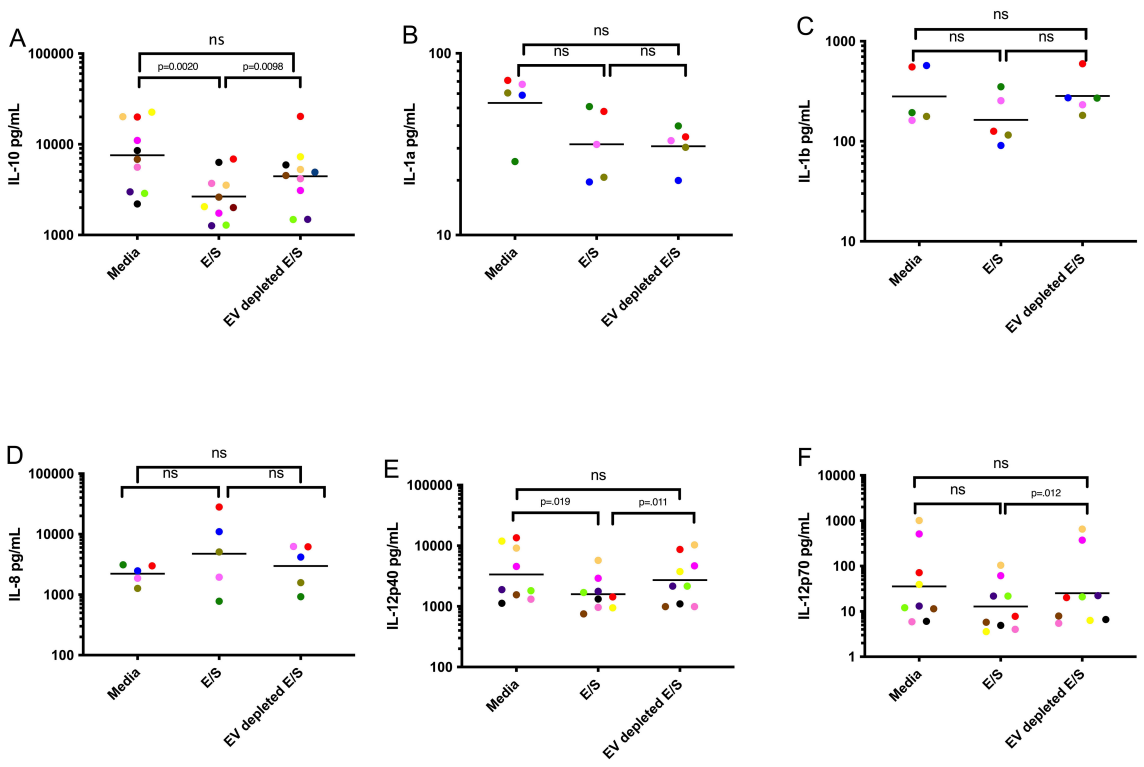

FIGURE 2
EVs contained within Mf E/S drive DC suppression of cytokine production following activation Human DC were exposed to media, Mf-derived E/S, and Mf-derived E/S depleted of EV for 48 hours and assessed for IL-10 **(A)**, IL1a **(B)**, IL1b **(C)**, IL8 **(D)**, IL-12p40 **(E)**, IL-12p70 **(F)**. Each dot represents an individual DC culture with the color matched for each donor among conditions. ns, non-significant.

observed in E/S products. Our findings highlight the central role of EVs derived from Mf in altering the gene expression and function of DC.

Ingenuity Pathway Analysis (IPA) was used to uncover pathways in DC modulated by exposure to microfilariae (Mf)-derived EVs. The analysis identified two predominant enriched canonical pathways: "DC Maturation" and "Th1 and Th2 Activation Pathways" (Figure 4A). Within the IPA-identified DC Maturation canonical pathway, genes associated with antigen processing (HLA-DMA, HLA-DMB) and immune complex recognition (Fc-gamma receptor, FcγR) were found to be downregulated. The Fc-gamma receptor component encompassed annotations for inhibitory molecules and demonstrated downregulatory relationships between MHC Class I and II activation and IL-10 production. Notably, the MHC Class II genes HLA-DMA and HLA-DMB, crucial for antigen presentation, exhibited marked downregulation within this pathway. This downregulation aligns with the overall inhibitory pattern observed in the DC Maturation pathway, suggesting a potential mechanism by which Mf-derived EVs may modulate DC function and subsequent immune responses. These findings provide insights into the molecular mechanisms underlying the immunomodulatory effects of Mf-derived EVs on DC, potentially contributing to our understanding of host-parasite interactions in filarial infections.

Because APCs drive activation of T cells, it is not surprising that the second most important canonical pathway was that associated with Th1 and Th2 activation. Th1 and Th2 activation is pleiotropic with multiple molecules within the pathway responsible for elements of cellular proliferation regulation. As can be seen (Figures 4A–C), EV-treated cells demonstrate inhibition in Th2 cell proliferation indicated by a significantly downregulated, negative z score describing the pathway regulatory networks.

We next used real-time quantitative RT-PCR to confirm the differential gene expression found in the RNAseq analysis. DC were either exposed to EVs or media and RNA was prepared from these cells. Using genes identified to be relevant to both viral and helminth immune response, we were able to independently corroborate the EV-induced alteration of M1 (Signaling Lymphocytic Activation Molecule Family Member 1), TLR7 (Toll-Like Receptor 7), SLC (Solute Carrier Family 7 Member 11), MT1 (Metallothionein 1F) and mTOR (Mechanistic Target of Rapamycin Kinase) (Supplementary Figure 3).

3.4 Mf-derived EVs alter DC activation and activity of antigen-specific T-cells

To determine the impact of Mf-derived EVs as modifiers of DC function, we investigated the impact of EVs on DC activation of antigen-specific CD4+ TCLs (19). Using autologous DC derived from the 6 donors from whom the TCLs were derived, these DC

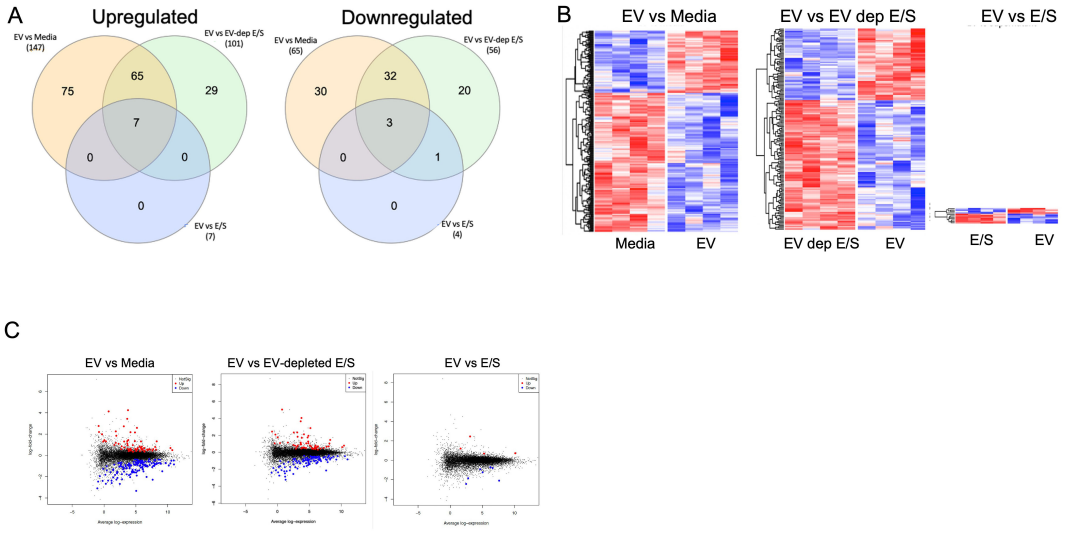

FIGURE 3
Differentially expressed genes (DEGs) in antigen presenting cells exposed to filarial helminth byproducts RNA sequencing results from 4 separate human DC donors left unexposed (media) or exposed to Live Mf, EVs, EV-depleted E/S, and E/S. **(A)** Shows two Venn diagrams of the number of upregulated (Left) and downregulated (Right) DEGs among the various conditions. **(B)** Shows the unsupervised hierarchal clustering of DEGs for EV vs Media (Left, heatmap), EV vs EV-depleted E/S (middle, heatmap), and EV vs E/S (right, heatmap). **(C)** Depicts volcano plots of the various comparisons with blue dots represents statistically significant downregulated DEG and the red dots representing significantly upregulated DEG.

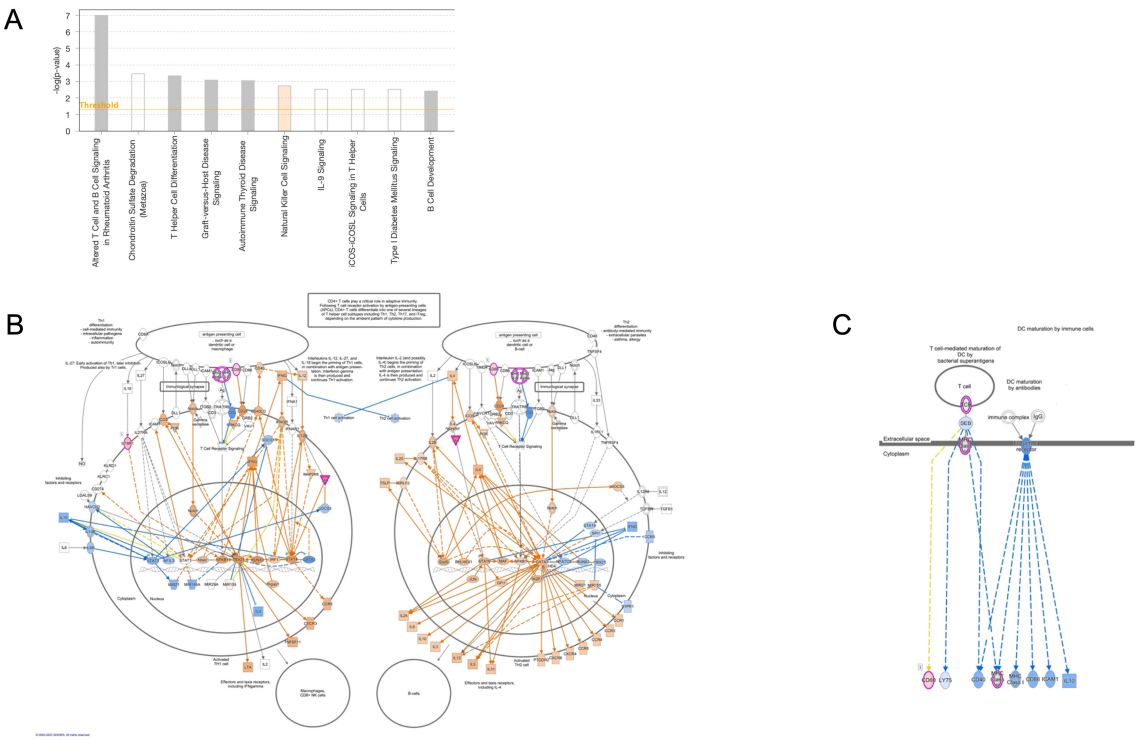

FIGURE 4
Ingenuity Pathway Analysis of annotated canonical pathways in EV-conditioned DC Top Canonical signaling pathways of biological relevance in human DC **(A)**. Map of the Th1 and Th2 activation pathway with blue indicating downregulated genes in the pathway **(B)**. A map of the DC Maturation canonical pathway indicate annotated molecules are associated with suppression (blue) of Fc gamma receptor signaling **(C)**.

were exposed to Mf-derived EVs or media for 48hrs. After 48hrs, the cells were washed and loaded with SARS CoV-2 Membrane peptide pools. Concurrently, Membrane-specific (n=6) TCLs were thawed and co-incubated with their matched (and conditioned) DC. Flow cytometry to assess intracellular CD154, a marker of antigen-experienced CD4 T cells, and IFN-γ, a marker of an anti-viral cytokine response were assessed (Supplementary Figure 3). As can be seen in Figure 5, using SARS CoV-2 Membrane-specific CD4+ T cell derived from the same 6 donors and DC conditioned with Mf-derived EVs, we were able to find fewer activated SARS CoV-2 Membrane-specific CD3+ CD4+ CD154+ cells (p=.0001) when compared to unconditioned DC. Additionally, Mf-derived EV-conditioning of DC induced fewer SARS CoV-2 Membrane-specific CD3+ CD4+ cells capable of producing IFN-γ (p=.0001).

4 Discussion

Brugia malayi represent a class of parasitic (filarial) organisms that inhabit the lymphatic system and can induce subclinical chronic infections in their hosts. The disease associated with infection (lymphatic filariasis) can be characterized by significant morbidity resulting from the inflammatory responses elicited by the filarial worms. Recent studies have revealed that filarial helminths secrete EVs containing a variety of biomolecules, including small RNAs, proteins, lipids, and glycans, which are then internalized by host cells (13, 17). Our research group has previously demonstrated that both the Mf and the EVs derived from them are capable of modulating host mTOR-associated pathways which play critical roles in the regulation of cellular proliferation, autophagy, and

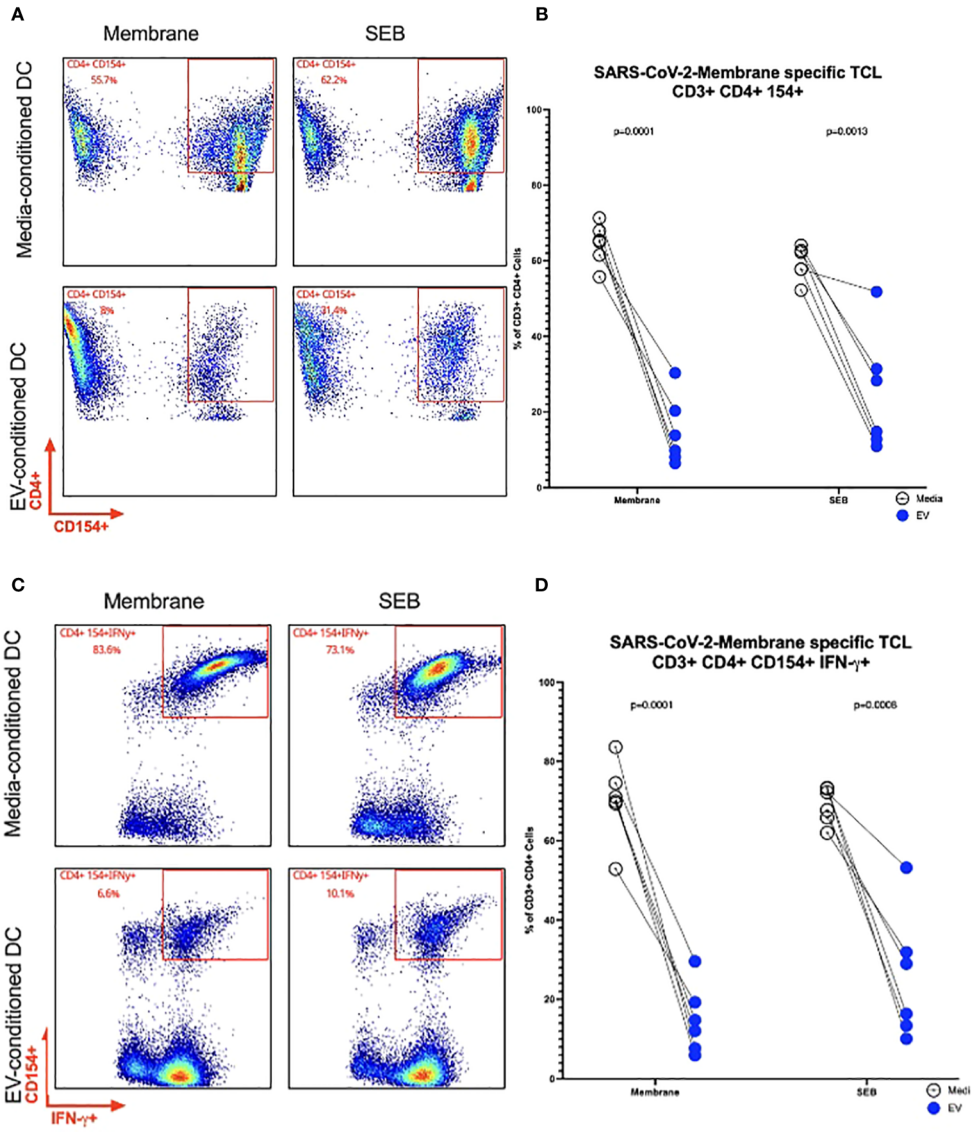

FIGURE 5
Frequency of SARS CoV-2 Membrane TCLs following activation by EV-conditioned human DC Representative flow cytometry plots of a single patient for SARS-CoV-2 Membrane-specific CD3+ CD4+CD154+ T cells **(A)**. Frequencies of SARS-CoV-2 Membrane-specific CD3+ CD4+CD154+ T cells **(B)**. Representative flow cytometry plots of a single patient for SARS-CoV-2 Membrane-specific CD3+ CD4+ CD154+ IFN-γ+ **(C)**. Frequencies of SARS-CoV-2 Membrane-specific CD3+ CD4+CD154+ T cells detected in coincubations with EV-conditioned dendritic cell **(D)** n= 6.

apoptosis. The unique characteristics of EVs, including their ability to transport immunomodulatory cargo, have made them the focus of increasing attention as a potential therapeutic tool for targeted delivery of these biomolecules. Our investigations have shown that EVs are readily internalized by human DC, where they can modulate key intercellular functions (17). 21 proteins unique to *Loa loa* EVs have been found in patient sera, indicating potential use of EVs as a biomarker of infection (23). Additionally, the immunomodulatory functions of EVs have been explored as a potential therapeutic approach for reducing clinical symptoms and inflammatory markers in models of inflammation (24). In particular, studies of the effects of helminth infections on immune responses to viral antigen and vaccines have revealed that these infections induce a cytokine response that diminishes bystander antigen-specific immune responses (25). In the present study, we aimed to characterize the role of EVs in mediating alterations of human APC functions and to evaluate the immunomodulatory effects of these EVs on viral-specific immune responses.

EVs contain cargo that modulate the functions of DC and influence their interactions with immune cells. Through RNA sequencing analysis, we demonstrated that EVs are a potent modulator of DC gene expression, as the gene expression in EV-exposed cells was found to be distinct from both EV-depleted E/S- and media-exposed cells (Figures 3A-C). These findings provide strong evidence that EVs, rather than unencapsulated soluble mediators, are responsible for driving the observed changes in DC functions. Our previous research has established that EVs, like Mfs can alter immune activation functions in APCs through their internalization within the cell cytosol; in so doing they appear to suppress the production of proinflammatory cytokines (26). In line with these findings, in the present study, exposure to Mf-derived EVs resulted in a suppression of DC cytokine production, including IL-12p40, IL-12p70, IL-1b, and RANTES in activated human DC (Figures 1A, B). Additionally, depletion of EVs from Mf E/S resulted in a return of these cytokines to their baseline levels. The impact of EVs on reducing cytokine secretion demonstrate their immunomodulatory capacity. The results presented in this study underscore the potential utility of EVs as a therapeutic tool, owing to their ability to internalize within a diverse range of target cells and transfer molecules that modulate intracellular machinery. Specifically, the findings of this study implicate EVs as important regulators of host-parasite immune responses and suggest that they have great promise as a means of manipulating immune activation and suppression. A deeper understanding of the underlying mechanisms by which EVs modulate these processes could inform the development of novel therapeutic strategies for the treatment of helminth infections.

In addition to their potential application in the context of parasitic infections, the results of this study further support the growing body of literature that indicates that EVs are key players in the regulation of APC function and, thus, are capable of shaping the host immune response (13, 27–29). We found EVs downregulate pathways for DC maturation that in turn have consequences for Th1 differentiation. The impact of reduced Th1-associated effector function include limitations to expansion of immune subsets, and dysregulated immune effector functions for antiviral responses.

We found that EVs downregulated MHC-II expression in DC as well as HLA-DMA and HLA-DMB, a marker of DC maturation. The enzyme HLA-DM facilitates CLIP dissociation from MHC-II, which enables the binding of a peptide to MHC-II. DM stabilizes MHC-II during peptide exchange and selects for peptides with higher binding affinities. Therefore, HLA-DM may play a role in DC antigen presentation by facilitating the exchange of peptides bound to MHC-II. EVs may alter HLA-DMA and HLA-DMB, preventing antigen-processing of filarial antigens to avoid immune detection.

As stated above, HLA-DM is a nonclassical MHCII-like protein that plays a pivotal role in selecting high specificity epitopes, ultimately shaping the adaptive immune response. By acting as a peptide exchange catalyst, HLA-DM helps to shape the MHCII immunopeptidome by editing the repertoire of presented peptides (30). The interaction between T-cell receptor (TCR), peptide and major histocompatibility complex (MHC) can determine Th1/Th2 dominance and selection of CD4+ T cell functions (31). In other parasitic infections, HLA-DM genes are also downregulated (32), suggesting EVs may inhibit high MHCII density on DC and alter Th1/Th2 differentiation (31). We also found that EVs altered the expression of FcγRs, receptors found on many myeloid cells that recognize targets coated with IgG, such as opsonized pathogens or immune complexes (33). Plasma from *Brugia* spp. Mf+ infected individuals actively impair granulocyte activation and degranulation, a process governed by FcgR-signalling, suggesting a possible role for EVs in altering the functionality of FcγRs (34).

Patent lymphatic filariasis, a chronic infection caused by B. *malayi* and the related parasite, *Wuchereria bancrofti*, is also characterized by defects in DC function and antigen-specific T-cell unresponsiveness (35). Previous research has shown that Mf exposure can reduce the expression of innate antiviral immune ligand receptors, such as TLR3 and TLR4 which can lead to a diminution of antigen-specific responses (36).

These alterations in the immune environment can have long-lasting consequences for vaccine and viral bystander memory. Our current study found that virus (SARS CoV-2 Membrane)-specific TCLs had lower frequencies of activated cells and fewer IFN-γ producing cells when cultured with EV-conditioned DC (Figure 5) This suppression of T-cell activation is consistent with the findings of previous studies, which have shown that chronic filarial infections are associated with lower levels of inflammatory cytokines such as IFN-γ, which is partially due to T-cell exhaustion. Helminth infections, including *B. malayi* infections, produce exhausted T cells with increased expression of inhibitory receptors (PD-1, LAG3, CTLA4) that are capable of downregulating T-cell proliferative responses and increasing the potential for apoptosis (2, 37–39).

In conclusion, our study provides further evidence of the potential of EVs as downmodulatory of host immune responses. These findings suggest that many of the modulatory effects seen in chronic filarial infection are mediated through the internalization of EVs on APCs. Further research will be needed to fully characterize the fine intracellular details of EV trafficking and immune modulation, as well as to investigate the therapeutic implications of these.

Data availability statement

The data presented in the study are deposited in the GEO repository and is publicly available under accession number GSE263690.

Ethics statement

The studies involving humans were approved by NIH Institutional Review Board. The studies were conducted in accordance with the local legislation and institutional requirements. The human samples used in this study were acquired from a by-product of routine care or industry. Written informed consent for participation was not required from the participants or the participants' legal guardians/next of kin in accordance with the national legislation and institutional requirements.

Author contributions

GS: Conceptualization, Formal analysis, Methodology, Visualization, Writing – original draft, Writing – review & editing. AR: Conceptualization, Data curation, Investigation, Methodology, Supervision, Visualization, Writing – original draft, Writing – review & editing. NR: Investigation, Methodology, Software, Writing – review & editing. PS: Investigation, Supervision, Writing – review & editing. JL: Methodology, Software, Supervision, Validation, Writing – review & editing. PG-G: Formal analysis, Methodology, Supervision, Validation, Writing – review & editing. TN: Conceptualization, Data curation, Formal analysis, Funding acquisition, Investigation, Methodology, Project administration, Resources, Software, Supervision, Validation, Visualization, Writing – original draft, Writing – review & editing.

Funding

The author(s) declare financial support was received for the research, authorship, and/or publication of this article. This work was supported by the Division of Intramural Research (DIR) National Institute of Allergy and Infectious Diseases.

Acknowledgments

We would also like to acknowledge the NIAID Integrated Data Science Section (IDDS) for their support in the analysis.

Conflict of interest

The authors declare that the research was conducted in the absence of any commercial or financial relationships that could be construed as a potential conflict of interest.

Publisher's note

Supplementary material

The Supplementary Material for this article can be found online at: https://www.frontiersin.org/articles/10.3389/fimmu.2024.1436818/full#supplementary-material

References

1. Babu S, Nutman TB. Immunology of lymphatic filariasis. *Parasite Immunol.* (2014) 36:338–46. doi: 10.1111/pim.12081

2. Babu S, Blauvelt CP, Kumaraswami V, Nutman TB. Regulatory networks induced by live parasites impair both Th1 and Th2 pathways in patent lymphatic filariasis: implications for parasite persistence. *J Immunol.* (2006) 176:3248–56. doi: 10.4049/jimmunol.176.5.3248

3. Babu S, Ganley LM, Klei TR, Shultz LD, Rajan TV. Role of gamma interferon and interleukin-4 in host defense against the human filarial parasite Brugia malayi. *Infect Immun.* (2000) 68:3034–5. doi: 10.1128/IAI.68.5.3034-3035.2000

4. Hartmann W, Brunn M-L, Stetter N, Gagliani N, Muscate F, Stanelle-Bertram S, et al. Helminth infections suppress the efficacy of vaccination against seasonal influenza. *Cell Rep.* (2019) 29:2243–2256.e4. doi: 10.1016/j.celrep.2019.10.051

5. White MPJ, McManus CM, Maizels RM. Regulatory T-cells in helminth infection: induction, function and therapeutic potential. *Immunology.* (2020) 160:248–60. doi: 10.1111/imm.13190

6. Narasimhan PB, Akabas L, Tariq S, Huda N, Bennuru S, Sabzevari H, et al. Brugia malayi Microfilariae Induce Autophagy through an Interferon-γ Dependent Mechanism on Human Monocytes. *Am J Trop Med Hyg.* (2022) 106:1254–62. doi: 10.4269/ajtmh.21-1134

7. Weinkopff T, Mackenzie C, Eversole R, Lammie PJ. Filarial excretory-secretory products induce human monocytes to produce lymphangiogenic mediators. *PloS Negl Trop Dis.* (2014) 8:e2893. doi: 10.1371/journal.pntd.0002893

8. Narasimhan PB, Bennuru S, Meng Z, Cotton RN, Elliott KR, Ganesan S, et al. Microfilariae of Brugia malayi Inhibit the mTOR Pathway and Induce Autophagy in Human Dendritic Cells. *Infect Immun.* (2016) 84:2463–72. doi: 10.1128/IAI.00174-16

9. Terrazas CA, Sánchez-Muñoz F, Mejía-Domínguez AM, Amezcua-Guerra LM, Terrazas LI, Bojalil R, et al. Cestode antigens induce a tolerogenic-like phenotype and inhibit LPS inflammatory responses in human dendritic cells. *Int J Biol Sci.* (2011) 7:1391–400. doi: 10.7150/ijbs.7.1391

10. Maldonado RA, von Andrian UH. How tolerogenic dendritic cells induce regulatory T cells. *Adv Immunol.* (2010) 108:111–65. doi: 10.1016/B978-0-12-380995-7.00004-5

11. Sun S, Wang X, Wu X, Zhao Y, Wang F, Liu X, et al. Toll-like receptor activation by helminths or helminth products to alleviate inflammatory bowel disease. *Parasit Vectors.* (2011) 4:186. doi: 10.1186/1756-3305-4-186

12. Drurey C, Maizels RM. Helminth extracellular vesicles: Interactions with the host immune system. *Mol Immunol.* (2021) 137:124–33. doi: 10.1016/j.molimm.2021.06.017

13. Harischandra H, Yuan W, Loghry HJ, Zamanian M, Kimber MJ. Profiling extracellular vesicle release by the filarial nematode Brugia malayi reveals sex-specific differences in cargo and a sensitivity to ivermectin. *PloS Negl Trop Dis*. (2018) 12: e0006438. doi: 10.1371/journal.pntd.0006438

14. Zamanian M, Fraser LM, Agbedanu PN, Harischandra H, Moorhead AR, Day TA, et al. Release of small RNA-containing exosome-like vesicles from the human filarial parasite brugia malayi. *PloS Negl Trop Dis*. (2015) 9:e0004069. doi: 10.1371/journal.pntd.0004069

15. Marshall FA, Grierson AM, Garside P, Harnett W, Harnett MM, et al. ES-62, an immunomodulator secreted by filarial nematodes, suppresses clonal expansion and modifies effector function of heterologous antigen-specific T cells in vivo1. *J Immunol*. (2005) 175:5817–26. doi: 10.4049/jimmunol.175.9.5817

16. Buck AH, Akabas L, Tariq S, Huda N, Bennuru S, Sabzevari H, et al. Exosomes secreted by nematode parasites transfer small RNAs to mammalian cells and modulate innate immunity. *Nat Commun*. (2014) 5:5488. doi: 10.1038/ncomms6488

17. Ricciardi A, Bennuru S, Tariq S, Kaur S, Wu W, Elkahloun AG, et al. Extracellular vesicles released from the filarial parasite Brugia malayi downregulate the host mTOR pathway. *PloS Negl Trop Dis*. (2021) 15:e0008884. doi: 10.1371/journal.pntd.0008884

18. Coakley G, Maizels RM, Buck AH. Exosomes and other extracellular vesicles: the new communicators in parasite infections. *Trends Parasitol*. (2015) 31:477–89. doi: 10.1016/j.pt.2015.06.009

19. Gazzinelli-Guimaraes PH, Sanku G, Sette A, Weiskopf D, Schaughency P, Lack J, et al. Antigenic determinants of SARS-coV-2-specific CD4. *Front Immunol*. (2022) 13:883159. doi: 10.3389/fimmu.2022.883159

20. Robinson MD, Oshlack A. A scaling normalization method for differential expression analysis of RNA-seq data. *Genome Biol*. (2010) 11:R25. doi: 10.1186/gb-2010-11-3-r25

21. Semnani RT, Liu AY, Sabzevari H, Kubofcik J, Zhou J, Gilden JK, et al. Brugia malayi microfilariae induce cell death in human dendritic cells, inhibit their ability to make IL-12 and IL-10, and reduce their capacity to activate CD4+ T cells. *J Immunol*. (2003) 171:1950–60. doi: 10.4049/jimmunol.171.4.1950

22. Narasimhan PB, Akabas L, Tariq S, Huda N, Bennuru S, Sabzevari H, et al. Similarities and differences between helminth parasites and cancer cell lines in shaping human monocytes: Insights into parallel mechanisms of immune evasion. *PloS Negl Trop Dis*. (2018) 12:e0006404. doi: 10.1371/journal.pntd.0006404

23. Yates D, Maggio Di LS, Rosa BA, Sprung RW, Erdmann-Gilmore P, Townsend RR, et al. Identification of biomarker candidates for filarial parasite infections by analysis of extracellular vesicles. *Front Parasitol*. (2023) 2. doi: 10.3389/fpara.2023.1281092

24. Cortes-Serra N, Gualdron-Lopez M, Pinazo MJ, Torrecilhas AC, Fernandez-Becerra C, et al. Extracellular vesicles in. *J Immunol Res*. (2022) 2022:5230603. doi: 10.1155/2022/5230603

25. Wait LF, Dobson AP, Graham AL. Do parasite infections interfere with immunisation? A review and meta-analysis. *Vaccine*. (2020) 38:5582–90. doi: 10.1016/j.vaccine.2020.06.064

26. O'Regan NL, Steinfelder S, Venugopal G, Rao GB, Lucius R, Srikantam A, et al. Brugia malayi microfilariae induce a regulatory monocyte/macrophage phenotype that suppresses innate and adaptive immune responses. *PloS Negl Trop Dis*. (2014) 8:e3206. doi: 10.1371/journal.pntd.0003206

27. Loghry HJ, Sondjaja NA, Minkler SJ, Kimber MJ. Secreted filarial nematode galectins modulate host immune cells. *Front Immunol*. (2022) 13:952104. doi: 10.3389/fimmu.2022.952104

28. Hertz MI, Glaessner PM, Rush A, Budge PJ. Brugia malayi galectin 2 is a tandem-repeat type galectin capable of binding mammalian polysaccharides. *Mol Biochem Parasitol*. (2020) 235:111233. doi: 10.1016/j.molbiopara.2019.111233

29. Daniłowicz-Luebert E, Oregan NL, Steinfelder S, Hartmann S. Modulation of specific and allergy-related immune responses by helminths. *J BioMed Biotechnol 2011*. (2011) p:821578. doi: 10.1155/2011/821578

30. Álvaro-Benito M, Wieczorek M, Sticht J, Kipar C, Freund C. HLA-DMA polymorphisms differentially affect MHC class II peptide loading. *J Immunol*. (2015) 194:803–16. doi: 10.4049/jimmunol.1401389

31. Murray JS. How the MHC selects Th1/Th2 immunity. *Immunol Today*. (1998) 19:157–63. doi: 10.1016/S0167-5699(97)01237-1

32. Knight JS, Baird DB, Hein WR, Pernthaner A. The gastrointestinal nematode Trichostrongylus colubriformis down-regulates immune gene expression in migratory cells in afferent lymph. *BMC Immunol*. (2010) 11:51. doi: 10.1186/1471-2172-11-51

33. Guilliams M, Bruhns P, Saeys Y, Hammad H, Lambrecht BN. The function of Fcγ receptors in dendritic cells and macrophages. *Nat Rev Immunol*. (2014) 14:94–108. doi: 10.1038/nri3582

34. Prodjinotho UF, Horn von C, Debrah AY, Debrah Batsa L, Albers A, Layland LE, et al. Pathological manifestations in lymphatic filariasis correlate with lack of inhibitory properties of IgG4 antibodies on IgE-activated granulocytes. *PloS Negl Trop Dis*. (2017) 11:e0005777. doi: 10.1371/journal.pntd.0005777

35. Talaat KR, Bonawitz RE, Domenech P, Nutman TB. Preexposure to live Brugia malayi microfilariae alters the innate response of human dendritic cells to Mycobacterium tuberculosis. *J Infect Dis*. (2006) 193:196–204. doi: 10.1086/498912

36. Semnani RT, Venugopal PG, Leifer CA, Mostbock S, Sabzevari H, Nutman TB. Inhibition of TLR3 and TLR4 function and expression in human dendritic cells by helminth parasites. *Blood*. (2008) 112:1290–8. doi: 10.1182/blood-2008-04-149856

37. Steel C, Nutman TB. CTLA-4 in filarial infections: implications for a role in diminished T cell reactivity. *J Immunol*. (2003) 170:1930–8. doi: 10.4049/jimmunol.170.4.1930

38. Babu S, Bhat SQ, Kumar Pavan N, Lipira AB, Kumar S, et al. Filarial lymphedema is characterized by antigen-specific Th1 and th17 proinflammatory responses and a lack of regulatory T cells. *PloS Negl Trop Dis*. (2009) 3:e420. doi: 10.1371/journal.pntd.0000420

39. Rajamanickam A, Munisankar S, Dolla C, Nutman TB, Babu S. Cytotoxic T-lymphocyte-associated antigen 4 (CTLA-4)- and programmed death 1 (PD-1)-mediated regulation of monofunctional and dual functional CD4(+) and CD8(+) T-cell responses in a chronic helminth infection. *Infect Immun*. (2019) 87. doi: 10.1128/IAI.00469-19

frontiers | Frontiers in Immunology

TYPE Original Research
PUBLISHED 25 October 2024
DOI 10.3389/fimmu.2024.1459961

OPEN ACCESS

EDITED BY
Anisuzzaman Anisuzzaman,
Bangladesh Agricultural University,
Bangladesh

REVIEWED BY
Christoph Siegfried Niki Klose,
Charité University Medicine Berlin, Germany
Thomas Nutman,
National Institutes of Health (NIH),
United States

*CORRESPONDENCE
Mübeccel Akdis
muebeccel.akdis@siaf.uzh.ch

RECEIVED 05 July 2024
ACCEPTED 12 September 2024
PUBLISHED 25 October 2024

CITATION
López J-F, Zakzuk J, Satitsuksanoa P, Lozano A, Buergi L, Heider A, Alvarado-Gonzalez JC, Babayev H, Akdis C, van de Veen W, Caraballo L and Akdis M (2024) Elevated circulating group-2 innate lymphoid cells expressing activation markers and correlated tryptase AB1 levels in active ascariasis.
Front. Immunol. 15:1459961.
doi: 10.3389/fimmu.2024.1459961

Elevated circulating group-2 innate lymphoid cells expressing activation markers and correlated tryptase AB1 levels in active ascariasis

Juan-Felipe López[1,2], Josefina Zakzuk[2], Pattraporn Satitsuksanoa[1], Ana Lozano[2], Laura Buergi[1], Anja Heider[1], Juan Carlos Alvarado-Gonzalez[2], Huseyn Babayev[1], Cezmi Akdis[1], Willem van de Veen[1], Luis Caraballo[2] and Mübeccel Akdis[1]*

[1]Swiss Institute of Allergy and Asthma Research (SIAF), University of Zurich, Davos, Switzerland, [2]Institute for Immunological Research, University of Cartagena, Cartagena, Colombia

Introduction: *Ascaris lumbricoides* infection is one of the most common soil-transmitted helminthiasis and IgE response to this helminth may increase the risk of asthma, bronchial hyperreactivity and atopy. There is not enough evidence showing the role of group-2 innate lymphoid cells (ILC2) in the pathogenesis of helminth infections in humans. Here, we aimed to investigate and characterize the influence of *Ascaris lumbricoides* infection on circulating ILCs in endemically exposed subjects.

Methods: Non-infected (NI; n=16) and Ascaris-infected (AI; n=16) subjects from an endemic area were included. Two consecutive stool samples from each subject were examined by Kato-Katz to define parasite infection. Antibodies to the ABA-1 antigen of Ascaris and Ascaris extract were measured by ELISA. ILC subsets and their activation markers (CD25, CD69, thymic stromal lymphopoietin receptor (TSLPR) were evaluated in its PBMC by flow cytometry. Proximity extension assay (PEA) was performed to explore plasma proteins associated to infection.

Results: No significant differences in the relative or absolute frequencies of total ILCs, ILC1, ILC2 and ILC3 cells were observed regarding the infection status. However, within AI group, IgE-sensitized subjects to ABA-1 had higher frequencies and counts of ILC2 ($p<0.05$). Frequencies of CD25+, CD69+ and TSLPR+ ILC2 were higher in AI compared to the NI ($p<0.01$). Additionally, egg burden was positively correlated with CD69+ ILC2 frequencies ($r=0.67$; $p=0.005$). Tryptase alpha/beta 1 (TPSAB1), GP6 and several plasma proteins associated with cell growth and granulocyte chemotaxis were highly expressed in the AI group ($p<0.05$). Interestingly, TPSAB1 levels were positively correlated with ILC2 expressing activation markers frequencies, egg burden and IgE levels against Ascaris.

Discussion: Ascaris infection is associated with increased expression of ILC2 activation markers and TPSAB1, which may contribute to the type-2 response.

KEYWORDS

ascariasis, helminth, IgE, immune regulation, innate lymphoid cells, type-2 immunity, Tryptase AB1

1 Introduction

Ascaris lumbricoides infection is one of the most prevalent and neglected tropical helminthiasis worldwide (global prevalence around 11.9%) (1). In addition, several studies have shown that sensitization to its components is associated with indicators of poorly hygienic conditions and asthma risk (2–8). Similar to allergy, helminth infection induces a strong type-2 (T2) response that is orchestrated by alarmins, cytokines, and cells from innate and adaptive immune systems (9).

Innate lymphoid cells (ILCs) are mainly tissue-resident lymphocytes that do not express antigen-recognition receptors (10). They produce cytokines essential for the maintenance of tissue homeostasis and communication between the innate and adaptive immune systems (10). Recent studies have demonstrated the importance of ILCs and alarmins (IL-25, IL-33) in the promotion of T2 immunity and inflammation following helminth infection or allergen exposure (11–14). ILC2s, a subtype of ILCs discovered in a mouse model of helminth infection, are essential for Th2-differentiation and worm expulsion due to their role in the production of IL-4 and IL-13, respectively (15–18). Observations from human studies in *Schistosoma haematobium* and filarial infection have demonstrated that ILC frequencies fluctuate according to the infection status (19, 20). However, these findings are heterogeneous and were reported in different helminth species.

Since mice are not a natural host for Ascaris spp. and larvae do not develop into adult stages, there is no clear evidence that *A. lumbricoides* induces changes in ILCs in this species. Due to the strong promoting effect of Ascaris on T2 responses, it is hypothesized that this infection may induce ILC2 development and activation. Epithelial alarmins stimulation and different status of disease can induce changes in the different surface markers associated with this population. Several studies in different models have shown that activation of ILCs could be represented by global lymphoid cell activation markers like CD69 (21–23) and CD25 (24, 25), and thymic stromal lymphopoietin receptor (TSLPR) represents a proxy of T2 response susceptibility of this cell subset (26, 27).

Understanding how helminths shape the immune system provides the opportunity to gain insight into natural T2 responses and how they might be regulated. Additionally, exploration of helminth targets in the immune system may help to elucidate the mechanisms by which potential vaccine candidates fail to provide sustained immunity (28). Hence, this study aimed to investigate and characterize specifically the influence of helminth infection by *A. lumbricoides* on circulating ILCs of exposed subjects living in an endemic town of Colombia.

2 Materials and methods

2.1 Study subjects

From March 2022 to September 2022, subjects were recruited through a cross-sectional survey in Santa Catalina, a small tropical farming/fishing town in the North of Colombia (10° 36′ 0″ N, 75° 18′ 0″ W) that includes five villages (153 km2, 12.500 inhabitants, no sewage) where *Ascaris lumbricoides* infection is endemic (prevalence of 63%) (7, 29). In a last survey, half of its inhabitants had at least one unsatisfied basic need, only 4.5% of the population has a sewage system and 56% has tap water.

Eligible participants were adults (between 18 to 75 years old), who had lived in the town for at least 2 years. They were visited by a trained physician, who examined the subjects, filled out the questionnaires to assess the demographic risk factors for infection, and collected blood and stool samples. Exclusion criteria were co-infection by another helminth, pregnancy, received anti-helminthic in the last 3 months and/or any antecedent of cancer or autoimmune diseases. Controls were non-infected but exposed subjects (inhabitants from this village) with similar sociodemographic conditions, age and sex, without records of worm expulsion in the last 2 years and two consecutives (least than one week apart) negative stool examinations. Once an infected case was identified, a neighbor of the same age and sex without consanguinity (to avoid genetic susceptibility bias) was invited to participate as a control.

Infection status was determined by stool parasitological analyses in two stool samples obtained by spontaneous evacuation on different days and donors were categorized as non-infected (NI) or Ascaris infected (AI). Briefly, all donors were tested under direct fecal smear and Kato-Katz method which allows to determine counting helminth egg per gram (e.p.g) of feces which has a sensitivity and specificity over 90% to detect different soil-transmitted helminth infections (30, 31). If protozoan or

helminth parasites different than Ascaris were found, the subject was excluded from the study. Peripheral mononuclear cells (PBMC) were isolated from heparinized blood, cryopreserved and stored in liquid nitrogen until flow cytometry analysis.

The study was approved by the University of Cartagena Ethics Committee (Minutes #12811-2019). Informed consent was obtained from all participants.

2.2 Recombinant ABA-1, Ascaris-specific and total IgE antibody detection

Ascaris lumbricoides extract was prepared from adult worms after physical homogenization in PBS as reported previously (32). Recombinant ABA-1 was produced in *Escherichia coli* BL21 (Invitrogen Corporation, Carlsbad, CA, USA) as a GST fusion protein. After cleavage with thrombin, a 99% purity product is observed in SDS-PAGE (33). Recombinant ABA-1 and *A. lumbricoides* body extract were coated at 1 µg and 5 µg per well, respectively, on Nunc Maxisorb microtiter plate (Thermo Fisher Scientific, Waltham, MA, USA) and incubated at room temperature (RT) overnight and then blocked with blocking buffer (PBS pH 7.4, 2% BSA, 0.05% Tween 20). Plasma samples diluted 1:10 in blocking buffer were added and incubated for 2 hours at room temperature. Specific IgE was detected using a goat anti-human IgE antibody conjugated with HRP (Bethyl Laboratories, Cat N° A80-108P, Texas, USA). For the detection of specific IgG, goat anti-human IgG-peroxidase (Jackson Immuno Research Europe Ltd, Cambridgeshire, UK) was used. For total IgE detection, high-binding 96-well ELISA plates (Thermo Fisher Scientific, USA) were coated with mouse anti–human IgE clone 14-41 (gift from Christoph Heusser, Novartis, Basel, Switzerland). The plates were blocked and then incubated for 2 hours with 1:100 diluted plasma samples and the 8-step standard curve (300 to 0.13 ng/mL) of human IgE myeloma wild-type (Cat N° 401152; Sigma-Aldrich). Biotinylated mouse anti–IgE clone 6-7 (clone MZ01; Christoph Heusser, Novartis) was used as detection antibody and Extravidin peroxidase (Cat N° E2886; Sigma-Aldrich) was used as an enzymatic reagent (34). ELISAs were developed using tetramethylbenzidine (TMB) substrate (Thermo Fisher Scientific, Waltham, MA, USA) and the reaction was stopped with 1M H2SO4 sulfuric acid. Plates were read at 450 nm by a Mithras LB 940 spectrophotometer (Berthold Technologies, Bad Wildbad, Germany) (35).

2.3 Peripheral blood mononuclear cells isolation and cryopreservation

Blood samples were collected in heparinized tubes; subsequently, they were diluted in PBS and centrifuged with Ficoll Histopaque (Sigma Aldrich, St. Louis, MO, USA) to visualize and extract the mononuclear cell layer. Cells were washed three times with PBS/EDTA and resuspended in 1 mL of RPMI 1640 (Sigma Aldrich, St. Louis, MO, USA) supplemented medium and 1 mL of freezing medium (80% inactivated FBS and 20% DMSO). The samples were deposited in cryovials in a freezing container (Thermo Scientific™ Mr. Frosty™ Freezing Container) at -80°C and stored at −196°C in LN2 until analysis.

2.4 Flow cytometry

PBMCs were thawed and stained with a modified panel based from a well-established method for ILCs detection (36, 37). A monoclonal antibody mix containing FITC-labelled surface antibodies was used to exclude dendritic cells (CD11c), plasmacytoid dendritic cells (CD303, CD123), monocytes (CD14), macrophages (CD14), stem cells (CD34), NK cells (CD94), basophils (FceR1a), T lymphocytes (CD3) and B lymphocytes (CD19). CD45, CD161 and CD127 (IL-7Rα) were included to identify the circulating total ILC population (Supplementary Figure 1A), and CRTH2 (PGD2 receptor) and CD117(c-kit) to differentiate ILC1s, ILC2s and ILC3s (Figure 1A). The full stain panel (Supplementary Table 1) also includes TSLPR, and CD69 (c-type lectin protein) and CD25 (IL2Rα) for further phenotyping of ILC2 activation. Isotype and fluorescence minus one (FMO) tubes were used as controls to define the gating strategy (Supplementary Figure 1B). Flow cytometric measurements were made according to the compensation matrix of the ILC panel prepared on the BD LSR FORTESA (16-colour analyzer) and were analyzed using the Flowjo LLC Software (Version 10, San Jose, CA, USA).

2.5 Proximity extension assay

We used Target 96 Inflammation, Immune Response, Cardiovascular III and Organ Damage panels from Olink Biosciences (Uppsala, Sweden) to characterize 368 proteins in the obtained plasma samples. The PEA method involves binding of antibody-pairs labeled with unique DNA oligonucleotides to the target protein in the samples. The subsequent proximity extension creates unique DNA barcodes which are amplified by real time PCR. Measurements are presented as Normalized Protein eXpression (NPX) values, reflecting relative protein concentration with no absolute quantification, derived from Ct values after data pre-processing to minimize variation (38). Assay characteristics including quality control, detection limits, and measurements of assay performance and validation were done at the Olink Service Provider Lab in Davos, Switzerland. After excluding variables due to >40% missing data (values below the limit of detection; LOD), 239 products were selected for final analysis.

2.6 Statistical analysis

Statistical analyses were performed using SPSS version 20 software, GraphPad Prism 9 and R Studio programs. Distribution

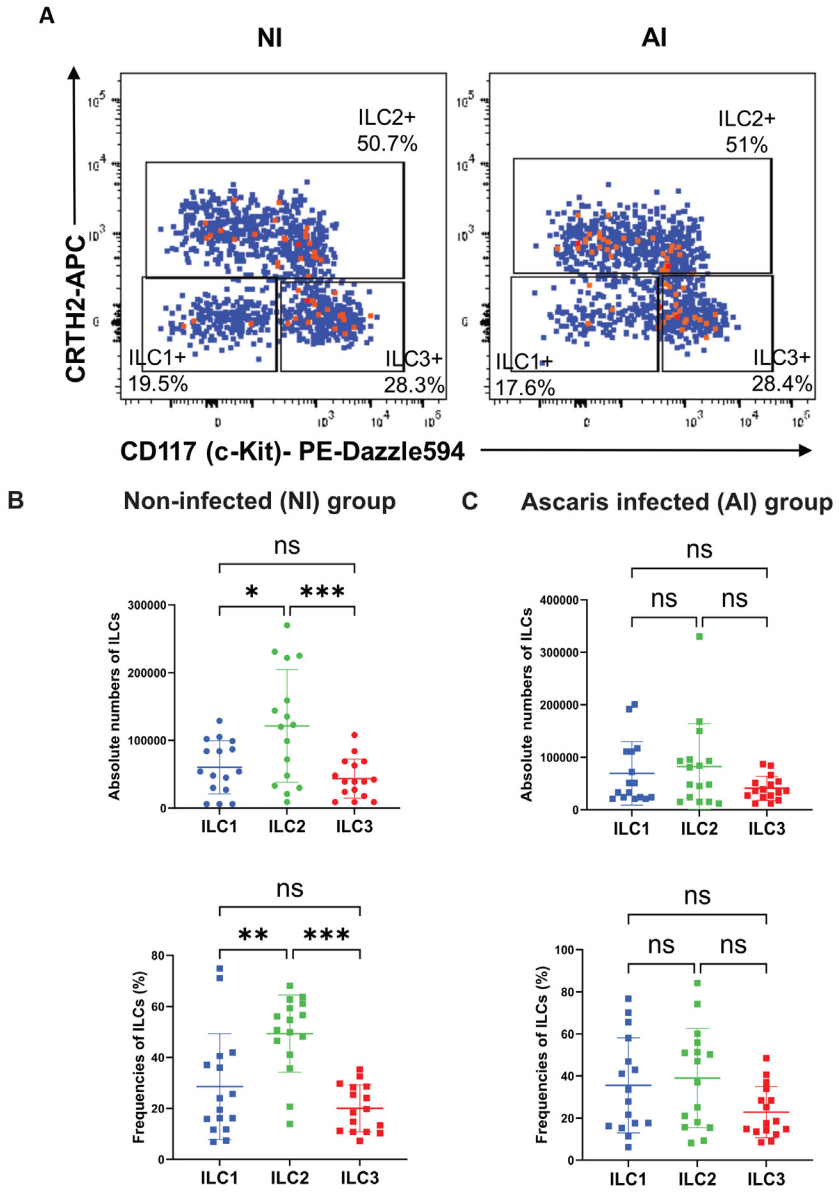

FIGURE 1
ILCs distribution between NI and AI groups. **(A)** Representative plot of ILC subsets according to infection status. Distribution of frequencies and absolute numbers of ILC subsets (ILC1, ILC2, ILC3) in **(B)** non-infected and **(C)** Ascaris infected. Comparisons were made using Friedman and Dunn's multiple comparison test. * p<0.05. **p<0.01, *** p<0.001. ns, non-significant.

of variables was examined using visual (histogram and probability graphs) and analytical methods (Kolmogrov-Smirnov/Shapiro-Wilk tests). Descriptive statistics were calculated by using the mean and standard deviation for normally distributed variables and the median and range for non-normally distributed variables.

Groups were compared with each other in terms of total ILCs and ILCs subsets and activated cells by marker expression. Parametric and non-parametric tests were used according to the Gaussian distribution of the variables. The bivariate tests included Pearson's Chi-square to compare categorical variables and the Mann-Whitney or Kruskal Wallis test to compare continuous variables between two or more groups, respectively.

Parametric statistics was applied for most analysis with data derived from Olink since measurements are expressed as NPX values, which are derived from a log2 transformation of the protein concentration values. This transformation helps to handle a wide range of protein concentrations and can normalize for variations in the assay. T-tests were used for two-group comparisons of proteins (NPX values) between AI and NI subjects. Heatmap was generated using Z-score data as input (which normalized the protein expression across all samples), clustering applied to columns (proteins), and custom colors assigned to the 'Infected' and 'Non-Infected' status. Euclidean distance metric was used for clustering the proteins. Protein enrichment pathway analysis was done with

Enrichr web-server. Nine upregulated proteins were input. Gene Ontology Biological Process 2023 pathways were selected. The top 10 significant pathways were selected according to the highest adjusted p-value and the representation corresponds to -log10 of these values (39).

For correlational analysis of relative counts of ILC2-related variables with Olink proteins, relative cell counts were first log-transformed, and then, Pearson correlation coefficients were obtained. P and adjusted p-values (False Discovery Rate, FDR) are presented. In addition, due to their highly skewed distribution, correlations of egg and specific-antibody data with other variables were determined by Spearman method.

Finally, we explored the importance of different immune variables (selected from previous mentioned analysis) on determining active infection using a random forest model. Corrplot, ggplot2 and pheatmap, random forest, Enhanced volcano packages were used for plotting with R software (version 4.3.0).

3 Results

The mean age of the subjects was 52 years proportionally distributed in terms of biological sex in both groups. The median egg burden was 359 eggs per gram (e.p.g). No cases of anemia were detected in the study population. There was not significant difference regarding concentration of total IgE, the strength of the antibody response IgG or IgE to the body-extract of Ascaris or the ABA-1 antigen. The frequency of IgG response to Ascaris body extract was lower in the AI group compared to NI (68.8% vs. 75%). In contrast, IgE response was significantly higher in AI group compared to NI (87% vs. 56%; $p<0.05$). Likewise, the frequencies of anti-ABA1 IgG (37.5% vs 31.3%) and anti-ABA1 IgE (31% vs 44%) followed the same trend but there were no significant differences between the groups (Table 1).

TABLE 1 Clinical features of the study population.

Variable	Non-Infected (n=16)	Ascaris infected (n=16)	p-value
Age (mean ± SD)	52.06 ± 16.5	52.1 ± 16.16	0.99
Female (%)	60%	50%	0.57
Egg count per gram [median (range)]	N/A	359 (1230)	N/A
Total IgE (ng/mL) [median (range)]	52.09 (12.14 – 1205.17)	122.19 (20.82 – 1187.21)	0.16
Anti-Ascaris sIgG (%)	75	68.8	0.69
OD Anti-Ascaris sIgG [median (range)]	0.85 (0.25 – 0.94)	0.76 (0.45 – 0.97)	0.49
Anti-ABA-1 sIgG (%)	37.5	31.3	0.71
OD Anti-ABA-1 sIgG [median (range)]	0.58 (0.37 – 1.14)	0.61 (0.18 – 0.87)	0.93
Anti-Ascaris sIgE (%)	56	87	0.049*
OD Anti-Ascaris sIgE (median, range)	0.13 (0.06 – 0.33)	0.16 (0.08 – 0.23)	0.25
Anti-ABA-1 sIgE (%)	31	44	0.47
OD Anti-ABA-1 sIgE (median, range)	0.10 (0.04 – 0.25)	0.11 (0.04 – 0.30)	0.54

IQR, Interquartil range; OD, Optical density; N/A, Non apply; SD, Standard deviation; sIgE, specific IgE, sIgG, specific IgG.*, Significantly different. Mann-Whitney test was used for 2-groups comparison of continuous variables.

3.1 Higher numbers and frequencies of circulating ILC2s are associated with ABA-1 IgE antibody response

Circulating total ILCs were defined as $Lin^{-}CD45^{+}CD127^{+}CD161^{+}$ (Supplementary Figure 1A); whereas c-kit and CRTH2 markers, were used to define ILC subpopulations (ILC1: c-$kit^{-}CRTH2^{-}$, ILC2: c-$kit^{-}CRTH2^{+}$, and ILC3: c-$kit^{+}CRTH2^{-}$) (Figure 1A). Although in NI subjects, ILC2s were the most frequent (49.3%) among the three ILC subpopulations (ILC1: 28.5%; ILC3: 20%) (Figure 1B), we did not observe significant differences in the relative frequencies or numbers of ILCs among AI individuals (ILC1: 35.6%; ILC2: 39%; ILC3: 22.8%; Figure 1C). No significant differences were found in relative or absolute numbers of total ILCs, ILC1, ILC2 or ILC3 between NI and AI subjects. However, we observed a bimodal distribution of ILC2 in AI individuals. Examining different variables, this behavior is likely explained by variations in the IgE response to ABA-1 among infected individuals for the relative and absolute numbers of ILC2. We observed that positive responders in this group had significantly higher frequencies of ILC2 ($p < 0.05$) (Figures 2A, B).

3.2 Frequencies of ILC2 expressing activation markers cells are higher in active Ascaris infection and correlated with the egg burden

Surface markers associated with activation and type 2 response (CD25+, CD69+ and TSLPR+) in ILC2 frequencies were also analyzed. In Figure 3A, a representative plot of gated CD25+, CD69+ and TSLPR+ ILC2 cells for FMO control as well as infected and NI groups are shown. The frequencies CD25+, CD69 + and TSLPR+ ILC2s were significantly higher in AI compared to the NI controls (Figure 3B). Additionally, Ascaris's egg burden in feces had a positive correlation ($r=0.67$; $p=0.005$) with the number of CD69+ ILC2 (Figure 3C).

3.3 Exploratory analysis of plasma proteins correlated with circulating ILC2s

A correlational analysis of blood ILC2s with circulating proteins in plasma samples, measured through the PEA method, was

10.3389/fimmu.2024.1459961

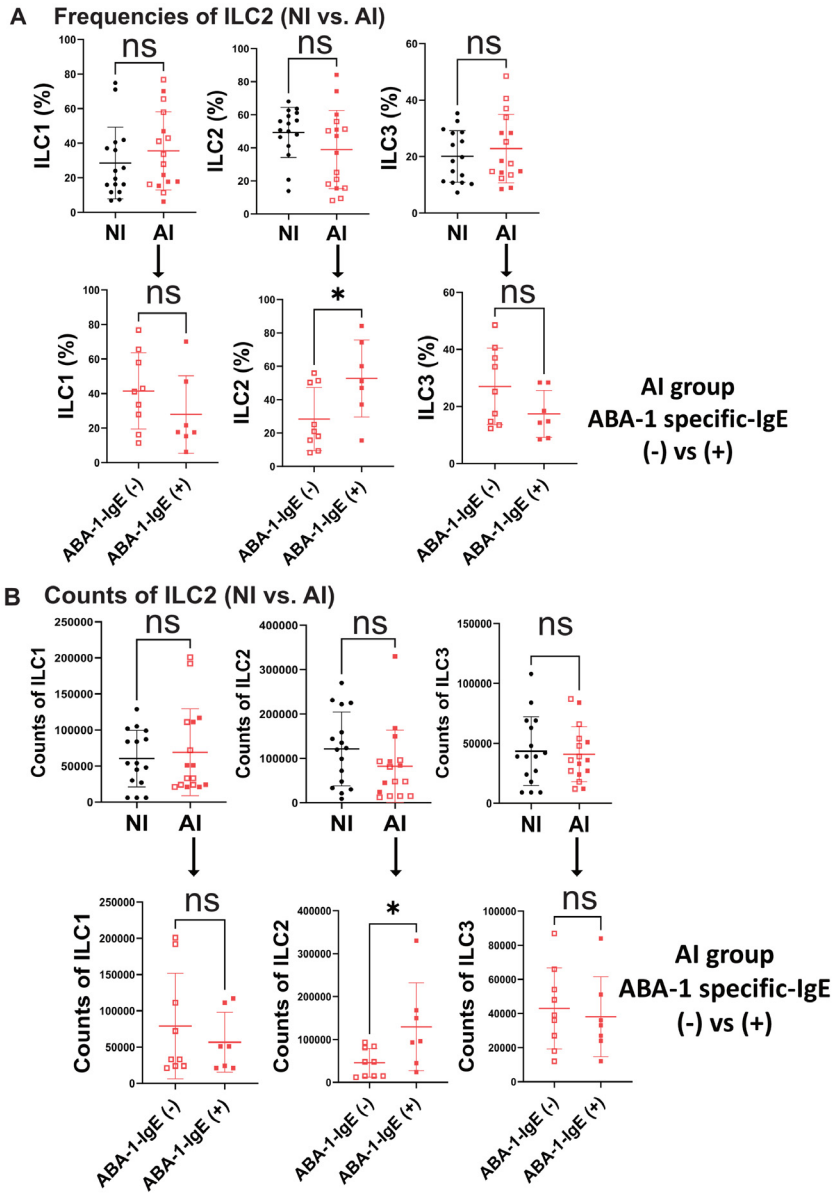

FIGURE 2
Higher ILC2 Higher frequencies and numbers are associated with anti-ABA-1 IgE sensitization status. Frequencies **(A)** and absolute numbers **(B)** of three mainly ILC subsets (ILC1, ILC2, ILC3) according to Ascaris infection status. Categorization by ABA-1 IgE sensitization is associated with higher ILC2 in the AI group. Comparisons were made using Mann–Whitney according to infection and unpaired T-test according sensitization. * p<0.05. ns, non-significant.

performed. Before multiple testing correction, there were 50 products associated with either log-transformed % total, CD25+, CD69+ or TSLPR+ ILC2 cells (Supplementary Figure 2). Negatively correlations of %ILC2 with granulocytes products and type 2 response proteins like myeloperoxidase (MPO), vascular endothelial growth factor A (VEGFA), amphiregulin (AREG), and chitinase-3 like-protein-1(CHI3L1) were found. Also, %CD25 + ILC2 were negatively correlated with chemokines like CCL3, CCL4, CCL19 and inflammatory cytokines like TNF and IFNγ. On the other hand, TPSAB1 and GP6 were positively correlated with CD25+ and CD69+ ILC2. However, after multiple testing correction (FDR < 0.1), only MMP1 (r=-0.62; p=0.003), VEGFA (r=-0.71; 0.0003) and MPO (r=-0.64; p=0.002) were significantly correlated with %ILC2.

3.4 Protein expression profile in active Ascaris infection and involved pathways

Eleven proteins that are differentially expressed in Ascaris infection were identified by targeted proteomics performed on plasma samples (Figures 4A, B). Tryptase alpha/beta 1 (TPSAB1)

10.3389/fimmu.2024.1459961

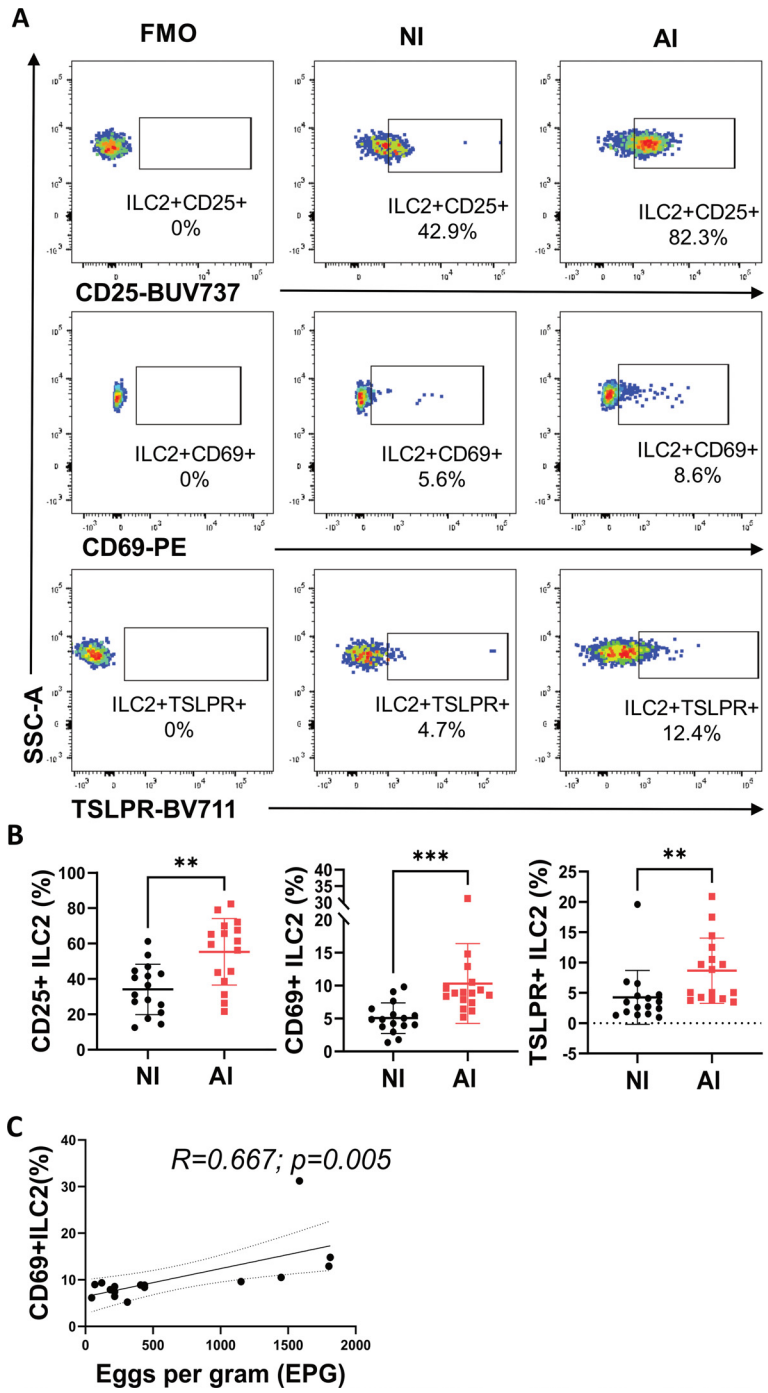

FIGURE 3
ILC2 expressing activation markers frequencies are associated with Ascaris infection and correlate with the egg burden. **(A)** Representative dot plot of the frequency of activation markers in ILC2s compared between non-infected (NI) and infected (AI) subjects. **(B)** Frequencies of different activation markers in ILC2s according to Ascaris infection status **(C)** Correlation plot between CD69+ILC2 and egg burden. Comparisons were made using the Mann–Whitney test and correlation analysis corresponds to Spearman correlation coefficient (r). ** p<0.01, *** p<0.001.

from mast cells, glycoprotein 6 (GP-6) which induces activation and aggregation of platelets, and junctional adhesion molecule A (JAM-A), involved in epithelium stability, were significantly high in infected individuals. In addition, the neutrophil (CXCL1) and granulocytes' (CXCL6) chemotactic proteins, AXIN1 a negative regulator of the wingless-type MMTV integration site family member 1 (WNT) signaling pathway, matrixin 1 (MMP-1) associated to tissue remodeling, eukaryotic translation initiation factor 4 gamma 1 (EIF4G1) and STAMBP, Signal Transducing Adaptor Molecule binding protein were significantly higher

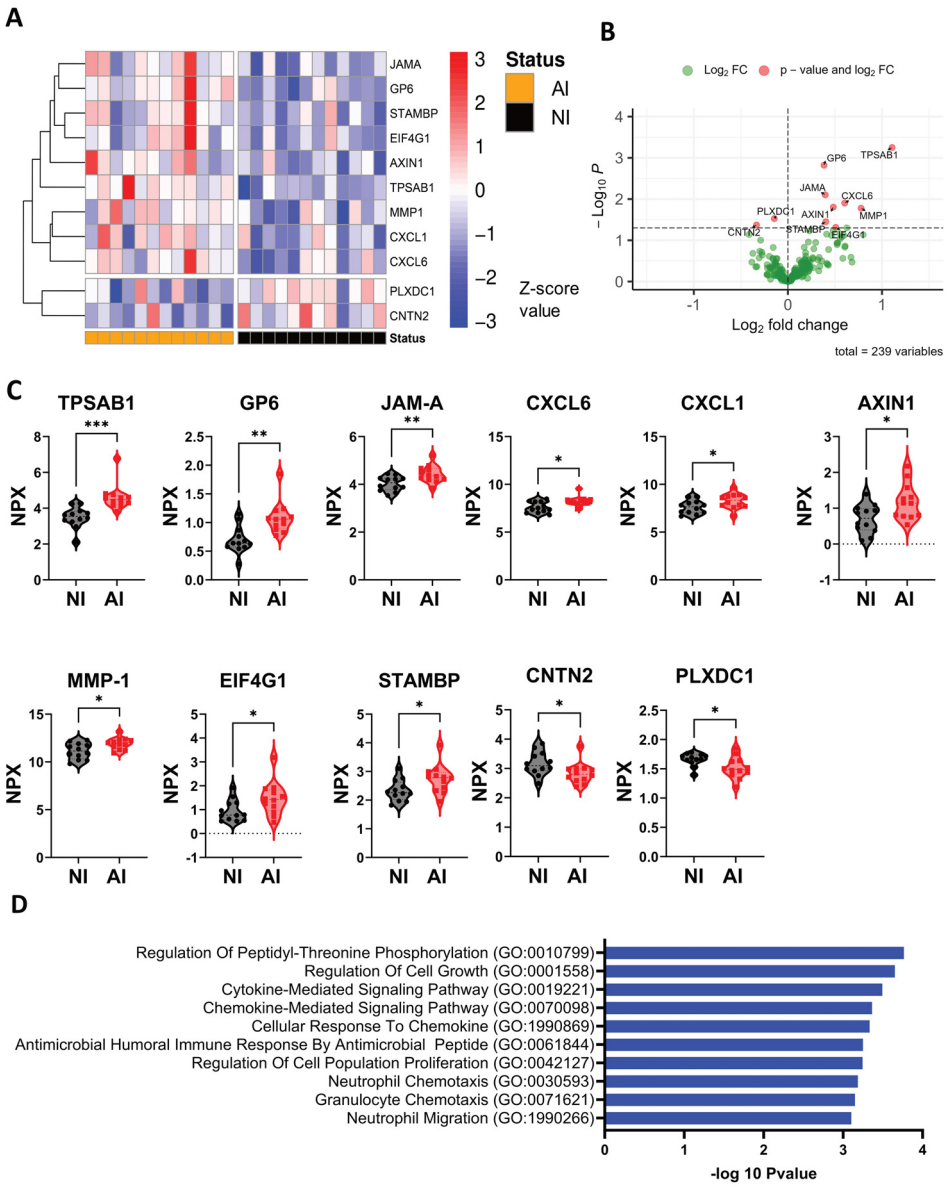

FIGURE 4
Protein expression profile associated with Ascaris infection and pathways involved during the infection. **(A, B)** The heatmap and volcano plot depicts significant differential protein expression profiles in the NI and AI groups. **(C)** Differential expressed plasma proteins are represented in violin plots: TPSAB1, GP-6, JAM-A, CXCL1, CXCL6, AXIN1, MMP-1, EIF4G1, STAMBP,CNTN2, and PLXDC1; **(D)** Ratio of 10 significant biological processes associated with high expressed protein profile. Comparisons were made using unpaired T-test * p<0.05, ** p<0.01, *** p<0.001.

expressed in plasma samples of AI compared to NI subjects (Figure 4C). In contrast, contactin-2 (CNTN2) a cell adhesion molecule, and plexin domain containing 1(PLXDC1) involved in angiogenesis and endothelial morphogenesis were significantly lower expressed in AI individuals (Figure 4C). Highly expressed proteins were included in the pathway analysis, which showed that most of them are involved in granulocyte chemotaxis and migration, regulation of peptidyl-threonine phosphorylation and cell growth, and disassembly of the extracellular matrix and cellular components (Figure 4D). In most patients, the alarmins, TSLP and IL-33, as well as Th2 cytokines (IL-4, IL-5 and IL-13) could not be detected in plasma samples. Other proteins related to inflammation, type 1 and type 2 responses and immune regulation pathways did not show any significant differences in regard to infection status (Supplementary Figure 3).

3.5 Tryptase AB1 levels are associated to ILC2 expressing activation markers, egg burden and IgE response to Ascaris

Plasma proteins significantly enhanced in active infection were correlated with antibody response intensity, egg burden and frequency of ILC2s and subsets of activation. Remarkably, we found that TPSAB1 levels were positively correlated with frequencies of ILC2 expressing activation markers ILC2 (CD25+,

CD69+, TSLPR+), egg counts and intensity of IgE antibody response to Ascaris (r>0.5; p<0.05) (Figures 5A, B). IL-10 levels showed a negative correlation with ILC2 frequencies (rho=-0.62; p<0.05) (Supplementary Figure 4A).

As an exploratory approach, we also used a random forest model to determine the importance of these variables on predicting *A. lumbricoides* infection. Notably, TPSAB1 values and different phenotypes of ILC2 expressing activation markers had the best performance to predict infection (Supplementary Figure 4B). ROC curve analysis found strong predictive performance for TPSAB1 (AUC: 0.95), CD25+ ILC2(AUC: 0.85), and CD69+ ILC2 (AUC: 0.88) over *A. lumbricoides* infection (Figure 5C).

4 Discussion

As a bridge between the innate and adaptive immune T2 response, ILC2s represent an essential cell subset in the immune response against helminths (40). Several studies, in animal models and humans, have evaluated the role of these cells in the pathophysiology of helminthiasis, however, findings differ among the different infecting helminth species. As a novelty, this study explores the relationship of ILC2 numbers with *A. lumbricoides* infection, finding that ILC2 expressing activation markers are more frequent in infected subjects. Also, we report for the first time the overexpression of three activation markers in ILC2 from humans with ascariasis and the significant correlation between this activation marker expression with egg burden. Finally, using a targeting proteomic approach, we identified different proteins associated with Ascaris infection and one particular mast cell product, TPSAB1, that also correlated with %CD25, %CD69 and % TSLPR+ ILC2s frequencies and, Ascaris IgE levels and egg burden.

To our knowledge, the relationship between *A. lumbricoides* active infection in humans and ILC2 frequencies has not been reported previously. Although Darboe et al. (41) studied the association between specific IgG antibodies against *Ascaris* spp. extract with the frequency of ILC2, this is not an informative measure for active infection, but mostly about exposure that may be almost universal in highly endemic populations. In fact, in our study sample, we observed a high frequency of IgG seropositive response against Ascaris extract or ABA-1 in both, actively infected and non-infected subjects. As we have previously published, in this rural town of Colombia, a prevalence of 63% of ascariasis have been found. Then, it is expected that most individuals are exposed during lifetime to this parasite (7, 29). In our study, ILC2 numbers and frequencies were not different between infected and non-infected subjects; however, we did observe that ILC2s were more abundant

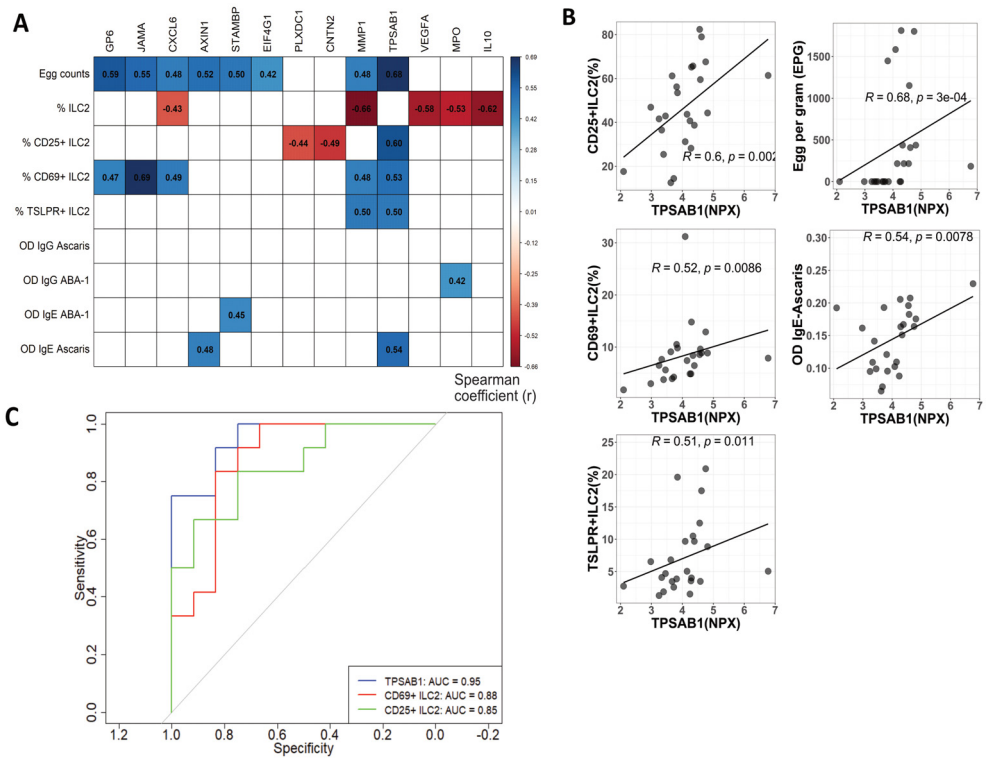

FIGURE 5
TPSAB1 is correlated to ILC2s expressing activation markers frequencies, egg burden and Ascaris IgE sensitization. **(A)** Correlation values are depicted between NPX of protein expression, humoral parameters, ILC2 and ILC2s expressing activation markers frequencies. Only significant correlations are shown as colored squares. Spearman coefficient (r) values from −0.66 to 0.69 on a red to-blue scale, respectively. **(B)** Plots depicting the positive correlation between TPSAB1 NPX values with frequencies of ILC2s expressing activation markers (CD69+, CD25+ and TSLPR+), egg counts and Ascaris IgE levels **(C)** Receiver operating characteristic (ROC) curves and area under the curve (AUC) obtained from logistic regression models to predict the Ascaris infection. Blue, red and green line corresponding to TPSAB1, CD69+ILC2 and CD25+ILC2, respectively.

in relation to ILC1 and ILC3 in the NI controls but did not in the infected group. Similar to other reports (41), we found ILC2s represented the 50% of ILCs in NI group, however, this significant difference in the distribution disappears in the infected subjects. Comparison of ILC2s in regard to helminth infection have yielded different results. IL-13-producing c-Kit+ ILCs were described as higher in the peripheral blood of adult individuals with filarial infection (20). In contrast, Nausch et al. reported a decrease of the ILC2 population in children infected with *Schistosoma haematobium*, which could be restored and become activated (reflected by the overexpression of TSLP) after anti-helminth treatment (19). Also, Tamadaho et al. found that non-infected subjects had higher number of ILC2 in comparison with patients with active *W. bancrofti* infection (lymphatic filariasis), and this distribution changed after pathogen clearance using deworming treatment (42). Our results are similar to the last two studies. During active infection, it is possible that cells migrate to tissue due to the production of alarmins and chemokines by epithelial cells in the gut, which could result in a reduction of circulating cell numbers. Notably, blood levels of granulocytes and ILC2 mediators (MPO and VEGFA) (43), are strongly and negatively correlated with the relative counts of ILC2 in the blood. This suggests that during infection, ILC2 cells may become activated and migrate to the infected tissues.

Even though, ILC2 tends to decrease in infected individuals, two groups could be identified in this population, one with high ILC2 numbers and the other one with low numbers. IgE sensitization to ABA-1 seems to be associated with the increase of ILC2s in the high group. IgE sensitization against ABA-1 has been reported as a marker of resistance to infection (44) and a factor associated with asthma and its severity (7, 45). In this context, it can be thought that the subjects who have a higher frequency of ILC2 tend to have a stronger T2 response to helminth infection and, similarly, higher ILC2 may contribute to the worsening of allergic diseases (46).

The activation markers CD25, CD69, and TSLPR were significantly more prevalent on ILC2 cells in AI individuals, reinforcing the association between ILC2 activation and active Ascaris infection. Several studies support that upon stimulation with alarmins and cytokines, ILC2 activates and expresses CD25, CD69 or TSLPR. In spite we did not confirm that expression of these surface markers is accompanied by type 2 cytokine production, there are studies that support that these phenotypes are related to enhanced activity in ILC2s. CD25+ ILCs and ILC2s produced higher amounts of type 2 cytokines (47, 48). Also, BAL fluid-derived ILC2s exhibited increased expression of IL-13, AHR, interferon regulatory factor 4 (IRF4), IL-33 receptor ST2 (IL1RL1), and several activation markers, including CD69 (49). Finally, ILC2s from individuals with eosinophilic asthma demonstrated increased TSLPR expression and cytokine release of IL-5 and IL-13 (50).

Moreover, molecules mainly related to granulocyte chemotaxis, tissue remodeling and cell growth were upregulated in AI individuals. Similar to our results, MMP-1, PLXDC1 and GP6 signaling pathways appear to be dysregulated after the stimulation of hepatic stellate cells with two peptides from Sm16, a product from *S. mansoni* (51). Additionally, Ascaris infection also increased circulating levels of JAM-A, a tight junction molecule that regulates the permeability of the epithelium (52), suggesting a possible increase in epithelial permeability due to the loss of this protein from the barrier cells to the circulation. As observed in our findings regarding CXCL6 and CXCL1, chemokines associated with granulocyte migration, like CXCL5, have been reported to be increased in serum from subjects infected with *A. lumbricoides* (53). Granulocytes play a fundamental role in the immune response against pathogens, and in the case of helminths, eosinophils are characterized by leading the fight against and expulsion of these parasites. Interestingly, neutrophil migration pathways are upregulated in subjects with ascariasis. The role of these cells in the defense against this helminth has been scarcely explored in humans. An early intestinal neutrophilic response has been found in a model of mice infected with *Ascaris* spp (54). and there is evidence that neutrophils can destroy larvae of *Ascaris suum* (55). Interestingly, a preliminary study in subjects living in Santa Catalina found lower relative numbers of neutrophils in individuals with ascariasis compared to sex- and age- matched, non-infected control subjects (56), which may be related to an increased migration to tissues where parasites reside (i.e. the gut or the lung).

TPSAB1 is an enzyme associated with mast cell regulation and function. Tryptase plays a role in immune responses and is involved in various physiological and pathological processes, including inflammation, mast cells disorders and allergic reactions (57, 58). Our findings regarding higher TPSAB1 levels indicates that mast cells may be one of the initial and essential sensors during Ascaris infection, which may indirectly activate ILC2s and boost the T2 response. Similar to our results, Ascaris-infected pigs had significantly increased expression of mast cell tryptase, TPSAB1 together with several T2-related molecules (59). These "feed-forward loop" of mast cell activation and T2 response have been supported in airway epithelium in asthma, where the T2 inflammation is associated with the expression of a specific set of mast cell genes (60). Additionally, mast cells seem to be critical in the induction of ILC2 and helminth expulsion as a main source of IL-33 (61). Interaction of mast cells and ILC2 remains to be further studied, as well as the functional role of these cells in infection and resistance to parasites. Our finding of an increase of TPSAB1 has also been reported in eosinophilic chronic obstructive pulmonary disease (62), suggesting that an interaction between ILC2, mast cells and eosinophilic inflammation could be present in ascariasis.

Additional support to this T2 boost is the negative correlation of IL-10 levels with ILC2 frequency. It has been demonstrated that ILC2s can switched to IL-10 regulatory innate lymphoid cells under specific conditions or cytokine milieu (63, 64), so it would be interesting to understand this negative correlation in helminthiasis as compared to allergen immunotherapy where the high dose of allergen could lead to another mechanism of immune regulation.

Several limitations must be acknowledged in this study. The sample size is small, which reduces the power to detect associations. The activation status of ILC2s was not confirmed by measuring type 2 cytokine production, mainly due to limitations in the amount of biological material available. Additionally, it is important to note that under cell culture conditions, cells might develop phenotypes

that are induced and do not accurately represent the *in vivo* circulating status of ILC2 cells, which was the main objective of this study. Other surface markers, such as ST2, IL17RB, KLRG1, ICOS, CCR6, and MHCII, as well as transcription factors like GATA3, were not evaluated in the ILC2 subset. Finally, despite its high sensitivity, PEA could not detect type 2 cytokines and alarmins in circulation, which limits our ability to draw conclusions about the systemic type 2 response and its correlation with circulating ILCs.

In summary, this study demonstrates the increase of circulating ILC2 with an activated phenotype and higher TPSAB1 levels associated with *A. lumbricoides* infection, supporting the role of ILC2 in a network of interacting with other cells through increased cytokines and chemokines in the boosting of the T2 immune response and helminth immunity.

Data availability statement

The raw data supporting the conclusions of this article will be made available by the authors, without undue reservation.

Ethics statement

The studies involving humans were approved by University of Cartagena Ethics Committee (Minutes #12811-2019). The studies were conducted in accordance with the local legislation and institutional requirements. The participants provided their written informed consent to participate in this study.

Author contributions

J-FL: Formal analysis, Investigation, Methodology, Visualization, Writing – original draft, Writing – review & editing, Project administration. JZ: Conceptualization, Funding acquisition, Investigation, Methodology, Project administration, Supervision, Writing – original draft, Writing – review & editing, Formal analysis. PS: Investigation, Methodology, Writing – review & editing. AL: Investigation, Writing – review & editing. LB: Investigation, Methodology, Writing – review & editing. AH: Investigation, Methodology, Writing – review & editing, Validation. JA-G: Writing – review & editing, Investigation. HB: Formal analysis, Writing – review & editing, Visualization. CA: Investigation, Resources, Writing – review & editing, Conceptualization. WV: Formal analysis, Methodology, Resources, Supervision, Validation, Writing – review & editing. LC: Conceptualization, Funding acquisition, Investigation, Project administration, Resources, Supervision, Writing – review & editing. MA: Conceptualization, Formal analysis, Funding acquisition, Investigation, Project administration, Resources, Supervision, Writing – review & editing, Writing – original draft.

Funding

The author(s) declare financial support was received for the research, authorship, and/or publication of this article. This study was funded by the Colombian Ministry of Science (Minciencias) in the framework of the grant numbers BPIN2020000100405 -BPIN2020000100364 (PI: LC) and 699-2017 (PI: JZ) and by The Latin-American-Swiss Center (CLS-HSG) from University of St. Gallen under the grant Agreement No. SMG1929 (PI: MA) and the Swiss National Science Foundation No. 310030-201053/320030-159870/310030_201053/1(PI: MA).

Acknowledgments

We thank all the individuals who voluntarily participated in this study, the Colombian Ministry of Science, University of Cartagena, University of Zurich (UZH) and University of St. Gallen for financing this project.

Conflict of interest

The authors declare that the research was conducted in the absence of any commercial or financial relationships that could be construed as a potential conflict of interest.

The author(s) declared that they were an editorial board member of Frontiers, at the time of submission. This had no impact on the peer review process and the final decision.

Publisher's note

Supplementary material

The Supplementary Material for this article can be found online at: https://www.frontiersin.org/articles/10.3389/fimmu.2024.1459961/full#supplementary-material

References

1. Holland C, Sepidarkish M, Deslyper G, Abdollahi A, Valizadeh S, Mollalo A, et al. Global prevalence of Ascaris infection in humans (2010–2021): a systematic review and meta-analysis. *Infect Dis Poverty*. (2022) 11:113. doi: 10.1186/s40249-022-01038-z

2. Zakzuk J, Acevedo N, Cifuentes L, Bornacelly A, Sanchez J, Ahumada V, et al. Early life IgE responses in children living in the tropics: a prospective analysis. *Pediatr Allergy Immunol*. (2013) 24:788–97. doi: 10.1111/pai.2013.24.issue-8

3. Hawlader MD, Ma E, Noguchi E, Itoh M, Arifeen SE, Persson LA, et al. Ascaris lumbricoids infection as a risk factor for asthma and atopy in rural Bangladeshi children. *Trop Med Health*. (2014) 42:77–85. doi: 10.2149/tmh.2013-19

4. Alcantara-Neves NM, Badaro SJ, dos Santos MC, Pontes-de-Carvalho L, Barreto ML. The presence of serum anti-Ascaris lumbricoides IgE antibodies and of Trichuris trichiura infection are risk factors for wheezing and/or atopy in preschool-aged Brazilian children. *Respir Res*. (2010) 11:114. doi: 10.1186/1465-9921-11-114

5. Moncayo AL, Vaca M, Oviedo G, Workman LJ, Chico ME, Platts-Mills TA, et al. Effects of geohelminth infection and age on the associations between allergen-specific IgE, skin test reactivity and wheeze: a case-control study. *Clin Exp Allergy*. (2013) 43:60–72. doi: 10.1111/cea.2012.43.issue-1

6. Ahumada V, Garcia E, Dennis R, Rojas MX, Rondon MA, Perez A, et al. IgE responses to Ascaris and mite tropomyosins are risk factors for asthma. *Clin Exp Allergy*. (2015) 45:1189–200. doi: 10.1111/cea.2015.45.issue-7

7. Zakzuk J, Casadiego S, Mercado A, Alvis-Guzman N, Caraballo L. Ascaris lumbricoides infection induces both, reduction and increase of asthma symptoms in a rural community. *Acta Trop*. (2018) 187:1–4. doi: 10.1016/j.actatropica.2018.07.016

8. Caraballo L, Acevedo N, Buendía E. Human ascariasis increases the allergic response and allergic symptoms. *Curr Trop Med Rep*. (2015) 2:224–32. doi: 10.1007/s40475-015-0058-7

9. Loke P, Lee SC, Oyesola OO. Effects of helminths on the human immune response and the microbiome. *Mucosal Immunol*. (2022) 15:1224–33. doi: 10.1038/s41385-022-00532-9

10. Vivier E, Artis D, Colonna M, Diefenbach A, Di Santo JP, Eberl G, et al. Innate lymphoid cells: 10 years on. *Cell*. (2018) 174:1054–66. doi: 10.1016/j.cell.2018.07.017

11. Hung LY, Tanaka Y, Herbine K, Pastore C, Singh B, Ferguson A, et al. Cellular context of IL-33 expression dictates impact on anti-helminth immunity. *Sci Immunol*. (2020) 5. doi: 10.1126/sciimmunol.abc6259

12. Lok LSC, Walker JA, Jolin HE, Scanlon ST, Ishii M, Fallon PG, et al. Group 2 innate lymphoid cells exhibit tissue-specific dynamic behaviour during type 2 immune responses. *Front Immunol*. (2021) 12:711907. doi: 10.3389/fimmu.2021.711907

13. Löser S, Smith KA, Maizels RM. Innate lymphoid cells in helminth infections-obligatory or accessory? *Front Immunol*. (2019) 10:620. doi: 10.3389/fimmu.2019.00620

14. Bartemes KR, Kita H. Roles of innate lymphoid cells (ILCs) in allergic diseases: The 10-year anniversary for ILC2s. *J Allergy Clin Immunol*. (2021) 147:1531–47. doi: 10.1016/j.jaci.2021.03.015

15. Neill DR, Wong SH, Bellosi A, Flynn RJ, Daly M, Langford TK, et al. Nuocytes represent a new innate effector leukocyte that mediates type-2 immunity. *Nature*. (2010) 464:1367–70. doi: 10.1038/nature08900

16. Price AE, Liang HE, Sullivan BM, Reinhardt RL, Eisley CJ, Erle DJ, et al. Systemically dispersed innate IL-13-expressing cells in type 2 immunity. *Proc Natl Acad Sci USA*. (2010) 107:11489–94. doi: 10.1073/pnas.1003988107

17. Pelly VS, Kannan Y, Coomes SM, Entwistle LJ, Ruckerl D, Seddon B, et al. IL-4-producing ILC2s are required for the differentiation of T(H)2 cells following Heligmosomoides polygyrus infection. *Mucosal Immunol*. (2016) 9:1407–17. doi: 10.1038/mi.2016.4

18. Fallon PG, Ballantyne SJ, Mangan NE, Barlow JL, Dasvarma A, Hewett DR, et al. Identification of an interleukin (IL)-25-dependent cell population that provides IL-4, IL-5, and IL-13 at the onset of helminth expulsion. *J Exp Med*. (2006) 203:1105–16. doi: 10.1084/jem.20051615

19. Nausch N, Appleby LJ, Sparks AM, Midzi N, Mduluza T, Mutapi F. Group 2 innate lymphoid cell proportions are diminished in young helminth infected children and restored by curative anti-helminthic treatment. *PloS Negl Trop Dis*. (2015) 9:e0003627. doi: 10.1371/journal.pntd.0003627

20. Boyd A, Ribeiro JM, Nutman TB. Human CD117 (cKit)+ innate lymphoid cells have a discrete transcriptional profile at homeostasis and are expanded during filarial infection. *PloS One*. (2014) 9:e108649. doi: 10.1371/journal.pone.0108649

21. Munneke JM, Bjorklund AT, Mjosberg JM, Garming-Legert K, Bernink JH, Blom B, et al. Activated innate lymphoid cells are associated with a reduced susceptibility to graft-versus-host disease. *Blood*. (2014) 124:812–21. doi: 10.1182/blood-2013-11-536888

22. Salimi M, Wang R, Yao X, Li X, Wang X, Hu Y, et al. Activated innate lymphoid cell populations accumulate in human tumour tissues. *BMC Cancer*. (2018) 18:341. doi: 10.1186/s12885-018-4262-4

23. Ishimori A, Harada N, Chiba A, Harada S, Matsuno K, Makino F, et al. Circulating activated innate lymphoid cells and mucosal-associated invariant T cells are associated with airflow limitation in patients with asthma. *Allergol Int*. (2017) 66:302–9. doi: 10.1016/j.alit.2016.07.005

24. Li BWS, Stadhouders R, de Bruijn MJW, Lukkes M, Beerens D, Brem MD, et al. Group 2 innate lymphoid cells exhibit a dynamic phenotype in allergic airway inflammation. *Front Immunol*. (2017) 8:1684. doi: 10.3389/fimmu.2017.01684

25. Roediger B, Kyle R, Tay SS, Mitchell AJ, Bolton HA, Guy TV, et al. IL-2 is a critical regulator of group 2 innate lymphoid cell function during pulmonary inflammation. *J Allergy Clin Immunol*. (2015) 136:1653–63 e7. doi: 10.1016/j.jaci.2015.03.043

26. Camelo A, Rosignoli G, Ohne Y, Stewart RA, Overed-Sayer C, Sleeman MA, et al. IL-33, IL-25, and TSLP induce a distinct phenotypic and activation profile in human type 2 innate lymphoid cells. *Blood Adv*. (2017) 1:577–89. doi: 10.1182/bloodadvances.2016002352

27. Toki S, Goleniewska K, Zhang J, Zhou W, Newcomb DC, Zhou B, et al. TSLP and IL-33 reciprocally promote each other's lung protein expression and ILC2 receptor expression to enhance innate type-2 airway inflammation. *Allergy*. (2020) 75:1606–17. doi: 10.1111/all.14196

28. Nausch N, Mutapi F. Group 2 ILCs: A way of enhancing immune protection against human helminths? *Parasite Immunol*. (2018) 40. doi: 10.1111/pim.12450

29. Zakzuk J, Casadiego S, Mercado A, Peñaranda D, Alvis Guzman N, Caraballo L. PIN58 PREVALENCE OF PARASITE INTESTINAL INFECTIONS IN A RURAL COMMUNITY OF THE CARIBBEAN NORTH OF COLOMBIA. *Value Health*. (2019) 22:S204. doi: 10.1016/j.jval.2019.04.928

30. Mbong Ngwese M, Prince Manouana G, Nguema Moure PA, Ramharter M, Esen M, Adegnika AA. Diagnostic techniques of soil-transmitted helminths: impact on control measures. *Trop Med Infect Dis*. (2020) 5:93. doi: 10.3390/tropicalmed5020093

31. Tarafder MR, Carabin H, Joseph L, Balolong E Jr., Olveda R, McGarvey ST. Estimating the sensitivity and specificity of Kato-Katz stool examination technique for detection of hookworms, Ascaris lumbricoides and Trichuris trichiura infections in humans in the absence of a 'gold standard'. *Int J Parasitol*. (2010) 40:399–404. doi: 10.1016/j.ijpara.2009.09.003

32. Ahumada V, Manotas M, Zakzuk J, Aglas L, Coronado S, Briza P, et al. Identification and physicochemical characterization of a new allergen from ascaris lumbricoides. *Int J Mol Sci*. (2020) 21:9761. doi: 10.3390/ijms21249761

33. Acevedo N, Sanchez J, Erler A, Mercado D, Briza P, Kennedy M, et al. IgE cross-reactivity between Ascaris and domestic mite allergens: the role of tropomyosin and the nematode polyprotein ABA-1. *Allergy*. (2009) 64:1635–43. doi: 10.1111/j.1398-9995.2009.02084.x

34. Starrenburg ME, Bel Imam M, Lopez JF, Buergi L, Nguyen NT, Nouwen AEM, et al. Dupilumab treatment decreases MBC2s, correlating with reduced IgE levels in pediatric atopic dermatitis. *J Allergy Clin Immunol*. (2024). doi: 10.1016/j.jaci.2024.06.023

35. Acevedo N, Mercado D, Vergara C, Sanchez J, Kennedy MW, Jimenez S, et al. Association between total immunoglobulin E and antibody responses to naturally acquired Ascaris lumbricoides infection and polymorphisms of immune system-related LIG4, TNFSF13B and IRS2 genes. *Clin Exp Immunol*. (2009) 157:282–90. doi: 10.1111/j.1365-2249.2009.03948.x

36. Miljkovic D, Bassiouni A, Cooksley C, Ou J, Hauben E, Wormald PJ, et al. Association between group 2 innate lymphoid cells enrichment, nasal polyps and allergy in chronic rhinosinusitis. *Allergy*. (2014) 69:1154–61. doi: 10.1111/all.2014.69.issue-9

37. Celebi Sozener Z, Cevhertas L, Satitsuksanoa P, van de Veen W, Jansen K, Secil D, et al. Innate lymphoid cell subsets in obese asthma patients: Difference in activated cells in peripheral blood and their relationship to disease severity. *Allergy*. (2022) 77:2835–9. doi: 10.1111/all.15378

38. Greenwood C, Ruff D, Kirvell S, Johnson G, Dhillon HS, Bustin SA. Proximity assays for sensitive quantification of proteins. *Biomol Detect Quantif*. (2015) 4:10–6. doi: 10.1016/j.bdq.2015.04.002

39. Evangelista JE, Xie Z, Marino GB, Nguyen N, Clarke DJB, Ma'ayan A. Enrichr-KG: bridging enrichment analysis across multiple libraries. *Nucleic Acids Res*. (2023) 51:W168–W79. doi: 10.1093/nar/gkad393

40. Zaiss DMW, Pearce EJ, Artis D, McKenzie ANJ, Klose CSN. Cooperation of ILC2s and T(H)2 cells in the expulsion of intestinal helminth parasites. *Nat Rev Immunol*. (2023) 24:294–302. doi: 10.1038/s41577-023-00942-1

41. Darboe A, Nielsen CM, Wolf AS, Wildfire J, Danso E, Sonko B, et al. Age-related dynamics of circulating innate lymphoid cells in an African population. *Front Immunol*. (2020) 11:594107. doi: 10.3389/fimmu.2020.594107

42. Tamadaho RSE, Osei-Mensah J, Arndts K, Debrah LB, Debrah AY, Layland LE, et al. Reduced type 2 innate lymphocyte cell frequencies in patent wuchereria bancrofti-infected individuals. *Pathogens*. (2023) 12:665. doi: 10.3390/pathogens12050665

43. Shen X, Pasha MA, Hidde K, Khan A, Liang M, Guan W, et al. Group 2 innate lymphoid cells promote airway hyperresponsiveness through production of VEGFA. *J Allergy Clin Immunol*. (2018) 141:1929–31 e4. doi: 10.1016/j.jaci.2018.01.005

44. McSharry C, Xia Y, Holland CV, Kennedy MW. Natural immunity to Ascaris lumbricoides associated with immunoglobulin E antibody to ABA-1 allergen and inflammation indicators in children. *Infect Immun*. (1999) 67:484–9. doi: 10.1128/IAI.67.2.484-489.1999

45. Buendia E, Zakzuk J, Mercado D, Alvarez A, Caraballo L. The IgE response to Ascaris molecular components is associated with clinical indicators of asthma severity. *World Allergy Organ J*. (2015) 8:8. doi: 10.1186/s40413-015-0058-z

46. Smith SG, Chen R, Kjarsgaard M, Huang C, Oliveria JP, O'Byrne PM, et al. Increased numbers of activated group 2 innate lymphoid cells in the airways of patients with severe asthma and persistent airway eosinophilia. *J Allergy Clin Immunol*. (2016) 137:75–86.e8. doi: 10.1016/j.jaci.2015.05.037

47. Engelbertsen D, Foks AC, Alberts-Grill N, Kuperwaser F, Chen T, Lederer JA, et al. Expansion of CD25+ Innate lymphoid cells reduces atherosclerosis. *Arterioscler Thromb Vasc Biol*. (2015) 35:2526–35. doi: 10.1161/ATVBAHA.115.306048

48. Sheikh A, Lu J, Melese E, Seo JH, Abraham N. IL-7 induces type 2 cytokine response in lung ILC2s and regulates GATA3 and CD25 expression. *J Leukoc Biol*. (2022) 112:1105–13. doi: 10.1002/JLB.3AB1220-819RRR

49. Winkler C, Hochdorfer T, Israelsson E, Hasselberg A, Cavallin A, Thorn K, et al. Activation of group 2 innate lymphoid cells after allergen challenge in asthmatic patients. *J Allergy Clin Immunol*. (2019) 144:61–9 e7. doi: 10.1016/j.jaci.2019.01.027

50. Malik B, Bartlett NW, Upham JW, Nichol KS, Harrington J, Wark PAB. Severe asthma ILC2s demonstrate enhanced proliferation that is modified by biologics. *Respirology*. (2023) 28:758–66. doi: 10.1111/resp.14506

51. Carson JP, Robinson MW, Ramm GA, Gobert GN. Synthetic peptides derived from the Schistosoma mansoni secretory protein Sm16 induce contrasting responses in hepatic stellate cells. *Exp Parasitol*. (2022), 236-7:108255. doi: 10.1016/j.exppara.2022.108255

52. Laukoetter MG, Nava P, Lee WY, Severson EA, Capaldo CT, Babbin BA, et al. JAM-A regulates permeability and inflammation in the intestine in vivo. *J Exp Med*. (2007) 204:3067–76. doi: 10.1084/jem.20071416

53. Asemota OO, Nmorsi OP, Isaac C, Odoya EM, Akinseye J, Isaac O. Chemokines responses to ascaris lumbricoides sole infection and co-infection with hookworm among Nigerians. *N Am J Med Sci*. (2014) 6:84–8. doi: 10.4103/1947-2714.127750

54. Gazzinelli-Guimaraes PH, Gazzinelli-Guimaraes AC, Silva FN, Mati VL, Dhom-Lemos Lde C, Barbosa FS, et al. Parasitological and immunological aspects of early Ascaris spp. infection in mice. *Int J Parasitol*. (2013) 43:697–706. doi: 10.1016/j.ijpara.2013.02.009

55. Thompson JM, Meola SM, Ziprin RL, Jeska EL. An ultrastructural study of the invasion of Ascaris suum larvae by neutrophils. *J Invertebr Pathol*. (1977) 30:181–4. doi: 10.1016/0022-2011(77)90217-8

56. Lozano A, Marrugo V, Alvarado JC, Hernandez K, Caballero KL, Acevedo N, et al. Characterization of peripheral blood cellular populations in relation to Ascaris Lumbricoides infection in rural areas of Bolivar. *Rev Alerg Mex*. (2024) 71:69. doi: 10.29262/ram.v71i1.1372

57. Lang A, Kubala S, Grieco MC, Mateja A, Pongracic J, Liu Y, et al. Severe food allergy reactions are associated with alpha-tryptase. *J Allergy Clin Immunol*. (2023) 152:933–9. doi: 10.1016/j.jaci.2023.07.014

58. Wilcock A, Bahri R, Bulfone-Paus S, Arkwright PD. Mast cell disorders: From infancy to maturity. *Allergy*. (2019) 74:53–63. doi: 10.1111/all.2019.74.issue-1

59. Solano-Aguilar G, Shea-Donohue T, Madden KB, Quinones A, Beshah E, Lakshman S, et al. Bifidobacterium animalis subspecies lactis modulates the local immune response and glucose uptake in the small intestine of juvenile pigs infected with the parasitic nematode Ascaris suum. *Gut Microbes*. (2018) 9:422–36. doi: 10.1080/19490976.2018.1460014

60. Altman MC, Lai Y, Nolin JD, Long S, Chen CC, Piliponsky AM, et al. Airway epithelium-shifted mast cell infiltration regulates asthmatic inflammation via IL-33 signaling. *J Clin Invest*. (2019) 129:4979–91. doi: 10.1172/JCI126402

61. Shimokawa C, Kanaya T, Hachisuka M, Ishiwata K, Hisaeda H, Kurashima Y, et al. Mast cells are crucial for induction of group 2 innate lymphoid cells and clearance of helminth infections. *Immunity*. (2017) 46:863–74 e4. doi: 10.1016/j.immuni.2017.04.017

62. Higham A, Dungwa J, Pham TH, McCrae C, Singh D. Increased mast cell activation in eosinophilic chronic obstructive pulmonary disease. *Clin Transl Immunol*. (2022) 11:e1417. doi: 10.1002/cti2.v11.9

63. Morita H, Kubo T, Rückert B, Ravindran A, Soyka MB, Rinaldi AO, et al. Induction of human regulatory innate lymphoid cells from group 2 innate lymphoid cells by retinoic acid. *J Allergy Clin Immunol*. (2019) 143:2190–201.e9. doi: 10.1016/j.jaci.2018.12.1018

64. Golebski K, Layhadi JA, Sahiner U, Steveling-Klein EH, Lenormand MM, Li RCY, et al. Induction of IL-10-producing type 2 innate lymphoid cells by allergen immunotherapy is associated with clinical response. *Immunity*. (2021) 54:291–307.e7. doi: 10.1016/j.immuni.2020.12.013

frontiers | Frontiers in Immunology

TYPE Perspective
PUBLISHED 28 October 2024
DOI 10.3389/fimmu.2024.1449495

OPEN ACCESS

EDITED BY
Anisuzzaman Anisuzzaman,
Bangladesh Agricultural University,
Bangladesh

REVIEWED BY
Nahla Galal Metwally,
Bernhard Nocht Institute for Tropical Medicine (BNITM), Germany
Anita Rani Dey,
Bangladesh Agricultural University,
Bangladesh

*CORRESPONDENCE
Yamei Jin
yameijin@shvri.ac.cn

RECEIVED 15 June 2024
ACCEPTED 06 September 2024
PUBLISHED 28 October 2024

CITATION
Zhong H, Guan G and Jin Y (2024) Roles of helminth extracellular vesicle-derived let-7 in host–parasite crosstalk.
Front. Immunol. 15:1449495.
doi: 10.3389/fimmu.2024.1449495

Roles of helminth extracellular vesicle-derived let-7 in host–parasite crosstalk

Haoran Zhong[1,2], Guiquan Guan[3,4] and Yamei Jin[1,2]*

[1]National Reference Laboratory for Animal Schistosomiasis, Shanghai Veterinary Research Institute, Chinese Academy of Agricultural Sciences, Shanghai, China, [2]Key Laboratory of Animal Parasitology of Ministry of Agriculture and Rural Affairs, Shanghai Veterinary Research Institute, Chinese Academy of Agricultural Sciences, Shanghai, China, [3]State Key Laboratory for Animal Disease Control and Prevention, Lanzhou Veterinary Research Institute, Chinese Academy of Agricultural Science, Lanzhou, Gansu, China, [4]Key Laboratory of Veterinary Parasitology of Gansu Province, Lanzhou Veterinary Research Institute, Chinese Academy of Agricultural Science, Lanzhou, Gansu, China

Helminth infections are a major public health problem as they can cause long-term chronic infections in their hosts for which there is no effective vaccine. During the long-term interaction between helminths and their hosts, helminth-derived extracellular vesicles (EVs) can participate in host immunomodulatory processes by secreting bioactive molecules (BMAs). Growing data suggests that microRNAs (miRNAs) in helminth EVs have a significant impact on the host's immune system. The let-7 family is highly conserved among helminth EVs and highly homologous in the host, and its function in host–parasite crosstalk may reflect active selection for compatibility with the host miRNA machinery. In-depth studies targeting this aspect may better elucidate the mechanism of parasite-host interactions. Hence, this review summarizes the current studies on the cross-species involvement of helminth EV-derived let-7 in host immune regulation and discusses the barriers to related research and potential applications of helminth EVs.

KEYWORDS

helminth, extracellular vesicles, microRNA, Let-7 family, host-parasite interaction

Introduction

Helminthiosis, caused by nematodes, cestodes, and trematodes, are a major public health concern and result in ~60 million disability-adjusted life years (DALYs) globally (1). Recent estimates indicate that 2 billion people in low- and middle-income countries, mostly in endemic areas of Asia, the Americas, and Africa, have been infected by one or more parasitic worms (2). Unfortunately, there are currently no broad-spectrum anthelmintic vaccines available (3). Therefore, most helminth infections are controlled with the use of anthelmintic drugs, which do not prevent reinfection (4). However, prolonged and over use of these drugs can lead to the development of anthelmintic resistance (5–7). Hence, new control and prevention strategies against helminth infections are urgently needed.

As a result of complex life cycles and long-term symbiosis with the host, helminths release various mediators involved in host–parasite crosstalk, which promote immunomodulation, immune evasion, and pathogenesis (8, 9). Previous studies have primarily focused on helminth excretory/secretory products (ESPs) involved in regulating the host immune response (10, 11). However, as the study of host–parasite interactions has entered a deeper molecular realm, there has been a gradual emergence of helminth-derived microRNAs (miRNAs), mainly loaded in extracellular vesicles (EVs), involved in this intricate crosstalk (9, 12, 13).

EVs are small membrane-bounded secretory vesicles released by almost all cell types. EVs play essential roles in cell–cell communication via a wide variety of bio-active molecules (BMAs), including small RNAs, DNAs, messenger RNAs (mRNAs), proteins, lipids, and glycans (14, 15). These BMAs are encapsulated by EVs that are protected by a membrane to prevent degradation in the extracellular environment (16). Among these diverse BMAs conveyed by EVs, miRNAs are regarded as multifunctional regulators of various biological functions (17). MiRNAs play a pivotal role in regulating gene expression, affecting critical cellular functions such as growth, differentiation, and apoptosis (18). Their biogenesis begins with the transcription of primary miRNA (pri-miRNA) by RNA polymerase II. This pri-miRNA is processed in the nucleus by the Drosha-DGCR8 complex into precursor miRNA (pre-miRNA), which is then transported to the cytoplasm via Exportin-5. In the cytoplasm, Dicer further processes the pre-miRNA into mature miRNA. The mature miRNA is then integrated into the RNA-induced silencing complex (RISC), where it directs the repression of target mRNAs through sequence-specific binding, thereby modulating various biological processes and contributing to disease mechanisms (19). However, little is known about the mechanisms that drive and regulate the incorporation of miRNAs into helminth EVs and how specific miRNAs are preferentially selected as cargo (20). Nonetheless, both helminth EV-derived miRNAs and corresponding host targets are remarkably similar, suggesting that the packaging and release mechanisms of specific miRNAs during long-term host–parasite interactions and related immunomodulatory functions are evolutionarily conserved (13).

The most common miRNA clusters in helminth EVs are let-7, miR-2, miR-9, miR-10, miR-31, miR-71, miR-87, and miR-125 (21). As a conserved miRNA family that is highly homologous to the host, the function of helminth EV-derived let-7 in host–parasite interactions may reflect active selection for compatibility with the host miRNA machinery. This is because the let-7 miRNA from helminths and hosts may function similarly due to their similar sequences, and that the parasite miRNA, once taken up by the host cell, may rely on the host miRNA machinery to modulate gene expression (13). As one of the earliest identified miRNAs, let-7 is associated with reproductive development of *Caenorhabditis elegans*, while deficiency or overexpression of let-7 can lead to developmental abnormalities (22, 23). Although the importance in reproductive development of helminths remains unclear, let-7 can regulate host immune responses through EVs (24–27). Target gene prediction software is often used to analyze host target genes against the let-7 family-specific seed sequence (GAGGUAG) or the full-length sequence of helminth let-7 (26–29). Most of these target genes are associated with the TGF-β, MAPK, and Wnt signaling pathways, which play crucial roles not only in cell proliferation and differentiation but also in host immune and inflammatory reactions. This multiple involvement suggests different roles of helminth EV-derived let-7 in host–parasite crosstalk (13). Therefore, an in-depth study of helminth EV-derived let-7 will further enrich our understanding of this crosstalk and may further clarify the mechanisms underlying the crosstalk between helminth EVs and host cells.

Therefore, the aim of this article is to summarize current studies on the cross-species involvement of helminth EV-derived let-7 in host immune regulation (Table 1), while addressing shortcomings of related research and potential applications of helminth EVs.

Helminth EV-derived let-7 in host-parasite crosstalk

Trematodes

Diseases caused by blood fluke (e.g. schistosomiasis), liver flukes (clonorchiosis, opisthorchiosis, fascioliosis etc.) and lung flukes (paragonimiosis) severely hamper health and productivity of humans and animals (24, 26, 30, 31). These diseases induce severe pathological impacts, including chronic inflammation, fibrosis, and extensive tissue damage in affected organs. Specifically, schistosomiasis and fascioliosis primarily target the liver, clonorchiosis and opisthorchiosis lead to biliary obstruction and elevate the risk of cholangiocarcinoma, while paragonimiosis causes pulmonary fibrosis and systemic symptoms due to parasite migration (32, 33).

Schistosomes are dioecious, presenting as separate male and female sexes (34). Following dialysis, ultrafiltration, and ultracentrifugation combined with a commercial kit, EVs derived from male and female *S. japonicum* were successfully enriched from the supernatant of *in vitro* cultures and contained a high abundance of sja-let-7 (24, 31, 35). Our group recently reported that *Sj*EVs reduced expression of collagen type I alpha 2 chain (Col1α2), one of the host target genes of sja-let-7, thereby alleviating liver fibrosis (24). The same relationship between helminth let-7 and host Col1α2 was also reported in *S. mansoni* (21). Since sja-let-7 is not highly abundant in *S. japonicum* egg ESPs or EVs (36, 37), this regulatory effect might not be caused by eggs deposited in the host liver, but rather remotely mediated via worm-derived EVs, suggesting that worms can manipulate the host immune responses to alleviate pathological damage, thereby preventing expulsion and promoting a state of tolerance that benefits the parasite by prolonging the host's life (12). Therefore, it is not surprising that helminth miRNAs can inhibit the pathological processes underlying the establishment of chronic infection (Figure 1). However, due to the large number of mRNAs targeted by miRNAs, the consequent biological functions may vary at different stages of infection (18). Fontenla et al. (30) reported that EVs from *F. hepatica* contained fhe-let-7 that could potentially interact with target genes related to different regulatory roles, although the specific mechanisms remain unclear. Notably, let-7 of *C. sinensis* promotes inflammation in the host (26). Yan et al. (26) isolated EVs from *C. sinensis* (*Cs*EVs) by ultracentrifugation combined with iodixanol-based density gradient centrifugation. Further analysis revealed that csi-let-7a, a highly

10.3389/fimmu.2024.1449495

TABLE 1 Current research involving helminth EV-derived let-7 and their target genes.

Category	miRNA name	Species	EV Origin	EV Purification method	Target gene	Reference
Trematodes	sja-let-7	*Schistosoma japonicum*	Adult worm ESPs	Dialysis, ultrafiltration, and ultracentrifugation combined with commercial kit	COL1A2	(24)
	sma-let-7	*Schistosoma mansoni*	Adult worm ESPs	Differential centrifugation followed by membrane filtration and sucrose density ultracentrifugation	COL1A2, MAP3K1, MSN, RASGRP1, SMAD2, FBXO32, LTN1, MUC20, RANBP2, RICTOR	(21)
	fhe-let-7	*Fasciola hepatica*	Adult worm ESPs	Ultracentrifugation	CD200R1, CNOT4, HIF1AN, HOXA9, HSPA14, MAP3K1, MAPK8, PMAIP1, PTAFR, SMAD4, SNAP23, TNFRSF1B, TP53, TRIM71, ZBTB16	(30)
	csi-let-7	*Clonorchis sinensis*	Adult worm ESPs	Ultracentrifugation, iodixanol-based density gradient centrifugation	SOCS1, CLEC7A	(26)
	dde-let-7	*Dicrocoelium dendriticum*	Adult worm ESPs	Ultracentrifugation coupled to membrane filtration	Not validated	(52)
	tsp-let-7	*Trichinella Spiralis*	Larvae ESPs	Ultracentrifugation	Not validated	(53)
Cestodes	tpi-let-7	*Taenia pisiformis*	Larvae ESPs	Ultracentrifugation	C/EBP δ, NFκB2	(25, 27)
	egr-let-7	*Echinococcus granulosus*	Protoscolece ESPs Hydatid fluid	Ultracentrifugation	IGF2R	(43)
Nematodes	hpo-let-7	*Heligmosomoides polygyrus*	Adult worm ESPs	Ultracentrifugation	DUSP1	(16)
	bma-let-7	*Brugia malayi*	Adult worm ESPs	Commercial kit	EIF4E	(50)
	asu-let-7	*Ascaris suum*	Adult worm, L3, L4 larvae ESPs Adult worm body fluid	Ultracentrifugation, size exclusion chromatography	CD86, PARP8, SENP1, TRIM32 USP15	(49)

EVs, Extracellular vesicles; ESPs, Excretory/secretory products.

enriched miRNA delivered by CsEVs, plays a pivotal role in the activation of M1-like macrophages and subsequent proinflammatory responses to biliary injury by targeting the host genes suppressor of cytokine signaling 1 and c-type lectin domain containing 7A (26).

Cestodes

Cestodes are zoonotic parasites that are usually widely spread in susceptible impoverished areas with poor hygiene practices, especially urban settings with livestock (38). In taenid cestodes such as *Taenia solium*, *T. saginata*, and *Echinococcus* spp., an intermediate host ingests contaminated vegetation or food containing cestode eggs, which hatch into larvae in the intestines. These larvae are then transported through the bloodstream to various tissues where they develop into cysts or metacestodes. When the definitive host consumes the infected meat, the infection is established. These metacestodes can cause chronic pathology, reflecting the parasite's evolved mechanisms to evade the host's immune response. In humans, *T. solium* can lead to cysticercosis, causing severe neurological damage, while *Echinococcus* spp. may result in hydatid disease with life-threatening cysts in the liver and lungs. In livestock, these infections cause economic losses due to reduced productivity, meat condemnation, and increased veterinary costs (39).

Cysticercus pisiformis, the larval stage of *Taenia pisiformis*, can infect rabbits and cause digestive disorders and growth retardation, resulting in great economic losses to the breeding industry. Co-incubation of RAW264.7 macrophages with EVs of *T. pisiformis* (*Tp*EVs) collected by ultracentrifugation increased levels of tpi-let-7 in the cell, which reduced M1 phenotype expression and enhanced M2 phenotype polarization by inhibiting the target gene transcription factor CCAAT/enhancer-binding protein δ (27, 40). Likewise, co-incubation of rabbit peritoneal macrophages with *Tp*EVs resulted in detectable levels of tpi-let-7 in the host cells, demonstrating the delivery of tpi-let-7 by *Tp*EVs (25). Moreover, another potential target gene of tpi-let-7, nuclear factor kappa B subunit 2, was differentially expressed, as determined by proteomic analysis of the same cell samples, suggesting that the tpi-let-7/NFκB2 axis may also be involved in modulating the host immune response by *Tp*EVs (25).

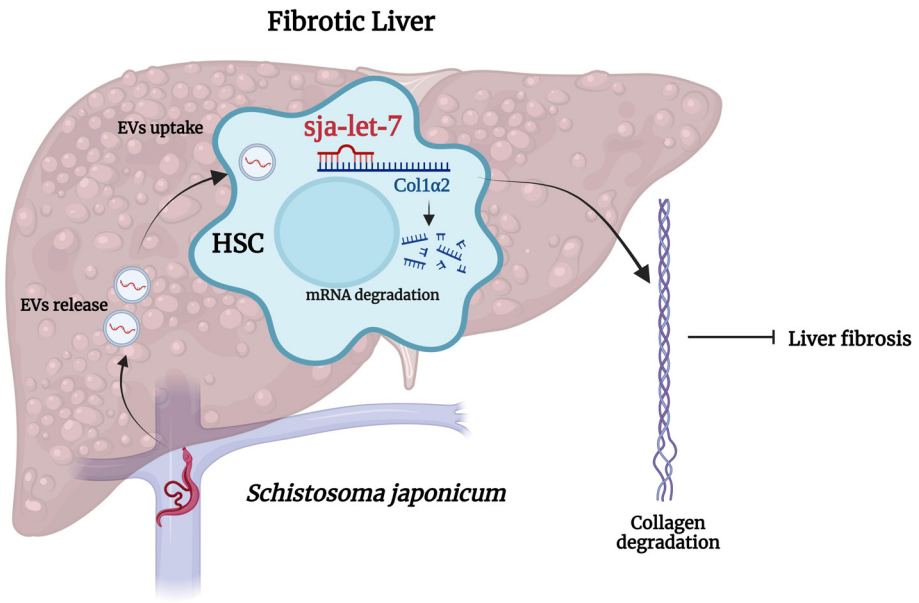

FIGURE 1
Cross-species sja-let-7 mediates host–parasite interactions in schistosome-induced liver fibrosis. *Schistosoma japonicum* worms residing in the host portal vein release *Sj*EVs that contain sja-let-7, which alleviates schistosome-induced liver fibrosis through the regulation of Col1α2. This figure was created with Biorender.com.

Echinococcosis is a zoonotic disease induced by adult or larval cestodes of the genus *Echinococcus* (41). *Echinococcus granulosus* is a medically significant cestode and a public health concern (42). EVs of *E. granulosus* collected by ultracentrifugation contained high levels of egr-let-7, which might play an immunomodulatory role by targeting insulin like growth factor 2 receptor, although the specific mechanisms remain unclear (43).

Nematodes

Nematodes are highly diverse, widely distributed, and well-adapted to almost all habitats. Based on complex and varied evolutionary histories, nematodes can be categorized into three main groups: free-living, saprophytic, and parasitic (44).

Heligmosomoides polygyrus is a gastrointestinal nematode that infects mice and belongs to the same nematode clade as *C. elegans* (45). During long-term interactions with the host, *H. polygyrus* may induce a strong Th2 response and simultaneously secrete immunomodulatory molecules, which can suppress the host immune response (46). EVs isolated from *H. polygyrus* (*Hp*EVs) by ultracentrifugation were reported to suppress type 2 innate responses and reduce eosinophilia in mice (16). Subsequent microarray analysis revealed that hpo-let-7 from *Hp*EVs could suppress expression of dual specificity phosphatase 1, which is a crucial regulator of inflammation and immunity, to manipulate host cells. In addition to *H. polygyrus*, *Haemonchus contortus* is another significant gastrointestinal nematode that affects livestock, particularly small ruminants such as sheep and goats (47). *H. contortus* is a major cause of parasitic gastroenteritis, leading to severe anemia, reduced productivity, and significant economic losses in the livestock industry (48). Although the specific role of let-7 in *Hc*EVs remains underexplored, understanding its involvement in parasite-host interactions could open new avenues for developing targeted therapies and diagnostic tools for managing infections in livestock.

Interactions between helminth EV-derived let-7 and host targets have also been reported in other nematodes (49, 50). *Brugia malayi* is a pathogen of lymphatic filariasis, commonly known as elephantiasis, a neglected tropical disease that affects millions of people, and an important public health issue due to the high prevalence. Ricciardi et al. (50) isolated EVs from *B. malayi* with a commercial kit that were absorbed by human dendritic cells and monocytes, which downregulated the mammalian target of rapamycin pathway in host cells via the bma-let-7/eukaryotic translation initiation factor 4E axis. *Ascaris suum* is a prevalent parasitic nematode that infects pigs and was found to reduce nutrient utilization and weight gain, ultimately resulting in production loss (51). Through ultracentrifugation and size exclusion chromatography (SEC), EVs were obtained from *A. suum* adults, as well as L3 and L4 larvae, for miRNA profiling (49). The results of target gene prediction showed that asu-let-7 interacted with CD86, which facilitates T-cell activation, suggesting that this axis might be involved in host–parasite interactions (49).

In addition to these species, let-7 has been identified in the EVs of other helminths, although the specific target genes have not yet been identified (52, 53). Details can be found in Table 1.

Current challenges and future perspectives

Although current evidence confirms that the helminth EV-derived let-7 cluster is involved in various pathological and

physiological processes, considerable challenges still exist to gain a deeper understanding of the roles of let-7 in host–parasite crosstalk.

First, helminth EVs are typically isolated from *in vitro* culture supernatants of a single formulation, such as Dulbecco's modified Eagle's medium or Roswell Park Memorial Institute 1640 medium supplemented with EV-free fetal bovine serum and antibiotics (24–26, 52–55). However, the viability of the worms is gradually decreased in these mediums, which may compromise the quality of helminth EVs. In addition, the evolutionary history of helminths is complex and the acquisition of essential substances from the host varies among parasitized stages. Whether there are differences between helminth EVs collected by *in vitro* culture and those involved in host–parasite interactions remain unknown. Recent studies have reported medium suitable for the reproductive development of some helminths *in vitro* (56, 57). Thus, the use of such a medium to obtain helminth EVs may be a direction for further research.

Second, in most studies, helminth EVs are collected by ultracentrifugation of ESPs as the primary separation and isolation method (25–27, 37, 39, 40, 53–55, 58). However, there has been a recent shift towards the use of other methods, such as SEC (59). While ultracentrifugation is commonly used to isolate EVs, it can compromise vesicle integrity due to high shear forces (60). SEC offers an alternative by separating molecules based on size through a column of porous beads, which enables high-purity isolation of EVs, preserving their biological activity and ensuring reproducibility. Additionally, SEC is scalable for larger volumes, making it ideal for studies requiring substantial quantities of purified EVs (61). Since the collection method influences the number, purity and type of enriched helminth EVs, each study should include detailed information based on a recent publication, titled "Special considerations for studies of extracellular vesicles from parasitic helminths: A community-led roadmap to increase rigor and reproducibility" (62).

Third, further studies are needed to determine whether helminth miRNAs are delivered to host cells as primary or precursor miRNAs, how miRNAs are processed and loaded in the EVs, and whether there are differences in the predicted target genes *in vivo* vs. *in vitro*. Investigating these mechanisms is crucial for advancing our understanding of host-parasite interactions. Future research should focus on exploring the molecular machinery involved in miRNA incorporation into EVs and identifying factors that determine the selectivity of miRNA cargo. These studies will provide valuable insights into how helminth EVs modulate host immune responses and contribute to parasite survival. To preliminarily confirm the interactions *in vitro*, our group conducted fluorescence *in situ* hybridization to label co-localized sja-let-7 and the related target gene Col1α2 in liver sections of mice with schistosome-induced liver fibrosis (24).

Fourth, to explore the biological functions of helminth EVs or miRNAs, recent studies have applied mimics either directly to a single cell type or directly to mice via tail vein injection. However, the use of mimics differs from natural helminth infection. Also, since miRNAs target a large number of mRNAs, potential side effects in the host should be considered. Interestingly, our group administered a mimic of sja-let-7, which resulted in a relatively high abundance miRNAs in *Sj*EVs and an anti-fibrotic effect in mice with schistosome-induced liver fibrosis, as well as carbon tetrachloride-induced liver fibrosis, which alleviated pathological changes, demonstrating the potential application of helminth-derived miRNAs (63). Certainly, it is also necessary to assess safety in future studies.

Conclusions

This article summarized the roles of helminth EV-derived let-7 in host–parasite interactions. In addition to helminth let-7, in-depth studies are warranted to clarify the biological functions of other BMAs, such as miR-71 (21, 37) and miR-125 (43, 64), to further elucidate potential roles on host–parasite crosstalk and provide a theoretical basis for helminth prevention and control. Moreover, the potential therapeutic and diagnostic applications of let-7 are promising areas for future research. As understanding of the molecular mechanisms governing let-7 and its role in modulating host immune responses deepens, targeted therapies could be developed to inhibit or enhance specific pathways affected by let-7. Similarly, the presence of let-7 in extracellular vesicles could serve as a biomarker for parasitic infections, aiding in the early diagnosis and monitoring of disease progression.

Author contributions

HZ: Writing – original draft. GG: Writing – original draft. YJ: Writing – review & editing.

Funding

The author(s) declare that financial support was received for the research, authorship, and/or publication of this article. This work was supported by the Agricultural Science and Technology Innovation Program (ASTIP) (no. CAAS-ASTIP-2021-SHVRI), the Natural Science Foundation of Shanghai (no. 20ZR1469300) and partially funded by the Key Laboratory of Veterinary Etiological Biology, Ministry of Agricultural and Rural Affairs, China (no. XKQ2024002). The funders had no role in study design, data collection and analysis, decision to publish, or preparation of the manuscript.

Acknowledgments

We thank International Science Editing for revising the manuscript and their valuable comments.

Conflict of interest

The authors declare that the research was conducted in the absence of any commercial or financial relationships that could be construed as a potential conflict of interest.

Publisher's note

References

1. Anisuzzaman, Hossain MS, Hatta T, Labony SS, Kwofie KD, Kawada H, et al. Food- and vector-borne parasitic zoonoses: global burden and impacts. *Adv Parasitol*. (2023) 120:87–136. doi: 10.1016/bs.apar.2023.02.001

2. Weatherhead JE, Hotez PJ, Mejia R. The global state of helminth control and elimination in children. *Pediatr Clinics North America*. (2017) 64:867–77. doi: 10.1016/j.pcl.2017.03.005

3. Fissiha W, Kinde MZ. Anthelmintic resistance and its mechanism: A review. *Infection Drug resistance*. (2021) 14:5403–10. doi: 10.2147/idr.S332378

4. Shao B, Gui X, Lu Z, Lv R, Li H, Lu K, et al. Praziquantel promotes protection against *schistosoma japonicum* infection in mice. *Acta tropica*. (2023) 241:106874. doi: 10.1016/j.actatropica.2023.106874

5. Wang N, Peng HQ, Gao CZ, Cheng YH, Sun MT, Qu GL, et al. *In vivo* efficiency of praziquantel treatment of single-sex *schistosoma japonicum* aged three months old in mice. *Int J Parasitol Drugs Drug Resist*. (2022) 20:129–34. doi: 10.1016/j.ijpddr.2022.11.002

6. Liu Y, Luo X, Li J, Wang P, Teng B, Wang R, et al. Using feeding and motility patterns for ivermectin resistance detecting in *haemonchus contortus* larvae. *Exp Parasitol*. (2022) 238:108230. doi: 10.1016/j.exppara.2022.108230

7. Liu Y, Wang P, Wang R, Li J, Zhai B, Luo X, et al. An epidemiological investigation and drug-resistant strain isolation of nematodirus oiratianus in sheep in inner Mongolia, China. *Animals*. (2022) 13(1):30. doi: 10.3390/ani13010030

8. Mu Y, McManus DP, Hou N, Cai P. Schistosome infection and schistosome-derived products as modulators for the prevention and alleviation of immunological disorders. *Front Immunol*. (2021) 12:619776. doi: 10.3389/fimmu.2021.619776

9. Mu Y, McManus DP, Gordon CA, Cai P. Parasitic helminth-derived micrornas and extracellular vesicle cargos as biomarkers for helminthic infections. *Front Cell infection Microbiol*. (2021) 11:708952. doi: 10.3389/fcimb.2021.708952

10. Donnelly S, Dalton JP, Loukas A. Proteases in helminth- and allergen- induced inflammatory responses. *Chem Immunol Allergy*. (2006) 90:45–64. doi: 10.1159/000088880

11. Hewitson JP, Grainger JR, Maizels RM. Helminth immunoregulation: the role of parasite secreted proteins in modulating host immunity. *Mol Biochem Parasitol*. (2009) 167:1–11. doi: 10.1016/j.molbiopara.2009.04.008

12. He X, Pan W. Host-parasite interactions mediated by cross-species micrornas. *Trends Parasitol*. (2022) 38(6):478–88. doi: 10.1016/j.pt.2022.02.011

13. Chowdhury S, Sais D, Donnelly S, Tran N. The knowns and unknowns of helminth–host mirna cross-kingdom communication. *Trends Parasitol*. (2024) 40:176–91. doi: 10.1016/j.pt.2023.12.003

14. Deolindo P, Evans-Osses I, Ramirez MI. Microvesicles and exosomes as vehicles between protozoan and host cell communication. *Biochem Soc Trans*. (2013) 41:252–7. doi: 10.1042/BST20120217

15. van Niel G, D'Angelo G, Raposo G. Shedding light on the cell biology of extracellular vesicles. *Nat Rev Mol Cell Biol*. (2018) 19:213–28. doi: 10.1038/nrm.2017.125

16. Buck AH, Coakley G, Simbari F, McSorley HJ, Quintana JF, Le Bihan T, et al. Exosomes secreted by nematode parasites transfer small rnas to mammalian cells and modulate innate immunity. *Nat Commun*. (2014) 5:5488. doi: 10.1038/ncomms6488

17. Zhong H, Jin Y. Multifunctional roles of micrornas in schistosomiasis. *Front Microbiol*. (2022) 13:925386. doi: 10.3389/fmicb.2022.925386

18. Bartel DP. Micrornas: genomics, biogenesis, mechanism, and function. *Cell*. (2004) 116:281–97. doi: 10.1016/s0092-8674(04)00045-5

19. Bartel DP. Micrornas: target recognition and regulatory functions. *Cell*. (2009) 136:215–33. doi: 10.1016/j.cell.2009.01.002

20. Ding J, He G, Wu J, Yang J, Guo X, Yang X, et al. Mirna-seq of echinococcus multilocularis extracellular vesicles and immunomodulatory effects of mir-4989. *Front Microbiol*. (2019) 10:2707. doi: 10.3389/fmicb.2019.02707

21. Ovchinnikov VY, Kashina EV, Mordvinov VA, Fromm B. Ev-transported micrornas of *schistosoma mansoni* and *fasciola hepatica*: potential targets in definitive hosts. *Infection Genet evolution: J Mol Epidemiol evolutionary Genet Infect Dis*. (2020) 85:104528. doi: 10.1016/j.meegid.2020.104528

22. Ding XC, Slack FJ, Grosshans H. The let-7 microrna interfaces extensively with the translation machinery to regulate cell differentiation. *Cell Cycle*. (2008) 7:3083–90. doi: 10.4161/cc.7.19.6778

23. Reinhart BJ, Slack FJ, Basson M, Pasquinelli AE, Bettinger JC, Rougvie AE, et al. The 21-nucleotide let-7 rna regulates developmental timing in *caenorhabditis elegans*. *Nature*. (2000) 403:901–6. doi: 10.1038/35002607

24. Zhong H, Dong B, Zhu D, Fu Z, Liu J, Jin Y. Sja-let-7 suppresses the development of liver fibrosis *via schistosoma japonicum* extracellular vesicles. *PloS Pathog*. (2024) 20(4):e1012153. doi: 10.1371/journal.ppat.1012153

25. Wang L, Liu T, Pu G, Chen G, Li H, Zhang S, et al. Global profiling of mirna and protein expression patterns in rabbit peritoneal macrophages treated with exosomes derived from *taenia pisiformis* cysticercus. *Genomics*. (2023) 115:110690. doi: 10.1016/j.ygeno.2023.110690

26. Yan C, Zhou Q-Y, Wu J, Xu N, Du Y, Li J, et al. Csi-let-7a-5p delivered by extracellular vesicles from a liver fluke activates M1-like macrophages and exacerbates biliary injuries. *Proc Natl Acad Sci*. (2021) 118(46):e2102206118. doi: 10.1073/pnas.2102206118

27. Wang L, Liu T, Chen G, Li Y, Zhang S, Mao L, et al. Exosomal microrna let-7-5p from *taenia pisiformis* cysticercus prompted macrophage to M2 polarization through inhibiting the expression of C/ebp delta. *Microorganisms*. (2021) 9(7):1403. doi: 10.3390/microorganisms9071403

28. Krüger J, Rehmsmeier M. Rnahybrid: microrna target prediction easy, fast and flexible. *Nucleic Acids Res*. (2006) 34:W451–4. doi: 10.1093/nar/gkl243

29. Peterson SM, Thompson JA, Ufkin ML, Sathyanarayana P, Liaw L, Congdon CB. Common features of microrna target prediction tools. *Front Genet*. (2014) 5:23. doi: 10.3389/fgene.2014.00023

30. Fontenla S, Langleib M, de la Torre-Escudero E, Domínguez MF, Robinson MW, Tort J. Role of *fasciola hepatica* small rnas in the interaction with the mammalian host. *Front Cell infection Microbiol*. (2022) 11:812141. doi: 10.3389/fcimb.2021.812141

31. Zhu L, Liu J, Dao J, Lu K, Li H, Gu H, et al. Molecular characterization of S. Japonicum exosome-like vesicles reveals their regulatory roles in parasite-host interactions. *Sci Rep*. (2016) 6:25885. doi: 10.1038/srep25885

32. Yongvanit P, Pinlaor S, Loilome W. Risk biomarkers for assessment and chemoprevention of liver fluke-associated cholangiocarcinoma. *J hepato-biliary-pancreatic Sci*. (2014) 21:309–15. doi: 10.1002/jhbp.63

33. Mas-Coma S, Bargues MD, Valero MA. Human fascioliasis infection sources, their diversity, incidence factors, analytical methods and prevention measures. *Parasitology*. (2018) 145:1665–99. doi: 10.1017/s0031182018000914

34. van Hellemond JJ, van Balkom BW, Tielens AG. Schistosome biology and proteomics: progress and challenges. *Exp Parasitol*. (2007) 117:267–74. doi: 10.1016/j.exppara.2007.05.004

35. Du P, Giri BR, Liu J, Xia T, Grevelding CG, Cheng G. Proteomic and deep sequencing analysis of extracellular vesicles isolated from adult male and female *schistosoma japonicum*. *PloS Negl Trop Dis*. (2020) 14:e0008618. doi: 10.1371/journal.pntd.0008618

36. Zhu S, Wang S, Lin Y, Jiang P, Cui X, Wang X, et al. Release of extracellular vesicles containing small rnas from the eggs of *schistosoma japonicum*. *Parasit Vectors*. (2016) 9:574. doi: 10.1186/s13071-016-1845-2

37. Wang L, Liao Y, Yang R, Yu Z, Zhang L, Zhu Z, et al. Sja-mir-71a in schistosome egg-derived extracellular vesicles suppresses liver fibrosis caused by schistosomiasis *via* targeting semaphorin 4d. *J Extracell Vesicles*. (2020) 9:1785738. doi: 10.1080/20013078.2020.1785738

38. Craig P, Ito A. Intestinal cestodes. *Curr Opin Infect Dis*. (2007) 20:524–32. doi: 10.1097/QCO.0b013e3282ef579e

39. Ancarola ME, Marcilla A, Herz M, Macchiaroli N, Perez M, Asurmendi S, et al. Cestode parasites release extracellular vesicles with micrornas and immunodiagnostic protein cargo. *Int J Parasitol*. (2017) 47:675–86. doi: 10.1016/j.ijpara.2017.05.003

40. Wang L-Q, Liu T-L, Liang P-H, Zhang S-H, Li T-S, Li Y-P, et al. Characterization of exosome-like vesicles derived from *taenia pisiformis* cysticercus and their immunoregulatory role on macrophages. *Parasites Vectors*. (2020) 13(1):318. doi: 10.1186/s13071-020-04186-z

41. Wen H, Vuitton L, Tuxun T, Li J, Vuitton DA, Zhang W, et al. Echinococcosis: advances in the 21st century. *Clin Microbiol Rev*. (2019) 32(2):e00075-18. doi: 10.1128/cmr.00075-18

42. McManus DP, Gray DJ, Zhang W, Yang Y. Diagnosis, treatment, and management of echinococcosis. *BMJ (Clinical Res ed)*. (2012) 344:e3866. doi: 10.1136/bmj.e3866

43. Zhang X, Gong W, Cao S, Yin J, Zhang J, Cao J, et al. Comprehensive analysis of non-coding rna profiles of exosome-like vesicles from the protoscoleces and hydatid cyst fluid of echinococcus granulosus. *Front Cell infection Microbiol*. (2020) 10:316. doi: 10.3389/fcimb.2020.00316

44. Antonopoulos A, Gilleard JS, Charlier J. Next-generation sequencing technologies for helminth diagnostics and surveillance in ruminants: shifting diagnostic barriers. *Trends Parasitol*. (2024) 40(6):511–26. doi: 10.1016/j.pt.2024.04.013

45. Blaxter ML, De Ley P, Garey JR, Liu LX, Scheldeman P, Vierstraete A, et al. A molecular evolutionary framework for the phylum nematoda. *Nature*. (1998) 392:71–5. doi: 10.1038/32160

46. Finney CA, Taylor MD, Wilson MS, Maizels RM. Expansion and activation of cd4(+)Cd25(+) regulatory T cells in heligmosomoides polygyrus infection. *Eur J Immunol*. (2007) 37:1874–86. doi: 10.1002/eji.200636751

47. Liu Y, Wang X, Luo X, Wang R, Zhai B, Wang P, et al. Transcriptomics and proteomics of *haemonchus contortus* in response to ivermectin treatment. *Animals*. (2023) 13(5):919. doi: 10.3390/ani13050919

48. Tuersong W, Zhou C, Wu S, Qin P, Wang C, Di W, et al. Comparative analysis on transcriptomics of ivermectin resistant and susceptible strains of *haemonchus contortus*. *Parasites Vectors*. (2022) 15(1):159. doi: 10.1186/s13071-022-05274-y

49. Hansen EP, Fromm B, Andersen SD, Marcilla A, Andersen KL, Borup A, et al. Exploration of extracellular vesicles from ascaris suum provides evidence of parasite-host cross talk. *J Extracell Vesicles*. (2019) 8:1578116. doi: 10.1080/20013078.2019.1578116

50. Ricciardi A, Bennuru S, Tariq S, Kaur S, Wu W, Elkahloun AG, et al. Extracellular vesicles released from the filarial parasite *brugia malayi* downregulate the host mtor pathway. *PloS Negl Trop Dis*. (2021) 15:e0008884. doi: 10.1371/journal.pntd.0008884

51. Nansen P, Roepstorff A. Parasitic helminths of the pig: factors influencing transmission and infection levels. *Int J Parasitol*. (1999) 29:877–91. doi: 10.1016/s0020-7519(99)00048-x

52. Bernal D, Trelis M, Montaner S, Cantalapiedra F, Galiano A, Hackenberg M, et al. Surface analysis of *dicrocoelium dendriticum*. The molecular characterization of exosomes reveals the presence of mirnas. *J Proteomics*. (2014) 105:232–41. doi: 10.1016/j.jprot.2014.02.012

53. Wu J, Liao Y, Li D, Zhu Z, Zhang L, Wu Z, et al. Extracellular vesicles derived from *trichinella spiralis* larvae promote the polarization of macrophages to M2b type and inhibit the activation of fibroblasts. *Front Immunol*. (2022) 13:974332. doi: 10.3389/fimmu.2022.974332

54. Kondo Y, Ito D, Taniguchi R, Tademoto S, Horie T, Otsuki H. Extracellular vesicles derived from *spirometra erinaceieuropaei* plerocercoids inhibit activation of murine macrophage raw264.7 cells. *Parasitol Int*. (2023) 95:102742. doi: 10.1016/j.parint.2023.102742

55. Nowacki FC, Swain MT, Klychnikov OI, Niazi U, Ivens A, Quintana JF, et al. Protein and small non-coding rna-enriched extracellular vesicles are released by the pathogenic blood fluke *schistosoma mansoni*. *J Extracell Vesicles*. (2015) 4:28665. doi: 10.3402/jev.v4.28665

56. Wang J, Chen R, Collins JJ 3rd. Systematically improved in vitro culture conditions reveal new insights into the reproductive biology of the human parasite *schistosoma mansoni*. *PloS Biol*. (2019) 17:e3000254. doi: 10.1371/journal.pbio.3000254

57. You Y, Chen X, Huo L, Chen L, Chen G, Gu M, et al. An improved medium for in vitro studies of female reproduction and oviposition in *schistosoma japonicum*. *Parasites Vectors*. (2024) 17(1):116. doi: 10.1186/s13071-024-06191-y

58. Wang Y, Gong W, Zhou H, Hu Y, Wang L, Shen Y, et al. A novel mirna from egg-derived exosomes of *schistosoma japonicum* promotes liver fibrosis in murine schistosomiasis. *Front Immunol*. (2022) 13:860807. doi: 10.3389/fimmu.2022.860807

59. Li C, Li X. Exosome-derived circ_0094343 promotes chemosensitivity of colorectal cancer cells by regulating glycolysis *via* the mir-766-5p/trim67 axis. *Contrast Media Mol Imaging*. (2022) 2022:2878557. doi: 10.1155/2022/2878557

60. Baranyai T, Herczeg K, Onódi Z, Voszka I, Módos K, Marton N, et al. Isolation of exosomes from blood plasma: qualitative and quantitative comparison of ultracentrifugation and size exclusion chromatography methods. *PloS One*. (2015) 10:e0145686. doi: 10.1371/journal.pone.0145686

61. Konoshenko MY, Lekchnov EA, Vlassov AV, Laktionov PP. Isolation of extracellular vesicles: general methodologies and latest trends. *BioMed Res Int*. (2018) 2018:8545347. doi: 10.1155/2018/8545347

62. White R, Sotillo J, Ancarola ME, Borup A, Boysen AT, Brindley PJ, et al. Special considerations for studies of extracellular vesicles from parasitic helminths: A community-led roadmap to increase rigour and reproducibility. *J Extracellular Vesicles*. (2023) 12(1):e12298. doi: 10.1002/jev2.12298

63. Zhong H, Dong B, Zhu D, Li H, Lu K, Fu Z, et al. Sja-let-7 attenuates carbon tetrachloride-induced liver fibrosis in a mouse model *via* col1α2. *Biology*. (2023) 12 (12):1465. doi: 10.3390/biology12121465

64. Liu J, Zhu L, Wang J, Qiu L, Chen Y, Davis RE, et al. *Schistosoma japonicum* extracellular vesicle mirna cargo regulates host macrophage functions facilitating parasitism. *PloS Pathog*. (2019) 15:e1007817. doi: 10.1371/journal.ppat.1007817

frontiers | Frontiers in Immunology

TYPE Original Research
PUBLISHED 31 January 2025
DOI 10.3389/fimmu.2024.1453742

OPEN ACCESS

EDITED BY
Joydeep Paul,
Adamas University, India

REVIEWED BY
Katherine Figarella,
University of Texas Health Science Center at Houston, United States
Manoj Kumar Singh,
Adamas University, India

*CORRESPONDENCE
Inssaf Berkiks
berkiksinssaf@gmail.com

†These authors share last authorship

RECEIVED 23 June 2024
ACCEPTED 02 December 2024
PUBLISHED 31 January 2025

CITATION
Berkiks I, Abdel Aziz N, Moses B, Brombacher T and Brombacher F (2025) Moderate regular physical exercise can help in alleviating the systemic impact of schistosomiasis infection on brain cognitive function.
Front. Immunol. 15:1453742.
doi: 10.3389/fimmu.2024.1453742

Moderate regular physical exercise can help in alleviating the systemic impact of schistosomiasis infection on brain cognitive function

Inssaf Berkiks[1,2]*, Nada Abdel Aziz[1,2,3], Blessing Moses[1,2], Tiroyaone Brombacher[1,2†] and Frank Brombacher[1,2†]

[1]Cytokines and Diseases Group, International Centre for Genetic Engineering and Biotechnology, Cape Town Component, Division of Immunology, Institute of Infectious Diseases and Molecular Medicine, Faculty of Health Sciences, University of Cape Town, Cape Town, South Africa, [2]Wellcome Centre for Infectious Diseases Research in Africa, Institute of Infectious Diseases and Molecular Medicine (IDM), Faculty of Health Sciences, University of Cape Town, Cape Town, South Africa, [3]Biotechnology Department, Faculty of Science, Cairo University, Cairo, Egypt

One of the major consequences of schistosomiasis is its impact on brain function, and despite its severity, the underlying mechanism(s) remain inadequately understood, highlighting a knowledge gap in the disease. The symptoms can vary from headaches to profound cognitive impairment. Besides, the potential influence of physical exercise in mitigating cognitive deficits has received little attention. In our study, we utilized a murine model of *Schistosoma mansoni* infection to investigate the cognitive impact of schistosomiasis. Our aims were multifaceted: to pinpoint the specific cognitive domains affected during the infection in adult mice, to unravel the complex interplay between glial and immune cells within the central nervous system (CNS), and crucially, to explore the potential therapeutic role of regular physical exercise in counteracting the deleterious effects of schistosomiasis on the CNS. Our findings unveiled that while acute infection did not disrupt simple and complex learning or spatial reference memory, it did induce significant deficits in recall memory—a critical aspect of cognitive function. Furthermore, our investigation unearthed profound alterations in the immune and glial cell populations within the CNS. Notably, we observed marked changes in $CD4^+$ T cells and eosinophils in the meninges, as well as alterations in glial cell dynamics within the hippocampus and other brain regions. These alterations were characterized by heightened microglial activation, diminished astrocyte reactivity and a shift towards a proinflammatory milieu within the CNS. We also provided insights into the transformative potential of regular moderate physical exercise in partially alleviating cognitive and neuroinflammatory consequences of schistosomiasis. Remarkably, exercise decreased glial cell production of TNFα, suggesting a shift towards a less pro-inflammatory environment. Collectively, our study provided compelling evidence of the intricate interplay between schistosomiasis infection and cognitive function,

underscoring the critical need for further exploration in this area. Furthermore, our findings demonstrated the positive effects of physical activities on mitigating the cognitive burden of schistosomiasis, offering new hope for patients afflicted by this debilitating disease.

KEYWORDS

shistosomiasis, morris water maze, neuroinfection, physical activities, *Schistosoma mansoni*

Introduction

Schistosomiasis is one of the most debilitating neglected tropical diseases, afflicting approximately 240 million individuals and resulting in around 280,000 deaths annually (1–3). Furthermore, it imposes a staggering burden of up to 4 million disability-adjusted life years (DALYs) (3). Schistosomiasis typically progresses from an acute phase characterized by non-specific symptoms like fever and muscle aches to a chronic phase where the worms reside in the host's blood vessels, leading to organ damage (3). The pathology of schistosomiasis stems from the systemic immune response triggered by the presence of eggs trapped within the tissues leading to granuloma formation (4). Although it is rare, schistosomiasis can be also directly involved in the brain and spinal cord, causing a condition known as neuroschistosomiasis. Despite being under-diagnosed, this form affects at least 2-5% of the 200 million individuals infected worldwide (5, 6) making it the second most common presentation of *S. mansoni* infection (7).

The systemic effects of *S. mansoni* infection on neurological function can develop at any stage of the disease (5, 6). The key pathologic feature is driven by schistosome eggs in the central nervous system (CNS) resulting in granulomatous formation. Over time, these granulomas can cause focal neurological damage. Some neurological symptoms may also occur due to systemic inflammatory responses to the parasitic infection, which can be secondary to the release of cytokines and other inflammatory mediators (5, 6). There are two main forms of neuroschistosomias which are cerebral and spinal. Cerebral schistosomiasis is mediated by *S. japonicum*, and rarely *S. mansoni*, whereby the frontal and parietal lobes are often affected. Symptoms may include seizures, headaches, focal neurologic deficits, and altered mental status. On the other hand, spinal schistosomiasis is more commonly associated with *S. mansoni* infection whereby the thoracic spinal cord is predominantly affected. The clinical presentation can include paraparesis, quadriparesis, back pain, sensory deficits, and bladder and bowel dysfunction (5, 6). Of note, schistosomiasis also negatively impacts cognitive function. Research indicates that children who are moderately to heavily infected with helminths tend to score lower on cognitive function tests and achieve less in education compared to children who are either uninfected or lightly infected (8, 9). A recent attempt to understand the underlying mechanism demonstrated that *S. mansoni* infection led to impairment of spatial learning and memory capacity. The phenotype was associated with enhanced microglia and astrocytes number and reactivity (10). This was however characterized in mice at the post-natal stage, leaving the mechanisms underlying the impact of schistosomiasis on the adult brain unclear. It is worth mentioning that murine models to study neuroschistosomiasis provides valuable insights due to their genetic tractability, allowing for the exploration of pathogen-host interactions and therapeutic strategies. However, one of the main limitations is the significant biological differences between murine and human hosts that may not fully recapitulate the complexity of human neurological involvement or the diverse clinical presentations seen in neuroschistosomiasis. Consequently, while murine studies can highlight potential mechanisms and treatments, they may always need translational validation directly on human patients.

Praziquantel is the mainstay drug for treating schistosomiasis. However, in cases of neuroschistosomiasis, its efficacy in reducing neurological symptoms is unclear, as the drug may not always effectively cross the blood-brain barrier (8). Corticosteroids are typically administered alongside praziquantel to reduce inflammation caused by the dying parasites (5, 6). However, corticosteroids carry significant side effects that can potentially harm the host, making the exploration of safe natural alternatives imperative. One such non-invasive approach known for its ability to downregulate immune response and confer protection against chronic inflammation is physical activities (PA) (11). Reports demonstrated that regular moderate exercise have protective and anti-inflammatory impacts, thereby enhancing CNS functionality (12). This is achieved through various pathways i) transient increase in IL-6 that drives the production of anti-inflammatory mediators IL-10 and Interleukin-1 receptor antagonist (IL-1RA), ii) stimulating the adrenal gland cortex and medulla to produce adrenaline and glucocorticoid, respectively, iii) reducing the expression of toll-like receptor on monocytes, and/or iv) diminishing the circulating number of pre-inflammatory monocytes. These pathways collectively contribute to the reduction of pro-inflammatory mediators and bolster the ability of immune cells within the CNS to adopt an anti-inflammatory phenotype (11, 12). Generation of the anti-inflammatory phenotype fosters neuroplasticity, neurogenesis, neuroprotection, and support hippocampus-mediated learning and memory (13, 14). The

question of whether PA can effectively mitigate the pro-inflammatory impact of schistosomiasis on the brain remains open and warrants further investigation.

In the present study, we aimed to 1) dissect the impact of *S. mansoni* infection on the specific learning and memory domains in adult mice, 2) characterize the cellular changes in CNS in response to schistosomiasis infection, and to 3) finally to evaluate the impact of PA in alleviating schistosomiasis-induced changes in the CNS.

Materials and methods

Animals

Wildtype mice on BALB/c background were used, ad all mice were maintained in specific-pathogen-free barrier conditions in individually ventilated cages at the University of Cape Town biosafety level 2 animal facility. Experimental mice were sex and age-matched and used at 8 weeks of age. All the experimental work was done in strict accordance with the recommendations of the South African national guidelines and of the University of Cape Town practice for laboratory animal procedures as in ethics protocols, 020-007, approved by the Animal Research Ethics Committee of the Faculty of Health Science, University of Cape Town. All efforts were made to minimize animal suffering. Upon reaching the study experimental endpoint and/or the protocol-defined humane endpoint, animals were euthanized under this study by exposure to an excess of Halothane (4% in air) for 5 minutes. Death was confirmed either by neck dislocation or exsanguination by cardiac puncture. Death was not a pre-determined endpoint in any of the arms of this study.

S. mansoni infection

Prior to percutaneous infection with *S. mansoni* cercariae, animals between 7 to 8 weeks age were anesthetized by intraperitoneal injection of a cocktail of Ketamine (100 mg/kg) and Xylazine (10 mg/kg) and monitored for 5 mins to confirm deep anesthesia. Anesthesia was confirmed by the absence of pedal reflex (toe pinch) and eyeblink reflex amid a regular respiratory rate. The anesthesia duration was of a maximum of 30 minutes. During the anesthesia phase, animals were exposed to an infra-red lamp to help them maintain their core body temperature. This procedure was performed and dully cared for by trained and authorized researchers. Then, mice were percutaneously infected via the abdomen, using stainless-steel rings, with 0 or 35 viable cercariae of a Puerto Rican strain of *S. mansoni* obtained from infected *Biomphalaria glabrata* snails (NMRI strain, NR-21962, provided by Biomedical Research Institute, Rockville, MD) for control or infected group, respectively. Post-infection, animals were monitored until regaining of consciousness and moistened food was added to the cage bedding.

Morris Water Maze

The Morris Water Maze (MWM) is a widely-used behavioral testing procedure designed to study spatial learning and memory in rodents, particularly rats and mice (15). The MWM task involved a training phase where mice performed four swim trials 1 min each per day (with 5 minutes interval between trials) for 4 consecutive days to locate a plexiglass circular platform (10cm in diameter), which was placed approximately 0.5 cm below the water level in an open circular 123cm diameter MWM. The water temperature was controlled using an automated water heater and made to equilibrate with the room temperature maintained at 20-24˚C. During the training phase of the task, each mouse was allowed a maximum of 60 seconds to locate and climb onto the platform. Once the mouse had located the platform, it was given approximately 10 seconds to remain on the platform. Mice that failed to locate the platform within 60 seconds were gently guided to the platform and allowed to acclimatize for 10 seconds before returning to the home cage. During this phase, the test was measuring learning memory and spatial cues. On the 5th day, a probe trial was performed with the platform removed in order to test reference memory (observations were based on the number of and latency to platform crossings). Each mouse was given a maximum of 60 seconds in the MWM to find and cross the platform location. On days 6 and 7, the platform is placed in the quadrant opposite the original training quadrant, and the mouse was retrained for four trials each day (i.e. 60sec swim with approximately 5mins interval x 4 trials). On day 8 mice were introduced to the pool with a visible platform in a third quadrant, placed approximately 0.5 cm above water level to test learning memory. All data was recorded using the EthoVision XT 8 automated tracking system (Noldus Information Technology, VA).

Experiments design

The MWM put mice to a swimming task for 8 consecutive days, hence right after day 8 of MWM we attribute potential biological effects to the immediate impact of physical activity. To evaluate the long-term effects of the initial physical activities on the animals, we repeated the MWM test at 11 weeks post-infection, during the chronic stage, to further examine any lasting impacts. Thus, our experimental design included physical activities as a factor, and infection status as another independent factor, generating 4 experimental groups: non-infected non-trained (NINT), non-infected trained (NIT), infected non-trained (INT), and infected trained (IT).

Eggs detection

Mice were euthanized at acute stage (8 weeks post-infection). Eggs were purified from KOH digested liver, ileum, and spinal cord and counted at 40x magnifications as previously described (16–18). The method for determining collagen production through

hydroxyproline content was conducted as outlined in reference (18). Briefly, liver samples of specific weight were hydrolyzed in 6 M hydrochloric acid at 110°C overnight, followed by filtration using Whatman filter papers. The resulting filtrate was then neutralized using 1% phenolphthalein and titrated with 10 M sodium hydroxide. A portion of this filtrate was combined with isopropanol and introduced to a solution of chloramine-T and citrate buffer (pH 6.0). To this mixture, Ehrlich's reagent (comprising 25 g of p-dimethyl-amino-benzaldehyde and 37.5 ml of 60% perchloric acid) was added. The absorbance was measured at 570 nm employing a VersaMax microplate spectrophotometer from Molecular Devices. The concentration of hydroxyproline was determined using a standard of 4-hydroxy-L-proline (Calbiochem, San Diego, CA, US) with the results being reported in micrograms of hydroxyproline per weight of liver tissue, which contained 10^4 eggs.

Physical exercise using Morris Water Maze

Cognitive function was assessed at the acute stage, 8 weeks post-infection, using the Morris Water Maze (MWM) task for 8 consecutive days to verify the immediate impact of exercise. To evaluate the long-term effects of the initial exercise on the animals, we repeated the Morris Water Maze (MWM) test at 11 weeks post-infection, during the chronic stage, to further examine any lasting impacts. using Morris Water Maze (MWM) platform for 8 consecutive days. MWM is a widely-used behavioral testing procedure designed to study spatial learning and memory in rodents, particularly rats and mice (15). The MWM task involved a training phase During the training phase, where mice were given performed four swim trials per day (with 5 minutes interval between trials) for 4 consecutive days to locate a plexiglass circular platform (10cm in diameter), which was placed approximately 0.5 cm below the water level in an open circular 123cm diameter MWM. The water temperature normally was controlled using an automated water heater and made to equilibrate with the room temperature maintained at 20-24˚C. During the training phase of the task, each mouse was allowed a maximum of 60 seconds to locate and climb onto the platform. Once the mouse has had located the platform, it was given approximately 10 seconds to remain on the platform. Mice that failed to locate the platform within 60 seconds were gently guided to the platform and allowed to acclimatize for 10 seconds before returning to the home cage. During this phase, the test help in measuring learning memory and spatial cues On the 5th day, a probe trial was performed with the platform removed in order to test reference memory (observations were based on helped in measuring learning memory and spatial cues. On the 5th day, a probe trial was performed with the platform removed in order to test reference memory (observations were based on the number of and latency to platform crossings). Each mouse was given a maximum of 60 seconds in the MWM to find and cross the platform location. On days 6 and 7, the platform is placed in the quadrant opposite the original training quadrant, and the mouse was retrained for four trials each day (i.e 60sec swim with approximately 5mins interval x 4 trials). On day 8 mice were introduced to the pool with a visible platform in a third quadrant, placed approximately 0.5 cm above water level to test learning memory. All data will be recorded using the EthoVision XT 8 automated tracking system (Noldus Information Technology, VA).

Intestinal contractility

A measure of schistosomiasis infection was conducted 8 weeks post-infection. After euthanizing the mice, Approximately 1 cm of jejunum segments were removed from the small intestine of all groups. The smooth muscle contractile responses were measured using a water-jacketed organ bath (Panlab, Spain), connected to transducers and the PowerLabTM system (ADInstruments, Australia). This setup feeds and translates the signals to a computer for measuring tissue isometric tensions. The tissues were weighed on an analytical scale before being stimulated with varying concentrations of ACh (−9 to −3 LOG [M]) to determine the isometric contractile responses.

Cells isolation

One day after MWM, animals were euthanized and perfused thoroughly with ice-cold PBS (pH 7.4) for 5 minutes. Following perfusion, heads were removed, and skulls were cleared of all tissue. Surgical scissors were utilized to sequentially remove the tops of the skulls in a clockwise manner. Subsequently, the skulls were promptly placed in ice-cold RPMI media. Meninges were meticulously extracted from the interior surfaces of the skulls and the brain surfaces using forceps (19). The hippocampus and prefrontal cortex were then separated from the brain parenchyma using surgical forceps. Part of hippocampus and prefrontal cortex was used for histology while the rest was used for single cell suspension. Single-cell suspensions from the meninges, hippocampus, and prefrontal cortex were prepared through enzymatic digestion in RPMI containing 220 U/mg Collagenase IV (Gibco, Waltham, Massachusetts), 13 U/mg DNase I (Sigma, St. Louis, Missouri), and 5% iFCS (inactivated fetal calf serum) (Gibco) in RPMI supplemented with 2mM MgCl2, 2mM CaCl2, 20% FBS, and 2 mM HEPES. The digested tissue was mechanically disrupted, filtered through a 100µm mesh, and then enriched for leukocytes by centrifugation (600 g, 10 minutes, no brakes) through 40% Percoll (Merck) (20).

Flow cytometry

Antibodies used for flow cytometry analysis were as follows: CD3ε (500A2), CD4 (RM4-5), CD8α (53-6.7), CD19 (1D3), CD44 (IM7), CD62L (MEL-14), IFN-γ (XMG1.2), IL-4 (11B11), IL-13 (eBio13A), TNFα, CXCR5, CD11b, SiglecF, NK1.1, CD45, F4/80, MHC II, PD1, and GFAP purchased from BD Biosciences (Franklin Lakes, New Jersey) and eBioscience (San Diego, California). For staining of cell surface markers, cells (1 x 10^6) were labeled and washed in PBS containing 1% BSA (Roche, Switzerland) and 0.1% NAN_3 (FACS buffer). For detection of intracellular cytokines, cells

were seeded at a density of 2 x 10^6 cells/well in a complete RPMI culture medium and stimulated with 50 ng/ml phorbol myristate acetate (PMA), 250 ng/ml ionomycin and 200 µM monensin (all from Sigma) for 8-12 hr at 37°C in a humidified atmosphere containing 5% CO_2. After the incubation period, cells were harvested, washed, fixed in 2% (w/v) paraformaldehyde, permeabilized with 0.5% saponin buffer, and then stained for cytokine production as previously described (17, 18). The acquisition was performed using BD LSRFortessa (BD Biosciences), and data were analyzed using FlowJo software (Treestar, Ashland, Oregon). Uniform Manifold Approximation and Projection (UMAP) was used for data visualization. It is a nonlinear dimensionality-reduction technique (21) available as a FlowJo plugin.

Quantitative real-time RT-PCR

RNA from parenchyma single cell suspension was reverse transcribed by Transcriptor First Strand cDNA Synthesis Kit (Roche) according to manufacturer's instructions. Real-time reverse transcribed PCR (QRT-PCR) was performed with LightCycler 480 SYBR Green I Master mix in LightCycler 480 II (Roche) and gene-specific primers (IDT, CA, USA). Fold change in gene expression was calculated by the ΔΔCt method and normalized to *Hprt1* which was used as internal control as described (22).

The primers used are as follow (Table 1):

TABLE 1 The primers used in qPCR.

No	Gene	Direction	Sequences
1	HPRT	Forward	5'– GTT GGA TAT GCC CTT GAC – 3'
		Reverse	5'– AGG ACT AGA ACA CCT GCT – 3'
2	Muscarinic M5	Forward	5' – CTC TGC TGG CAG TAC TTG GTC – 3'
		Reverse	5' – GTG AGC CGG TTT TCT CTT CTT – 3'
3	Muscarinic M2	Forward	5' – TGA AAA CAC GGT TTC CAC TTC – 3'
		Reverse	5' – GAT GGA GGA GGC TTC TTT TTG – 3'
4	Muscarinic M 1	Forward	5' – GGA CAA CAA CAC CAG AGG AGA – 3'
		Reverse	5' – CGA GGT CAC TTT AGG GTA GGG – 3'
5	IL-4	Forward	5' –TCG GCA TTT TGA ACG AGG TC– 3'
		Reverse	5' – GAA AAG CCC GAA AGA GTC TC– 3'
6	IL-6	Forward	5' – CGT GGA AAT GAG AAA AGA GTT GTG– 3'
7	IL-13	Forward	5' – CTC CCT CTG ACC CTT AAG GAG – 3'
		Reverse	5' – GAA GGG GCC GTG GCG AAA CAG – 3'
8	CCL2	Forward	5' – CTC TCT CTT CCT CCA CCA CCA T – 3'
		Reverse	5' – TGG GGC GTT AAC TGC ATC TG – 3'
9	TNFα	Forward	5' – TCT CAT CAG TTC TAT GGC CC – 3'
		Reverse	5' – GGG AGT AGA CAA GGT ACA AC– 3'

(Continued)

TABLE 1 Continued

Tissue homogenate for cytokine analysis

Brain parenchyma (hippocampus and prefrontal cortex) was collected and homogenized in RIPA buffer. Cytokines (TNFα, IL-6, and MCP all from BD Pharmingen) were measured in the protein extracts by sandwich ELISA as described previously (17, 18). Cytokine values were normalized according to the protein content measured by Pierce BCA Protein Assay Kit (Thermo Fisher Scientific, catalogue no. 23225).

Immunofluorescence

First, mice were anesthetized using isoflurane and perfused with ice-cold PBS and 4% paraformaldehyde (PFA) through the heart. Next, free-floating coronal sections from the brain or spinal cord were sectioned at 30 µm using a Leica cryostat. The sections were then immersed in a blocking solution consisting of PBS with 2% Normal Goat Serum, 1% BSA, 1% Triton-X, 0.05% Tween-20, and 0.05% sodium azide for 1 hour at room temperature. The sections were subsequently incubated overnight at 4°C with primary antibodies, including rabbit anti-Ach (Abcam), rabbit anti-Iba1 (Abcam) at a concentration of 1:500 and 1:400, and rabbit anti-Iba1(Abcam), at a concentration of 1:500 and 1:400, respectively. After washing the sections with PBS, they were incubated with fluorophore-conjugated secondary antibodies at a dilution of 1:400 for 2 hours. Finally, the sections were stained with DAPI at a concentration of 10 µg/ml for 10 minutes at room temperature, mounted on glass slides using moviol and antifade mounting medium from Thermo Fisher Scientific.

Immunohistochemistry

Brain or spinal cord tissue was sectioned at a thickness of 9 µm using OCT compound and a cryostat. The sections were mounted on glass slides and dried for 2 hours. Following this, the slides were

stained in 0.1% cresyl violet solution for 5 minutes, then rinsed with running distilled water. The sections were further dehydrated using graded alcohols, cleared in xylene, and finally mounted with antifade medium (Mowiol).

Statistics

Statistical analysis was conducted using GraphPad Prism 6 software and SPSS 20. Data were calculated as mean ± SEM. Statistical significance was determined using the unpaired Student's t-test and One-Way ANOVA with Bonferroni's post-test after testing for normality and homogeneity in one category independent data. Two-way ANOVA was used to compare two categorical independent variables (infection and PA), and also the interaction between them, defining differences to uninfected mice as significant (*, $P \leq 0.05$; **, $P \leq 0.01$; ***, $P \leq 0.001$). Two-way ANOVA was also employed to examine the interaction effects of infection and training, enabling an understanding of both the separate and combined effects of these factors. This comprehensive approach provided a nuanced understanding of the collective impact of infection and training on experimental outcomes.

Results

Acute schistosomiasis causes recall memory impairment

In order to understand how systemic Schistosomiasis infection may affect the brain function, especially the behavior, we conducted MWM test at the acute stage (8 weeks post-infection to assess cognitive abilities.

The MWM analysis revealed some key findings. Firstly, *S. mansoni* infection did not significantly alter locomotor activity, as shown by the consistent distance moved (Figure 1A). Similarly, velocity measurements (Figure 1B) indicated no signs of anxiety-like behavior. Furthermore, there were no significant differences in immobility time (Figure 1C), center-moving duration (Figure 1D), or immobility time ratio (Figure 1E), suggesting the absence of any phenotypes-like behavior in infected mice.

Both infected and non-infected mice demonstrated comparable spatial learning abilities, with a similar reduction in the time taken to reach the platform across learning sessions (Figure 1F). To further assess spatial reference memory, a probe test was performed 24 hours after the last learning trial. No significant differences were observed between the groups in time spent in the platform's quadrant (Figure 1Gi), latency to cross the platform area (Figure 1Gii), or the number of platform crossings (Figure 1Giii), indicating that spatial memory remained intact in infected mice after 8 weeks post infection.

However, during the reversal trial, when the platform was relocated to a different quadrant, infected mice displayed a significant increase in latency to find the platform on day 8 compared to controls (Figure 1H). Additionally, infected mice spent more time in the arena (Figure 1I), although the distance they travelled remained similar to that of non-infected mice (Figure 1J). These results suggest that while complex learning abilities were not impaired, schistosomiasis infection negatively impacted recall memory.

To our knowledge, this is the first study to dissect cognitive behavior in this context and shed light on the impact of schistosomiasis on recall system rather than the entire cognitive outcomes.

Impact of physical activities on peripheral and CNS responses following schistosomiasis infection

Research shows that schistosomiasis infection harms intestinal function by causing inflammation and fibrosis, which disrupt normal muscle contractions needed for gut movement. When parasite eggs lodge in intestinal tissues, they trigger immune responses that lead to chronic inflammation, tissue damage, and changes in muscle activity, impairing digestion and nutrient absorption. In our study, we specifically looked at how physical activity (PA) impacts intestinal contractility after infection. Surprisingly, despite infection, the hypercontractility of the intestine was similar between non-infected, non-trained (NINT) and infected, non-trained (INT) groups (Supplementary Figure S1A). These results suggest that at this stage of infection, the presence of parasite eggs may not significantly alter muscle contractility. However, as noted in other studies, exercise slightly increased hypercontractility in both non-infected trained (NIT) and infected trained (IT) groups (Supplementary Figure S1A). While increased intestinal contractility can enhance gut motility and digestion, the implications of this change in the context of infection warrant further investigation.

Considering the potential link between enhanced intestine contractility and the expulsion of schistosomiasis eggs (23), we examined the effects of PA on egg burden and egg-driven immunopathology. Unexpectedly, our findings indicated that PA led to an increase in egg burden in the liver (Supplementary Figure S1B) and small intestine (Supplementary Figure S1C) in the IT group compared to the INT group. Furthermore, histopathological analysis revealed that training exacerbated liver granuloma size (Supplementary Figures S1F, G) and increased tissue fibrosis in the liver (Supplementary Figure S1H). These unexpected outcomes underscore the intricate relationship between PA and schistosomiasis progression, necessitating further exploration to unravel underlying mechanisms and potential implications for disease management.

In our investigation of egg infiltration in the central nervous system (CNS), specifically the spinal cord and brain parenchyma, histological assessments yielded noteworthy results. As we expected, there was a lack of egg infiltration in the spinal cord (Supplementary

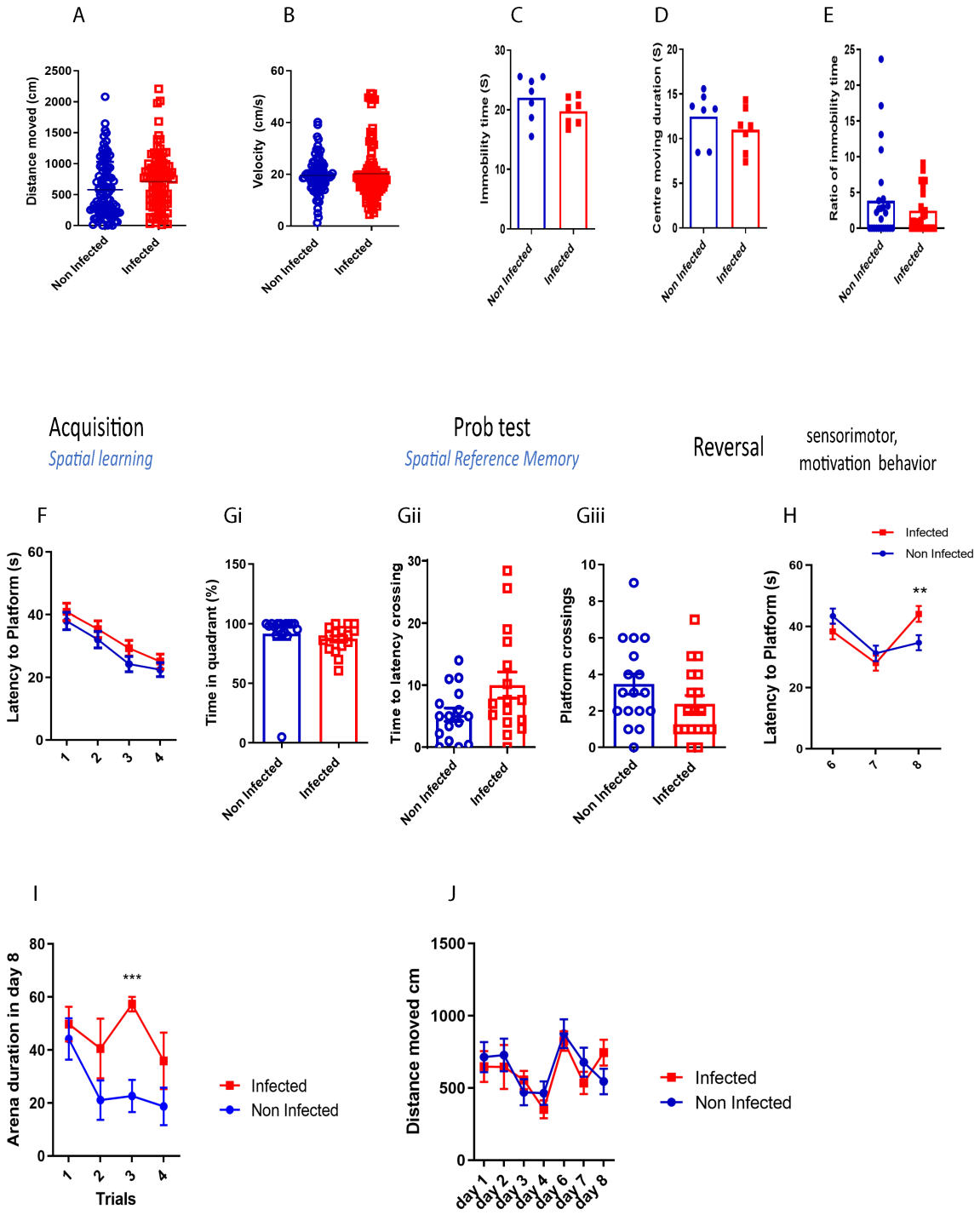

FIGURE 1
Acute schistosomiasis infection can impair recall memory. **(A)** Distance moved by the mice in MWM, **(B)** the villosity, **(C)** Immubility time, **(D)** Centre moving duration, **(E)** Ratio of immobility time, **(F)** Spatial learning was assessed during the first four days whereby latency to platform was assessed. A probe test was then done on day 5, and **(Gi)** the time percentage spent in the right training quadrant, **(Gii)** the latency to cross the virtual platform, and **(Gii)** the number of times the mice crossed the platform were recorded. **(H)** Reversal trial was then performed from day 6 to day 8 and the latency to the new platform was measured. **(I)** Duration spent on the arena during each trial on day 8. **(J)** Distance travelled in each day. Results are pooled from two different experiments with 6-8 mice per group. Data are expressed as mean ± S.E.M. NS, P > 0.05; *$P < 0.05$, ** $P < 0.001$, ***$P < 0.0001$ by two-tailed unpaired *Student t* test and repeated measures ANOVA.

Figures S2A, B) and brain parenchyma, particularly in the prefrontal cortex (PFC) and hippocampus (HPC), for both the infected non-trained (INT) and infected trained (IT) groups (Figure 2A).

Our study found that while schistosomiasis infection and PA did not affect intestinal muscle contractility in non-trained infected groups. Exercise increased egg burden in the liver and intestines, worsened liver granuloma size, and increased fibrosis,

highlighting a complex interaction between PA and infection progression.

Impact of schistosomiasis infection and physical activity on cholinergic system and cytokine expression in the nervous system

We next analyzed the impact of schistosomiasis infection and its interaction with PA on the cholinergic system. In spinal cord, the number of cells producing acetylcholine (ACh) showed a significant increase in the INT group compared to the NINT group (Supplementary Figures S2Ci-C). This indicated that schistosomiasis infection affected ACh production in the spinal cord. However, PA in the IT group restored ACh production to the baseline level, suggesting that exercise could mitigate the impact of infection on ACh production (Supplementary Figures S2C-Ci). On other hand, the expression of muscarinic receptors (*M1*, *M2*, and *M5*) (Figures 2Fi-Fiii) was examined in the HPC and PFC (Supplementary Figures S2Diii, Dvi). In the hippocampus, M1, M2, and M5 expression levels were remarkably increased in the INT group compared to the NINT group. However, M5 was the only receptor to decrease significantly in the IT group with PA, and statistical analysis showed a significant interaction effect. This suggests that while M1 and M2 are generally upregulated with infection, M5 expression may be uniquely modulated by the combination of infection and PA. For PFC, no change was noted in either *Ccl2*, *Il13*, *Il4*, *M1*, *M2*, *or M5* expression between the different groups Supplementary Figures S2Di, Dvi.

We further characterized cytokine expression in brain parenchyma. Significant effect was observed in the expression of TNFα in the HPC, with PA modulating its impact on *tnfα* expression dependent on infection presence (Figure 2Di). PA restored *tnfα* expression to baseline levels compared to the INT group (Figure 2Di). Similar, but not significant, *tnfα* trend was noted between the different groups (Figure 2Dii).

For *Il6*, the INT group exhibited a significant elevation in *Il6* expression compared to the NINT group in HPC (Figure 2Diii) and PFC (Figure 2Ei). However, PA did not significantly alter *Il6* expression. Training of the infected mice helped in partially restoring *Il6* expression (Figures 2Diii, Ei). Similar to *Il6*, the INT group showed a significant increase in *Il4* expression compared to the NINT group (Figure 2Dvi), and PA did not have a significant impact on *Il4* expression.

Analyzing the expression of *Ccl2* (Figure 2Div) and *Il13* (Figure 2Dv), no significant differences were observed between the INT, NINT, and NIT groups. However, it was worth noting that PA in the infected group significantly enhanced *Il13* expression compared to the rest (Figure 2Dv). In summary, Muscarinic receptors, particularly the M2 subtype, can modulate inflammation by inhibiting pro-inflammatory cytokines like TNFα and IL-6. Conversely, elevated cytokines can alter muscarinic receptor expression and function, impacting neuroinflammation and cognitive processes. This reciprocal relationship suggests that schistosomiasis-induced cytokine changes may influence muscarinic receptor activity, affecting neuroinflammatory responses and brain function.

Physical activities helps reduce the impact of schistosomiasis on microglia and myeloid cell phenotypes in the brain

In the prefrontal cortex, PA's impact on cell numbers depended on the presence of infection (Figures 2B, 2Ci), with infection and PA independently influencing microglia accumulation (Figures 2B, 2Ci). Moreover, the INT group exhibited higher cell numbers compared to the non-infected trained (NIT) and non-infected non-trained (NINT) groups (Figures 2B, 2Ci).

The occupied area or cell distribution in the PFC revealed significant interaction effects, indicating the dependency of PAs impact on infection presence (Figure 2Cii). Additionally, main effects of PA and infection were observed, influencing the occupied area independently (Figure 2Cii). The INT group had a reduced occupied area compared to the NIT and IT groups (Figure 2Cii). Microglia in the HPC were not significantly affected by infection or PA (Figures 2Ciii, Civ), indicating the resilience of this cell population to the experimental conditions. Next, we delved into the impact of schistosomiasis infection in brain cells parenchyma using flow cytometry (Figures 3A, Bii). The findings revealed a significant increase in microglia frequency (Figure 3Aiii), TNFα production (Figures 3Ai, Aii), and activation status, marked by higher MHC class II (MHCII) expression (Figure 3Aiii) in HPC in response to schistosomiasis infection compared to the NINT group. In contrast, PA had no effect on microglia activation level in infected animals (Figure 3Aiv).Notably, a statistical analysis highlighted a significant interaction effect between the infection and training for TNFα production in the HPC (Figures 3Ai, Aii),. Of interest, and consistent with our previous observation (Figure 2Di), PA in IT group restored TNFα production to a level similar to NINT and NIT groups. Furthermore, PA did not impact microglia MHCII expression or the production of IL-4 or IL-13 in the HPC (Figures 3iii, Aiv). In the PFC comparable microglia frequency (Figures 3Bii, Biii), activation (Figure 3Biv), and TNFα production (Figures 3B, Bi) were observed in response to schistosomiasis infection and/or PA. Statistical analysis did not reveal significant effects on TNFα production in the PFC (Figure 3Bi).

Considering the anticipated type 2 immune response induced by *S. mansoni* infection, we examined microglia's production of IL-4 and IL-13. Surprisingly, infected non-trained animals produced similar levels of IL-4 and IL-13 in the HPC compared with the non-infected group (Figure 3Aiii). In the PFC, while no significant change in IL-4 production was noted, the INT group exhibited a notable reduction in IL-13 production (Figure 3Biii). After PA, no noticeable differences in IL-4 or IL-13 production by microglia in the PFC were observed in the IT group compared to the NIT group (Figure 3Biv).

For myeloid cell subsets, there were similar frequency of monocytes and eosinophils before (Supplementary Figure S3Ci)

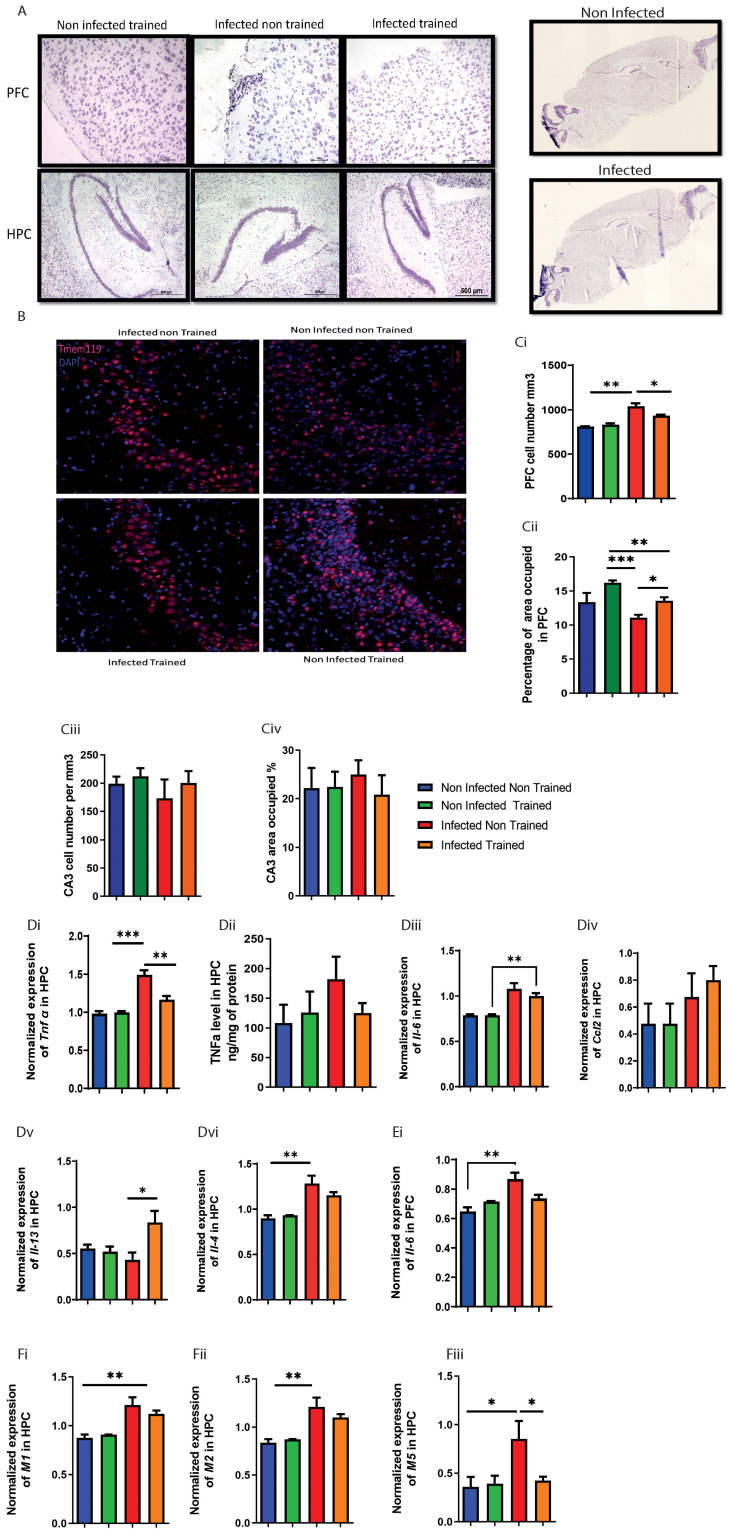

FIGURE 2
Impact of schistosomiasis infection and/or physical activities on brain parenchyma. **(A)** Eggs infiltration in prefrontal cortex (upper row) and hippocampus (lower row) was assessed using H&E staining (original magnification 500um). **(B)** Immunofluorescence staining of CA3 area in hippocampus to to show Tmem 119 positive cells area occupied 50um, (the quantification of cell presence within a defined spatial with 50um dept, specifically calculated as the number of cells per cubic millimeter (mm^3) **(Ci)** Total cell number in mm^2 and **(Cii)** area occupied in prefrontal cortex. **(Ciii)** Total cell number in mm^2 and **(Civ)** area occupied in hippocampus. **(Di)** *Tnfa* mRNA expression relative to HPRT housekeeping gene determined using qRT-PCR from hippocampus. **(Dii)** TNFα concentration in hippocampus homogenate using ELISA. mRNA expression level of **(Diii)** *Il6*, **(Div)** *Ccl2*, **(Dv)** *Il13*, and **(Dvi)** *Il4* relative to HPRT housekeeping gene determined using qRT-PCR in hippocampus. mRNA expression level of **(Ei)** *Il6* relative to HPRT housekeeping gene determined using qRT-PCR in prefrontal cortex. Muscarinic receptors expression was assessed using qPCR, mRNA expression level of **(Fi)** *M1*, **(Fii)** *M2*, and **(Fiii)** *M5* relative to HPRT housekeeping gene determined using qRT-PCR in hippocampus. Results are pooled from two different experiments with 6-8 mice per group. Data are expressed as mean ± S.E.M. NS, $P > 0.05$; $^{*}P < 0.05$, $^{**}P < 0.001$, $^{***}P < 0.0001$ by two-way ANOVA followed by Bonferroni.

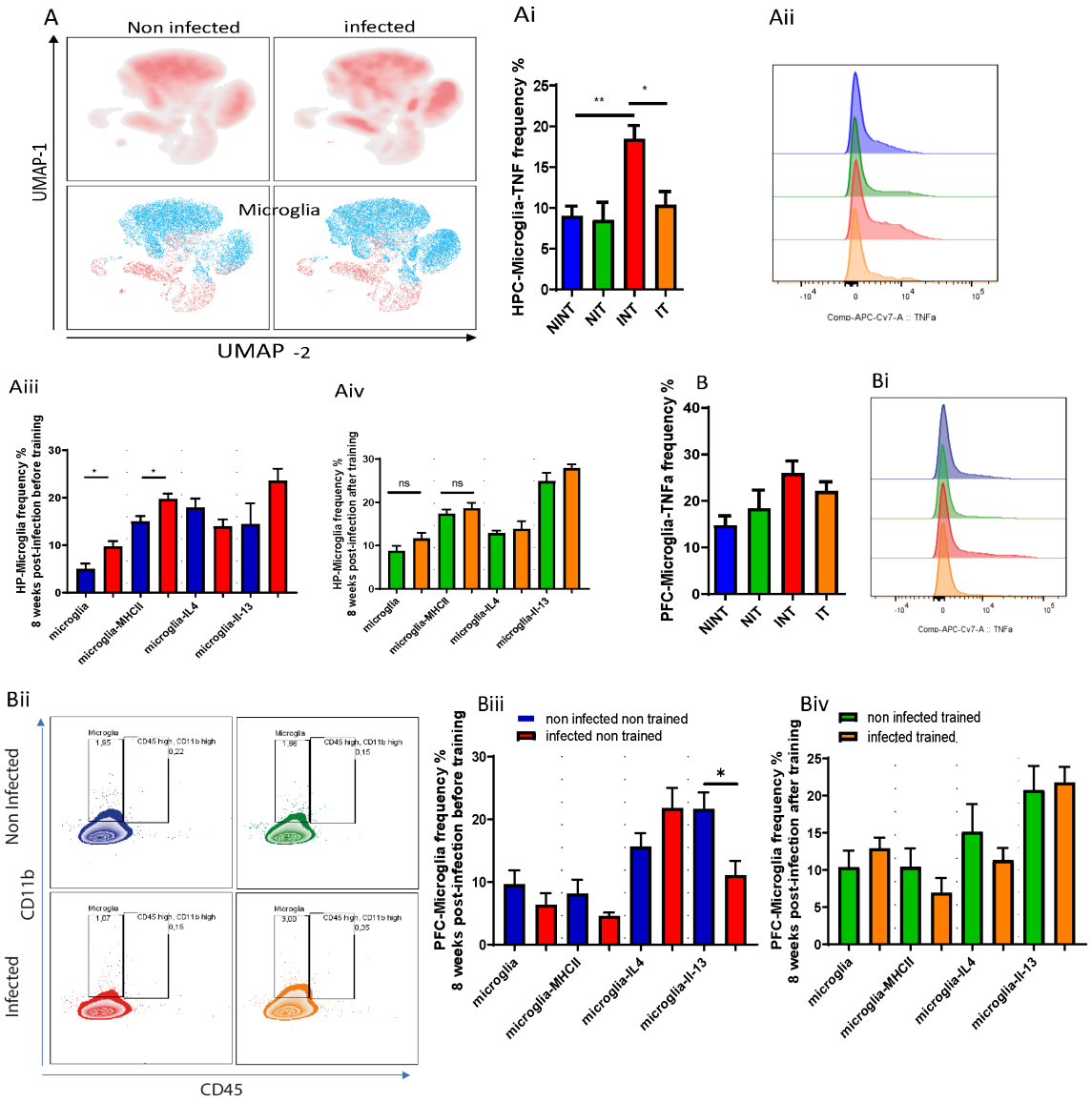

FIGURE 3
The impact of schistosomiasis infection and/or physical activities on microglia and myeloid cells phenotype. Wildtype BALB/c mice were infected with 0 or 35 *S. mansoni* cercariae and then euthanized 8 weeks post-infection and different brain regions were collected for characterization using flow cytometry. **(A)** UMAP visulaization of Microglia in hippocampus (HPC) using flow cytometry. **(Ai)** Frequency of microglia producing TNFα in hippocampus. **(Aii)** TNFα expression by microglia depicted in **(Aii)**. **(Aiii)** microglia frequency, MHC class II expression, IL-4, and IL-13 production before and after PA in hippocampus **(Aiv)**. Frequency of microglia producing TNFα in prefrontal cortex **(B)**. TNFα expression by microglia depicted in **(Bi, Bii)** Representative flow cytometry of microglia and $CD45^+$ $CD11b^+$ population. **(Biii)** microglia frequency, MHC class II expression, IL-4, and IL-3 production before and after PA in prefrontal cortex **(Biii, Biv)**. Results are pooled from two different experiments with 6-8 mice per group. Data are expressed as mean ± S.E.M. NS, $P > 0.05$; $^*P < 0.05$, $^{**}P < 0.001$ by two-way ANOVA followed by Bonferroni or non-parametric test after testing the homogeneity and normality.

and after PA (Supplementary Figure S3Cii) of *S. mansoni* infected animals compared with non-infected controls in HPC and PFC. We also noted comparable frequency of $CD11b^+$ cells (Supplementary Figure S3A, B) and their production of IL-4 (Supplementary Figures S3Aiii, Biii) and IL-13 (Supplementary Figures S3Aiv, Biv) in HPC and PFC, respectively, in NINT, INT and IT groups. to summarize this part, our results suggest that while schistosomiasis infection did not significantly impact the $CD11b^+$ cell phenotype, it did enhance microglia polarization towards an microglia producing TNFα phenotype, particularly in the hippocampus. Importantly, PA might play a role in mitigating microglia adoption of the microglia producing TNFα phenotype by restoring TNFα production to baseline levels. These findings underscore the potential influence of PA in modulating microglia response in the context of schistosomiasis infection and emphasize the need for further investigation into the underlying mechanisms and implications for disease progression.

Impact of schistosomiasis and training on astrocytes phenotype

Expanding our examination to include other glial cells, specifically astrocytes-GFAP+ cells, we probed into their activity, antigen presentation capacity, and cytokine production in response to schistosomiasis infection.

GFAP-positive astrocytes are generally associated with functions like forming glial scars, modulating inflammation, and protecting surrounding neural tissue.

To understand the changed happening in GFAP+Astrocytes, we measured GFAP expression (Figure 4A). Surprisingly, our results revealed a reduction in GFAP expression due to *S. mansoni* infection in the infected non-trained (INT) compared to non-infected non-trained (NINT) group (Figure 4Bi). Additionally, PA did not alter astrocyte reactivity, with the IT group showing similar GFAP expression compared to the NIT group (Figure 4Bii).

Furthermore, our results indicated that schistosomiasis infection and/or PA led to a significant reduction in astrocyte antigen presentation capacity, marked by lower MHCII expression (Figures 4Bi, Bii). The statistical analysis revealed a significant interaction effect, emphasizing the interdependence of infection and PA on astrocyte antigen presentation capacity (Figures 4Bi, Bii. However, no significant main effects of PA or infection alone on MHCII expression were observed. These changes may signify a loss of GFAP+ astrocytes that maybe responsible for modulating the inflammation or protecting the neural tissue induced by infection. Importantly, there were no significant alterations in the production of type 2 cytokines, namely IL-4 and IL-13, between the INT and NINT groups (Figure 4Bi) or between the NIT and IT groups (Figure 4Bii). Of particular note, PA exerted a positive influence on astrocyte production of TNFα compared to the NINT control group. Similarly, schistosomiasis infection induced a significant increase in TNFα production by astrocytes, which returned to baseline levels after training. These compelling

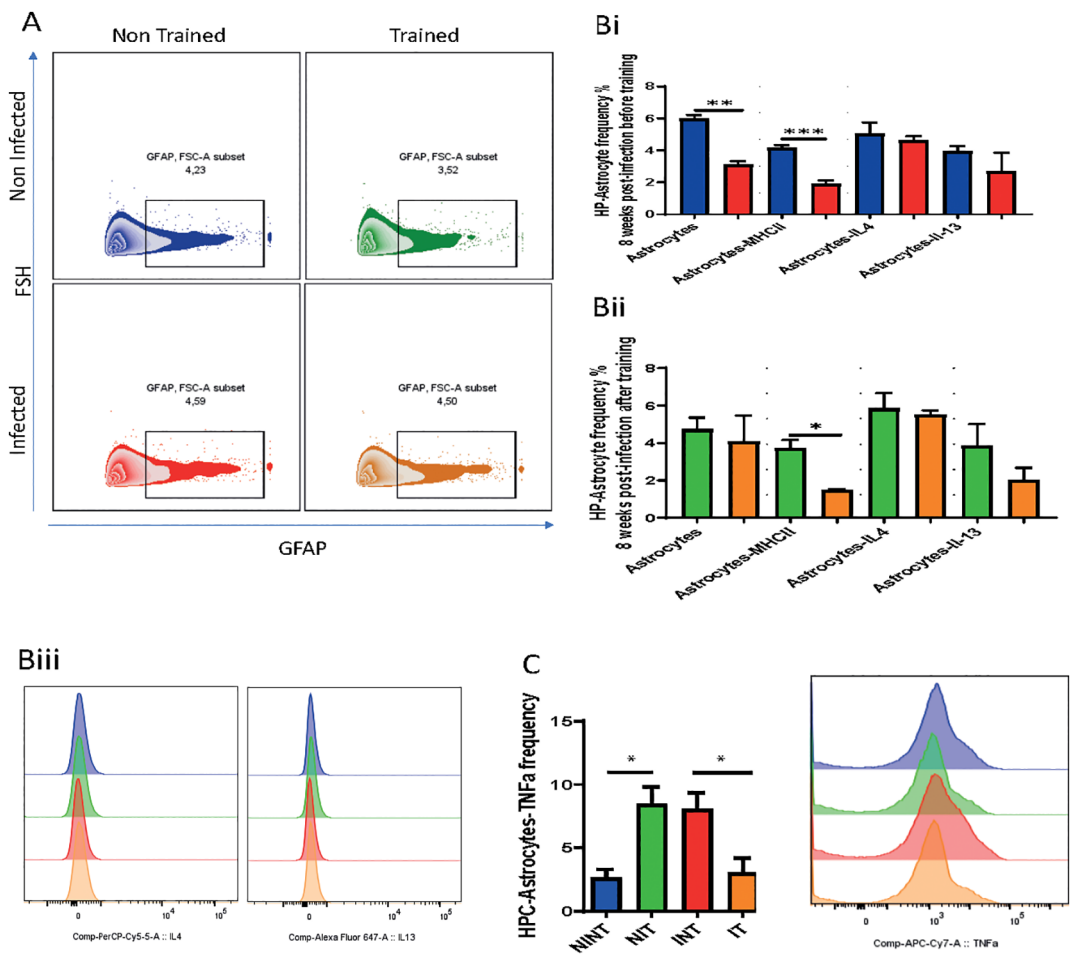

FIGURE 4
Impact of schistosomiasis infection and/or physical activities on astrocyte phenotype. **(A)** Representative flow cytometry of GFAP$^+$ astrocytes in hippocampus. **(Bi)** Frequency of GFAP$^+$ astrocytes, MHC class II expression, and astrocytes producing IL-4 and IL-13 before and **(Bii)** after training. **(Biii)** IL-4 (left) and IL-13 (right) expression by astrocytes depicted in **(Bi, Bii)**. **(C)** Frequency of astrocytes producing TNFα assessed using flow cytometry. Results are pooled from two different experiments with 6-8 mice per group. Data are expressed as mean ± S.E.M. NS, $P > 0.05$; $^*P < 0.05$, $^{**}P < 0.001$, $^{***}P < 0.0001$ by two-way ANOVA followed by Bonferroni.

findings highlight that, akin to microglia, PA effectively restored TNFα production by astrocytes to baseline levels post-*S. mansoni* infection. We can conclude that, our investigation into GFAP + astrocyte responses underlined the intricate dynamics influenced by schistosomiasis infection and PA. The restoration of TNFα production emphasizes the potential of exercise to modulate astrocyte GFAP+, offering valuable insights into the broader implications for disease progression and therapeutic strategies. In here, It's important to note that *GFAP* does not capture the full diversity of astrocyte subtypes and states, such as those involved in metabolic support, neurotransmitter regulation, or synaptic modulation. Thus additional study should be conducted.

Schistosomiasis infection alters meningeal lymphocyte composition

In our pursuit to characterize the influence of schistosomiasis infection on meningeal lymphocyte composition, we employed flow cytometry to phenotype lymphoid and myeloid cell subsets in the meninges of both non-infected and schistosomiasis-infected mice, both before and after PA. Examining T cell subsets (Figure 5A), we noted that while a similar frequency of naïve $CD4^+$ T cells in the meninges upon *S. mansoni* infection (Figure 5Bi), the infection led to a significant increase in the frequency of effector T cells (TEM, Figure 5Bii). This effect was influenced by PA,. Additionally, infection alone had a significant effect on both TEM and central memory T cell (TCM) subsets (Figures 5Bii, Biii), highlighting an increase in these T cell subsets in the meninges. However, PA alone did not significantly affect the frequency of TEM or TCM $CD4^+$ T cell subsets.

Further characterization of the $CD4^+$ T cell population in the meninges revealed higher PD1 expression, indicating T cell exhaustion (Figure 5Biv). While PA alone did not significantly impact PD1 expression, it effectively countered the schistosomiasis-induced alteration of CD4+ T cell populations. PA reduced the frequency of TEM $CD4^+$ T populations without affecting other subpopulations or PD1 expression compared to the infected (INT) group (Figures 5Bi-Biv).

Analyzing the $CD8^+$ T cell population, schistosomiasis infection led to a significant increase in the naïve $CD8^+$ T cell population (Figure 5Ci). The impact of training on the frequency of naïve $CD8^+$ T cells was influenced by schistosomiasis infection, as indicated by a significant interaction. Notably, PA did not alter the frequency of $CD8^+$ T cell subsets (naïve, TEM, and TCM) compared to the training group (Figures 5Ci-Ciii). Moreover, PA helped in partially restoring the basal frequency of naïve CD8 (Figure 5Ci) and TEM-CD8 (Figure 5Cii) subsets, demonstrating its beneficial impact on these subsets in the meninges after infections. Additionally, PA reduced $CD8^+$ T cell exhaustion, indicated by decreased PD1 expression (Figure 5Civ),.

Further analyses unveiled a significant interaction between PA and infection in the eosinophil population, emphasizing the positive influence of training in mitigating the increase in eosinophils induced by schistosomiasis infection (Figure 5D). Additionally, wide-screen analyses demonstrated an increase in various markers (CD62L, CXCR5, SiglecF, CD44, CD45) in response to *S. mansoni* infection, which was reduced through PA in the IT group compared to the INT group (Supplementary Figure S4). Furthermore, no significant changes were observed in the $CD19^+$ B cell population (Figure 5E) or $NK1.1^+$ cell population (Figure 5F) in the meninges of INT compared to NINT group.

In the brain parenchyma, particularly the HPC, schistosomiasis infection did not induce major changes in lymphoid cell populations. However, PA had a notable impact, enhancing the $CD4^+$ T cell (Figure 5G) and $CD19^+$ B cell populations (Figure 5I). Interestingly, the increase in the $CD4^+$ T cell population was not driven by the central memory T cell (TCM) population, which was downregulated before and after schistosomiasis infection (Figure 5H) but possibly through another T cell subset like TEM. Moreover, an increase in the hippocampus CD 19 $^+$ cell population was observed in the *S. mansoni* infection group after PA (IT) compared to the INT group (Figure 5I), this increase is not related to the infection but is related to the benefit impact of PA on hippocampus.

In conclusion, our data illustrate the nuanced effects of schistosomiasis infection and PA on lymphoid and myeloid populations in the meninges and brain parenchyma. PA emerges as a potential mitigator of infection-induced changes in these populations, providing valuable insights into the intricate interplay between PA and immune responses in the context of schistosomiasis.

Discussion

Schistosomiasis infection correlated with diminished cognitive performance, particularly evident in school-aged children afflicted with heavy or moderate infections, leading to educational, learning, and memory deficits (24, 25). Both the specific cognitive domain affected and the mechanism underlying its pathogenesis is incompletely understood. The current therapeutic approaches carry a lot of side effects, thereby finding a natural alternative is imperative. Whether PA may help in alleviating these consequences is an open question that yet to be explored. In our study, we investigated the effects of schistosomiasis infection on cognitive function in adult mice, delved into the cellular-level alterations in the CNS during the acute stage of infection, and evaluated the potential benefits of PA in mitigating schistosomiasis-induced systemic inflammation on CNS. First, our findings revealed that during the acute infection in adult mice, schistosomiasis infection did not significantly impair simple and complex learning or spatial reference memory, however; it did adversely affect recall memory. At the cellular level, we observed significant alterations in T cell populations and eosinophils within the meninges, accompanied by dysregulated cytokine production in the hippocampus. Additionally, an increase in microglial frequency and activation status, along with heightened TNFα production in response to the infection. Moreover, the infection promoted the expression of muscarinic receptors in the hippocampus, while reducing the number and antigen presentation capacity of astrocytes. Interestingly, PA in infected animals partially mitigated schistosomiasis-induced changes in glial and immune cell phenotypes within the brain parenchyma and meninges, respectively. Most notably, exercise reduced the production of TNFα by glial cells, indicating a shift towards a less pro-inflammatory environment. Collectively, these unprecedented findings shed light on the immune and glial cell alterations within

10.3389/fimmu.2024.1453742

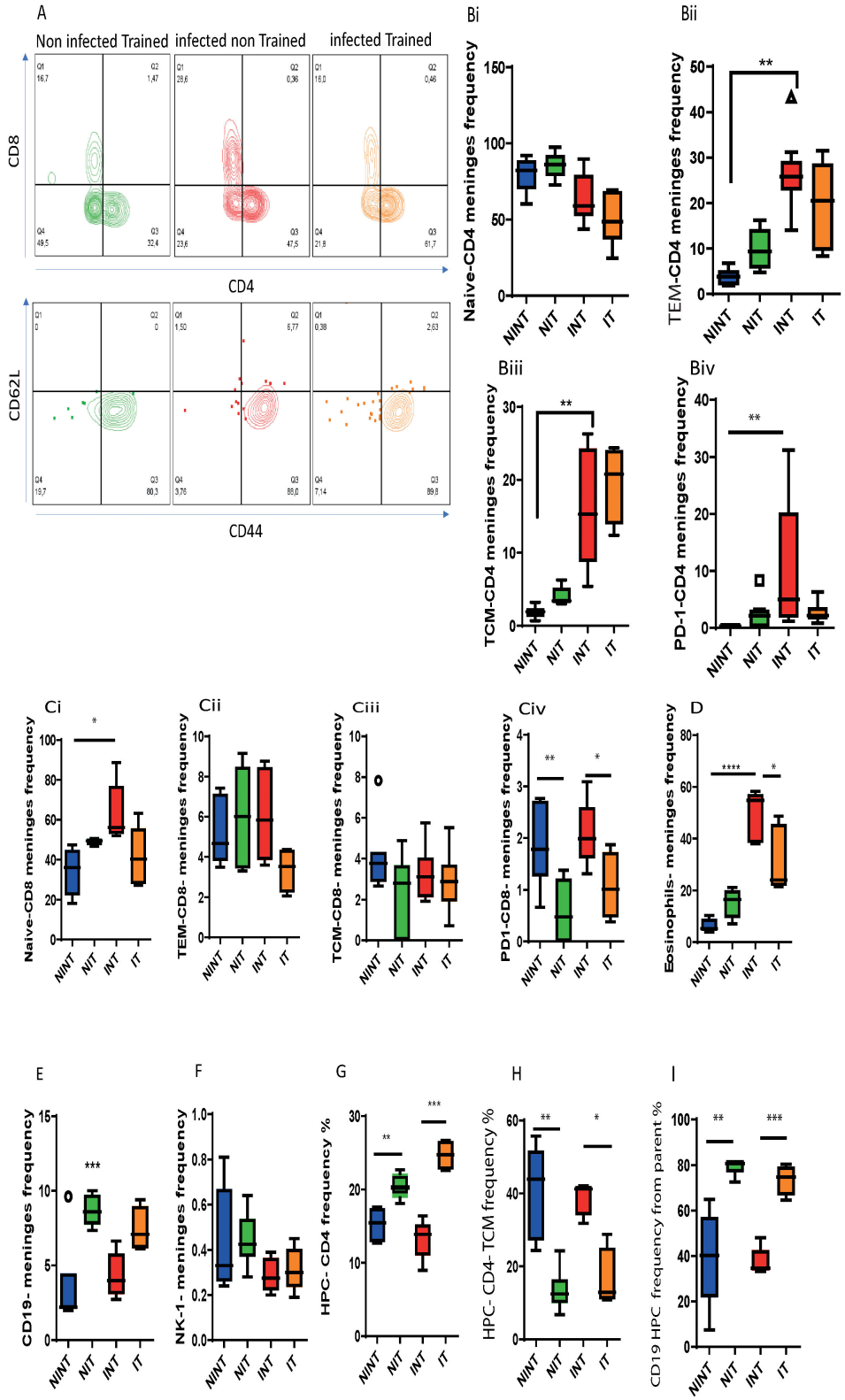

FIGURE 5
Impact of schistosomiasis infection and/or physical activities on lymphoid and myeloid cells in meninges and brain parenchyma. **(A)** Representative flow cytometry of $CD4^+$ and $CD8^+$ T cell populations (upper row) and $CD62L^+$ $CD44^+$ central memory and $CD62L^-$ $CD44^+$ effector T cell subsets (lower row) in the meninges. **(Bi)** Frequency of naïve, **(Bii)** effector memory (TEM), and **(Biii)** central memory (TCM) subsets and **(Biv)** the expression of PD1 by $CD4^+$ T cells. **(Ci)** Frequency of naïve, **(Cii)** effector memory (TEM), and **(Ciii)** central memory (TCM) subsets and **(Civ)** the expression of PD1 by $CD8^+$ T cells. Frequency of **(D)** eosinophils, **(E)** $CD19^+$ B cells, and $NK1.1^+$ cells in the meninges. **(G)** Frequency of total $CD4^+$ T cells and **(H)** TCM subset in the HPC. **(I)** Frequency of $CD19^+$ B cells in the HPC. Results are pooled from two different experiments with 6-8 mice per group. Data are expressed as mean ± S.E.M. NS, $P > 0.05$; *$P < 0.05$, **$P < 0.001$, ***$P < 0.0001$, ****$P < 0.000$. by ANOVA followed by Bonferoni, or unparametric test.

the CNS induced by schistosomiasis and underscore the potential of PA in ameliorating schistosomiasis-induced CNS alterations.

Several studies have indicated that schistosomiasis infection causes significant impairment of brain cognitive functions (3, 25). Whereas schistosomiasis impact on cognitive functions were assessed at the pre-clinical and clinical stages (5, 10), information is very scarce about the specific cognitive domain(s) impacted in adult age. Recent paper on the impact of schistosomiasis in post-natal mice showed that infected animals suffered from impairment in spatial learning and memory formation during acute schistosomiasis (10). By contrast, our findings indicated unaffected simple and complex learning as well as spatial reference memory in adult mice. The infection, however; resulted in impairment in the recall cognitive behavior. Two potential explanations may elucidate these disparities: firstly, schistosomiasis may exert varying impacts on cognitive domains depending on the host's maturation stage; and secondly, a higher infection inoculum used in the previous study could lead to more severe impacts of schistosomiasis infection on CNS function. Future experiments involving different infection doses administered to mice at various maturation stages will be instrumental in developing a more comprehensive understanding in that regard. Regarding affective behavior, emotions-associated behaviour, schistosomiasis infection did neither alter locomotor activity nor anxiety levels, as infected mice exhibited similar distances moved and velocities compared to uninfected controls. These findings are consistent with a previous report showing that infection of postnatal mice did neither alter locomotion nor anxiety level (10), and in contrast with others that demonstrated impact of helminth infection on the locomotion, suggesting specific species-neurobehavior impact (26, 27). Together, these findings suggested that while schistosomiasis infection had a specific effect on spatial reference memory, it had minimal influence on motor performance and affective behavior in adult mice.

Due to the spine and the large size of *S. mansoni* eggs, they are almost unable to traverse the blood brain barrier and they usually infiltrate the lower domain of the spinal cord (5, 28, 29). In agreement, our histological examination of brain sections indicated absence of eggs translocation into the brain. We also noted absence of egg infestation in the spinal cord likely due to the acute stage of the disease, which is one of the limitation in this study. Therefore, the noted schistosomiasis impact on the CNS was most likely through the systemic inflammation. This systemic inflammation led to significant alteration in T cell profile in meninges. In fact, there was a remarkable increase in effector and central memory $CD4^+$ T cell population that was associated with increased cell exhaustion as indicated by higher level of PD-1 expression. We also noted an increase in naïve $CD8^+$ T cell population. These alterations in T cell population in the brain could be the causal of significant impairment of hippocampal-dependent spatial learning and memory acquisition (30, 31). Hence, the changes in T cell population could be driving the schistosomiasis-induced impairment of the recall cognitive functions.

Schistosomiasis infection led also to a significant increase in the frequency of eosinophil population in the meninges, the phenomenon previously demonstrated in *T. regenti* infection (26). Further investigation is warranted to determine whether the elevated infiltration of eosinophils was driven by increased production of IL-5 by T cells (32).

By affecting the cell dynamics in the meninges, neuroinflammation in the brain parenchyma was highly anticipated. In agreement, there was an increase in microglia frequency and activation in hippocampus, while maintaining similar frequency and reactivity in prefrontal cortex, suggesting a profound impact of schistosomiasis infection on HPC compared to prefrontal cortex at adult stage. Significant increase in microglia was also recorded in the CNS of schistosomatidae infected mice (26). Investigating microglia polarization indicated a significant increase in TNFα production in the infected group compared to non-infected non-trained control. While TNFα production can promote inflammation and edema in addition to its toxic effects on neuronal structure and myelin, it could also promote neural cell survival and proliferation (13). The tendency of one effect over another is context dependent. In the present study, the predominant production of TNFα over type 2 cytokines (IL-4 and IL-13) could suggest the domination of pro-inflammatory effects of TNFα during neuroschistosomiasis after 8 weeks post-infections. Microglia production of TNFα may initiated neuroinflammation and aggravate neural tissue injury. It could further impair the neurogenesis and synaptogenesis in hippocampus (33) which may explain the dysregulation in recall memory (34, 35). The predomination of pro-inflammatory environment in hippocampus during neuroschistosomiasis could be the cause of the increased cell infiltration and reduction in the area occupied [the quantification of cell presence within a defined spatial area, specifically calculated as the number of cells per cubic millimeter (mm^3)] in the prefrontal cortex but not the hippocampus.

Cytokine profile in brain parenchyma was also significantly altered. We noted a consistent increase in IL-6 in hippocampus and prefrontal cortex, and IL-4 and TNFα in HPC. The higher level of IL-6 and IL-4 is consistent with the previous study demonstrated an increase in the same cytokines in cerebrospinal fluid (CSF) in spinal cord schistosomiasis (SCS) patients (36). Schistosomiasis infection at oviposition stage, > 6 weeks post-infection, is characterized by the domination of type 2 immunity (4). Hence, the production of IL-4 and IL-6 could be helping in skewing the immune response to type 2 immunity in the CNS to downmodulate pro-inflammatory immune response and diminish reactive oxygen and nitrogen species production that may damage the tissue. In fact, they could possibly mitigate the increased expression level of TNFα in hippocampus produced by microglia and astrocytes in response to the infection. The increase in TNFα is in disagreement with previous attempts by other investigator showing lower TNFα in CSF of SCS patients (36) and similar TNFα in prefrontal cortex in schistosomiasis-infected mice at postnatal stage (10). Of note, IL-6 may also induce nervous tissue lesion. Future studies will be needed to dissect the independent functional contributions of these cytokine to schistosomiasis effects on CNS.

Schistosomiasis infection further induced alteration in the cholinergic system. This could be due to the reliance of schistosomiasis parasites on the neurotransmitters produced by the host for the activation of their nervous system (37). Schistosomiasis nervous system is principal in the parasites survival, motility, nutrient uptake, and reproduction. ACh is one of the most important neurotransmitters needed for muscles contraction and nutrient absorption (38–40). Enhanced ACh expression by the cells in the spinal cord could then be driven by

the parasites in favor of their survival. The increased production of ACh was paralleled by enhanced expression of the muscarinic receptors in the hippocampus namely, M1, M2 and M5. Recently, it was shown that systemic schistosomiasis infection results in enhanced phosphorylation of Tau, microtubule associated protein (10). Increased uptake of Tau by neurons through M1 and M3 receptors enhanced microglia activation while maintaining similar GFAP expression level (41). Our results partially goes in line with these findings as we noted increase in microglia population and similar GFAP expression. However, the frequency of $GFAP^+$ astrocytes was significantly diminished in infected animals and were characterized by their potency of producing higher level of TNFα. The changes in muscarinic receptors expression could be playing a role in the noted immune dysregulation (42).

The utilization of physical activity (PA) as an adjunctive therapy in the treatment of neuroschistosomiasis represents an innovative approach to modulate host immune responses and potentially ameliorate disease outcomes. Praziquantel (PZQ) remains the primary antihelmintic drug for treating schistosomiasis, and its efficacy is well-established; it can reduce neuroschistosomiasis symptoms as school-aged children treated with PZQ often show enhanced cognitive performance, including improvements in attention, memory, and problem-solving skills. However, while PZQ effectively kills the parasites, it does not directly address the inflammatory symptoms and complications associated with neuroschistosomiasis. Consequently, adjunctive therapies like corticosteroids are frequently needed to manage symptoms, which comes with their own set of potential side effects (5, 6). Previous studies have found a protective effect of PA against inflammation-associated diseases (11, 12).

Therefore, in our study, we explored the intricate effects of an 8-day PA regimen on glial and immune cells within the CNS of schistosomiasis-infected subjects. Our data revealed that PA not only mitigated neuroinflammation but also fostered a milieu conducive to neuroprotection. The dampening of TNFα production and the concurrent increase in IL-13 within the hippocampus suggested a potential shift toward an anti-inflammatory state. This was particularly pertinent given the neurotoxic potential of chronic TNFα elevation and the neuroprotective role IL-13 can play. Exercise-induced modulation of glial cell activity, characterized by the normalization of pro-inflammatory cytokine expression, indicated that PA exerted a regulatory influence over CNS innate immunity, which could have broad implications for limiting the neurological impact of schistosomiasis.

Furthermore, PA had a restorative effect on neurotransmitter system markers, such as ACh in the spinal cord and M5 muscarinic receptors in the hippocampus, which may indicate a broader impact on CNS function and disease resilience. The PA regimen positively influenced lymphocyte populations, reducing the frequency of CD4 + and CD8+ effector memory T cells and eosinophils within the meninges. These could further alleviate meningeal inflammation and reduce the risk of long-term structural CNS damage. These neuro-immunological adjustments underscored the capacity of PA to act beyond a simple physical enhancer and position it as a powerful modulator of central immune and neural processes.

However, despite these beneficial CNS effects, PA unexpectedly influenced other disease dynamics. We previously demonstrated that gut smooth muscles hypercontractility is crucial for egg expulsion and any defects in this process led to higher susceptibility to the infection and premature death (23). Consequently, we expected that enhancing gut smooth muscle hypercontractility by PA would help in reducing egg burden but in contrary we noted significant increase in the egg burden after training. This unexpected finding suggested that PA could somehow have interfered with the egg expulsion process, possibly by redirecting the body's activity in another direction. We also noted worsened the egg-induced granuloma and fibrosis. One possible explanation could be that increase in IL-6 and C-reactive protein usually generated during PA could have led to the exacerbation of the disease immunopathology (11). Given these findings, it is crucial to understand the balance between beneficial and potentially detrimental effects of PA. Our results thus necessitate a careful consideration of the role of exercise in the management of schistosomiasis, highlighting the importance of future research to delineate the optimal types and intensities of PA that could improve disease outcomes without worsening the peripheral pathology, particularly concerning liver health and fibrosis, which are not ameliorated by PA according to previous studies.

Overall, our results demonstrated the impact of schistosomiasis infection on the cognitive function and cellular composition and phenotype in the CNS and how regular moderate PA could help in mitigating the impact of schistosomiasis on the CNS. Our results indicated impairment specifically in the recall memory during acute stage of the infection in adult mice. We further demonstrated the changes in glial and immune cells in CNS. Our results illustrated changes in T cells and eosinophils in the meninges which were accompanied by higher the propensity of glial cell to produce pro-inflammatory cytokines, particularly TNFα during schistosomiasis infection. We then highlighted how PA alleviated the schistosomiasis-induced impacts on the CNS. Together, our data support that moderate regular PA could be a natural non-invasive strategy that could help in mitigating the impact of *S. mansoni* infection on CNS.

Data availability statement

The datasets presented in this study can be found in online repositories. The names of the repository/repositories and accession number(s) can be found in the article/Supplementary Material.

Ethics statement

The animal study was approved by 1. Cytokines and Diseases Group, International Centre for Genetic Engineering and Biotechnology, Cape Town Component, Division of Immunology, Institute of Infectious Diseases and Molecular Medicine, Faculty of Health Sciences, University of Cape Town, Cape Town, South Africa; Wellcome Centre for Infectious Diseases Research in Africa, Institute of Infectious Diseases and Molecular Medicine (IDM), Faculty of Health Sciences, University of Cape Town, Cape Town 7925, South Africa. The study was conducted in accordance with the local legislation and institutional requirements.

Author contributions

IB: Conceptualization, Data curation, Methodology, Software, Writing – original draft, Writing – review & editing. NA: Writing – original draft, Writing – review & editing. BM: Data curation, Writing – review & editing. TB: Supervision, Writing – review & editing. FB: Supervision, Validation, Writing – review & editing.

Funding

The author(s) declare financial support was received for the research, authorship, and/or publication of this article. The research presented was supported by the South African National Research Foundation (NRF), SAMRC and South African Research Chair Initiative (SARCHi) for F. Brombacher and ICGEB south africa.

Conflict of interest

The authors declare that the research was conducted in the absence of any commercial or financial relationships that could be construed as a potential conflict of interest.

Publisher's note

Supplementary material

The Supplementary Material for this article can be found online at: https://www.frontiersin.org/articles/10.3389/fimmu.2024.1453742/full#supplementary-material

SUPPLEMENTARY FIGURE 1
Impact of physical activities on the periphery response to schistosomiasis infection. 8 weeks p.i. 1 cm jejunum segment was removed from the small intestine of both non-infected and *S. mansoni* infected mice to assess the smooth muscle hypercontractility. **(A)** Smooth muscle hypercontractility measured using acetylcholine (ACh). jejunum segment was stimulated with varying concentrations of ACh −9 to −3 LOG [M] to determine isometric contractile responses. **(B)** Egg burden in liver, **(C)** intestine, **(D)** spleen, and **(E)** lung. **(F)** Representative H&E staining of liver sections from mice infected with *S. mansoni* for 8 weeks before (INT) and after training (IT) (4x). **(G)** Liver Granuloma size determined from **(F)** by using a computerized morphometric analysis program (NIS elements by NIKON) by measuring 100 granulomas/group. **(H)** Liver hydroxyproline content measured by colorimetry 8 weeks p.i. **(I)** Schema of second postinfection Training (11weeks PI) **(Ii)** Latency to platform after 11 weeks postinfection, **(Iii)**, latency of platform in day 6,7,8, after 11 days postinfection, **(Iiii)** Percentage time in quadrant 11 weeks postinfections. Results are pooled from two different experiments with 6-8 mice per group. Data are expressed as mean ± S.E.M. NS, $P > 0.05$; * $P < 0.05$, ** $P < 0.001$, *** $P < 0.0001$ by two-tailed unpaired *Student t* test,.

SUPPLEMENTARY FIGURE 2
Impact of schistosomiasis infection and/or physical activities on spinal cord. **(A)** Representative H&E sections for spinal cord to assess eggs infiltration (original magnification 4 and10x). **(B)** Egg burden in spinal cord. **(Ci)**) cholinergic neurons in coronal sections of spinal cord For astrocytes producing acetylcholine in the spinal cord (original magnification 10x). **(Cii)** Number of cell producing ACh in the spinal cord. **(Di)** *Ccl2*, **(Dii)** *Il13*, and **(Diii)** *Il4* relative to HPRT housekeeping gene determined using qRT-PCR in prefrontal cortex, mRNA expression level of **(Div)** *M1*, **(Dv)** *M2*, and **(Dvi)** *M5* relative to HPRT housekeeping gene determined using qRT-PCR in prefrontal cortex Results are pooled from two different experiments with 6-8 mice per group. Data are expressed as mean ± S.E.M. NS, $P > 0.05$; * $P < 0.05$, ** $P < 0.001$, *** $P < 0.0001$ by two-tailed by ANOVA followed by Bonferoni,.

SUPPLEMENTARY FIGURE 3
Impact of schistosomiasis infection and/or physical activities on $CD11b^+$ cells in brain parenchyma. **(A)** Frequency of $CD11b^+$ cells in HPC 8 weeks p.i. **(Ai)** IL-4 and **(Aii)** IL-13 expression by $CD11b^+$ cells in hippocampus. **(B)** Frequency of $CD11b^+$ cells in PFC 8 weeks p.i. **(Bi)** IL-4 and **(Bii)** IL-13 expression by $CD11b^+$ cells in prefrontal cortex. **(Ci)** Frequency of monocytes and eosinophils in hippocampus and prefrontal cortex before and **(Cii)** after mice training. **(D)** Parenchyma gating strategy, **(E)** Meningeal gating strategy. Results are pooled from two different experiments with 6-8 mice per group. Data are expressed as mean ± S.E.M. NS, $P > 0.05$; * $P < 0.05$, ** $P < 0.001$, *** $P < 0.0001$ by two-tailed by ANOVA followed by Bonferoni, or unparametric test.

SUPPLEMENTARY FIGURE 4
UMAP for the Impact of schistosomiasis infection and/or physical activities on immune cells in brain, Wide screen analyses of CD62L, CXCR5, SiglecF, CD3, CD4, NK1.1, CD45, PD-1, CD8 demonstrated a remarkable increase in CXCR5, SiglecF, CD44, CD45 expression in the meninges in response to *S. mansoni* infection.

References

1. Steinmann P, Keiser J, Bos R, Tanner M, Utzinger J. Schistosomiasis and water resources development: systematic review, meta-analysis, and estimates of people at risk. *Lancet Infect Dis*. (2006) 6:411–25. doi: 10.1016/S1473-3099(06)70521-7

2. Utzinger J, Raso G, Brooker S, De Savigny D, Tanner M, Ornbjerg N, et al. Schistosomiasis and neglected tropical diseases: towards integrated and sustainable control and a word of caution. *Parasitology*. (2009) 136:1859–74. doi: 10.1017/S0031182009991600

3. McManus DP, Dunne DW, Sacko M, Utzinger J, Vennervald BJ, Zhou XN. Schistosomiasis. *Nat Rev Dis Primers*. (2018) 4:13. doi: 10.1038/s41572-018-0013-8

4. Abdel Aziz N, Musaigwa F, Mosala P, Berkiks I, Brombacher F. Type 2 immunity: a two-edged sword in schistosomiasis immunopathology. *Trends Immunol*. (2022) 43:657–73. doi: 10.1016/j.it.2022.06.005

5. Ferrari TC, Moreira PR. Neuroschistosomiasis: clinical symptoms and pathogenesis. *Lancet Neurol*. (2011) 10:853–64. doi: 10.1016/S1474-4422(11)70170-3

6. Ross AG, McManus DP, Farrar J, Hunstman RJ, Gray DJ, Li YS. Neuroschistosomiasis. *J Neurol*. (2012) 259:22–32. doi: 10.1007/s00415-011-6133-7

7. Carod Artal FJ, Vargas AP, Horan TA, Marinho PB, Coelho Costa PH. *Schistosoma mansoni* myelopathy: clinical and pathologic findings. *Neurology*. (2004) 63:388–91. doi: 10.1212/01.WNL.0000130190.67613.BE

8. Caumes E, Vidailhet M. Acute neuroschistosomiasis: a cerebral vasculitis to treat with corticosteroids not praziquantel. *J Travel Med*. (2010) 17:359; author reply 60. doi: 10.1111/j.1708-8305.2010.00452_1.x

9. Jaureguiberry S, Paris L, Caumes E. Acute schistosomiasis, a diagnostic and therapeutic challenge. *Clin Microbiol Infect*. (2010) 16:225–31. doi: 10.1111/j.1469-0691.2009.03131.x

10. Gasparotto J, Senger MR, Telles de Sa Moreira E, Brum PO, Carazza Kessler FG, Peixoto DO, et al. Neurological impairment caused by *Schistosoma mansoni* systemic

infection exhibits early features of idiopathic neurodegenerative disease. *J Biol Chem*. (2021) 297:100979. doi: 10.1016/j.jbc.2021.100979

11. Gleeson M, Bishop NC, Stensel DJ, Lindley MR, Mastana SS, Nimmo MA. The anti-inflammatory effects of exercise: mechanisms and implications for the prevention and treatment of disease. *Nat Rev Immunol*. (2011) 11:607–15. doi: 10.1038/nri3041

12. Khazaei M. Chronic low-grade inflammation after exercise: controversies. *Iran J Basic Med Sci*. (2012) 15:1008–9.

13. Hanisch UK. Microglia as a source and target of cytokines. *Glia*. (2002) 40:140–55. doi: 10.1002/glia.10161

14. Vitkovic L, Maeda S, Sternberg E. Anti-inflammatory cytokines: expression and action in the brain. *Neuroimmunomodulation*. (2001) 9:295–312. doi: 10.1159/000059387

15. Vorhees CV, Williams MT. Morris water maze: procedures for assessing spatial and related forms of learning and memory. *Nat Protoc*. (2006) 1:848–58. doi: 10.1038/nprot.2006.116

16. Cheever AW. Relative resistance of the eggs of human schistosomes to digestion in potassium hydroxide. *Bull World Health Organization*. (1970) 43:601–3.

17. Nono JK, Ndlovu H, Abdel Aziz N, Mpotje T, Hlaka L, Brombacher F. Host regulation of liver fibroproliferative pathology during experimental schistosomiasis via interleukin-4 receptor alpha. *PloS Negl Trop Dis*. (2017) 11:e0005861. doi: 10.1371/journal.pntd.0005861

18. Abdel Aziz N, Nono JK, Mpotje T, Brombacher F. The Foxp3+ regulatory T-cell population requires IL-4Ralpha signaling to control inflammation during helminth infections. *PloS Biol*. (2018) 16:e2005850.

19. Abdel Aziz N, Berkiks I, Mosala P, Brombacher TM, Brombacher F. Environmental and microbial factors influence affective and cognitive behavior in C57BL/6 sub-strains. *Front Immunol*. (2023) 14:1139913. doi: 10.3389/fimmu.2023.1139913

20. Pasciuto E, Burton OT, Roca CP, Lagou V, Rajan WD, Theys T, et al. Microglia require CD4 T cells to complete the fetal-to-adult transition. *Cell*. (2020) 182:625–40 e24. doi: 10.1016/j.cell.2020.06.026

21. McInnes L, Healy J, Melville J. UMAP: uniform manifold approximation and projection for dimension reduction. *arXiv*. (2018). doi: 10.21105/joss.00861

22. Tamgue O, Gcanga L, Ozturk M, Whitehead L, Pillay S, Jacobs R, et al. Differential Targeting of c-Maf, Bach-1, and Elmo-1 by microRNA-143 and microRNA-365 Promotes the Intracellular Growth of Mycobacterium tuberculosis in Alternatively IL-4/IL-13 Activated Macrophages. *Front Immunol*. (2019) 10:421. doi: 10.3389/fimmu.2019.00421

23. Marillier RG, Brombacher TM, Dewals B, Leeto M, Barkhuizen M, Govender D, et al. IL-4Ralpha-responsive smooth muscle cells increase intestinal hypercontractility and contribute to resistance during acute Schistosomiasis. *Am J Physiol Gastrointest Liver Physiol*. (2010) 298:G943–51. doi: 10.1152/ajpgi.00321.2009

24. Jukes MC, Nokes CA, Alcock KJ, Lambo JK, Kihamia C, Ngorosho N, et al. Heavy schistosomiasis associated with poor short-term memory and slower reaction times in Tanzanian schoolchildren. *Trop Med Int Health*. (2002) 7:104–17.

25. Ezeamama AE, Bustinduy AL, Nkwata AK, Martinez L, Pabalan N, Boivin MJ, et al. Cognitive deficits and educational loss in children with schistosome infection-A systematic review and meta-analysis. *PloS Negl Trop Dis*. (2018) 12:e0005524. doi: 10.1371/journal.pntd.0005524

26. Machacek T, Leontovyc R, Smidova B, Majer M, Vondracek O, Vojtechova I, et al. Mechanisms of the host immune response and helminth-induced pathology during Trichobilharzia regenti (Schistosomatidae) neuroinvasion in mice. *PloS Pathog*. (2022) 18:e1010302.

27. Janecek E, Waindok P, Bankstahl M, Strube C. Abnormal neurobehaviour and impaired memory function as a consequence of Toxocara canis- as well as Toxocara cati-induced neurotoxocarosis. *PloS Negl Trop Dis*. (2017) 11:e0005594. doi: 10.1371/journal.pntd.0005594

28. Carod-Artal FJ. Neurological complications of Schistosoma infection. *Trans R Soc Trop Med Hyg*. (2008) 102:107–16. doi: 10.1016/j.trstmh.2007.08.004

29. Cervellati C, Trentini A, Pecorelli A, Valacchi G. Inflammation in neurological disorders: the thin boundary between brain and periphery. *Antioxid Redox Signal*. (2020) 33:191–210. doi: 10.1089/ars.2020.8076

30. Derecki NC, Cardani AN, Yang CH, Quinnies KM, Crihfield A, Lynch KR, et al. Regulation of learning and memory by meningeal immunity: a key role for IL-4. *J Exp Med*. (2010) 207:1067–80. doi: 10.1084/jem.20091419

31. Serre-Miranda C, Roque S, Santos NC, Portugal-Nunes C, Costa P, Palha JA, et al. Effector memory CD4(+) T cells are associated with cognitive performance in a senior population. *Neurol Neuroimmunol Neuroinflamm*. (2015) 2:e54. doi: 10.1212/NXI.0000000000000054

32. Kouro T, Takatsu K. IL-5- and eosinophil-mediated inflammation: from discovery to therapy. *Int Immunol*. (2009) 21:1303–9. doi: 10.1093/intimm/dxp102

33. Butovsky O, Ziv Y, Schwartz A, Landa G, Talpalar AE, Pluchino S, et al. Microglia activated by IL-4 or IFN-gamma differentially induce neurogenesis and oligodendrogenesis from adult stem/progenitor cells. *Mol Cell Neurosci*. (2006) 31:149–60. doi: 10.1016/j.mcn.2005.10.006

34. Monje ML, Toda H, Palmer TD. Inflammatory blockade restores adult hippocampal neurogenesis. *Science*. (2003) 302:1760–5. doi: 10.1126/science.1088417

35. Steadman PE, Xia F, Ahmed M, Mocle AJ, Penning ARA, Geraghty AC, et al. Disruption of oligodendrogenesis impairs memory consolidation in adult mice. *Neuron*. (2020) 105:150–64 e6. doi: 10.1016/j.neuron.2019.10.013

36. Ferrari TC, Moreira PR, Sampaio MJ, da Cunha AS, de Oliveira JT, Gazzinelli G, et al. Intrathecal cytokines in spinal cord schistosomiasis. *J Neuroimmunol*. (2006) 177:136–41. doi: 10.1016/j.jneuroim.2006.05.008

37. Ribeiro P, El-Shehabi F, Patocka N. Classical transmitters and their receptors in flatworms. *Parasitology*. (2005) 131 Suppl:S19–40. doi: 10.1017/S0031182005008565

38. Camacho M, Agnew A. Schistosoma: rate of glucose import is altered by acetylcholine interaction with tegumental acetylcholine receptors and acetylcholinesterase. *Exp Parasitol*. (1995) 81:584–91. doi: 10.1006/expr.1995.1152

39. Jones AK, Bentley GN, Oliveros Parra WG, Agnew A. Molecular characterization of an acetylcholinesterase implicated in the regulation of glucose scavenging by the parasite Schistosoma. *FASEB J*. (2002) 16:441–3. doi: 10.1096/fj.01-0683fje

40. You H, Liu C, Du X, McManus DP. Acetylcholinesterase and nicotinic acetylcholine receptors in schistosomes and other parasitic helminths. *Molecules*. (2017) 22. doi: 10.3390/molecules22091550

41. Morozova V, Cohen LS, Makki AE, Shur A, Pilar G, El Idrissi A, et al. Normal and pathological tau uptake mediated by M1/M3 muscarinic receptors promotes opposite neuronal changes. *Front Cell Neurosci*. (2019) 13:403. doi: 10.3389/fncel.2019.00403

42. Kudlak M, Tadi P. *Physiology, Muscarinic Receptor*. Treasure Island (FL: StatPearls (2022).

frontiers | Frontiers in Immunology

TYPE Original Research
PUBLISHED 19 February 2025
DOI 10.3389/fimmu.2025.1521295

OPEN ACCESS

EDITED BY
Muhammad Tofazzal Hossain,
Bangladesh Agricultural University,
Bangladesh

REVIEWED BY
Jayaraman Tharmalingam,
University of Wisconsin-Madison,
United States
Yibeltal Akelew,
Debre Markos University, Ethiopia

*CORRESPONDENCE
Yakobo Leonard Lema
yakobolema@gmail.com
Clarissa Prazeres da Costa
clarissa.dacosta@tum.de

RECEIVED 01 November 2024
ACCEPTED 28 January 2025
PUBLISHED 19 February 2025

CITATION
Lema YL, Prodjinotho UF, Makasi C, Nanyaro M-WA, Kilale AM, Godfrey Mfinanga S, Schmidt V, Carabin H, Winkler AS, Lyamuya EF, Ngowi BJ and Prazeres da Costa C (2025) Cytokine profiles and CD4 counts in HIV-positive individuals with cysticercosis: implications for sex-specific immune responses in co-endemic regions of Tanzania. *Front. Immunol.* 16:1521295. doi: 10.3389/fimmu.2025.1521295

Cytokine profiles and CD4 counts in HIV-positive individuals with cysticercosis: implications for sex-specific immune responses in co-endemic regions of Tanzania

Yakobo Leonard Lema[1*], Ulrich Fabien Prodjinotho[2,3], Charles Makasi[1,4], Mary-Winnie A. Nanyaro[1], Andrew Martin Kilale[1], Sayoki Godfrey Mfinanga[1,5,6], Veronika Schmidt[3], Hélène Carabin[7,8,9,10], Andrea Sylvia Winkler[3,11,12], Eligius F. Lyamuya[13], Bernard James Ngowi[1,14] and Clarissa Prazeres da Costa[2,3,15*]

[1]Muhimbili Medical Research Center, National Institute for Medical Research (NIMR), Dar es Salaam, Tanzania, [2]Institute for Medical Microbiology, Immunology, and Hygiene, School of Medicine and Health, Technical University of Munich (TUM), Munich, Germany, [3]Center for Global Health, School of Medicine and Health, Technical University of Munich, Munich, Germany, [4]Institute of Public Health, Kilimanjaro Christian Medical University College, Moshi, Tanzania, [5]Department of Public Health, Kampala International University, Dar Es Salaam, Tanzania, [6]School of Public Health, Muhimbili University of Health and Allied Sciences (MUHAS), Dar Es Salaam, Tanzania, [7]Faculty of Veterinary Medicine, University of Montreal, Saint-Hyacinthe, QC, Canada, [8]School of Public Health, University of Montreal, Montreal, QC, Canada, [9]Research Group on Epidemiology of Zoonoses and Public Health (GREZOSP), Saint-Hyacinthe, QC, Canada, [10]Department of Epidemiology, Public Health Research Center of the Centre intégré universitaire de santé et de services sociaux (CIUSSS) of Center-Sud-de-l'Île-de-Montréal (CReSP), Montreal, QC, Canada, [11]Department of Community Medicine and Global Health, Institute of Health and Society, University of Oslo, Oslo, Norway, [12]Department of Global Health and Social Medicine, Harvard Medical School, Boston, MA, United States, [13]Department of Microbiology and Immunology, Muhimbili University of Health and Allied Sciences (MUHAS), Dar Es Salaam, Tanzania, [14]Mbeya College of Health and Allied Sciences, University of Dar Es Salaam, Mbeya, Tanzania, [15]Department of Infectious Diseases, German Center for Infection Research (DZIF), Partner Site Munich, Munich, Germany

Introduction: The interplay between HIV and *Taenia solium* cysticercosis in co-endemic regions remains poorly understood, particularly regarding the immune responses but is relevant for an effective treatment strategy. This study aimed to investigate the relationship between peripheral cytokine profiles, $CD4^+$ T-cell counts, and cysticercosis infection status in HIV-positive individuals in Tanzania's southern highlands.

Methods: We conducted a cross-sectional study involving 110 HIV-positive individuals. Cysticercosis was diagnosed using antibody and antigen tests, with neurocysticercosis confirmed by CT imaging. CD4 counts and serum cytokine levels (pro- and anti-inflammatory) were analyzed using multivariate regression and MANOVA, including sex-stratified analyses.

Results: Among participants, 20.9% tested positive for cysticercosis antibodies, 43.6% for antigens and 20.2% presented with brain cysts, with 10.6% showing active neurocysticercosis. Cysticercosis-positive individuals showed positive correlations between CD4 counts and pro-inflammatory cytokines (e.g., TNF-α,

IL-1β), contrasting with negative correlations in cysticercosis-negative individuals. Sex-stratified analysis showed stronger regulatory cytokine responses in males compared to females, particularly involving higher levels of IL-10 and IL-4 indicating sex-specific immune modulation in co-infected individuals. However, overall cytokine profiles were not significantly influenced by CD4 categories or cysticercosis status.

Conclusion: These results contribute to our understanding of immunological interactions in HIV-cysticercosis co-infection and underscore the need for further research with larger sample sizes to elucidate the clinical implications of these findings. Such studies could inform the development of more effective, sex-personalized treatment strategies for HIV patients in cysticercosis-endemic regions.

KEYWORDS

Taenia solium cysticercosis, HIV, cytokine profiles, CD4 count, sex-dependent responses

1 Introduction

Taenia solium, a zoonotic parasite, significantly impacts human and animal health in many low-income countries, leading to substantial economic losses and healthcare burden (1, 2). Neurocysticercosis (NCC), caused by presence of the larval stage of *T. solium* in the central nervous system (CNS), is recognized as a leading cause of epilepsy and is associated with significant morbidity and mortality in the endemic areas especially in sub-Sahara Africa (SSA) (2, 3). According to the WHO Foodborne Disease Burden Epidemiology Reference Group, NCC is the third leading cause of death from food-borne diseases, resulting in an estimated 2.8 million disability-adjusted life-years (DALYs) (4).

In humans, while the adult tapeworm resides in the intestines causing taeniasis, the larval cysticerci can infect various tissues causing cysticercosis (CC), including CNS leading to NCC (5, 6). NCC can present as symptomatic or asymptomatic disease, with up to 50% of cases being asymptomatic, contributing to underdiagnosis and continued transmission of the parasite (7–9). When symptomatic, the most common manifestations include severe progressive headaches and epileptic seizures (acute or chronic), which can be associated with reduced quality of life, and social stigma (10–12). Seroprevalence studies have shown significant regional variation in *T. solium* infection rates. In SSA, community surveys using antigen ELISA reported prevalences ranging from 5.8% to 22% (9, 13, 14). In northern Tanzania, a hospital-based cross-sectional study reported definitive and probable NCC in 2.4% and 11.3% of people with epilepsy, respectively (6, 15).

Many *T. solium* endemic areas in SSA are also disproportionately burdened by the human immunodeficiency virus (HIV). Approximately 25 million people living with HIV/AIDS reside in SSA which is also home to an estimated 3 million people suffering from NCC-related epilepsy (2, 6, 16). Thus, the interplay between HIV and parasitic infections is an important area of research, with studies showing that some parasitic infections can enhance susceptibility to HIV and potentially accelerate disease progression (17).

While interactions between HIV and certain soil-transmitted parasitic infections have been well-documented, the main findings indicate that helminths are potent immunomodulators, suggesting that HIV patients might benefit from anthelminthic treatment (18, 19). However, the relationship between HIV and CC, particularly NCC, remains less understood (20–23).

Studies from Mexico have demonstrated significant immunological alterations in patients with NCC. Fleury et al. found that viable cysticerci release immunomodulatory molecules that induce a shift towards a Th2-type immune response, characterized by increased levels of anti-inflammatory cytokines such as interleukin-4 (IL-4) and interleukin-10 (IL-10) (24). This shift can suppress the pro-inflammatory Th1 response, leading to decreased production of cytokines like interferon-gamma (IFN-γ) and interleukin-2 (IL-2), which are crucial for cell-mediated immunity. This suppression may jeopardize anti-bacterial and anti-viral immune responses. Restrepo et al. observed that NCC patients exhibit altered cytokine profiles with elevated IL-5 and IL-6 levels, alongside reduced IFN-γ production, suggesting a compromised immune response (25). These immunological changes could contribute to the persistence of the parasite and exacerbate immunosuppression.

Research findings on the interaction between HIV and NCC have been varied and inconclusive. Some evidence suggests that HIV-associated immunosuppression-particularly in individuals with $CD4^+$ T-cell counts below 200 cells/mm^3, may influence *T. solium* infection, leading to more asymptomatic cases due to a

reduced inflammatory response (26–28). However, the relationship between low CD4+ counts and an increased risk of NCC infection remains uncertain, with no clear consensus as to whether immunosuppression increases susceptibility or merely alters symptomatology. Noormahomed et al. (2014) found no significant correlation between CC antibodies and $CD4^+$ T-cell counts in HIV patients (29). Additionally, a study by Schmidt et al. (2016) did not observe a higher prevalence of CC in HIV-positive individuals compared to HIV-negative controls (6).

Regarding NCC, multiple studies have demonstrated that HIV infection is not associated with a higher prevalence of NCC, and in some cases, the prevalence may even be lower compared to HIV-negative populations (6, 29–33). These findings highlight the need for further research into how HIV-associated immunosuppression could alter the course of *T. solium* infection, and thereby CC disease prevalence, symptoms, and treatment outcomes (34). Specifically, HIV-positive patients with higher CD4+ T-cell counts may be more likely to exhibit symptomatic NCC when they acquire the infection due to a more robust immune response leading to inflammation, whereas immunocompromised patients might present asymptomatically or with atypical forms of the disease (35, 36). To investigate the peripheral immune responses and clinical presentation in relation to CD4 T cell counts in HIV and CC/NCC co-infected patients, we recently conducted a study in Southern Tanzania and could show that HIV infection itself significantly modulates levels of key cytokines such as TNF-α, IL-8, and IFN-γ (20). However, HIV did not alter cytokine levels induced by CC or NCC. These immunological findings highlight the complex interplay between HIV and NCC but leave unclear how CC-induced cytokine profiles might influence $CD4^+$ T-cell counts in HIV-infected individuals.

The present study addresses this gap by investigating the influence of cytokine profiles modulated by CC infection on $CD4^+$ T-cell counts in HIV-positive patients in Tanzania's southern highlands.

2 Materials and methods

2.1 Study design and participants

We conducted a nested cross-sectional immunological study within a larger paired cross-sectional investigation in the Southern Highlands of Tanzania between June 2018 and March 2021. The study focused on Chunya district (Mbeya region) and Iringa rural district (Iringa region), areas characterized by high HIV prevalence (9.0% and 9.1%, respectively) and significant porcine CC prevalence (7.6% and 8.4%, respectively) (37).

The parent study recruited 1,291 people living with HIV/AIDS (PLWH/A) on antiretroviral therapy (ART) aged 14 years and above from HIV clinics in the study regions. Exclusion criteria included opportunistic infections, neurological symptoms predating HIV diagnosis, and anthelminthic treatment within the previous 12 months. All participants underwent clinical evaluation, neurological examination, and serological testing for *T. solium* CC.

For our nested investigation, we included 110 HIV-positive participants from the parent study who had complete data on CC serological status, CD4 counts, cytokine profiles, and CT scan examinations, allowing for a comprehensive analysis of the interplay between HIV infection, (neuro-)cysticercosis, and immune responses.

2.2 Ethics statement

This cross-sectional study was conducted in accordance with the Declaration of Helsinki. Ethical approval was obtained from the Directorate of Research and Publications at Muhimbili University of Health & Allied Sciences (MUHAS), Dar es Salaam (Ref.No.DA.282/298/01.C/), and the National Institute for Medical Research (NIMR) in Tanzania (Ref. NIMR/HQ/R.8a/Vol. IX/2529) as part of the broader Cystinet Africa project. The Technical University of Munich, School of Medicine and Health, Ethics Committee also provided clearance (Ref: 537/18 and 215/18S).

All participants provided written informed consent prior to enrollment. Participants were informed about the study procedures, potential risks, and benefits, including those associated with diagnostic tests and CT imaging where applicable. The study protocol ensured appropriate care for PLWHA participants throughout the research process. Participants' privacy and confidentiality were maintained through data anonymization during collection and analysis. The study design prioritized the well-being and rights of people living with HIV, adhering to principles of respect for autonomy, beneficence, and justice. No children or pregnant women were included in this study.

2.3 Sample collection and handling

Venous blood samples (15 mL) were collected from each participant using standard aseptic technique. Blood was drawn into two types of Vacutainer tubes (BD Biosciences, Franklin Lakes, NJ, USA): a 5 mL Serum Separator Tube (SST) and a 10 mL EDTA tube. For serum collection, SST tubes were inverted 5 times after collection and allowed to clot at room temperature for 30 minutes. Samples were then centrifuged at 1500 x g for 10 minutes at 4°C. The resulting serum was aliquoted into separate vials: 50 µL each for CC antigen testing, antibody testing, and cytokine analysis, with the remaining serum stored in 0.5 mL aliquots. EDTA tubes were inverted 8-10 times immediately after collection to ensure proper mixing with the anticoagulant. These samples were used for CD4 count analysis using the BD FACSPresto™ System (BD Biosciences, San Jose, CA, USA) within 6 hours of collection, and HIV-1 viral load quantification using the Xpert HIV-1 Viral Load Assay on the GeneXpert platform (Cepheid, Sunnyvale, CA, USA) (38).

All aliquots were stored at -80°C within 2 hours of processing. Samples were transported on dry ice to the respective laboratories for analysis. Freeze-thaw cycles were minimized, with samples thawed only once for each analysis.

2.4 Diagnosis of NCC and CC

(Neuro-) Cysticercosis diagnosis was based on serological testing and neuroimaging. We employed two serological tests: the CYSTICERCOSIS Western Blot (WB) IgG test (LDBio Diagnostics SARL, Lyon, France) for antibody detection and the CC Ag ELISA (apDia bvba, Turnhout, Belgium) for circulating antigen detection.

The WB IgG test utilizes antigens from *T. solium* cysticerci of porcine origin, separated by electrophoresis and bound to nitrocellulose strips. Serum samples (1:50 dilution) were incubated with individual strips for 90 minutes at 20-26°C. After washing, alkaline phosphatase-anti human IgG conjugate was added and incubated for 60 minutes. Following additional wash steps, strips were developed with NBT/BCIP substrate for 60 minutes. The reaction was then stopped, and strips were dried and interpreted. A positive result was indicated by the presence of at least two well-defined bands among five main bands (P6-8, P12, P23-26, P39, and P50-55). This test has a reported sensitivity of 97.5% and specificity of 100% based on manufacturer's data.

The Ag ELISA detects circulating antigens from viable *Taenia* spp. metacestodes. Serum samples were pre-treated with 5% trichloroacetic acid (1:1 ratio) for 5 minutes at room temperature, then centrifuged at 12,000g for 5 minutes. Supernatants were neutralized with an equal volume of 0.156M carbonate/bicarbonate buffer. Pre-treated samples (100 µL) were added to wells coated with B158C11A10 monoclonal antibodies and incubated for 15 minutes at 37°C. After washing, peroxidase conjugated B60H8A4 monoclonal antibodies were added and incubated for 15 minutes at 37°C. Following washing, chromogen substrate was added and incubated for 15 minutes at room temperature. The reaction was stopped, and absorbance was read at 450 nm within 15 minutes. Results were expressed as an antigen index (Ag Index), with ≥ 1.3 considered positive, ≤ 0.8 negative, and 0.8-1.3 doubtful. This test has a reported sensitivity of 90% and specificity of 98% (39).

Participants with positive serological results underwent cerebral computed tomography (CT) at Mbeya Zonal Referral Hospital. The CT images were evaluated by experienced radiologists and neurologists who were blinded to the serological results. Based on combined serological and imaging findings, participants were classified as NCC, CC or negative for CC.

2.4.1 Case definition of NCC and CC

For this study, we established specific criteria to define CC cases based on the combination of serological and imaging results. NCC was diagnosed in individuals with active, mixed, or calcified cysts in the brain on cerebral CT scan, regardless of serological test results. CC was defined for individuals who had positive results on the antigen ELISA (apDia test), the antibody Western Blot IgG, or both, with a negative CT scan or without CT scan results, this suggests possible CC infection, potentially with viable cysts located outside the central nervous system. Negative cases were those individuals with negative results on all performed tests, including the antigen ELISA, antibody Western Blot IgG, and CT scan when available.

2.5 Multiplex cytokine assay

Serum cytokine levels were quantified using a Human Magnetic Luminex Assay (14-Plex) kit (Catalogue # LXSAHM-14, R&D Systems Europe Ltd.) on a Luminex xMAP 100 MAGPIX system (Luminex Corporation, Austin, TX, USA). The multiplex panel included pro-inflammatory and Th1 cytokines (TNF-α, IFN-γ, IL-1β, IL-6, IL-8, IL-12 p40, IL-17A, IL-18), Th2 cytokines (IL-4, IL-5), anti-inflammatory cytokines (IL-10, IL-13), and cell adhesion molecules (VCAM-1/CD106, ICAM-1/CD54).

Serum samples were centrifuged at 16,000 x g for 4 minutes immediately prior to use. Samples were diluted at least 2-fold (75 µL sample + 75 µL Calibrator Diluent RD6-52) as per kit instructions. Briefly, the assay employs color-coded magnetic microspheres pre-coated with analyte-specific antibodies. 50 µL of standard or diluted serum sample was added to each well of a 96-well plate, followed by 50 µL of diluted microparticle cocktail. The plate was incubated for 2 hours at room temperature on a horizontal orbital shaker (800 ± 50 rpm)., This allowed the analytes to bind to the immobilized antibodies. After washing away unbound substances, 50 µL of diluted biotin-antibody cocktail specific to the analytes of interest was added and incubated for 1 hour. Following another wash step, 50 µL of diluted streptavidin-PE was added and incubated for 30 minutes. After a final wash, the microparticles were resuspended in 100 µL of wash buffer for analysis.

The plate was read within 90 minutes using the Luminex MAGPIX analyzer. Instrument settings were as follows: 50 µL sample volume, 50 count/region, and collection of Median Fluorescence Intensity (MFI). Standard curves for each analyte were generated using a five-parameter logistic (5-PL) curve-fit in xPONENT software version 4.3 (Luminex Corporation). Sample concentrations were determined from the standard curve and multiplied by the appropriate dilution factor. To normalize their distribution before statistical analysis, log transformation was applied to the cytokine concentrations.

Quality control measures included the use of kit-provided standards and controls, as well as inter-assay and intra-assay coefficient of variation calculations to assess precision.

2.6 CD4 counts and HIV testing

$CD4^+$ T-cell counts were measured using the BD FACSPresto™ Near-Patient CD4 Counter System (BD Biosciences, San Jose, CA, USA). Whole blood samples were collected in 10 mL EDTA Vacutainer tubes (BD Biosciences, Franklin Lakes, NJ, USA). Immediately after collection, tubes were inverted 8-10 times to ensure proper mixing with the anticoagulant. CD4 count analysis was performed within 6 hours of collection to ensure sample integrity. For the assay, 30 µL of EDTA-anticoagulated whole blood was added to the inlet port of the BD FACSPresto cartridge containing dried fluorochrome-conjugated antibody reagents. After an 18-minute incubation period at room temperature (20-25°C), the cartridge was inserted into the BD FACSPresto instrument for analysis. The system employs fluorescence microscopy and

absorbance spectrophotometry to provide absolute CD4 count (cells/μL), CD4 percentage of lymphocytes, and hemoglobin concentration (g/dL) results within 4 minutes.

Based on the $CD4^+$ T-cell counts, participants were categorized into three groups: severe immunosuppression (SIM) (<200 cells/mm^3), moderate immunosuppression (MIS) (200–499 cells/mm^3), and normal immune status (NIS) (≥500 cells/mm^3). This stratification is widely adopted in HIV research and clinical practice and follows the standard guidelines established by both the World Health Organization (WHO) and the Centers for Disease Control and Prevention (CDC), which use similar thresholds to classify the degree of immunodeficiency in HIV-infected individuals. This stratification allowed for the analysis of immune responses across different levels of HIV-associated immunosuppression.

HIV-1 viral load was quantified using the Xpert HIV-1 Viral Load Assay on the GeneXpert platform (Cepheid, Sunnyvale, CA, USA). This assay is an *in vitro* reverse transcriptase polymerase chain reaction (RT-PCR) test for the detection and quantification of HIV-1 RNA in human plasma. The test can quantify HIV-1 RNA over the range of 40 to 10,000,000 copies/mL and is validated for quantification of RNA from HIV-1 Group M (subtypes A, B, C, D, F, G, H, J, K, CRF01_AE, CRF02_AG, and CRF03_AB), Group N, and Group O. For viral load testing, plasma was separated from the EDTA whole blood samples by centrifugation at 1500 x g for 10 minutes at 4°C. One milliliter of plasma was then pipetted directly into the Xpert HIV-1 Viral Load cartridge. The GeneXpert System automated all steps of nucleic acid amplification testing, including sample preparation, nucleic acid extraction and amplification, and detection of the target sequence using real-time RT-PCR. Results were available within 90 minutes.

Viral loads were classified as detectable (≥40 copies/mL) or undetectable (<40 copies/mL) based on the assay's lower limit of quantification. For analysis purposes, viral load results were log-transformed to normalize their distribution.

2.7 Statistical analyses

All statistical analyses were performed using IBM SPSS Statistics, Version 29.0 (IBM Corp., 2021). Descriptive statistics were calculated for demographic and clinical characteristics, stratified by CD4 count categories. Chi-square tests were used to assess associations between categorical variables.

To examine the relationship between CD4 counts and cytokine levels in HIV patients with and without CC, we conducted correlation analyses. Fisher's Z-test was employed to compare the strength of these correlations between groups. Cytokine concentrations were log-transformed to normalize their distribution.

Multivariate regression analyses were performed to investigate the effects of CD4 counts, CC status, and potential confounding factors (age, sex, viral load, HIV stage, and ART duration) on cytokine levels. Interaction terms (CD4 count × cysticercosis status and sex × cysticercosis status) were included to assess potential effect modifications. Variance Inflation Factors (VIF) were calculated to check for multicollinearity among predictor variables.

Sensitivity analyses were conducted sequentially excluding each confounding factor to assess their impact on the relationship between CD4 counts and cytokine levels. Additionally, we performed stratified analyses by sex to explore potential sex-specific differences in cytokine predictors.

A two-way Multivariate Analysis of Variance (MANOVA) was conducted to examine differences in overall cytokine profiles across CD4 categories and CC status, as well as their interaction. Wilks' Lambda, Pillai's Trace, Hotelling-Lawley Trace, and Roy's Greatest Root were used to assess the overall significance of the model. Partial eta squared (η^2) values were calculated to estimate effect sizes. To account for multiple comparisons in the multivariate regression analyses (Tables 1B, C, 2), we applied the Benjamini-Hochberg procedure to control the false discovery rate at 0.05 for all reported p-values.

For all analyses, a p-value < 0.05 was considered statistically significant. Where applicable, 95% confidence intervals were reported alongside effect estimates.

3 Results

3.1 Baseline characteristics of study participants

A total of 110 PLWHA individuals were included in this study. The median age of participants was 43 years (interquartile range [IQR]: 17 years). Participants were categorized into three CD4 count groups: normal (NIS) (>500 cells/mm^3), moderate (MIS) (200-499 cells/mm^3), and severe (SIM) (<200 cells/mm^3). Most participants fell into the normal and moderate ranges, with 47 (43%) in the normal range and 54 (49%) in the moderate range. A smaller proportion, 9 (8%) of participants, were in the severe range. Significant differences were observed in the distribution of participants across CD4 categories based on region ($p = 0.035$) and sex ($p = 0.020$). Most participants were from Mbeya (70.0%), with a higher proportion in the moderate CD4 category (76%) compared to Iringa. Male participants predominated overall 69 (63%) but were overrepresented in the moderate category 38 (70%) and severe category 8 (89%).

Many participants had secondary education 63 (57%), were farmers 87 (79%), and were single 79 (72%). BMI distribution showed that most participants were of normal weight 75 (68%), with some variations across CD4 categories, though not statistically significant ($p = 0.137$) (Table 3).

3.2 Serological and neuroradiological findings

Serological tests for CC revealed that all 110 participants underwent both *T. solium* (TsAb) antibody and *T. solium* (TsAg) antigen testing, while 94 participants also received cerebral CT imaging to assess for NCC. Of the total participants, 47 (43%) were found to be CC+, with 22 (20%) being diagnosed with NCC based

TABLE 1A A sensitivity analysis of CD4 count as a predictor for cytokine levels.

Cytokine	Confounder Excluded	β (CD4 count)	SE	p-value
TNF-a	None	-0.0012	0.000403	0.003
	Age	-0.0012	0.000403	0.003
	Sex	-0.0012	0.000403	0.003
	Viral Load	-0.0012	0.000403	0.003
	HIV Stage	-0.0012	0.000403	0.003
	ART Months	-0.0012	0.000403	0.003
	CC+	-0.0012	0.000403	0.003
	CD4_count_CC+	-0.0007	0.000303	0.004
	Sex_CC+	-0.0012	0.000403	0.003
IL-1β	None	-0.0007	0.000357	0.083
	Age	-0.0007	0.000357	0.083
	Sex	-0.0007	0.000357	0.083
	Viral Load	-0.0007	0.000357	0.083
	HIV Stage	-0.0007	0.000357	0.083
	ART Months	-0.0007	0.000357	0.083
	CC+	-0.0007	0.000357	0.083
	CD4_count_CC+	-0.0005	0.000357	0.123
	Sex_CC+	-0.0007	0.000357	0.083
IFN-γ	None	-0.001	0.0004	0.021
	Age	-0.001	0.0004	0.021
	Sex	-0.001	0.0004	0.021
	Viral Load	-0.001	0.0004	0.021
	HIV Stage	-0.001	0.0004	0.021
	ART Months	-0.001	0.0004	0.021
	CC+	-0.001	0.0004	0.021
	CD4_count_CC+	-0.0006	0.0003	0.088
	Sex_CC+	-0.001	0.0004	0.021

β, Regression coefficient representing the effect size of CD4 count on cytokine levels; SE, Standard Error of the regression coefficient; CD4_count × CC+, Interaction term between CD4 count and cysticercosis status; TNF-α, Tumor Necrosis Factor-alpha; IL-1β, Interleukin-1 beta; IFN-γ, Interferon-gamma. $p < 0.05$ indicates statistical significance.
Each confounding factor was sequentially excluded to assess its impact on the associations.

TABLE 1B Multivariate regression analysis of cytokine levels in male HIV-positive patients.

Cytokine	Variables	β (SE)	95% CI	p-value	Adj p-value (BH)
TNF-a	CD4 count	-0.0017 (0.0006)	(-0.0030, -0.0005)	0.008	0.045
	CC+	-0.4029 (0.23)	(-0.8627, 0.0570)	0.085	0.199
	Age	-0.0081 (0.0077)	(-0.0235, 0.0074)	0.302	0.453
	Viral Load	-0.000002 (0.000002)	(-0.000005, 0.000002)	0.285	0.452
	HIV_Stage	0.2647 (0.0947)	(0.0754, 0.4541)	0.007	0.047
	ART Months	0.0002 (0.0021)	(-0.0039, 0.0043)	0.916	0.951
	Sex_CC+	-0.4029 (0.23)	(-0.8627, 0.0570)	0.085	0.199

(Continued)

10.3389/fimmu.2025.1521295

TABLE 1B Continued

Cytokine	Variables	β (SE)	95% CI	p-value	Adj p-value (BH)
	CD4_count_CC+	0.0022 (0.0009)	(0.0003, 0.0040)	0.026	0.118
IL-1β	CD4 count	-0.0012 (0.0007)	(-0.0026, 0.0002)	0.088	0.182
	CC+	-0.4779 (0.2567)	(-0.9912, 0.0354)	0.067	0.192
	Age	-0.0076 (0.0086)	(-0.0249, 0.0096)	0.379	0.539
	Viral Load	0.0000001 (0.000002)	(-0.000004, 0.000004)	0.944	0.944
	HIV_Stage	0.0584 (0.1057)	(-0.1529, 0.2697)	0.583	0.655
	ART Months	0.0015 (0.0023)	(-0.0031, 0.0061)	0.512	0.628
	Sex_CC+	-0.4779 (0.2567)	(-0.9912, 0.0354)	0.067	0.192
	CD4_count_CC+	0.0022 (0.0011)	(0.0001, 0.0043)	0.043	0.146
IFN-γ	CD4 count	-0.0014 (0.0007)	(-0.0027, -0.0001)	0.040	0.153
	CC+	-0.199 (0.2448)	(-0.6885, 0.2906)	0.420	0.553
	Age	-0.01 (0.0082)	(-0.0265, 0.0065)	0.230	0.388
	Viral Load	0.0000005 (0.000002)	(-0.000003, 0.000004)	0.795	0.858
	HIV_Stage	0.1431 (0.1008)	(-0.0584, 0.3447)	0.161	0.289
	ART Months	0.0014 (0.0022)	(-0.0030, 0.0058)	0.521	0.611
	Sex_CC+	-0.199 (0.2448)	(-0.6885, 0.2906)	0.420	0.553
	CD4_count_CC+	0.0015 (0.001)	(-0.0005, 0.0036)	0.129	0.248

β, Regression coefficient; SE, Standard Error; CI, Confidence Interval; CD4_count × CC+, Interaction term between CD4 count and cysticercosis status; TNF-α, Tumor Necrosis Factor-alpha; IL-1β, Interleukin-1 beta; IFN-γ, Interferon-gamma; ART, Antiretroviral Therapy; CC+, Cysticercosis-positive status.
Statistical Notes: Adjusted p-values were calculated using the Benjamini-Hochberg correction to control the false discovery rate at 0.05.

TABLE 1C Multivariate regression analysis of cytokine levels in female HIV-positive patients.

Cytokine	Variables	β (SE)	95% CI	p-value	Adj p-value (BH)
TNF-a	CD4 count	-0.0014 (0.0005)	(-0.0027, -0.0001)	0.042	0.281
	CC+	-0.5632 (0.2938)	(-1.1545, 0.0281)	0.065	0.196
	Age	0.0011 (0.0108)	(-0.0204, 0.0227)	0.922	0.922
	Viral Load	-0.000009 (0.00001)	(-0.000030, 0.000012)	0.387	0.551
	HIV_Stage	-0.0948 (0.1391)	(-0.3777, 0.1881)	0.5	0.5870
	ART Months	-0.0025 (0.0031)	(-0.0089, 0.0038)	0.422	0.518
	Sex_CC+	-0.4929 (0.2466)	(-0.9945, 0.0088)	0.054	0.208
	CD4_count_CC+	0.0013 (0.0009)	(-0.0006, 0.0033)	0.180	0.348
IL-1β	CD4 count	-0.0004 (0.0005)	(-0.0013, 0.0006)	0.409	0.552
	CC+	-0.2179 (0.1032)	(-0.4277, -0.0080)	0.042	0.208
	Age	0.0074 (0.009)	(-0.0109, 0.0257)	0.418	0.538
	Viral Load	0.000013 (0.000009)	(-0.000005, 0.000031)	0.143	0.321
	HIV_Stage	0.016 (0.1164)	(-0.2208, 0.2527)	0.892	0.926
	ART Months	-0.005 (0.0026)	(-0.0103, 0.0003)	0.063	0.213
	Sex_CC+	-0.4357 (0.2063)	(-0.8555, -0.0159)	0.042	0.208
	CD4_count_CC+	0.0009 (0.0008)	(-0.0007, 0.0026)	0.256	0.406

(Continued)

TABLE 1C Continued

Cytokine	Variables	β (SE)	95% CI	p-value	Adj p-value (BH)
IFN-γ	CD4 count	-0.0007 (0.0006)	(-0.0020, 0.0005)	0.252	0.424
	CC+	-0.215 (0.1343)	(-0.4883, 0.0583)	0.119	0.306
	Age	-0.0034 (0.0117)	(-0.0272, 0.0205)	0.776	0.838
	Viral Load	0.000012 (0.000011)	(-0.000011, 0.000035)	0.294	0.441
	HIV_Stage	0.0836 (0.1515)	(-0.2246, 0.3919)	0.585	0.658
	ART Months	-0.0048 (0.0034)	(-0.0117, 0.0021)	0.166	0.345
	Sex_CC+	-0.4301 (0.2687)	(-0.9767, 0.1166)	0.119	0.306
	CD4_count_CC+	0.0014 (0.001)	(-0.0007, 0.0035)	0.192	0.346

β, Regression coefficient; SE, Standard Error; CI, Confidence Interval; CD4_count × CC+, Interaction term between CD4 count and cysticercosis status and (Sex × CC+) interaction term between sex and cysticercosis status; TNF-α, Tumor Necrosis Factor-alpha; IL-1β, Interleukin-1 beta; IFN-γ, Interferon-gamma; ART, Antiretroviral Therapy; CC+, Cysticercosis-positive status. Statistical Notes: Adjusted p-values were Benjamini-Hochberg corrected to control the false discovery rate at 0.05.

on CT findings. Among the 47 CC+ participants, 46 were positive for TsAg. Of these, 33 (72%) were positive for TsAg alone, and 13 (28%) were positive for both TsAg and TsAb. Of the 33 who were TsAg positive alone, only 5 (15%) were also NCC positive. Additionally, 10 participants were positive for TsAb alone, with 5 of these (50%) also being NCC positive. The distribution of TsAb and TsAg positivity across CD4 categories showed no statistically significant differences (p = 0.7473 for TsAb; p = 0.4511 for TsAg) (Table 4). Among those with normal CD4 counts (>500 cells/mm^3), 10 (21%) were TsAb positive and 21(45%) were TsAg positive, compared to 12 (22%) and 23(43%) respectively in the moderate CD4 group (200-499 cells/mm^3), and 1 (11%) and 2 (22%) in the severe CD4 group (<200 cells/mm^3).

There was a statistically significant difference in the distribution of CC positivity across CD4 categories (p = 0.026). Notably, no participants in the severe CD4 group were positive for CC, while 22 (47%) and 25 (46%) were positive in the normal and moderate CD4 groups, respectively (Table 4).

Of the 94 HIV-positive participants who underwent cerebral CT imaging, 22 (23%) showed brain cysts indicative of NCC, with 9 (10%) showing active cysts and 13 (14%) showing inactive cysts. The distribution of NCC status across CD4 categories did not show statistically significant differences (p = 0.430) (Table 4).

Cyst stages varied across CD4 categories, but these differences were not statistically significant (p = 0.575). Vesicular cysts were found in 3 (8%) of the normal CD4 group, 2 (4%) of the moderate CD4 group, and none in the severe CD4 group. Calcified cysts were observed in 5 (13%), and 8 (17%), of the normal and moderate groups respectively; none in the severe CD4 group. Mixed-stage cysts were present in 1 (5%) of the normal CD4 group, 1 (2%) of the moderate CD4 group, and 1 (11%) of the severe CD4 group (Table 4).

The number of cysts also varied across CD4 categories, but these differences were not statistically significant (p = 0.452). Multiple cysts were found in 7 (18%) of the normal CD4 group, 10 (22%) of the moderate CD4 group, and 1 (11%) of the severe CD4 group. Single cysts were observed in 3 (8%) of the normal CD4 group, 1 (2%) of the moderate, and none of the severe CD4 group (Table 4).

3.3 Cytokine profiles by CD4 categories

Cytokine levels revealed complex patterns across CD4 categories and CC status. Notably, there were no CC+ individuals in the severe CD4 group (<200 cells/mm^3), which restricted comparisons to CC- individuals only in this category. Among CC- individuals, TNF-α, IL-18, and IL-1β levels were elevated in

TABLE 2 MANOVA results for cytokine levels across CD4 categories and cysticercosis status.

Variable	Test Statistic	Value	F-value	p-value	Partial η^2
Combined Cytokines	Λ	0.9159	1.41	0.1711	0.0841
	V	0.0841	1.41	0.1711	0.0841
	T^2	0.0918	1.41	0.1711	0.0841
	θ	0.0918	1.41	0.1711	0.0841
CD4 Categories	Λ	0.9159	1.41	0.1711	0.0841
Cysticercosis	Λ	0.9082	1.51	0.128	0.0918
Interaction	Λ	0.915	1.43	0.1654	0.085

Wilks' Lambda (Λ), Pillai's Trace (V), Hotelling-Lawley Trace (T^2), Roy's Greatest Root (θ), f-statistics (f-value) and η^2 (eta squared) represents effect size. Small effect ($\eta^2 \approx 0.01$), Medium effect ($\eta^2 \approx 0.06$), Large effect ($\eta^2 \approx 0.14$)."

TABLE 3 Demographics characteristics of the participants by CD4.

Variables	NIS	MIS	SIM	Total	P-value
Region					**0.035**
Iringa	14 (29.79%)	13 (24.07%)	6 (66.67%)	33 (30.00%)	
Mbeya	33 (70.21%)	41 (75.93%)	3 (33.33%)	77 (70.00%)	
Age Group					0.238
25 - 34	12 (25.53%)	7 (12.96%)	0 (0.00%)	19 (17.27%)	
35 - 49	19 (40.43%)	29 (53.70%)	6 (66.67%)	54 (49.09%)	
>50	16 (34.04%)	18 (33.33%)	3 (33.33%)	37 (33.64%)	
Sex					**0.020**
Male	23 (48.94%)	38 (70.37%)	8 (88.89%)	69 (62.73%)	
Female	24 (51.06%)	16 (29.63%)	1 (11.11%)	41 (37.27%)	
Edu_LvL					0.630
No formal Edu	6 (12.77%)	9 (16.67%)	1 (11.11%)	16 (14.55%)	
Primary Edu	9 (19.15%)	15 (27.78%)	2 (22.22%)	26 (23.64%)	
Secondary Edu	28 (59.57%)	29 (53.70%)	6 (66.67%)	63 (57.27%)	
Higher Edu	4 (8.51%)	1 (1.85%)	0 (0.00%)	5 (4.55%)	
Occupation					0.679
Farmer	36 (76.60%)	44 (81.48%)	7 (77.78%)	87 (79.09%)	
Employed	8 (17.02%)	9 (16.67%)	1 (11.11%)	18 (16.36%)	
Unemployed	3 (6.38%)	1 (1.85%)	1 (11.11%)	5 (4.55%)	
Marital Status					0.782
Single	33 (70.21%)	39 (72.22%)	7 (77.78%)	79 (71.82%)	
Married	4 (8.51%)	2 (3.70%)	0 (0.00%)	6 (5.45%)	
Prev. Married	10 (21.28%)	13 (24.07%)	2 (22.22%)	25 (22.73%)	
BMI					0.137
Underweight	4 (8.51%)	5 (9.26%)	0 (0.00%)	9 (8.18%)	
Normal weight	26 (55.32%)	41 (75.93%)	8 (88.89%)	75 (68.18%)	
Overweight	12 (25.53%)	5 (9.26%)	0 (0.00%)	17 (15.45%)	
Obese	5 (10.64%)	3 (5.56%)	1 (11.11%)	9 (8.18%)	

P-values were calculated using Chi-square test to assess associations between categorical variables. Statistical significance was defined as $p < 0.05$. Edu_LvL, Education Level; NIS, Normal Immune Status (>500 cells/mm^3); MIS, Moderate Immunosuppression (200-499 cells/mm^3); SIM, Severe Immunosuppression (<200 cells/mm^3). CD4 count is measured in cells per mm^3. All analyses were conducted using standard Chi-square assumptions without further correction.
Bold values indicate statistical significance at $p < 0.05$.

the severe immunosuppression (SIM) group compared to the moderate (MIS) and normal (NIS) groups, suggesting increased immune activation associated with severe immunosuppression. In contrast, in CC+ individuals, TNF-α and IL-1β levels were higher in the normal immune status (NIS) group compared to the moderate immunosuppression (MIS) group, suggesting that CC may influence cytokine regulation differently based on CD4 status (Figure 1).

IL-10 showed a relatively consistent pattern across CD4 categories for CC- individuals, while CC+ individuals in the normal CD4 group exhibited a wider range of IL-10 levels, suggesting a varied regulatory response (Figure 1). IL-18 levels were higher and more variable in CC- participants across all CD4 categories compared to CC+ individuals, suggesting a distinct immune modulation due to CC. No significant changes were observed for IL-6, IL-1β (in CC+ individuals), and IFN-γ across CD4 categories and CC status. In summary, these findings reveal differences in cytokine levels based on CD4 count and CC status, particularly with elevated TNF-α, IL-18, and IL-1β in CC- individuals with severe immunosuppression. This suggests that immune responses may vary depending on CD4 count and CC infection in HIV-positive individuals.

10.3389/fimmu.2025.1521295

TABLE 4 Distribution of clinical characteristics by CD4 categories.

Variable	NIS	MIS	SIM	Total	P-value
TsAb					0.747
Negative	37 (78.72%)	42 (77.78%)	8 (88.89%)	87 (79.09%)	
Positive	10 (21.28%)	12 (22.22%)	1 (11.11%)	23 (20.91%)	
TsAg					0.451
Negative	26 (55.32%)	31 (57.41%)	7 (77.78%)	64 (58.18%)	
Positive	21 (44.68%)	23 (42.59%)	2 (22.22%)	46 (41.82%)	
CC status					0.026
Negative	25 (53.19%)	29 (53.70%)	9 (100.00%)	63 (57.27%)	
Positive	22 (46.81%)	25 (46.30%)	0 (0.00%)	47 (42.73%)	
NCC status					0.430
No cyst	29 (74.36%)	35 (76.09%)	8 (88.89%)	72 (76.60%)	
Active	5 (12.82%)	3 (6.52%)	1 (11.11%)	9 (9.57%)	
Inactive	5 (12.82%)	8 (17.39%)	0 (0.00%)	13 (13.83%)	
Cyst stage					0.575
No Cysts	29 (74.36%)	35 (76.09%)	8 (88.89%)	72 (76.60%)	
Vesicular	3 (7.69%)	2 (4.35%)	0 (0.00%)	5 (5.32%)	
Calcified	5 (12.82%)	8 (17.39%)	0 (0.00%)	13 (13.83%)	
Mixed	2 (5.13%)	1 (2.17%)	1 (11.11%)	4 (4.26%)	
No. of Cysts					0.452
No Cyst	29 (74.36%)	35 (76.09%)	8 (88.89%)	72 (76.60%)	
Single	3 (7.69%)	1 (2.17%)	0 (0.00%)	4 (4.26%)	
Multiple	7 (17.95%)	10 (21.74%)	1 (11.11%)	18 (19.15%)	

P-values were calculated using the Chi-square test to assess associations between categorical clinical variables across CD4 categories. Statistical significance was determined at $p < 0.05$. TsAb, Taenia solium Antibody; TsAg, Taenia solium Antigen; CC+, Cysticercosis positive; NIS, Normal Immune Status (>500 cells/mm^3); MIS, Moderate Immunosuppression (200-499 cells/mm^3); SIM, Severe Immunosuppression (<200 cells/mm^3).

3.4 Correlation between CD4 counts, cytokine levels, and cysticercosis status

Figure 2 shows the relationships between CD4 counts and cytokine levels in HIV-positive individuals, both with and without CC. We conducted correlation analyses to explore the associations between CD4 counts, cytokine levels, and CC status. This helped us understand whether group-level trends are reflected at the individual level and provided deeper insights into how immune function (cytokine responses) might be influenced by both HIV and CC (Figure 2).

In CC-negative individuals, we observed weak negative correlations between CD4 counts and several cytokines, including TNF-α ($r = –0.236$, $p = 0.061$), IL-6 ($r = –0.115$, $p = 0.362$), IL-1β ($r = –0.166$, $p = 0.195$), IFN-γ ($r = –0.200$, $p = 0.109$), and the regulatory cytokine IL-10 ($r = –0.144$, $p = 0.260$). TNF-α, IL-6, IL-1β, IFN-γ, and IL-10. Although these correlations were not statistically significant, the trend suggested that higher CD4 counts might be linked to lower levels of these pro-inflammatory cytokines (Figure 2A).

In contrast, in CC-positive individuals, the correlations between CD4 counts and cytokine levels were generally positive for TNF-α ($r = 0.041$, $p = 0.772$), IL-6 ($r = 0.166$, $p = 0.269$), IL-10 ($r = 0.181$, $p = 0.226$), IL-1β ($r = 0.170$, $p = 0.255$), and IFN-γ ($r = 0.028$, $p = 0.854$), though none of these were statistically significant either. The positive trends may indicate a different immune response in the presence of CC (Figure 2B).

Although these results did not reach statistical significance, Fisher's Z-test indicated that the differences in correlation strength between CC-positive and CC-negative individuals for IL-10 (Z-diff = 1.655, $p = 0.098$) and IL-1β (Z-diff = 1.705, $p = 0.088$) were close to significant, suggesting there may be differences in how these cytokines are regulated depending on CC status.

In summary, these findings suggest that cytokine levels may correlate to CD4 counts in different ways depending on whether the individual has CC. While the correlations were not statistically significant, the trends observed imply that CC might affect immune responses in HIV-positive individuals, especially regarding pro-inflammatory and regulatory cytokines like IL-10 and IL-1β.

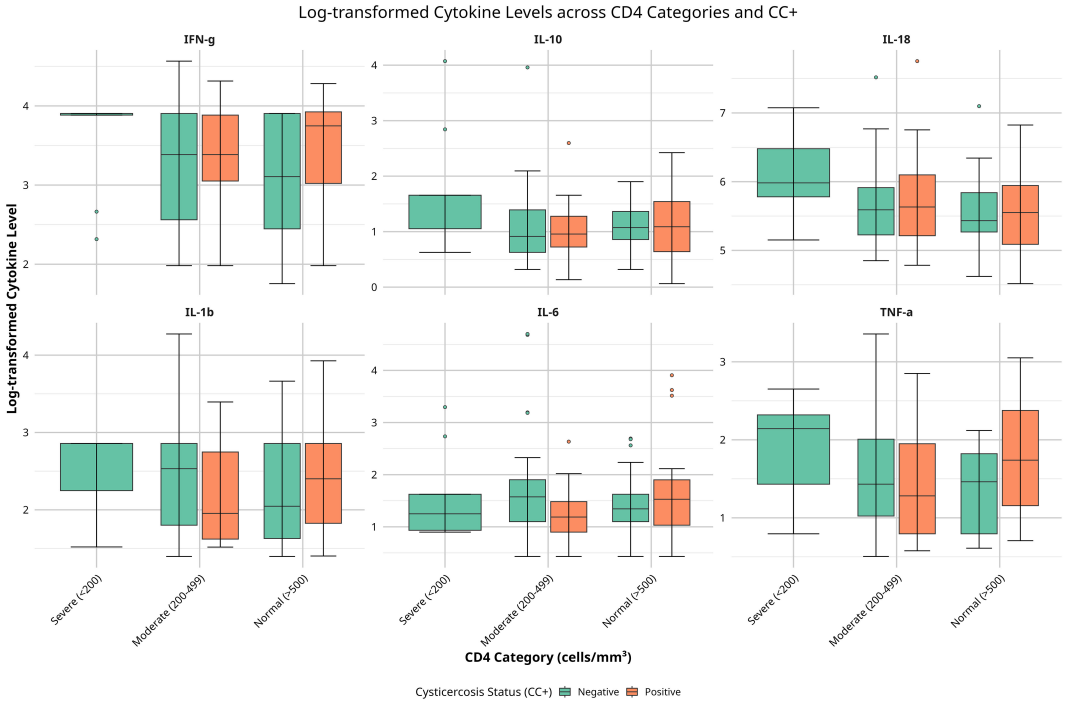

FIGURE 1
Boxplots of serum cytokine levels (TNF-α, IL-6, IL-10, IL-1β, IFN-γ, IL-18) across CD4 categories (<200, 200–499, ≥500 cells/mm^3) and cysticercosis status (positive or negative). Colors indicate cysticercosis status (orange: positive; green: negative). Data were log-transformed. Significant differences ($p < 0.05$) by Kruskal-Wallis tests are noted.

3.5 Multivariate analysis of cytokine predictors

To further investigate the relationships among CD4 counts, cytokine levels, and CC status, we performed a multivariate regression analysis. This analysis was adjusted for potential confounding factors such as age, sex, viral load, HIV stage, and duration on ART. This approach allows us to assess the independent effects of each factor on cytokine levels in HIV-positive individuals with and without CC. To account for multiple comparisons and control the false discovery rate at 0.05, we applied the Benjamini-Hochberg procedure (Table 5).

After adjustment, several significant associations emerged. TNF-α levels were negatively associated with CD4 count (β = –0.0012, 95% CI: –0.0020 to –0.0004, p = 0.003), meaning lower CD4 counts were linked to higher TNF-α levels. Additionally, there was a significant positive interaction between CD4 count and CC status (β = 0.0016, 95% CI: 0.0003 to 0.0029, p = 0.018), suggesting that CC may alter the effect of CD4 count on TNF-α levels. IFN-γ levels also showed a significant negative association with CD4 count (β = –0.0010, 95% CI: –0.0018 to –0.0002, p = 0.021). The interaction between sex and CC status was significant for TNF-α (β = –0.6666, 95% CI: –1.2662 to –0.0671, p = 0.030), indicating possible sex-based differences in immune response.

Other associations, such as those between IL-1β and CD4 count (β = –0.0007, 95% CI: –0.0015 to 0.0001, p = 0.083), or interactions involving IL-1β and CC status (β = 0.0014, 95% CI: 0.0001 to 0.0028, p = 0.036) or IFN-γ and CC status (β = 0.0013, 95% CI: –0.0001 to 0.0027, p = 0.074) did not remain statistically significant after adjustment. No significant associations were found for IL-6, IL-10, or IL-18 in relation to CD4 count or CC status (all p-values > 0.05) (Table 5). These findings highlight the complexity of cytokine regulation in HIV-positive individuals with CC and suggest that CC might affect immune function differently depending on a person's immune status.

3.6 Sensitivity and sex-stratified analyses of confounding factors

To ensure our multivariate regression findings were robust, we performed a sensitivity analysis to test whether individual confounding factors (age, sex, viral load, HIV stage, and ART duration) influenced the associations between cytokine levels and CD4 counts. We assessed how removing each confounder affected our results, and also checked for any sex-specific differences in these relationships. Before the sensitivity analysis, we confirmed that there was no multicollinearity between confounders. All variables exhibited low variance inflation factors (VIFs), with the highest being 1.267 for duration on ART (Supplementary Table S2), indicating that multicollinearity was not a concern in our multivariate regression models.

In the sensitivity analysis, we sequentially excluded each confounding factor from the model and observed the impact on the associations between cytokine levels and CD4 counts. For TNF-α, the association with CD4 count remained significant when excluding most confounders (β = –0.0012, 95% CI: –0.0020

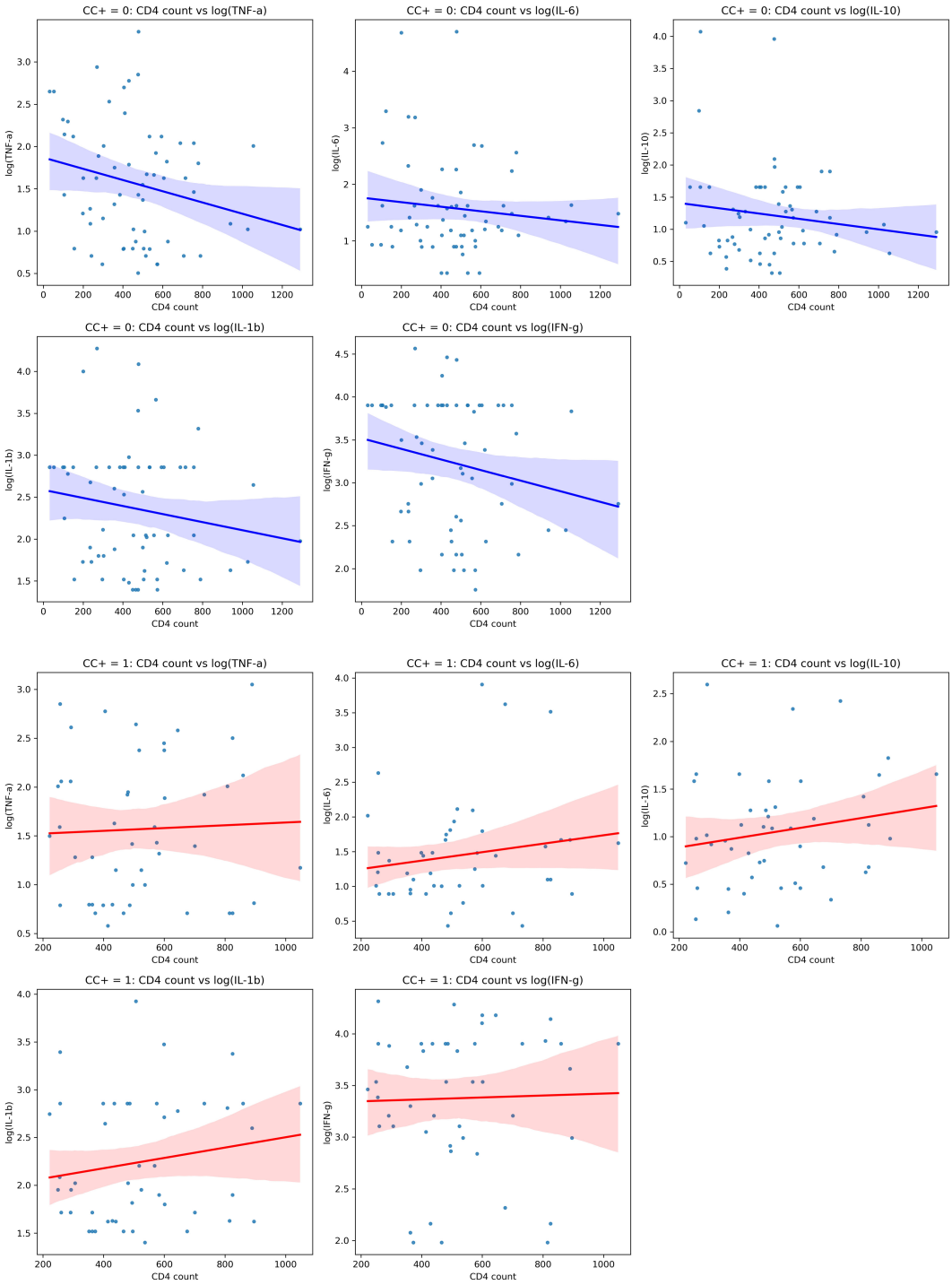

FIGURE 2
Scatterplots showing correlations between CD4 counts and cytokine levels (TNF-α, IL-6, IL-10, IL-1β, IFN-γ)in individuals with different cysticercosis (CC) statuses. The first panel (top) represents CC-negative individuals (blue), displaying weak negative correlations. The second panel (bottom) represents CC-positive individuals (red), showing weak positive correlations. The shaded areas indicate the 95% confidence intervals. Spearman's rank correlation coefficients (r) are provided for each plot; statistical significance is indicated where $p < 0.05$.

to –0.0004, p = 0.003). However, when the CD4 count × cysticercosis status interaction term was removed, the association slightly changed but remained significant (β = –0.0007, 95% CI: –0.0013 to –0.0001, p = 0.004) (Table 1A).

For IFN-γ, the association with CD4 count remained significant across most exclusions (β = –0.0010, 95% CI: –0.0018 to –0.0002, p = 0.021) but became non-significant when excluding the CD4 count × cysticercosis status interaction term (β = –0.0006, 95% CI: –0.0012 to 0.0000, p = 0.088). This suggests that the interaction between CD4 count and CC status plays a critical role in the association with IFN-γ levels (Table 1A).

TABLE 5 Multivariate regression analysis of cytokine levels in relation to CD4 count, cysticercosis status, and other confounding factors.

Cytokine	Variables	β (SE)	95% CI	p-value	Adj p-value (BH)
TNF-a	CD4 count	-0.0012 (0.0004)	(-0.0020, -0.0004)	0.003	**0.028**
	CC+	0.1450 (0.4751)	(-0.7976, 1.0876)	0.761	0.815
	Age	-0.0083 (0.0063)	(-0.0207, 0.0041)	0.188	0.452
	Sex	0.3764 (0.1956)	(-0.0117, 0.7645)	0.057	0.245
	Viral Load	-0.0000 (0.0000)	(-0.0000, 0.0000)	0.296	0.572
	HIV_Stage	0.1486 (0.0760)	(-0.0021, 0.2993)	0.053	0.266
	ART Months	-0.0009 (0.0017)	(-0.0043, 0.0025)	0.596	0.813
	Sex_CC+	-0.6666 (0.3022)	(-1.2662, -0.0671)	0.030	0.178
	CD4_count_CC+	0.0016 (0.0007)	(0.0003, 0.0029)	0.018	0.137
IL-6	CD4 count	-0.0005 (0.0005)	(-0.0014, 0.0005)	0.347	0.613
	CC+	-0.3694 (0.5707)	(-1.5016, 0.7628)	0.519	0.759
	Age	0.0022 (0.0075)	(-0.0127, 0.0172)	0.768	0.809
	Sex	-0.1258 (0.2350)	(-0.5920, 0.3404)	0.594	0.828
	Viral Load	-0.0000 (0.0000)	(-0.0000, 0.0000)	0.859	0.889
	HIV_Stage	0.0696 (0.0912)	(-0.1115, 0.2506)	0.448	0.746
	ART Months	0.0014 (0.0020)	(-0.0027, 0.0054)	0.506	0.759
	Sex_CC+	-0.3664 (0.3630)	(-1.0866, 0.3538)	0.315	0.573
	CD4_count_CC+	0.0014 (0.0008)	(-0.0001, 0.0030)	0.079	0.273
IL-10	CD4 count	-0.0005 (0.0004)	(-0.0013, 0.0003)	0.193	0.429
	CC+	-0.3113 (0.4562)	(-1.2163, 0.5938)	0.497	0.784
	Age	0.0006 (0.0060)	(-0.0114, 0.0125)	0.922	0.937
	Sex	0.2856 (0.1878)	(-0.0871, 0.6582)	0.1316	0.376
	Viral Load	0.0000 (0.0000)	(-0.0000, 0.0000)	0.693	0.785
	HIV_Stage	0.0331 (0.0729)	(-0.1116, 0.1777)	0.651	0.766
	ART Months	-0.0031 (0.0016)	(-0.0063, 0.0001)	0.059	0.236
	Sex_CC+	-0.1955 (0.2902)	(-0.7712, 0.3802)	0.502	0.772
	CD4_count_CC+	0.0008 (0.0006)	(-0.0004, 0.0021)	0.1905	0.440
IL-1β	CD4 count	-0.0007 (0.0004)	(-0.0015, 0.0001)	0.083	0.276
	CC+	-0.0135 (0.4840)	(-0.9738, 0.9467)	0.978	0.978
	Age	-0.0021 (0.0064)	(-0.0148, 0.0105)	0.738	0.805
	Sex	0.3018 (0.1993)	(-0.0936, 0.6972)	0.133	0.363
	Viral Load	0.0000 (0.0000)	(-0.0000, 0.0000)	0.658	0.760
	HIV_Stage	0.0441 (0.0774)	(-0.1094, 0.1976)	0.570	0.814
	ART Months	-0.0009 (0.0017)	(-0.0043, 0.0026)	0.621	0.793
	Sex_CC+	-0.5947 (0.3079)	(-1.2055, 0.0161)	0.056	0.259
	CD4_count_CC+	0.0014 (0.0007)	(0.0001, 0.0028)	0.036	0.194
IFN-γ	CD4 count	-0.0010 (0.0004)	(-0.0018, -0.0002)	0.021	0.142
	CC+	0.2650 (0.5026)	(-0.7321, 1.2622)	0.599	0.799
	Age	-0.0072 (0.0066)	(-0.0204, 0.0060)	0.281	0.562

(Continued)

TABLE 5 Continued

Cytokine	Variables	β (SE)	95% CI	p-value	Adj p-value (BH)
	Sex	0.3031 (0.2069)	(-0.1075, 0.7136)	0.146	0.381
	Viral Load	0.0000 (0.0000)	(-0.0000, 0.0000)	0.601	0.784
	HIV_Stage	0.1306 (0.0803)	(-0.0288, 0.2900)	0.107	0.321
	ART Months	-0.0009 (0.0018)	(-0.0044, 0.0027)	0.627	0.767
	Sex_CC+	-0.5285 (0.3197)	(-1.1627, 0.1058)	0.102	0.321
	CD4_count_CC+	0.0013 (0.0007)	(-0.0001, 0.0027)	0.074	0.260
IL-18	CD4 count	-0.0005 (0.0004)	(-0.0012, 0.0002)	0.185	0.463
	CC+	0.5246 (0.4227)	(-0.3140, 1.3633)	0.218	0.466
	Age	-0.0038 (0.0056)	(-0.0149, 0.0072)	0.494	0.801
	Sex	0.0622 (0.1741)	(-0.2831, 0.4075)	0.722	0.802
	Viral Load	-0.0000 (0.0000)	(-0.0000, 0.0000)	0.626	0.782
	HIV_Stage	0.0566 (0.0676)	(-0.0775, 0.1907)	0.404	0.693
	ART Months	-0.0018 (0.0015)	(-0.0048, 0.0011)	0.224	0.463
	Sex_CC+	-0.2738 (0.2689)	(-0.8073, 0.2596)	0.311	0.583
	CD4_count_CC+	-0.0003 (0.0006)	(-0.0014, 0.0009)	0.636	0.763

Multivariate regression analysis of cytokine predictors of CD4 count in HIV-positive individuals with and without cysticercosis, adjusted for age, sex, viral load, HIV stage, and duration on ART. cysticercosis status (CC+), their interaction terms (CD4 count × CC+), and (Sex × CC+). Regression coefficients (β), standard errors (SE), and Adj p-value BH - Benjamin Hochberg adjusted p-value. Bold values indicate statistical significance at $p < 0.05$.

3.6.1 Sex-stratified analysis

We also performed separate analyses for males and females, applying the Benjamini-Hochberg correction, to explore potential sex-specific differences in the associations between cytokine levels and CD4 counts. This investigates whether the patterns observed in the overall population persisted within each sex and to identify any differential effects that might inform sex-specific immune response dynamics (Tables 1B, C).

In males, significant predictors for TNF-α after correction were CD4 count and HIV stage. Higher CD4 counts were associated with lower TNF-α levels (β = –0.0017, 95% CI: –0.0030 to –0.0005, p = 0.045), while more advanced HIV stages were linked to higher TNF-α levels (β = 0.2647, 95% CI: 0.0754 to 0.4541, p = 0.047). However, the interaction between CD4 count and CC (β = 0.0022, 95% CI: 0.0003 to 0.0040, p = 0.118) was no longer significant after correction, implying that the interaction effect observed in the overall analysis was not pronounced in males (Table 1B). No significant predictors were found for IL-1β or IFN-γ after correction in males. These results suggest that TNF-α is influenced by both immune status (CD4 count) and disease progression (HIV stage) in males.

In females, after applying the Benjamini-Hochberg correction, no significant predictors were found for TNF-α, IL-1β, or IFN-γ (all adjusted p > 0.05). The associations that were previously significant before correction—for example, CD4 count with TNF-α (β = –0.0014, 95% CI: –0.0027 to –0.0001, p = 0.281), CC status with IL-1β (β = –0.2179, 95% CI: –0.4277 to –0.0080, p = 0.208), and the interaction between sex and CC status with IL-1β (β = –0.4357, 95% CI: –0.8555 to –0.0159, p = 0.208)—were no longer significant after correction. This suggests that in females, the associations between cytokine levels and CD4 counts are less pronounced or may be influenced by other factors not captured in our analysis (Table 1C).

Overall, the sensitivity analysis confirmed that the associations between cytokine levels and CD4 counts were generally robust, particularly for TNF-α. For IFN-γ, the association remained significant unless the interaction with CC status was excluded. The sex-stratified analysis showed that in males, TNF-α was significantly associated with both CD4 count and HIV stage, while no significant predictors were found in females after correction. These findings suggest that cytokine responses may vary between males and females, with males showing stronger associations between immune status and cytokine levels.

3.7 MANOVA analysis of overall cytokine profiles

To understand how CD4 categories and CC status together influence immune responses, we used a MANOVA to examine their effects on overall cytokine profiles. This method allowed us to analyze multiple cytokines at once to see if there were any significant differences across CD4 categories and CC status. The cytokines analyzed were TNF-α, IL-6, IL-10, IL-1β, IFN-γ, and IL-18. The results showed no significant effects for CD4 categories (Wilks' Lambda = 0.9159, F(12, 276) = 1.41, p = 0.1711, partial η^2 = 0.0841), CC status (Wilks' Lambda = 0.9082, F(6, 138) = 1.51, p = 0.1280, partial η^2 = 0.0918), or the interaction between CD4 categories and CC status (Wilks' Lambda = 0.9150, F(12, 276) =

1.43, p = 0.1654, partial η^2 = 0.0850) on the combined cytokine profiles (TNF-a, IL-6, IL-10, IL-1β, IFN-g, and IL-18) (Table 2). Other multivariate test criteria (Pillai's Trace, Hotelling-Lawley Trace, and Roy's Greatest Root) gave similar results, all yielding identical F-values and p-values to those obtained with Wilks' Lambda for each effect, confirming these findings (Table 2).

Although none of the effects reached statistical significance ($p < 0.05$), the effect sizes (partial η^2) suggested small to moderate contributions. CC status accounted for 9.18%of the variance in cytokine levels, followed by the interaction between CD4 categories and CC status (8.50%), and CD4 categories alone (8.41%) (Table 2).

In conclusion, the MANOVA did not identify any statistically significant effects of CD4 count categories, CC status, or their interaction on the overall cytokine profiles. This suggests that, when considered collectively, neither CD4 count, nor CC significantly influenced the immune response in this HIV-positive population.

4 Discussion

The primary aim of this study was to explore whether co-infection with *T. solium*, a potent immunomodulator, alters immune regulation in HIV-positive individuals, particularly by influencing cytokine profiles and CD4+ T-cell counts, in Tanzania's southern highlands. Our findings revealed that co-infection with *T. solium* significantly influenced immune responses, with TNF-α levels showing a strong negative association with CD4 counts, while this association was positively modulated by CC status. IFN-γ also displayed a significant negative relationship with CD4 counts, suggesting that *T. solium* co-infection may potentially alter immune regulation in HIV-positive individuals. While cytokines such as IL-1β, IL-6, IL-10, and IL-18, showed trends of immune modulation, these were not statistically significant.

Our sex-stratified analysis revealed important differences in immune regulation between male and female participants. In males, we found a significant negative association between TNF-α levels and CD4 counts, and a strong correlation between advanced HIV stages and elevated TNF-α levels. In contrast, females showed no significant associations between cytokine levels and CD4 counts after correction for multiple comparisons, suggesting more tightly regulated immune responses.

These sex-based differences align with previous research showing that testosterone typically suppresses both innate and adaptive immune responses, while estrogen enhances immune regulation (40). Female patients have been shown to exhibit stronger alterations in mucosal T-cell repertoire, with increased frequencies of Th1, Th17, and Th1/Th17-cell subsets compared to male patients (40, 41), which may explain our observation of fewer significant associations between CD4 counts and cytokine levels in the female cohort. Furthermore, female patients co-infected with HIV and helminths have been shown to exhibit better immunological recovery on ART compared to males (42), supporting our observation of more regulated immune responses in females. These findings suggest that sex-specific factors should be considered in developing therapeutic strategies for HIV-cysticercosis co-infection (43), with male patients potentially benefiting from modified anti-inflammatory interventions. Overall, these results highlight the potential impact of *T. solium* on immune function in PLWHA individuals, particularly in modulating pro-inflammatory and regulatory cytokine responses.

Similar patterns of immune dysregulation have been observed in other HIV-parasitic co-infections, such as schistosomiasis and soil-transmitted helminths, where elevated TNF-α and IL-6 persist, even in individuals on ART, indicating persistent immune activation (44–46). This occurs because helminths, including *T. solium*, release immunomodulatory molecules that drive a shift from a Th1 to a Th2 immune response, suppressing key pro-inflammatory cytokines like IFN-γ, while increasing IL-10 and IL-6, leading to continued but modulated immune activation (24, 25). In our study, this modulation was evident as *T. solium* co-infection altered the typical relationship between TNF-α and CD4 counts. While lower CD4 counts generally lead to increased TNF-α, the presence of CC moderated this increase, suggesting that the parasite's immunomodulatory effects dampened the expected pro-inflammatory response, even in the face of advanced immunosuppression. This highlights the need for targeted immunomodulatory interventions to manage immune activation in these patients (47).

Our findings suggest that the cytokines TNF-α, IL-1β, and IFN-γ are central to the immune response in HIV-CC co-infection whereas others like IL-18 are not. The elevated levels of these pro-inflammatory cytokines in CC-positive individuals with preserved immune function (with $CD4^+$ counts above 500 cells/μL) indicate an activated pro-inflammatory state, potentially driven by persistent antigenic stimulation from the parasite (48, 49). This continuous stimulation may modulate the balance between pro-inflammatory and regulatory cytokines, such as IL-10, exacerbating immune dysregulation despite partial immune recovery (50, 51). Similar patterns have been observed in studies where parasitic infections in HIV patients led to heightened immune activation, potentially exacerbating HIV progression (18, 52, 53). This persistent antigenic stimulation suggests that immune recovery, as measured by $CD4^+$ counts, may not fully mitigate ongoing inflammation and the clinical consequences thereof in such contexts (54, 55).

An unexpected finding in our study was the lack of significant differences in cytokine levels across $CD4^+$ categories based on individual cytokine analyses (e.g., TNF-α, IL-6, IL-10) and the absence of significant multivariate effects from the MANOVA, which assessed combined cytokine profiles across $CD4^+$ categories, CC status, and their interaction. This suggests that, while immune activation occurs in co-infected individuals, it does not lead to widespread alterations in cytokine profiles across the PLWHA population. Also, when considering all cytokines simultaneously, there are no clear distinctions based on $CD4^+$ categories or CC status alone. This finding supports the notion that immune modulation due to parasitic co-infections is targeted rather than systemic (49, 56), and indicates that the relationship between HIV, CC, and immune responses is more complex than initially hypothesized.

Comparative studies in HIV-negative individuals have reported varying immune responses to CC often with more regulated immune responses and less pronounced inflammation (25, 57). Our findings suggests that HIV infection alters this CC-driven immunological landscape, particularly in patients with low CD4 counts (SIM),

leading to heightened pro-inflammatory responses such as elevated TNF-α and IL-18 levels. This aligns with studies indicating that PLWHA individuals may experience more severe manifestations of parasitic infections due to immune dysregulation (27, 58). While our study focused on CC, similar interactions have been observed with other helminth infections in PLWHA populations. Co-infections with helminths such as schistosomiasis, soil-transmitted helminths and filarial infections (*Wuchereria bancrofti, Onchocerca volvulus, Loa loa*) have been linked to increased immune activation, and changes in cytokine profiles, including elevated IL-10 and TNF-α, which can exacerbate immune suppression and impact HIV disease progression (24, 25, 59). These effects are often contingent on $CD4^+$ counts, where severe immunosuppression is associated with greater immune dysregulation (elevated TNF-α and IL-18 levels, lower IFN-γ levels) (60, 61).

Several limitations of our study should be acknowledged. The sample size of 110 PLWHA patients may have limited our ability to detect certain associations, particularly in subgroup analyses. The cross-sectional design provides only a snapshot of immune status and cannot capture the dynamic nature of immune responses over time. Another limitation is the absence of an HIV-negative control group. However, previous studies have indicated that, under effective ART, cytokine profiles such as of IL-6, TNF and IL-1β of treated PLWHA individuals often closely resemble those of HIV-negative individuals (20). However, the primary goal of this study was to investigate the impact of CC on cytokines in relation to the CD4 counts in HIV positive individuals.

Despite these limitations, our study provides valuable insights into the complex interactions between HIV, CC, and immune responses. The observed persistence of elevated pro-inflammatory cytokines in CC-positive patients, along with the potential for differential immune responses based on $CD4^+$ counts, highlights the need for more nuanced and personalized approaches to HIV care in endemic areas.

Future research should aim to address the limitations of the current study and build upon its findings. Longitudinal studies with larger cohorts, including both PLWHA and HIV-negative individuals, could provide a more comprehensive understanding of the dynamic interplay between HIV, CC and other common helminths and immune responses over time. Such studies could also help elucidate the long-term clinical implications of the observed immune dysregulation in co-infected individuals such as on vaccine efficacy.

Furthermore, exploring the impact of antiparasitic treatment on immune responses and HIV disease progression in co-infected individuals could inform more effective treatment strategies. The potential use of cytokine profiles as biomarkers for CC in HIV patients warrants further investigation. If validated, such biomarkers could aid in the early detection and monitoring of CC in PLWHA individuals, potentially improving outcomes through timely intervention.

5 Conclusion

In conclusion, our study highlights the complex interactions between HIV infection, CC, and immune responses. Although we observed elevated levels of pro-inflammatory cytokines—such as TNF-α, IL-1β, and IFN-γ—in CC-positive patients with higher $CD4^+$ T-cell counts, these findings did not reach statistical significance. This suggests a trend toward immune activation that warrants further investigation. The lack of significant associations underscores the complexity of immune interactions in co-infected individuals and emphasizes the need for larger, longitudinal studies to better understand these dynamics. Considering parasitic co-infections and cytokine profiles in relation to the CD4 count in HIV management remains important, especially in endemic regions, to develop more targeted interventions that could improve patient outcomes.

Data availability statement

The raw data supporting the conclusions of this article will be made available by the authors, without undue reservation.

Ethics statement

The studies involving humans were approved by National Institute for Medical Research Ethics Review Committee, National Institute for Medical Research (NIMR), Ministry of Health, Community Development, Gender, Elderly and Children, P.O. Box 9653 Dar es Salaam, Tanzania. The studies were conducted in accordance with the local legislation and institutional requirements. Written informed consent for participation in this study was provided by the participants' legal guardians/next of kin.

Author contributions

YL: Conceptualization, Data curation, Formal analysis, Funding acquisition, Investigation, Methodology, Project administration, Resources, Software, Supervision, Validation, Visualization, Writing – original draft, Writing – review & editing. UP: Conceptualization, Data curation, Formal analysis, Investigation, Methodology, Resources, Software, Supervision, Writing – original draft, Writing – review & editing. CM: Data curation, Formal analysis, Investigation, Methodology, Project administration, Writing – review & editing. M-WN: Data curation, Formal analysis, Investigation, Methodology, Project administration, Validation, Writing – review & editing. AK: Conceptualization, Funding acquisition, Investigation, Methodology, Project administration, Resources, Supervision, Writing – review & editing. SM: Conceptualization, Funding acquisition, Investigation, Methodology, Project administration, Resources, Supervision, Writing – review & editing. VS: Conceptualization, Funding acquisition, Methodology, Project administration, Resources, Writing – review & editing. HC: Methodology, Resources, Writing – review & editing, Conceptualization, Funding acquisition. AW: Conceptualization, Data curation, Funding acquisition, Investigation, Methodology, Project administration, Resources, Supervision, Validation, Visualization, Writing – review & editing. EL: Methodology, Resources, Supervision, Writing – review & editing. BN: Conceptualization, Funding acquisition, Investigation, Methodology, Project administration, Resources, Supervision, Visualization, Writing –

review & editing. CP: Conceptualization, Data curation, Formal analysis, Funding acquisition, Investigation, Methodology, Project administration, Resources, Software, Supervision, Validation, Visualization, Writing – review & editing.

Funding

The author(s) declare financial support was received for the research, authorship, and/or publication of this article. The funders had no role in the design of the study, data collection, data analysis, decision to publish, or preparation of the manuscript. This work was supported by the German Federal Ministry of Education and Research (BMBF) through the project CYSTINET-Africa under the funding code 01KA161, which is part of the grant 81203604 from BMBF through the "Research Networks for Health Innovations in Sub-Saharan Africa" (RHISSA) initiative. In addition, CPdC received grants from the German Research Council (Deutsche Forschungsgemeinschaft, DFG) CO 1469/14-1/2 and 22-1. Further details about the funder can be accessed at https://www.cystinet-africa.net/funder/.

Acknowledgments

We would like to acknowledge Triphonia Mbena, Florida Mbwilo, and the entire NIMR Mbeya Research Lab for their invaluable support during this study. We also extend our heartfelt thanks to Frank Assenga for his guidance on the data analysis.

Conflict of interest

The authors declare that the research was conducted in the absence of any commercial or financial relationships that could be construed as a potential conflict of interest.

Generative AI statement

The author(s) declare that no Generative AI was used in the creation of this manuscript.

Publisher's note

Supplementary material

The Supplementary Material for this article can be found online at: https://www.frontiersin.org/articles/10.3389/fimmu.2025.1521295/full#supplementary-material

References

1. Fabiani S, Bruschi F. Neurocysticercosis in Europe: Still a public health concern not only for imported cases. *Acta Trop*. (2013) 128:18–26. doi: 10.1016/j.actatropica.2013.06.020

2. Winkler AS. Neurocysticercosis in sub-Saharan Africa: A review of prevalence, clinical characteristics, diagnosis, and management. *Pathog Glob Health*. (2012) 106:261–74. doi: 10.1179/2047773212Y.0000000047

3. Carabin H, Ndimubanzi PC, Budke CM, Nguyen H, Qian Y, Cowan LD, et al. Clinical manifestations associated with neurocysticercosis: A systematic review. *PloS Negl Trop Dis*. (2011) 5:1–13. doi: 10.1371/JOURNAL.PNTD.0001152

4. Torgerson PR, Devleesschauwer B, Praet N, Speybroeck N, Willingham AL, Kasuga F, et al. World health organization estimates of the global and regional disease burden of 11 foodborne parasitic diseases, 2010: A data synthesis. *PloS Med*. (2015) 12: e1001920. doi: 10.1371/journal.pmed.1001920

5. Garcia HH, Gonzalez AE, Gilman RH. Taenia solium cysticercosis and its impact in neurological disease. *Clin Microbiol Rev*. (2020) 33:1–23. doi: 10.1128/CMR.00085-19

6. Schmidt V, Kositz C, Herbinger KH, Carabin H, Ngowi B, Naman E, et al. Association between Taenia solium infection and HIV/AIDS in northern Tanzania: a matched cross sectional-study. *Infect Dis Poverty*. (2016) 5:1–15. doi: 10.1186/S40249-016-0209-7

7. Coral-Almeida M, Gabriël S, Abatih EN, Praet N, Benitez W, Dorny P. Taenia solium human cysticercosis: A systematic review of sero-epidemological data from endemic zones around the world. *PloS Negl Trop Dis*. (2015) 9:1–20. doi: 10.1371/JOURNAL.PNTD.0003919

8. Fogang YF, Savadogo AA, Camara M, Toffa DH, Basse A, Sow AD, et al. Managing neurocysticercosis: challenges and solutions. *Int J Gen Med*. (2015) 8:333. doi: 10.2147/IJGM.S73249

9. Zulu G, Stelzle D, Gabriël S, Trevisan C, Van Damme I, Mubanga C, et al. Neurocysticercosis prevalence and characteristics in communities of sinda district in Zambia: A cross-sectional study. *J Epidemiol Glob Health*. (2024) 14:1180–90. doi: 10.1007/s44197-024-00271-z

10. De Almeida SM, Gurjão SA. Quality of life assessment in patients with neurocysticercosis. *J Community Health*. (2011) 36:624–30. doi: 10.1007/S10900-010-9351-5

11. Gripper LB, Welburn SC. The causal relationship between neurocysticercosis infection and the development of epilepsy - a systematic review. *Infect Dis Poverty*. (2017) 6:31. doi: 10.1186/s40249-017-0245-y

12. Stelzle D, Abraham A, Kaminski M, Schmidt V, De Meijere R, Bustos JA, et al. Clinical characteristics and management of neurocysticercosis patients: a retrospective assessment of case reports from Europe. *J Travel Med*. (2022) 2022:1–13. doi: 10.1093/jtm/taac102

13. Assane YA, Trevisan C, Schutte CM, Noormahomed EV, Johansen MV, Magnussen P. Neurocysticercosis in a rural population with extensive pig production in Angónia district, Tete Province, Mozambique. *Acta Trop*. (2017) 165:155–60. doi: 10.1016/j.actatropica.2015.10.018

14. Mwape KE. An epidemiological study of human tapeworm infections in the Eastern Province of Zambia. *Ph.D. Thesis, University of Pretoria* (2012) 1–122.

15. Bhattarai R, Carabin H, Budke C. The burden of cysticercosis. *Nov Asp Cysticercosis Neurocysticercosis*. (2013) 13:1–19. doi: 10.5772/51668

16. Ngugi AK, Bottomley C, Kleinschmidt I, Wagner RG, Kakooza-Mwesige A, Ae-Ngibise K, et al. Prevalence of active convulsive epilepsy in sub-Saharan Africa and associated risk factors: cross-sectional and case-control studies. *Lancet Neurol*. (2013) 12:253–63. doi: 10.1016/S1474-4422(13)70003-6

17. Mbabazi PS, Andan O, Fitzgerald DW, Chitsulo L, Engels D, Downs JA. Examining the relationship between urogenital schistosomiasis and HIV infection. *PloS Negl Trop Dis*. (2011) 5:e1396. doi: 10.1371/journal.pntd.0001396

18. Walson JL, John-Stewart G. Treatment of helminth co-infection in individuals with HIV-1: A systematic review of the literature. *PloS Negl Trop Dis*. (2007) 1:e102. doi: 10.1371/journal.pntd.0000102

19. Means AR, Burns P, Sinclair D, Walson JL. Antihelminthics in helminth-endemic areas: effects on HIV disease progression. *Cochrane Database Syst Rev*. (2016) 4:1–9. doi: 10.1002/14651858.CD006419.pub4

20. Lema YL, Prodjinotho UF, Makasi C, Nanyaro M-WA, Kilale AM, Mfinanga S, et al. Evaluating the modulation of peripheral immune profile in people living with HIV and (Neuro)cysticercosis. *PloS Negl Trop Dis*. (2024) 18:e0012345. doi: 10.1371/journal.pntd.0012345

21. Prodjinotho UF, Lema J, Lacorcia M, Schmidt V, Vejzagic N, Sikasunge C, et al. Host immune responses during Taenia solium Neurocysticercosis infection and treatment. *PloS Negl Trop Dis*. (2020) 14:e0008005. doi: 10.1371/journal.pntd.0008005

22. Prodjinotho UF, Gres V, Henkel F, Lacorcia M, Dandl R, Haslbeck M, et al. Helminthic dehydrogenase drives PGE2 and IL-10 production in monocytes to potentiate Treg induction. *EMBO Rep*. (2022) 23:e54096. doi: 10.15252/embr.202154096

23. Prasad S, MacGregor RR, Tebas P, Rodriguez LB, Bustos JA, White AC. Management of potential neurocysticercosis in patients with HIV infection. *Clin Infect Dis*. (2006) 42:e30–4. doi: 10.1086/499359

24. Fleury A, Cardenas G, Adalid-Peralta L, Fragoso G, Sciutto E. Immunopathology in *Taenia solium* neurocysticercosis. *Parasite Immunol*. (2016) 38:147–57. doi: 10.1111/pim.12299

25. Restrepo BI, Alvarez JI, Castaño JA, Arias LF, Restrepo M, Trujillo J, et al. Brain granulomas in neurocysticercosis patients are associated with a Th1 and Th2 profile. *Infect Immun*. (2001) 69:4554–60. doi: 10.1128/iai.69.7.4554-4560.2001

26. Galan LEB, Gerolin LRM, Carvalho TJM, Filardi ETM, Ramos DLS, Dantas DSM, et al. Silent intruder: unusual presentation of neurocysticercosis in an HIV-infected patient from the far Northern Brazilian amazon. *Med Kaunas Lith*. (2024) 60:1–7. doi: 10.3390/medicina60030489

27. Jewell PD, Abraham A, Schmidt V, Buell KG, Bustos JA, Garcia HH, et al. Neurocysticercosis and HIV/AIDS co-infection: A scoping review. *Trop Med Int Health*. (2021) 26:1140–52. doi: 10.1111/TMI.13652

28. Stelzle D, Makasi C, Schmidt V, Trevisan C, Van Damme I, Ruether C, et al. Efficacy and safety of antiparasitic therapy for neurocysticercosis in rural Tanzania: a prospective cohort study. *Infection*. (2023) 51:1127–39. doi: 10.1007/s15010-023-02021-y

29. Noormahomed EV, Nhacupe N, Mascaró-Lazcano C, Mauaie MN, Buene T, Funzamo CA, et al. A cross-sectional serological study of cysticercosis, schistosomiasis, toxocariasis and echinococcosis in HIV-1 infected people in Beira, Mozambique. *PloS Negl Trop Dis*. (2014) 8:e3121. doi: 10.1371/journal.pntd.0003121

30. Lino-Junior Rde S, Faleiros ACG, Vinaud MC, de Oliveira FA, Guimarães JV, dos Reis MA, et al. Anatomopathological aspects of neurocysticercosis in autopsied patients. *Arq Neuropsiquiatr*. (2007) 65:87–91. doi: 10.1590/S0004-282X2007000100019

31. Serpa JA, Giordano TP, Goodman JC, White AC, Moran A. Neurocysticercosis in the HIV era: A case report and review of the literature. *Am J Trop Med Hyg*. (2007) 77:113–7. doi: 10.4269/ajtmh.2007.77.113

32. Ndimubanzi PC, Carabin H, Budke CM, Nguyen H, Qian Y-J, Rainwater E, et al. A systematic review of the frequency of neurocyticercosis with a focus on people with epilepsy. *PloS Negl Trop Dis*. (2010) 4:e870. doi: 10.1371/journal.pntd.0000870

33. Parija SC, Gireesh AR. A serological study of cysticercosis in patients with HIV. *Rev Inst Med Trop São Paulo*. (2009) 51:185–9. doi: 10.1590/S0036-46652009000400002

34. Herrera Vazquez O, Romo ML, Fleury A. Neurocysticercosis and HIV Infection: what can we learn from the published literature? *Arq Neuropsiquiatr*. (2019) 77:357–65. doi: 10.1590/0004-282X20190054

35. Moura VBL, Lima SB, Matos-Silva H, Vinaud MC, Loyola PRAN, Lino RS. Cellular immune response in intraventricular experimental neurocysticercosis. *Parasitology*. (2016) 143:334–42. doi: 10.1017/S0031182015001572

36. Mwanjali G, Kihamia C, Kakoko DVC, Lekule F, Ngowi H, Johansen MV, et al. Prevalence and risk factors associated with human taenia solium infections in Mbozi District, Mbeya Region, Tanzania. *PloS Negl Trop Dis*. (2013) 7:334–42. doi: 10.1371/JOURNAL.PNTD.0002102

37. Boa ME, Mahundi EA, Kassuku AA, Willingham AL, Kyvsgaard NC. Epidemiological survey of swine cysticercosis using ante-mortem and post-mortem examination tests in the southern highlands of Tanzania. *Vet Parasitol*. (2006) 139:1–9. doi: 10.1016/j.vetpar.2006.02.012

38. Nash M, Huddart S, Badar S, Baliga S, Saravu K, Pai M. Performance of the Xpert HIV-1 viral load assay: a systematic review and meta-analysis. *J Clin Microbiol*. (2018) 56:e01673–17. doi: 10.1128/JCM.01673-17

39. Erhart A, Dorny P, Van De N, Vien HV, Thach DC, Toan ND, et al. Taenia solium cysticercosis in a village in northern Viet Nam: seroprevalence study using an ELISA for detecting circulating antigen. *Trans R Soc Trop Med Hyg*. (2002) 96:270–2. doi: 10.1016/S0035-9203(02)90095-7

40. Klein SL, Flanagan KL. Sex differences in immune responses. *Nat Rev Immunol*. (2016) 16:626–38. doi: 10.1038/nri.2016.90

41. vom Steeg LG, Klein SL. SeXX matters in infectious disease pathogenesis. *PloS Pathog*. (2016) 12:e1005374. doi: 10.1371/journal.ppat.1005374

42. Zhao H, Feng A, Luo D, Yuan T, Lin Y-F, Ling X, et al. Factors associated with immunological non-response after ART initiation: a retrospective observational cohort study. *BMC Infect Dis*. (2024) 24:138. doi: 10.1186/s12879-024-09021-9

43. Scully EP. Sex differences in HIV infection: mystique versus machismo. *Pathog Immun*. (2018) 3:82–113. doi: 10.20411/pai.v3i1.238

44. Immunological and Haematological Changes in HIV Infection (2023). IntechOpen. Available online at: https://www.intechopen.com/chapters/49045 (Accessed September 22, 2024).

45. Mkhize-Kwitshana ZL, Taylor M, Jooste P, Mabaso ML, Walzl G. The influence of different helminth infection phenotypes on immune responses against HIV in co-infected adults in South Africa. *BMC Infect Dis*. (2011) 11:273. doi: 10.1186/1471-2334-11-273

46. Pasquereau S, Kumar A, Herbein G. Targeting TNF and TNF receptor pathway in HIV-1 infection: from immune activation to viral reservoirs. *Viruses*. (2017) 9:64. doi: 10.3390/v9040064

47. Zicari S, Sessa L, Cotugno N, Ruggiero A, Morrocchi E, Concato C, et al. Immune activation, inflammation, and non-AIDS co-morbidities in HIV-infected patients under long-term ART. *Viruses*. (2019) 11:1–17. doi: 10.3390/v11030200

48. Kallestrup P, Zinyama R, Gomo E, Butterworth AE, van Dam GJ, Erikstrup C, et al. Schistosomiasis and HIV-1 infection in rural Zimbabwe: implications of coinfection for excretion of eggs. *J Infect Dis*. (2005) 191:1311–20. doi: 10.1086/428907

49. van Riet E, Hartgers FC, Yazdanbakhsh M. Chronic helminth infections induce immunomodulation: Consequences and mechanisms. *Immunobiology*. (2007) 212:475–90. doi: 10.1016/j.imbio.2007.03.009

50. M'Bondoukwé NP, Moutongo R, Gbédandé K, Ngomo JMN, Hountohotegbé T, Adamou R, et al. Circulating IL-6, IL-10, and TNF-alpha and IL-10/IL-6 and IL-10/TNF-alpha ratio profiles of polyparasitized individuals in rural and urban areas of Gabon. *PloS Negl Trop Dis*. (2022) 16:e0010308. doi: 10.1371/journal.pntd.0010308

51. Mwape KE, Blocher J, Wiefek J, Schmidt K, Dorny P, Praet N, et al. Prevalence of neurocysticercosis in people with epilepsy in the Eastern Province of Zambia. *PloS Negl Trop Dis*. (2015) 9:e0003972. doi: 10.1371/journal.pntd.0003972

52. Modjarrad K, Vermund SH. Effect of treating co-infections on HIV-1 viral load: a systematic review. *Lancet Infect Dis*. (2010) 10:455–63. doi: 10.1016/S1473-3099(10)70093-1

53. Sandler NG, Douek DC. Microbial translocation in HIV infection: causes, consequences and treatment opportunities. *Nat Rev Microbiol*. (2012) 10:655–66. doi: 10.1038/nrmicro2848

54. Kanobana K, Ruiz A, Rojas L, Andrade R, Rosado F, Polman K, et al. Taenia solium cysticercosis: the case of Cuba. *PloS Negl Trop Dis*. (2013) 7:e2202. doi: 10.1371/journal.pntd.0002202

55. Morsica G, Galli L, Bossolasco S, Bagaglio S, Vercesi R, Salpietro S, et al. Brief report: outcome of acute hepatitis B virus infection in HIV-1–infected patients: possible factors associated with resolution or chronicity. *JAIDS J Acquir Immune Defic Syndr*. (2019) 82:175–80. doi: 10.1097/QAI.0000000000002106

56. Borkow G, Bentwich Z. Chronic immune activation associated with chronic helminthic and human immunodeficiency virus infections: role of hyporesponsiveness and anergy. *Clin Microbiol Rev*. (2004) 17:1012–30. doi: 10.1128/CMR.17.4.1012-1030.2004

57. Rodriguez S, Wilkins P, Dorny P. Immunological and molecular diagnosis of cysticercosis. *Pathog Glob Health*. (2013) 106:286–98. doi: 10.1179/2047773212y.0000000048

58. Sciutto E, Chavarria A, Fragoso G, Fleury A, Larralde C. The immune response in Taenia solium cysticercosis: protection and injury. *Parasite Immunol*. (2007) 29:621–36. doi: 10.1111/j.1365-3024.2007.00967.x

59. Kroidl I, Chachage M, Mnkai J, Nsojo A, Berninghoff M, Verweij JJ, et al. Wuchereria bancrofti infection is linked to systemic activation of CD4 and CD8 T cells. *PloS Negl Trop Dis*. (2019) 13:e0007623. doi: 10.1371/journal.pntd.0007623

60. Elias D, Britton S, Kassu A, Akuffo H. Chronic helminth infections may negatively influence immunity against tuberculosis and other diseases of public health importance. *Expert Rev Anti Infect Ther*. (2007) 5:475–84. doi: 10.1586/14787210.5.3.475

61. Walson JL, Otieno PA, Mbuchi M, Richardson BA, Lohman-Payne B, Macharia SW, et al. Albendazole treatment of HIV-1 and helminth co-infection: a randomized, double-blind, placebo-controlled trial. *AIDS Lond Engl*. (2008) 22:1601–9. doi: 10.1097/QAD.0b013e32830a502e

frontiers | Frontiers in Immunology

TYPE Original Research
PUBLISHED 28 February 2025
DOI 10.3389/fimmu.2025.1521022

OPEN ACCESS

EDITED BY
Anisuzzaman Anisuzzaman,
Bangladesh Agricultural University,
Bangladesh

REVIEWED BY
Esther Gathoni Kanduma,
University of Nairobi, Kenya
Simone Cristina Méo Niciura,
Embrapa Pecuária Sudeste, Brazil
Stefanía P. Bjarnarson,
National University Hospital of Iceland,
Iceland

*CORRESPONDENCE
Chunqun Wang
wangchunqun@mail.hzau.edu.cn
Min Hu
mhu@mail.hzau.edu.cn

†These authors have contributed equally to this work

RECEIVED 01 November 2024
ACCEPTED 07 February 2025
PUBLISHED 28 February 2025

CITATION
Liu H, Zhang Y, Li J, Liu F, Ye L, Liu X, Wang C and Hu M (2025) Identification and validation of protective glycoproteins in *Haemonchus contortus* H11. *Front. Immunol.* 16:1521022. doi: 10.3389/fimmu.2025.1521022

Identification and validation of protective glycoproteins in *Haemonchus contortus* H11

Hui Liu[1†], Yao Zhang[1†], Jiarui Li[1], Feng Liu[1], Lisha Ye[1], Xin Liu[2], Chunqun Wang[1*] and Min Hu[1*]

[1]National Key Laboratory of Agricultural Microbiology, College of Veterinary Medicine, Huazhong Agricultural University, Wuhan, China, [2]College of Life Science and Technology, Huazhong University of Science and Technology, Wuhan, China

Barbervax is the first and only available vaccine to protect animals against *Haemonchus contortus* - one of the most pathogenic parasites of small ruminants. This vaccine contains a kind of native antigen called H11, a glycoprotein complex derived from integral gut of this parasite. Native H11 has been shown to induce high levels (72-95%) of protection, but single or two recombinant molecules of H11 are consistently unsuccessful. An increasing number of aminopeptidases related to H11 have been characterized in the past three decades, but little is known about which ones are the key contributors to protective immunity. Our recent work has revealed that the immunoprotective effect of H11 is primarily associated with its N-glycan moieties. To identify key immunoprotective glycoproteins derived from H11 antigen, we employed glycan-related protective IgG antibodies combined with LC-MS/MS analysis and identified five glycosylated H11 proteins: H11, H11-1, H11-2, H11-4, and H11-5. Subsequently, we utilized the baculovirus-insect cell expression system and successfully expressed four H11 recombinant proteins including rH11, rH11-1, rH11-2 and rH11-4, which demonstrated similar aminopeptidase activity and comparable high-mannose and di-fucosylated N-glycan structures to those found on native H11. Immunization of goats with a cocktail of four rH11s induced a 66.29% reduction ($p > 0.05$) in total worm burden and cumulative fecal egg counts. High level of anti-rH11s IgG which could inhibit *H. contortus* intestinal aminopeptidase activity and larval development. Collectively, our study identified glycoprotein antigens from H11 and assessed their protective efficacy of a recombinant cocktail expressed in insect cells. This work will provide valuable insights into further development of recombinant vaccines against parasitic nematodes.

KEYWORDS

H11, vaccine, glycoprotein, N-glycan, recombinant antigen, insect cells, immunoprotection

Introduction

Roundworms (nematodes) form one of the largest and most diverse groups of animals. Many species, including gastrointestinal nematodes (GINs), result in serious threats to the health, welfare, and productivity of grazing animals (1, 2). GINs impose severe economic losses on livestock husbandry in numerous countries all over the world (3–6). Current strategies for controlling GINs rely on anthelmintic treatments, which have become increasingly costly and complicated due to the global rise in drug resistance (1, 5, 7, 8). Therefore, there is an urgent need for new and effective integrated prevention and management strategies to control the spread of drug-resistant GIN diseases.

Vaccination is regarded as an alternative and sustainable intervention strategy for controlling GIN parasitosis in livestock. Currently, the only GIN vaccine available is Barbervax, the first effective vaccine developed to control *Haemonchus contortus*. This parasite, commonly known as the barber's pole worm, is the most significant roundworm parasite of ruminants worldwide. This vaccine is based on intestinal membrane proteins from adult *H. contortus*. H11, a 110 kDa glycoprotein complex, which is the most important component in Barbervax. Administrated H11 alone could achieve > 75% reduction in worm burden and > 90% reduction in fecal egg counts (FECs) (9–13). Despite high protections induced by the native proteins, however, various recombinant forms of H11 expressed in different expression systems, such as bacteria (14), insect cells (15), and *Caenorhabditis elegans* (16, 17), have failed to provide the expected immune protection compared to native H11 (nH11).

Indeed, extensive research efforts have proven that nH11 is not a single protein but a collection of highly glycosylated proteins, containing a mixture of multiple glycoproteins from the microsomal M1 aminopeptidase family (18), which is believed to be involved in the degradation of small peptides during the digestion of host hemoglobin (19). Initially, three H11 isoforms (GenBank accession nos. AJ249941, AJ249942 and AJ311316) were cloned and sequenced based on gene analysis (14) and another isoform (GenBank accession no. X94187) was subsequently isolated using anti-H11 sera from the *H. contortus* cDNA library (18), In 2013, Roberts et al. identified a novel H11 sequence (GenBank accession no. KF381362.1) through *H. contortus* genomic data (17). With the rapid development of advanced omics techniques, an updating number of H11-related aminopeptidases have been characterized. There are 13 novel aminopeptidases (termed AP-1 to AP-13) that have been identified in the M1 aminopeptidase family through genomic and transcriptomic analyses (21), and 85 distinct proteins were identified in the N-glycoproteome of nH11 using glycoproteomic techniques (20). Moreover, as a highly glycosylated complex, our recent work demonstrated that the H11-induced immune protection was predominantly related to N-glycans (20). Nevertheless, it remains unclear which specific glycoproteins among them are the crucial contributors to immunoprotection and whether these H11 proteins exhibit redundant or synergistic immunological functions. Additionally, due to the abundant and unique N-glycan structures [e.g. core α1,3-linked fucoses, antennal fucosylated GalNAc-GlcNAc (LDNF)] present in nH11 (20), which are not commonly present in vertebrate glycans and are considered highly immunogenic (21–23). Accurately simulating these unusual glycan structures in the expression systems is another significant challenge in recombinant vaccine development.

Previously unsuccessful immune protection provided by single (14, 15, 24) or dual rH11s (17) suggests that identifying key protective glycoproteins derived from nH11 complex, preserving the integrity of glycan structures in rH11s, and fully combining them into a multivalent cocktail antigen may enhance immune protection in recombinant vaccines. Our previous study revealed that glycan-induced protective IgG antibodies confer specific and passive immunity in animals (20). Here, we identified the dominant glycoprotein antigens from nH11 by this glycan-related protective IgG antibodies. These identified glycoproteins were produced in the insect cell expression system that possesses the closest N-glycosylation pattern to nH11 among the available expression systems (25), and their aminopeptidase activities, N-glycan motifs, as well as protective effects in animals of these recombinant H11s (rH11s) were assessed. These findings have important implications for development of related parasite vaccines.

Materials and methods

Parasite materials

The infective third-stage larvae (iL3s) and female adult worms of *H. contortus* (Haecon-5 strain, a standard strain that has been preserved in our laboratory) were collected and maintained following previously established protocols (26). Briefly, the iL3s were isolated from feces cultured at 25°C for 7 days using the Baermann collecting procedure. To collect exsheathed L3s (xL3s) *in vitro*, the iL3s were exsheathed and sterilized by incubation in 0.15% v/v sodium hypochlorite solution at 37°C for 10 min, followed by centrifugation (1,000 *g*, 3 min) to remove sheaths. Female adult worms were collected from the abomasa of goats and distinguished according to morphological characteristics, such as red and white spiral stripes.

Immunoprecipitation

Four kinds of serum IgG antibodies used in immunoprecipitation assay were from our previous study (20), derived from four groups of goats vaccinated with three different H11 antigens (NA-native H11, DN-heat denatured H11 and PI-periodate treated H11) and adjuvant (AJ), respectively. Briefly, 50 μg of each IgG antibodies (NA, DN, PI and AJ) were added to 50 μL of Protein A+G magnetic beads (Beyotime Biotechnology) pre-washed with cold phosphate-buffered saline (PBS; pH 7.4) and incubated at 4°C for 2 h. Following incubation, a magnetic stand was employed to separate the beads, and unbound IgG antibodies were removed through multiple washes with cold PBS. Subsequently, 100 μg of nH11, extracted using Con A-Sepharose

(GE Healthcare) as described previously (9, 20), was added to each of the four groups of IgG antibodies and incubated at 4°C for 3 h to ensure complete binding of nH11 to the antibodies. Post-incubation, the beads were subjected to magnetic separation for 15 s, followed by the removal of the supernatant and thorough washing with PBS. The eluate was then analyzed by SDS-PAGE and reserved for subsequent LC-MS/MS analysis.

LC-MS/MS analysis

Four different sets of immunoprecipitated antigen-antibody complexes were thoroughly washed with 50 mM NH_4HCO_3 solution and subsequently incubated in 100% acetonitrile. The complexes were then rehydrated with trypsin at a concentration of 10 ng/μL, dissolved in 50 mM NH_4HCO_3 solution, and kept on ice for 1 h. Peptides were initially extracted with a solution of 50% acetonitrile and 5% formic acid, followed by extraction with 100% acetonitrile. The peptides were then completely dried and resuspended in a solution of 2% acetonitrile containing 0.1% formic acid. After preparation, the peptides were analyzed using a nano-spray ionization (NSI) source, followed by tandem mass spectrometry (MS/MS) on a Q Exactive™ Plus mass spectrometer (Thermo Fisher Scientific), which was coupled online to an ultra-performance liquid chromatography (UPLC) system. An electrospray voltage of 2.0 kV was applied, with a mass-to-charge (*m/z*) scan range set between 350 and 1,800 for full-scan analysis. Intact peptides were detected in the Orbitrap at a resolution of 70,000. Selection for MS/MS analysis was conducted with a normalized collision energy (NCE) setting of 28, and fragment ions were detected in the Orbitrap at a resolution of 17,500. A data-dependent acquisition method was employed, alternating between one MS scan followed by 20 MS/MS scans, incorporating a dynamic exclusion duration of 15 s. The automatic gain control (AGC) target was set to 5E4.

The resultant MS/MS data were processed using Proteome Discoverer 1.3 software. Tandem mass spectra were queried against the *H. contortus* database (UniProt, 24,551 sequences). Trypsin/P was designated as the proteolytic enzyme, permitting up to two missed cleavages. The precursor ion mass tolerance was set at 10 ppm, while the fragment ion mass tolerance was set at 0.02 Da. Carbamidomethylation of cysteine residues was specified as a fixed modification, and methionine oxidation was defined as a variable modification. Peptide identification confidence was set to high, with a peptide ion score threshold of >20.

Sf9 and High Five insect cells culture

Sf9 cells (Invitrogen) employed for recombinant virus production were maintained as adherent cultures at 28°C in Sf-900™ II medium (Thermo Fisher Scientific). High Five cells (Invitrogen) used for protein expression were maintained in suspension in cell shakers at 120 rpm at 28°C in Express Five™ medium (Thermo Fisher Scientific). Both cell lines were passaged every three days. Cell density was determined by Malassez hemocytometer (Marienfeld), and cell viability was assessed by Trypan blue staining (1 mg/mL, v/v).

Cloning, protein expression and purification of H11 molecules

To express the recombinant proteins in insect cells, five H11 coding sequences (GenBank accession nos. AJ249941.1, AJ249942.2, AJ311316.1, KF381362.1, Q10737 of H11-1, H11-2, H11-4, H11-5 and H11, respectively) were synthesized based on insect cell codon bias and subcloned into a baculovirus vector, pFastBac1, using BamHI and HindIII restriction sites. The original transmembrane sequence was removed, and the product was cloned downstream of an additional signal sequence (MKTIIALSYIFCLVFAAG) in the pFastBac1 expression vector, along with an N-terminal Flag tag and 10 × His tag for identification and purification. Diagrammatic representations of final expression constructs were shown in Supplementary Figure 1. Protein expression and purification followed well-established protocols. In brief, Sf9 cells were seeded onto six-well plates at 8 × 10^5 cells/mL and incubated in Sf-900™ II medium (Thermo Fisher Scientific) containing 1.5% fetal bovine serum (FBS; Invitrogen) at 28°C for 24 h before transfection. 1 μg of baculovirus plasmid was co-transfected with 8 μL of Cellfectin™ II Reagent (Thermo Fisher Scientific) into Sf9 cells according to the manufacturer's instructions. The transfection mixture was removed 5 h post-transfection and replaced with 2 mL of Sf-900™ II medium supplemented with 10% FBS. Sf9 cells were then cultured under the same conditions for 96 h, and then the transfection supernatant was harvested and amplified twice to obtain a high titer of recombinant virus. High Five cells were infected with the recombinant virus at a multiplicity of infection (MOI) of 5 in the exponential growth phase (1×10^6 cells/mL; 95% viability) in shake flasks at 28°C for 96 h. The culture media was collected and centrifuged at 3,000 *g* for 15 min, then purified utilizing affinity chromatography with Ni Sepharose™ excel (GE Healthcare) following eluted with 200 mM imidazole. The harvested eluent was dialyzed against PBS for 48 h and finally concentrated with sucrose. The concentrations of the final purified proteins were measured with the BCA Protein Assay Kit (Vazyme) and the purity was verified by SDS-PAGE staining with Coomassie brilliant blue.

Aminopeptidase activity assay of recombinant H11

Aminopeptidase catalyzes the conversion of the substrate L-leucine-p-nitroanilide (L-Leu-pNA) to yield the compound p-nitroaniline (pNA). The concentration of pNA, determined by absorbance at 405 nm, serves as an indicator of total aminopeptidase activity. To evaluate whether these rH11s exhibit aminopeptidase activity and to determine their optimal pH, 10 μg of each rH11 was incubated with 10 μL of 0.2 mM L-Leu-pNA (Sigma) at 37°C for 150 min at a shaking speed of 100 rpm. Phosphate buffers with varying pH values (ranging from 4.0 to

8.0) were added to achieve a final volume of 100 µL in 96-well microtiter plates. Absorbance was recorded at 405 nm using a multi-mode plate reader (BioTek Cytation 5), and the rate of optical density change per minute per microgram of protein was subsequently calculated.

Release, purification and permethylation of N-glycans of recombinant H11

The N-glycan preparation procedure was conducted as described previously (20). Briefly, 50 µg of each rH11 was denatured with 1 × glycoprotein denaturing buffer (0.5% SDS, 40 mM DTT) at 100°C for 10 min. Following the addition of NP-40 and GlycoBuffer 2 (50 mM sodium phosphate; pH 7.5), 2 µL of PNGase F (New England Biolabs) was added, and the reaction mixture was incubated overnight at 37°C. The glycan supernatant was isolated by centrifugation at 12,000 *g* for 15 min. To fully release all N-glycans, the remaining glycoprotein was washed, dried, denatured, and dissolved in GlycoBuffer 3 (50 mM sodium acetate; pH 6.0). Next, 2 µL of PNGase A (New England Biolabs) was added, and the reaction mixture was incubated at 37°C for 6 h. The glycan supernatant was harvested as above. Glycans released by PNGase F and PNGase A were further purified by porous graphitic carbon (PGC) cartridges, and the collected N-glycan eluent was dried at 37°C in a centrifugal evaporator. Permethylation was performed by published methods (27). Briefly, the dried N-glycan samples were dissolved in 50 µL of dimethyl sulfoxide (DMSO), followed by the addition of 100 µL of NaOH-DMSO suspension. Subsequently, the suspension was gently mixed, and 50 µL of methyl iodide was added. The mixture was fully vortexed for 20 min at room temperature and terminated by adding 500 µL of ultrapure water. The final methylated glycans were isolated by extraction with water/chloroform and the chloroform layer was dried as above.

Mass spectra were acquired utilizing the 5800 MALDI-MS (SCIEX, Concord) instrument operating in positive ionization mode. The dried glycan residues were reconstituted in 15 µL of 50% methanol, and the matrix solution was prepared by dissolving 10 mg/mL 2,5-dihydroxybenzoic acid (DHB) in 50% acetonitrile supplemented with 10 mM sodium acetate. A 1:1 mixture of permethylated glycan and DHB matrix (1 µL each) was applied to a MALDI plate and crystallized. Each sample spot received 1,000 laser shots. MS/MS was conducted with air as the CID gas at 2 kV. The resulting data were processed using Data Explorer 4.0 (SCIEX, Concord), and spectra were annotated with GlycoWorkbench 2.1. Theoretical fragmentation lists were generated for MS/MS interpretation.

Immunization trial

To evaluate whether the cocktail consisting of four rH11s could induce protective immunity against *H. contortus*, immunization and infection experiments were conducted in goats. All goat experiments were approved by the Animals Ethics Committee of Huazhong Agricultural University (permit code: HZAUGO-2024-0006). The workflow of the animal trials was shown in Figure 1. Briefly, 16 healthy Boer goats, aged 6-8 months and reared under conditions ensuring the absence of helminth infections, were randomly allocated into two groups of eight, matched by age and sex. Goats in the vaccinated group were administered 300 µg of a recombinant cocktail (comprising 75 µg each of rH11, rH11-1, rH11-2 and rH11-4) formulated with 500 µg of Quil A® adjuvant (InvivoGen). The adjuvant group, serving as the control, received an equivalent dose of the Quil A® adjuvant alone. Each goat was immunized subcutaneously thrice at three-week intervals (Figure 1). Following the third immunization on day 42, each goat was orally challenged with 7,000 iL3s and was then fasted for 8 h. An additional booster immunization was supplemented on day 56. Throughout the trial, blood and fecal samples were collected as described previously (20). Briefly, blood samples were obtained weekly from day 0 to the end of the trial. FECs were performed three to four times per week from 14 days post-iL3s challenge. On

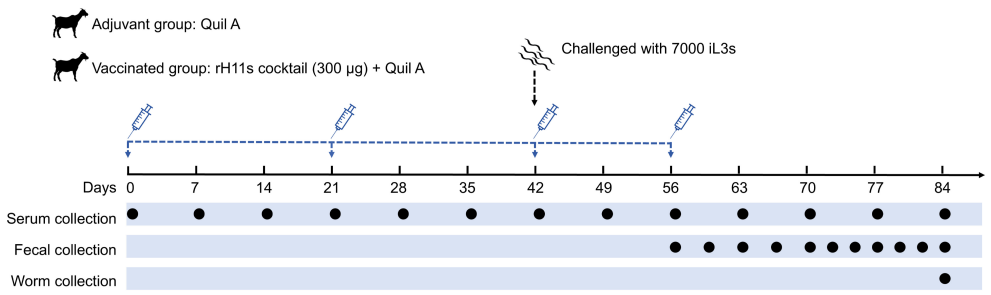

FIGURE 1
Diagram showing the procedure of animal vaccination trial. Two groups of eight goats each were immunized subcutaneously with adjuvant alone or 300 µg of rH11s cocktail four times (days 0, 21, 42 and 56). On the day of the third immunization (day 42), 7,000 infective third-stage larvae (iL3s) were challenged orally. The time points for immunization and challenge were identified with corresponding legends. Blood samples were collected weekly, and fecal samples were collected 2 to 3 times every week starting from 14 days post-challenge. On 28 days post-challenge, as the adult worms began to stably lay eggs, the frequency of fecal sample collection increased to 3 to 4 times every week. On day 84, all goats were euthanized, and the abomasa were dissected to collect adult parasites. The time points for blood collection (13 times), fecal collection (11 times) and adult worm collection (once) were indicated by black circles.

day 84, all goats were euthanized, and the number of adult male and female worms present in individual abomasum was quantified.

Western-blot analysis

To ascertain whether specific goat anti-rH11s IgG antibodies can be elicited following vaccination and whether these antibodies can recognize nH11, the following immunoblotting experiments were conducted. Serum (200 µL per goat) on day 42 was collected from blood samples and pooled, and the IgG antibodies were isolated using Protein A+G agarose (Beyotime Biotechnology) according to the manufacturer's instructions. Both rH11s and nH11 (50 µg of each protein) were denatured in a loading buffer with DTT and subjected to SDS-PAGE on 12.5% polyacrylamide gels. After electrophoresis, the proteins were transferred to a membrane and probed with primary IgG antibodies diluted 1:1,000. Horseradish peroxidase (HRP)-conjugated donkey anti-goat IgG (Abbkine) at a dilution of 1:5,000 was used as the secondary antibody. Detection was performed using an ECL reagent (Vazyme), and the results were visualized with a Tanon Imaging System.

Detecting the dynamics of anti-rH11s IgG antibody

The dynamics of goat anti-rH11s IgG antibodies from each animal were assessed by indirect enzyme-linked immunosorbent assay (ELISA). In brief, serum was obtained from blood samples after centrifugation at 500 *g* for 10 min at 4°C. 96-well microtiter plates were coated with a mixture of four rH11s (400 ng per well, with 100 ng of each protein) or individual rH11 (100 ng per well) diluted in carbonate buffer (50 mM; pH 9.6) and incubated at 4°C overnight, and then blocked with PBS (pH 7.4) containing 0.05% (v/v) Tween 20 and 1% (w/v) bovine serum albumin (BSA; Sigma) at 37°C for 2 h. Individual goat sera were diluted 1:2,000 and incubated at 37°C for 1 h. Subsequently, an HRP-conjugated donkey anti-goat IgG antibody (Abbkine) was applied as the secondary antibody at a dilution of 1:5,000 and further incubation at 37°C for 40 min. The assay was developed using tetramethylbenzidine (TMB) substrate at 37°C for 15 min, and the reaction was terminated by the addition of 10% H_2SO_4. Absorbance was measured at 450 nm using a microplate reader (BioTek Cytation 5).

Aminopeptidase activity and larval development inhibition assays

To determine whether anti-rH11s IgG antibodies could inhibit the aminopeptidase activity of nH11 enriched in the intestine, we isolated intestines of 30 female adults collected from non-vaccinated goats and extracted the gut proteins as previously described (28). Anti-rH11s IgG antibodies were purified from the goat serum collected on day 42 post-immunization by the protein A+G affinity chromatography (Beyotime Biotechnology). A total of 10 µg of gut proteins were pre-incubated with 5 µL of purified anti-rH11s IgG antibodies (1 mg/mL) at 37°C for 40 min. Meanwhile, 10 mM bestatin (Sigma) was employed as a positive control under identical conditions. Following the pre-incubation, 10 µL of 0.2 mM L-Leu-pNA (Sigma) was added to citrate-phosphate buffer (pH 7.0) and incubated at 37°C for 150 min. Absorbance readings were taken at 405 nm using a microplate reader (BioTek Cytation 5).

To further assess whether these anti-rH11s IgG antibodies can inhibit larval development, xL3s were cultured in 24-well plates (100 xL3s per well) in 200 µL of sterile Luria-Bertani (LB) medium, supplemented with 100 IU/mL of penicillin, 100 µg/mL of streptomycin (Sigma) and 0.25 µg/mL of amphotericin (Sigma). The larvae were treated with 50 µL of anti-rH11s IgG antibodies (1 mg/mL) and incubated at 39°C with 20% CO_2. The developmental rate was assessed on day 4 by identifying the presence of a buccal capsule, a defining characteristic of the L4s (29). Additionally, the length and width of individual L4s were measured on the same day.

Statistical analysis

All statistical analyses were conducted using Prism 8.0 software (GraphPad), and standard deviation (SD) or standard error of mean (SEM) was calculated. Non-parametric Mann-Whitney tests were used to perform the statistical analysis of cumulative FECs and worm burden. One-way analysis of variance (ANOVA) followed by Dunnett's test was used to compare the enzymatic activities of different rH11s as well as the inhibition of IgG antibodies. The $^{*}p < 0.05$, $^{**}p < 0.01$, $^{***}p < 0.001$, $^{****}p < 0.0001$ and ns (not significant) indicated the degree of statistical significance.

Results

Immunoprecipitation assay differentially identified five protective H11 isoforms

In this study, we conducted the immunoprecipitation assay using four groups of protective IgG antibodies (NA, DN, PI, and AJ) obtained from our previous study (20) to identify key protective antigens in nH11. nH11 was extracted and purified by ConA lectin (Figure 2A) from *H. contortus* adult worms and then used in the immunoprecipitation assay. On the SDS-PAGE gel with silver staining following immunoprecipitation, distinct protein bands within the range of 100-130 kDa were identified by the antibodies from the NA and DN groups with high levels of immune protection (20). In contrast, this region was absent in the PI group, which exhibited a lower level of immune protection (20) as well as in the AJ control group (Figure 2B). To further identify the key protective H11 components differentially recognized by the above four IgG antibodies, we performed LC-MS/MS analysis against *H. contortus* databases. In *H. contortus* genomic and transcriptomic databases (30), due to the usage of different sequencing methods and *H. contortus* strains (17, 18, 31, 32), several aminopeptidases were derived from the same transcript and have different accession

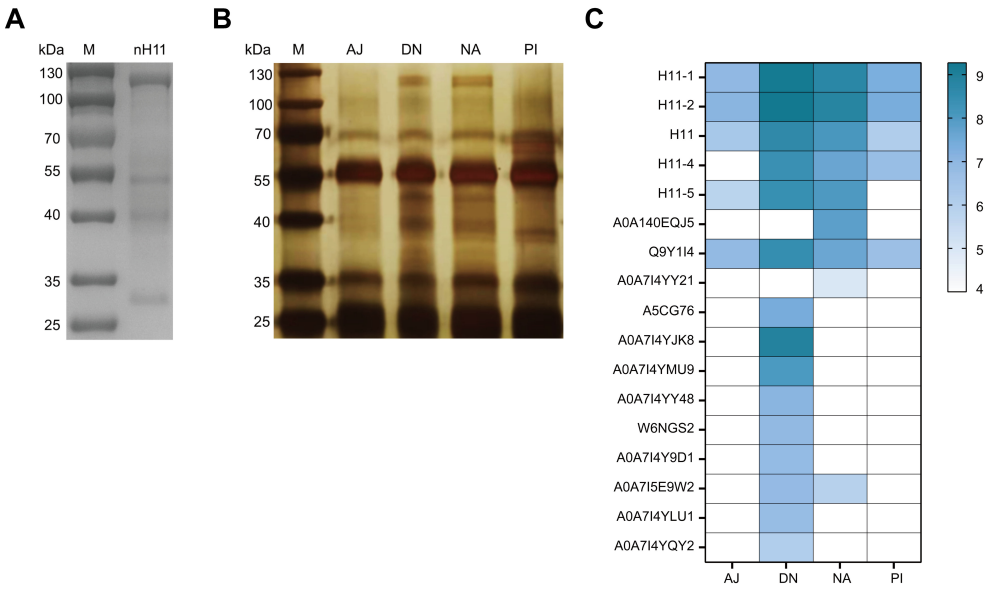

FIGURE 2
Identification of key immune protective antigens from native H11 protein complex.**(A)** SDS-PAGE analysis of nH11 purified using Con A-sepharose from *H. contortus* adult worms. M, protein marker. **(B)** Results of immunoprecipitation. SDS-PAGE with silver staining of nH11 proteins recognized by four groups of different IgG antibodies obtained from our previous vaccination trials in goats (20). M, protein marker. **(C)** Results of LC-MS/MS analysis. Heatmap of proteins (with molecular weights ranging from 100 to 130 kDa) abundance in different groups. AJ, IgG antibodies from adjuvant group; DN, IgG antibodies from high-temperature denatured H11 group; NA, IgG antibodies from native H11 group; PI: IgG antibodies from periodate treated H11 group.

numbers in the UniProt database, which created the redundancies and confusion to the analysis of mass spectrometry results. To clarify this, we analyzed detailed information on 41 aminopeptidases and 42 peptidase-related proteins retrieved from *H. contortus* databases (Supplementary Figure 2) and reclassified them according to the latest transcriptomic data (30). The analysis results were shown in Supplementary Table 1. Based on these data, the differential abundances of 21 aminopeptidases (with molecular weights ranging from 100 to 130 kDa) recognized by the four groups of antibodies were identified (Figure 2C, Supplementary Table 2). The abundances of five aminopeptidases including H11-1, H11-2, H11-4, H11-5 and H11, were significantly higher in NA and DN groups than those in PI and AJ groups, suggesting these five antigens could be main contributors to the immunoprotective properties of nH11.

Four H11 isoforms expressed in insect cells showed aminopeptidase activity

We employed High Five insect cells to produce the above identified five H11 isoforms, but only four of them (H11-1, H11-2 H11-4 and H11) were successfully expressed despite multiple attempts. As expected, molecular masses of these rH11s were all around 100-130 kDa, whereas the rH11 and rH11-4 were slightly larger than those of rH11-1 and rH11-2 (Figure 3A), which may be associated with different protein glycosylation. To detect whether these four rH11s possess aminopeptidase activity like nH11, we assessed their aminopeptidase activities using a standard Leu-PNA substrate. All four rH11s exhibited high-level aminopeptidase activity. Both rH11-1 and rH11 exhibited optimal activity at pH 7.0 (Figure 3B), consistent with that of previously described native intestinal aminopeptidases (20), while rH11-2 and rH11-4 exhibited better activities at pH of 6.0 (Figure 3B). Notably, rH11-1 demonstrated significantly higher enzymatic activity than the other three rH11s (Figure 3C).

N-glycome profiling of the recombinant H11 isoforms

To decode the N-glycomes of rH11s, we conducted MALDI-TOF/MS analysis on rH11s' N-glycans motifs. Based on the known N-glycomes data of nH11 and High Five cells (20, 25), a total of 15 glycan signal peaks, including 12 PNGase F-released glycans and three PNGase-A released glycans, were identified from four rH11s (Figures 4, 5, Table 1). We observed that the most abundant glycans were oligomannosidic ($Hex_{5-9}HexNAc_2$) and paucimannosidic forms ($Hex_{2-3}HexNAc_2$) with and without core fucoses (Figures 4, 5, Table 1). The majority of N-glycans were entirely released following treatment with the PNGase F, and the N-glycans released by the PNGase A served as additional components post-PNGase F treatment, as it can specifically cleave the core α1,3-linked fucose motif. rH11-2, rH11-4 and rH11 displayed

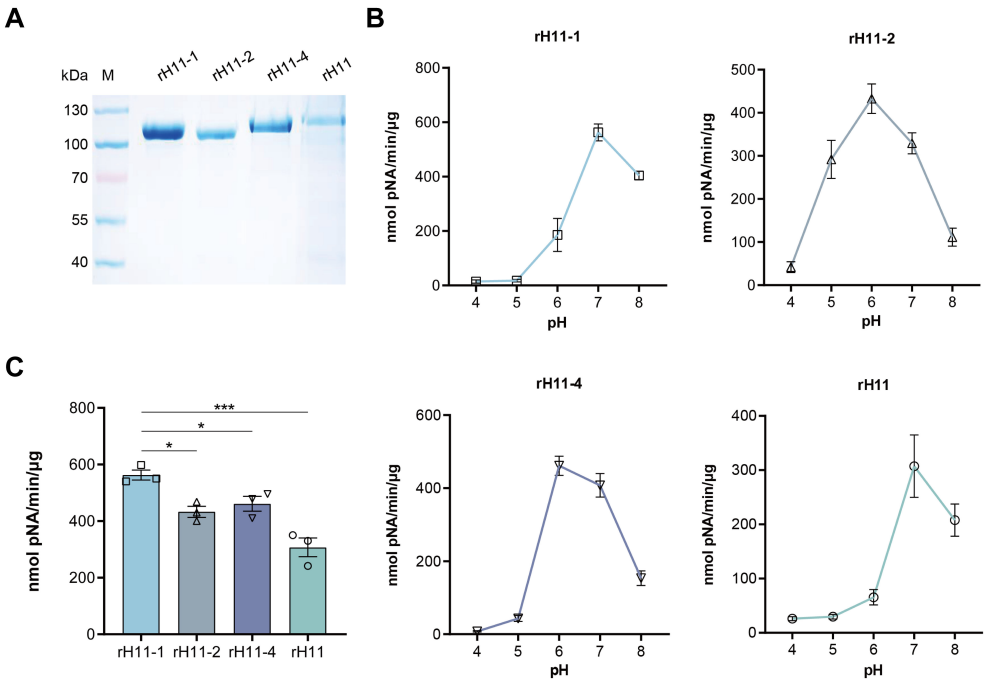

FIGURE 3
Aminopeptidase activity of four recombinant H11 proteins expressed in insect cells. **(A)** SDS-PAGE analysis of four purified rH11s expressed in insect cells. M, protein marker. **(B)** Optimal pH (ranging from 4.0 to 8.0) of aminopeptidase activity for each rH11. **(C)** Comparison of aminopeptidase activity among four rH11s. Data (absorbance at 405 nm) were pooled with the mean ± standard error of the mean (SEM) from three independent experiments, and statistically significant differences were analyzed using one-way ANOVA and indicated with *($p < 0.05$), ***($p < 0.001$), not significant was not marked.

characteristic N-glycan signal peaks after PNGase A digestion, predominantly featuring the $Hex_3HexNAc_2Fuc_2$ configuration (*m/z* 1519.9), indicating the presence of di-fucosylated glycan forms (Figure 5, Table 1). In rH11, two distinct α1,3-linked fucose glycans, $Hex_2HexNAc_2Fuc_1$ (*m/z* 1315.8) and $Hex_3HexNAc_2Fuc_1$ (*m/z* 1345.8) were additionally identified (Figure 5C, Table 1), which were absent in the other three rH11s (Figures 5A, B, Table 1). Besides, the unusual LDN glycans (*m/z* 2151.9) existed in rH11-4 and rH11 N-glycomes, although their abundance was limited (Figures 4C, D, Table 1).

Protective effect of recombinant H11 cocktail antigens on goats

To examine the immune protective effectiveness of this rH11s cocktail, we designed an animal vaccination trial as depicted in Figure 1. Between day 18 and day 21 post-challenge, both groups of goats began to excrete *H. contortus* eggs in feces. The result revealed that the mean cumulative FECs of the adjuvant control group continuously increased, peaking at 1,600 on day 40. In contrast, the mean cumulative FECs of goats vaccinated with rH11s remained below 550 over the course of trials. The reduction in mean cumulative FECs ultimately reached 66.29% compared to the adjuvant group (Table 2). Upon slaughter on day 42 post-challenge, the vaccinated group achieved a 66.29% reduction in total worm burden (Table 2), however, the reductions in both cumulative FECs and worm burden between the two groups were not statistically significant ($p > 0.05$).

rH11s induced high-level specific IgG antibody

Previous studies have shown that the excellent immune protective properties of nH11 are primarily mediated by IgG antibodies (9, 20, 33). To determine whether immunization with rH11s induces an antibody-mediated immune response, we isolated IgG antibodies from serum samples of two groups following the initial immunization. Immunoblotting results showed that antibodies from the immunized group specifically targeted four rH11s (Figure 6A), in contrast to those from the adjuvant group (Figure 6B). Furthermore, we demonstrated that anti-rH11s IgG antibody could obviously recognize the nH11 compared with the antibody from the control group (Figures 6C, D). We subsequently monitored the dynamic variation of IgG antibody levels throughout the trials between these two groups using indirect ELISA. Goats administered with rH11s showed significantly higher IgG antibody titers ($p < 0.001$) against the tested rH11s compared to those in the control group following the first vaccination, peaking on day 28 and sustaining high levels during the whole infection period (Figure 6E). In addition, we also examined antibody levels in response to each rH11, and there were no significant differences among four rH11s (Figure 6F).

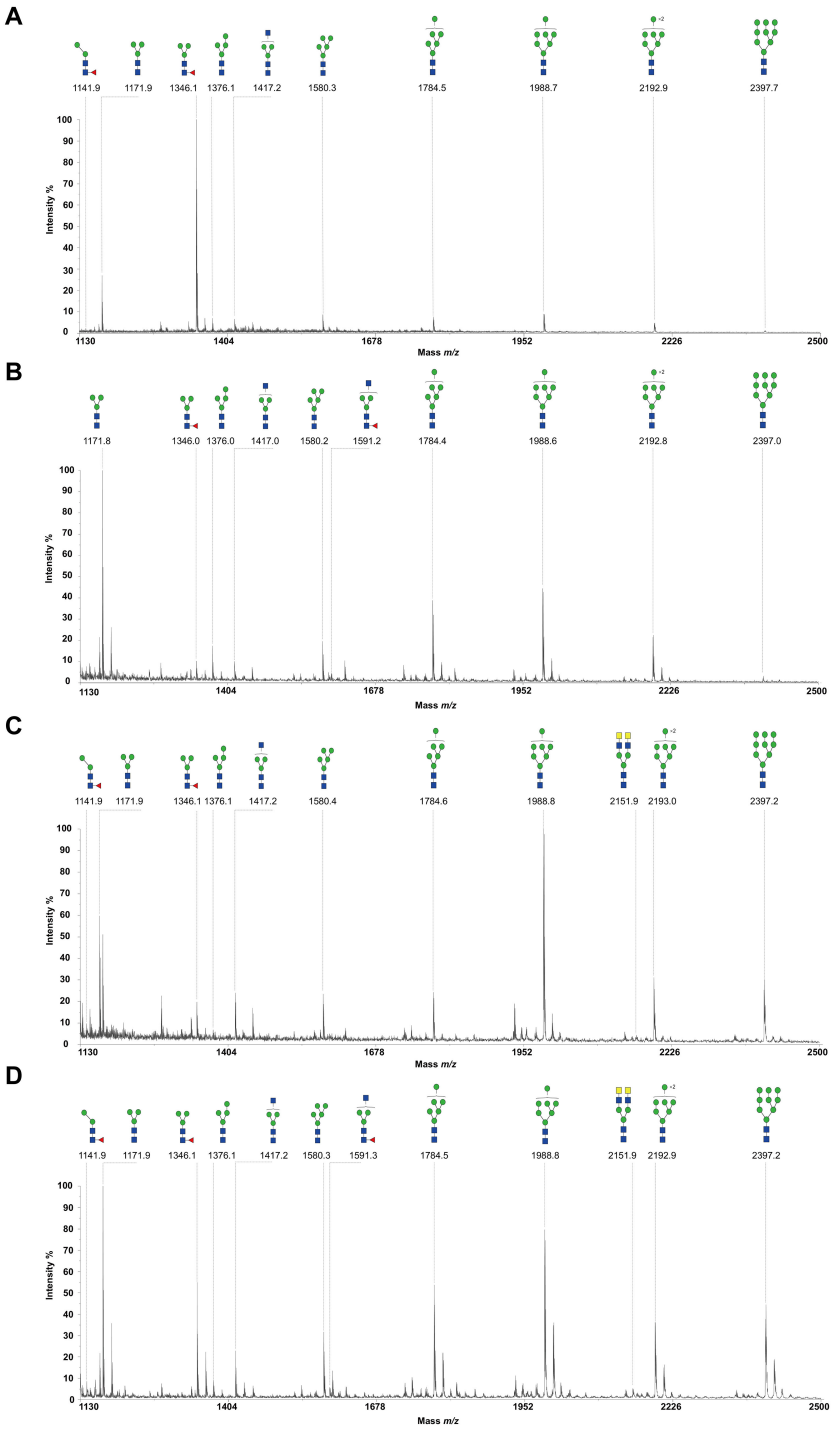

FIGURE 4
N-glycomes of four recombinant H11 proteins released by PNGase F digestion. MALDI-TOF-MS spectrum of the permethylated N-glycans of **(A)** rH11-1, **(B)** rH11-2, **(C)** rH11-4, and **(D)** rH11 released by PNGase F. Glycan species were presented primarily as $[M + Na]^+$ adducts. N-glycan signal peaks were annotated using the symbol nomenclature (green circle = mannose; blue square = GlcNAc; yellow square = GalNAc; red triangle = fucose). All N-glycan structures were deduced by the MALDI-TOF-MS/MS fragmentation and the current knowledge of N-glycomes of nH11 (20) and High Five cells (25).

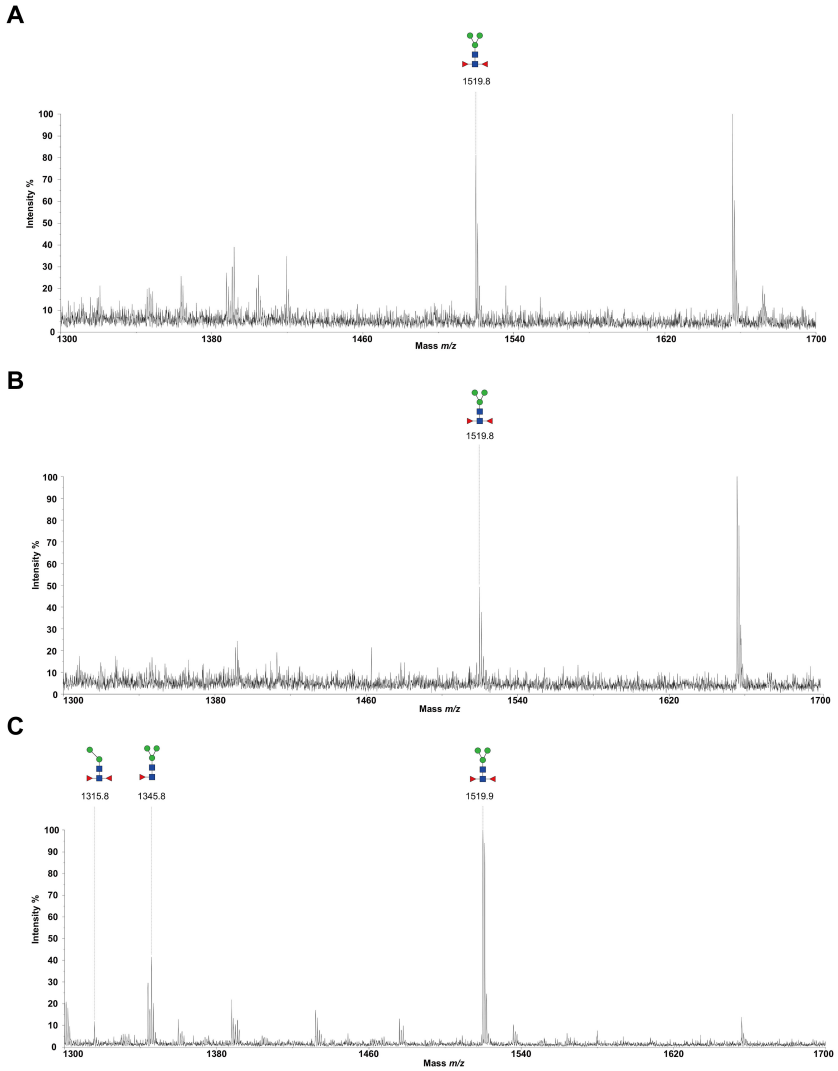

FIGURE 5
N-glycomes of three recombinant H11 proteins released by PNGase A digestion. MALDI-TOF-MS spectrum of the permethylated N-glycans of **(A)** rH11-2, **(B)** rH11-4, and **(C)** rH11, released by PPNGase A. Glycan species were presented primarily as $[M + Na]^+$ adducts. N-glycan signal peaks were annotated using the symbol nomenclature (green circle = mannose; blue square = GlcNAc; red triangle = fucose). All N-glycan structures were deduced by the MALDI-TOF-MS/MS fragmentation and the current knowledge of N-glycomes of nH11 (20) and High Five cells (25).

Anti-rH11s IgG antibody inhibited aminopeptidase activity and larval development

The effective protection of nH11 has been proven to be mediated by serum antibodies, whereby the parasite ingests host blood containing anti-H11 antibodies, which in turn inhibit the aminopeptidase activity and ultimately disrupt the digestion and absorption of nutrients (34, 35). In this study, we investigated whether the IgG antibodies generated against rH11s exhibit comparable inhibitory effects. The aminopeptidase activity of the native intestinal extract was significantly ($p < 0.001$) inhibited after incubation with serum IgG antibodies from the vaccinated group (30.45 nmol pNA/min/μg) compared to the adjuvant group (84.89 nmol pNA/min/μg) (Figure 7A). Furthermore, we showed that the inclusion of IgG antibodies from vaccinated goats at a final concentration of 0.25 mg/mL in LB medium for 7 days inhibited the development rate of xL3s to L4s compared to the control group (Figure 7B), as well as reduced the body length (Figure 7C) and width (Figure 7D) of L4s *in vitro*.

Discussion

In the present study, we utilized four kinds of IgG antibodies obtained from our previous study (20), which conferred distinct immunoprotective effects to screen and identify five glycoproteins from the nH11. We subsequently expressed four recombinants by insect cells, and confirmed that these rH11s possessed similar aminopeptidase activities and N-glycan motifs to nH11. Vaccination with a cocktail of the rH11s in goats gave a 66.29% reduction in both worm burden and cumulative FECs against *H.*

TABLE 1 N-glycan structures and abundances for four recombinant H11 proteins released by PNGase F and PNGase A.

NO.	Glycan	Composition	*m/z* [M + Na]$^+$	Relative abundance (%) [a]			
				rH11-1	rH11-2	rH11-4	rH11
1		$Hex_2HexNAc_2Fuc_1$	1141.90	3.50	1.38	2.39	1.67
2		$Hex_3HexNAc_2$	1171.92	33.09	13.45	13.88	17.38
3		$Hex_3HexNAc_2Fuc_1$	1346.10	4.07	54.28	5.69	9.74
4		$Hex_4HexNAc_2$	1376.15	5.79	4.23	2.21	1.72
5		$Hex_3HexNAc_3$	1417.19	4.01	4.15	7.36	4.48
6		$Hex_5HexNAc_2$	1580.00	7.07	5.18	7.25	6.87
7		$Hex_3HexNAc_3Fuc_1$	1591.37	1.42	2.61	–	1.14
8		$Hex_6HexNAc_2$	1784.56	14.52	5.00	7.07	13.07
9		$Hex_7HexNAc_2$	1988.79	17.07	5.88	34.37	21.61
10		$Hex_3HexNAc_6$	2151.94	–	–	0.97	1.22
11		$Hex_8HexNAc_2$	2192.99	8.39	3.13	9.83	10.03
12		$Hex_9HexNAc_2$	2397.22	1.06	0.70	8.97	11.07
13		$Hex_2HexNAc_2Fuc_2$	1315.85	–	–	–	7.17
14		$Hex_3HexNAc_2$ Fuc_1	1345.84	–	–	–	26.58
15		$Hex_3HexNAc_2Fuc_2$	1519.90	–	100	100	66.25

[a]Relative abundance of each glycan (%) = (Peak area of each glycan)/(Total of peak of all glycans) × 100%. The relative abundances of glycans released by PNGase F and PNGase A were calculated separately. Nos. 1-12: N-glycans of recombinant H11 proteins released by PNGase F; Nos. 13-15: N-glycans of recombinant H11 proteins released by PNGase A. N-glycan structures were annotated using the symbol nomenclature (green circle = mannose; blue square = GlcNAc; yellow square = GalNAc; red triangle = fucose).

contortus infection although there was no significantly statistical difference. We further demonstrated that this recombinant cocktail induced high-level anti-rH11 IgG antibodies which could bind to nH11 and inhibit the aminopeptidase activity of *H. contortus* adult worm's intestine as well as the *in vitro* larval development.

Protective efficacies of recombinant forms of one (14–16, 24) or two (17) of the above identified H11 isoforms have been tested in previous studies, but they barely induced immune protection. One of the primary reasons for the significantly decreased protective efficacy may be the exclusion of key immunogenic antigens in these recombinant vaccines, as the antigenic epitopes among H11 proteins may differ and potentially work synergistically to enhance the immune response. Cocktail vaccines against helminth infections have been proven to induce broader and more robust immune responses (36,

10.3389/fimmu.2025.1521022

TABLE 2 Fecal egg counts and worm burden of goats in the vaccination trial.

Group	Cumulative fecal egg count (FEC)				Intensity of infection			
	FEC	Mean	SD	Reduction[b] (%)	Worm count	Mean	SD	Reduction[b] (%)
AJ (n = 8)	600	9887.50	10651.28	Not applicable	5	238.63	253.80	Not applicable
	900				30			
	3150				44			
	4900				212			
	5500				187			
	9550				138			
	22350				775			
	32150				518			
Vaccinated (n = 7) [a]	750	3332.85	2818.54	66.29	16	80.43	59.31	66.29
	850				36			
	950				44			
	2400				83			
	3700				145			
	5930				49			
	8750				190			

Fecal samples were taken from individual goats at 11 time points from 14 days post-challenge (cf. Figure 1), and the number of *H. contortus* eggs per gram of fecal samples (Fecal egg count, FEC) was counted using the McMaster counting method. Cumulative FECs of individual goats and mean cumulative FECs (with standard deviations, SD) were calculated for each group. At the end of the experiment (day 84), the total worm numbers and mean worm numbers (with standard deviations, SD) in the abomasa were counted, and the reduction in the intensity of infection was calculated for each group.

[a] One goat died of a cause unrelated to haemonchosis on day 30. [b] The reduction (%) = 100 – [the mean value for vaccinated group ÷ mean value for adjuvant control (AJ) × 100%]. n: the number of goats. Statistical significance was determined by Mann - Whitney U-tests.

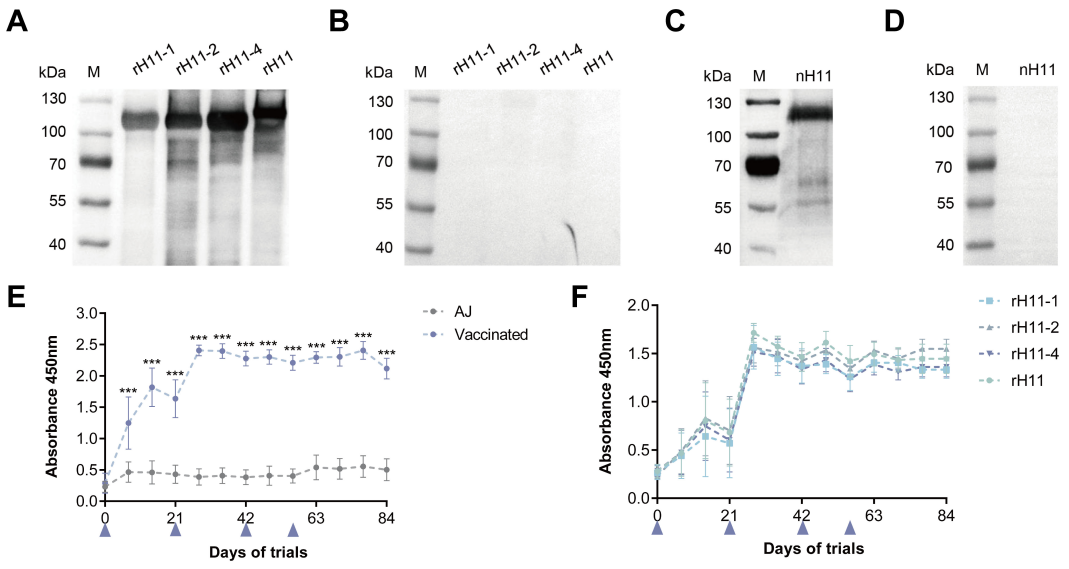

FIGURE 6
Serum IgG antibody response in goats vaccinated with recombinant H11 proteins. Western blot analysis showing serum IgG antibodies from the goats of the **(A)** vaccinated group and the **(B)** control group interacting with each of the four rH11s. Western blot analysis showing serum IgG antibodies from the goats of **(C)** vaccinated group and **(D)** control group interacting with nH11. IgG antibodies were isolated from serum samples collected from different groups on day 42 of the vaccination trial, and probed at a dilution of 1:1,000. **(E)** The dynamics of serum IgG antibodies from both vaccinated and control groups interacting with cocktail rH11s. **(F)** The dynamics of serum IgG antibodies from the vaccinated group interacting with each of the recombinant H11 proteins. Each data point (absorbance at 450 nm) represented the mean group antibody titers (mean ± SD; adjuvant control group, n = 8; vaccinated group, n = 7). The blue triangles indicated the four time points of vaccine administration. Statistically significant differences were assessed using Mann-Whitney U-tests, with significance denoted by ***(p < 0.001), not significant was not marked.

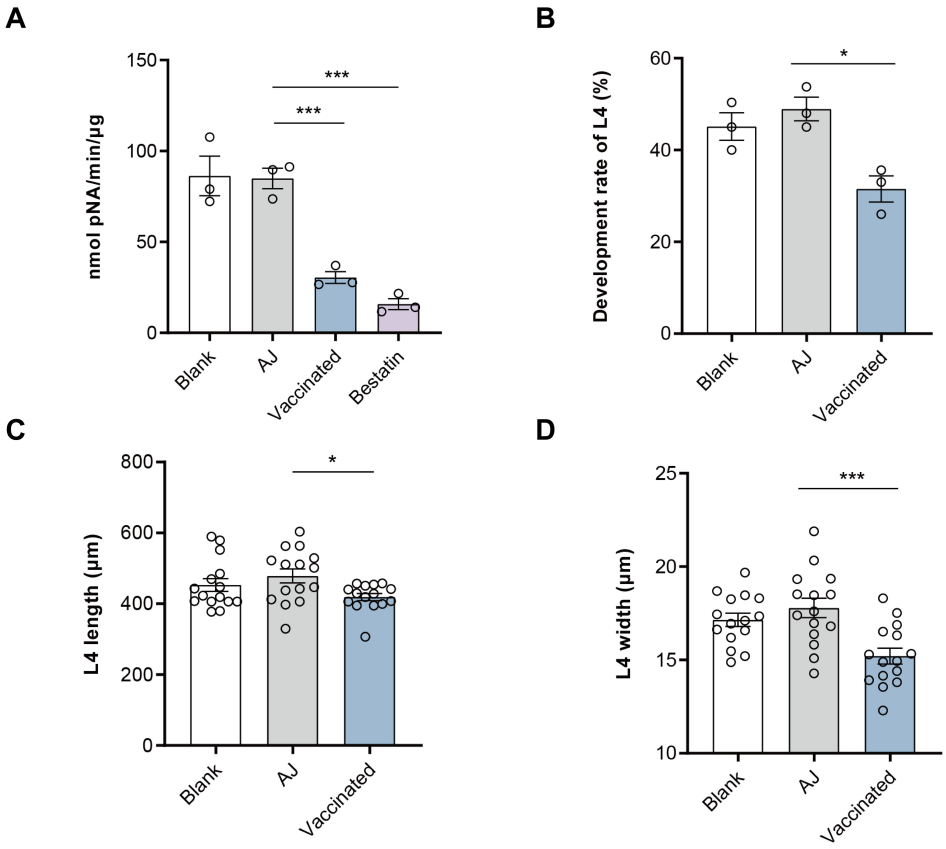

FIGURE 7
Anti-recombinant H11 IgG antibodies inhibited intestinal aminopeptidase activity and *in vitro* larval development of *Haemonchus contortus*. **(A)** Anti-rH11s antibodies inhibited intestinal aminopeptidase activity of adult worms. Inhibition assays were performed in a phosphate buffer, optimized to a pH of 7.0. Blank: IgG antibodies isolated from pre-immunization serum on day 0; AJ: IgG antibodies isolated from serum samples in the adjuvant group collected on day 42; Vaccinated: IgG antibodies isolated from serum samples in rH11s vaccinated group collected on day 42; Bestatin: a specific inhibitor of aminopeptidase. **(B)** Anti-rH11s antibodies inhibited the developmental rate of xL3s to L4s, and **(C)** the length (n = 15), and **(D)** the width (n = 15) of L4s developed *in vitro* on day 7 in the LB media containing anti-rH11 antibodies (vaccinated) or antibodies from the adjuvant group (AJ). Statistically significant differences were analyzed using one-way ANOVA and indicated with *($p < 0.05$), ***($p < 0.001$), not significant was not marked.

37). In our study, a cocktail comprising four rH11s was able to induce specific anti-rH11s IgG antibodies that were consistently maintained at high levels throughout the challenge infection and bound to both nH11 and rH11s. In contrast, a previous study reported that sheep immunized twice with the single rH11-1 expressed in insect cells displayed declining antibody responses at the eighth week post-immunization (15). Similarly, in another study, antibody levels induced by three immunizations with dual rH11s (rH11-4 + rH11-5) expressed in the free-living nematode *C. elegans* were not sustained throughout the trial, showing a significant decrease starting from the seventh week post-immunization (17). In addition to differences in the composition of recombinant vaccines, the duration of antibody responses observed in previous studies and ours may also be attributed to the number of immunizations. This suggests that further recombinant vaccine immunization strategies should emphasize the importance of booster immunizations. Regarding the immune protection induced by the nH11, it is believed that the anti-nH11 antibodies, upon ingestion with the blood meal, inhibit aminopeptidase activity and disrupt nutrient absorption (18, 20). In the present study, the anti-rH11s IgG antibodies could inhibit the aminopeptidase activities of adult worm's intestine and the larval growth and development, which was similar to the inhibition effect of the anti-nH11 IgG antibodies (20), suggesting that this cocktail vaccine could induce a sustained and protective antibody response. Our recombinant cocktail provided a 66.29% reduction in both worm burden and cumulative FECs in goats, this result has surpassed the efficacy (<30%) of previous rH11 that utilized either single (14–16) or dual rH11s (17) although there was no statistically significant difference. We speculated that individual variations among goats affected the statistical significance. These differences may result from genetic, immune, or environmental conditions affecting responses to infection and vaccination. To address this in future studies, grouping animals based on their immune responses or genetic traits may reduce variability, while increasing the sample scale and controlling environmental variables may improve the statistical power. Despite the lack of statistical significance, the trend toward increased protection suggests that using multiple H11 immunodominant components may further improve recombinant vaccine efficacy.

Our previous studies demonstrated that abundant and unique N-glycans in the nH11 play a decisive role in the protective immunity against *H. contortus* infection (20). Notably, α1,3-linked fucose in asparagine-linked GlcNAc residues, a non-vertebrate glycosylation, is regarded as highly immunologically relevant and serves as a key epitope for IgE antibodies of *H. contortus* infection (38). In *Schistosoma mansoni*, core α1,3-fucosylated glycans widely distributed in the eggs and miracidia are also believed to play a vital role in inducing the Th2 anti-parasite immune response (39–41), and IgG against these epitopes can kill schistosomula by a complement-dependent process *in vitro* (42). Besides being widely distributed in N-glycomes of helminths (20, 43–45), the crucial core fucosylated glycans are also present in insect cells (25, 46, 47), which gives them an inherent advantage for producing rH11s compared to other eukaryotic expression systems such as yeast or mammalian cells (48). Although the H11-1 isoform had been expressed in insect cells in a previous study (15), the N-glycan structures of rH11-1 were unknown. Here, we confirmed that rH11s expressed in insect cells possessed a total of 15 N-glycans and three rH11s (rH11, rH11-2 and rH11-4) exhibited both an α1,3 and an α1,6-linked fucose residue at the proximal GlcNAc which constitute an immunogenic core di-fucosylated glycans detected at *m/z* 1519.9 like nH11 (20). Except for the fucosylated core glycans, however, several more complex N-glycan unites, such as core tri-fucosylation, galactosylated fucose structures, antennal LDNF, Lewis^x, and galactosylated LDNF structures (20), were not detected in the N-glycome of the rH11s. Although an unusual signal peak for the LDN glycan (*m/z* 2151.9) was observed in the glycome of rH11-4 and rH11, its abundance (0.97-1.22%, cf. Table 1) was at a low level compared to those in nH11 (20). The variations in glycan composition or abundance may explain the decreased ability of rH11s to elicit protective immunity against *H. contortus* infection.

Glycan structural difference between rH11 and nH11 is attributed to the inadequacy or absence of specific glycosyltransferases required to elongate trimmed N-glycan processing intermediates and synthesize complex end products within the exogenous expression systems. Another factor is that insect cells possess an endogenous N-glycan trimming enzyme, which specifically removes terminal β1,2-linked GlcNAc residues to antagonize N-glycan elongation and thus cannot form glycan with complex antennal structures (49–51). Currently, glycoengineering is a promising strategy to mimic the properties of glycosylation of target glycoproteins by interfering with endogenous glycosidases or introducing heterogenous glycosyltransferases (52–55). More recent efforts to engineer insect N-glycosylation pathways have focused on the creation of transgenic insect cell lines that constitutively express mammalian glycosyltransferases (56–58), enabling precise synthesis of specific N-glycans. Although the N-glycosylation pathway of *H. contortus* has not been fully elucidated, a substantial number of glycosyltransferases have been characterized in *C. elegans*, a free-living nematode that belongs to the same evolutionary clade V as *H. contortus* and likely shares similar N-glycosylation pattern (59–61). A previous study using *C. elegans* as a novel expression system achieved N-glycans of rH11-4 closer in structure to those of nH11 (17). However, as a production system, *C. elegans* is not optimal due to its limitations in the production of foreign proteins, resulting in relatively low yields and the introduction of some additional redundant modifications (e.g. phosphorylcholine) to suppress immune responses (17). Therefore, introducing specific nematode glycosyltransferases of *C. elegans* into insect cells, such as Fut-6 (to synthesize distal core α1,3-linked fucose structure) (62), GalT-1 (to synthesize the core galactose-fucose structure) (55, 63), makes it feasible to convert trimmed N-glycans into complex structures and obtain completed N-glycosylated rH11s in the exogenous expression systems. This advancement will hold significant promise for enhancing the immune protection offered by recombinant vaccines.

In conclusion, we identified five immunoprotective glycoproteins from the nH11 and expressed four of them in the insect cell expression system. These rH11s have aminopeptidase activities and similar N-glycan profiles to those of nH11. A cocktail of rH11s resulted in a 66.29% reduction in both worm burden and cumulative FECs as well as a high level of anti-rH11s IgG that could inhibit the aminopeptidase activity of *H. contortus* adult intestine and larval development *in vitro*. Our study provides valuable insights for the future development of recombinant vaccines against *H. contortus* and other related parasites.

Data availability statement

The datasets presented in this study can be found in online repositories. The name of the repository and accession number can be found below: EMBL-EBI PRIDE Archive; PXD number PXD060969.

Ethics statement

The animal study was approved by Animals Ethics Committee of Huazhong Agricultural University. The study was conducted in accordance with the local legislation and institutional requirements.

Author contributions

HL: Investigation, Writing – original draft. YZ: Investigation, Writing – original draft. JL: Investigation, Writing – review & editing. FL: Investigation, Writing – review & editing. LY: Investigation, Writing – review & editing. XL: Software, Writing – review & editing. CW: Funding acquisition, Project administration, Supervision, Writing – review & editing. MH: Funding acquisition, Project administration, Resources, Supervision, Visualization, Writing – review & editing.

Funding

The author(s) declare that financial support was received for the research, authorship, and/or publication of this article. This work was supported by the National Natural Science Foundation of China (grant no. 32172881 to MH, grant no. 32402913 to CW), and the Natural Science Foundation of Hubei Province (grant no. 2023AFB486 to CW).

Conflict of interest

The authors declare that the research was conducted in the absence of any commercial or financial relationships that could be construed as a potential conflict of interest.

Generative AI statement

The author(s) declare that no Generative AI was used in the creation of this manuscript.

Publisher's note

Supplementary material

The Supplementary Material for this article can be found online at: https://www.frontiersin.org/articles/10.3389/fimmu.2025.1521022/full#supplementary-material

SUPPLEMENTARY FIGURE 1
Diagrams of construction of expression plasmids for five recombinant H11 proteins.

SUPPLEMENTARY FIGURE 2
Proportional distribution of aminopeptidase proteins retrieved from databases of *Haemonchus contortus*.

SUPPLEMENTARY TABLE 1
Information on the gene ID, gene name, transcript ID and UniprotKB accession number of 41 aminopeptidase proteins retrieved from the databases of *Haemonchus contortus*.

SUPPLEMENTARY TABLE 2
Information on molecules obtained from LC-MS/MS analysis of H11 components with molecular weights between 100-130 kDa recognized by four different IgG antibodies.

References

1. Maurizio A, Perrucci S, Tamponi C, Scala A, Cassini R, Rinaldi L, et al. Control of gastrointestinal helminths in small ruminants to prevent anthelmintic resistance: the Italian experience. *Parasitology*. (2023) 150:1105–18. doi: 10.1017/s0031182023000343

2. Hempstead MN, Waghorn TS, Gibson MJ, Sauermann CW, Ross AB, Cave VM, et al. Worms and welfare: Behavioural and physiological changes associated with gastrointestinal nematode parasitism in lambs. *Vet Parasitol*. (2023) 324:110056. doi: 10.1016/j.vetpar.2023.110056

3. Roeber F, Jex AR, Gasser RB. Impact of gastrointestinal parasitic nematodes of sheep, and the role of advanced molecular tools for exploring epidemiology and drug resistance - an Australian perspective. *Parasit Vectors*. (2013) 6:153. doi: 10.1186/1756-3305-6-153

4. Chagas ACS, Tupy O, Santos IBD, Esteves SN. Economic impact of gastrointestinal nematodes in Morada Nova sheep in Brazil. *Rev Bras Parasitol Vet*. (2022) 31:e008722. doi: 10.1590/s1984-29612022044

5. Rose Vineer H, Morgan ER, Hertzberg H, Bartley DJ, Bosco A, Charlier J, et al. Increasing importance of anthelmintic resistance in European livestock: creation and meta-analysis of an open database. *Parasite*. (2020) 27:69. doi: 10.1051/parasite/2020062

6. Strydom T, Lavan RP, Torres S, Heaney K. The economic impact of parasitism from nematodes, trematodes and ticks on beef cattle production. *Animals*. (2023) 13:1599. doi: 10.3390/ani13101599

7. Charlier J, Bartley DJ, Sotiraki S, Martinez-Valladares M, Claerebout E, von-Samson-Himmelstjerna G, et al. Anthelmintic resistance in ruminants: challenges and solutions. *Adv Parasitol*. (2022) 115:171–227. doi: 10.1016/bs.apar.2021.12.002

8. Voigt K, Geiger M, Jäger M. Five past twelve - the resistance situation in small ruminant gastrointestinal nematodes in Germany. *Tierarztl Prax Ausg G Grosstiere Nutztiere*. (2023) 51:153–9. doi: 10.1055/a-2097-9361

9. Smith TS, Munn EA, Graham M, Tavernor AS, Greenwood CA. Purification and evaluation of the integral membrane protein H11 as a protective antigen against *Haemonchus Contortus*. *Int J Parasitol*. (1993) 23:271–80. doi: 10.1016/0020-7519(93)90150-w

10. Newton SE, Munn EA. The development of vaccines against gastrointestinal nematode parasites, particularly *Haemonchus Contortus*. *Parasitol Today*. (1999) 15:116–22. doi: 10.1016/s0169-4758(99)01399-x

11. Graham M, Munn EA, Smith TS, Knox DP, Oliver JJ, Newton SE eds. Recombinant DNA molecules encoding aminopeptidase enzymes and their use in the preparation of vaccines against helminth infections. *United Kingdom patent WO 9323542* (1993).

12. Munn EA, Smith TS, Graham M, Tavernor AS, Greenwood CA. The potential value of integral membrane proteins in the vaccination of lambs against *Haemonchus Contortus*. *Int J Parasitol*. (1993) 23:261–9. doi: 10.1016/0020-7519(93)90149-s

13. Munn EA, Smith TS, Smith H, James FM, Smith FC, Andrews SJ. Vaccination against *Haemonchus contortus* with denatured forms of the protective antigen H11. *Parasite Immunol*. (1997) 19:243–8. doi: 10.1046/j.1365-3024.1997.d01-205.x

14. Newton SE, Meeusen EN. Progress and new technologies for developing vaccines against gastrointestinal nematode parasites of sheep. *Parasite Immunol*. (2003) 25:283–96. doi: 10.1046/j.1365-3024.2003.00631.x

15. Reszka N, Rijsewijk FA, Zelnik V, Moskwa B, Bieńkowska-Szewczyk K. *Haemonchus contortus*: characterization of the baculovirus expressed form of aminopeptidase H11. *Exp Parasitol*. (2007) 117:208–13. doi: 10.1016/j.exppara.2007.03.018

16. Zhou QJ, Yang Y, Guo XL, Duan LJ, Chen XQ, Yan BL, et al. Expression of *Caenorhabditis elegans*-expressed Trans-HPS, partial aminopeptidase H11 from *Haemonchus contortus*. *Exp Parasitol*. (2014) 145:87–98. doi: 10.1016/j.exppara.2014.08.005

17. Roberts B, Antonopoulos A, Haslam SM, Dicker AJ, McNeilly TN, Johnston SL, et al. Novel expression of *Haemonchus contortus* vaccine candidate aminopeptidase H11 using the free-living nematode *Caenorhabditis elegans*. *Vet Res*. (2013) 44:111. doi: 10.1186/1297-9716-44-111

18. Smith TS, Graham M, Munn EA, Newton SE, Knox DP, Coadwell WJ, et al. Cloning and characterization of a microsomal aminopeptidase from the intestine of the nematode *Haemonchus contortus*. *Biochim Biophys Acta*. (1997) 1338:295–306. doi: 10.1016/s0167-4838(96)00204-x

19. Williamson AL, Brindley PJ, Knox DP, Hotez PJ, Loukas A. Digestive proteases of blood-feeding nematodes. *Trends Parasitol*. (2003) 19:417–23. doi: 10.1016/s1471-4922(03)00189-2

20. Wang C, Liu L, Wang T, Liu X, Peng W, Srivastav RK, et al. H11-induced immunoprotection is predominantly linked to N-glycan moieties during *Haemonchus contortus* infection. *Front Immunol*. (2022) 13:1034820. doi: 10.3389/fimmu.2022.1034820

21. Prasanphanich NS, Mickum ML, Heimburg-Molinaro J, Cummings RD. Glycoconjugates in host-helminth interactions. *Front Immunol*. (2013) 4:240. doi: 10.3389/fimmu.2013.00240

22. van Die I, Cummings RD. Glycan gimmickry by parasitic helminths: a strategy for modulating the host immune response? *Glycobiology*. (2010) 20:2–12. doi: 10.1093/glycob/cwp140

23. Hokke CH, van Diepen A. Helminth glycomics - glycan repertoires and host-parasite interactions. *Mol Biochem Parasitol*. (2017) 215:47–57. doi: 10.1016/j.molbiopara.2016.12.001

24. Yan R, Li X. Expression of recombinant H11 of *Haemonchus contortus* in *Pichia pastoris*. *J Nanjing Agricult Univ*. (2005) 28:85–9. doi: 10.7685/j.issn.1000-2030.2005.02.018

25. Stanton R, Hykollari A, Eckmair B, Malzl D, Dragosits M, Palmberger D, et al. The underestimated N-glycomes of *lepidopteran* species. *Biochim Biophys Acta Gen Subj*. (2017) 1861:699–714. doi: 10.1016/j.bbagen.2017.01.009

26. Li F, Lok JB, Gasser RB, Korhonen PK, Sandeman MR, Shi D, et al. *Hc-daf-2* encodes an insulin-like receptor kinase in the barber's pole worm, *Haemonchus contortus*, and restores partial dauer regulation. *Int J Parasitol*. (2014) 44:485–96. doi: 10.1016/j.ijpara.2014.03.005

27. Ciucanu I, Costello CE. Elimination of oxidative degradation during the per-O-methylation of carbohydrates. *J Am Chem Soc*. (2003) 125:16213–9. doi: 10.1021/ja035660t

28. Munn EA, Greenwood CA. Endotube-brush border complexes dissected from the intestines of *Haemonchus contortus* and Ancylostoma caninum. *Parasitology*. (1983) 87:129–37. doi: 10.1017/s0031182000052471

29. Sommerville RI. The development of *Haemonchus contortus* to the fourth stage *in vitro*. *Int J Parasitol*. (1966) 52:127–36. doi: 10.2307/3276403

30. Doyle SR, Tracey A, Laing R, Holroyd N, Bartley D, Bazant W, et al. Genomic and transcriptomic variation defines the chromosome-scale assembly of *Haemonchus contortus*, a model gastrointestinal worm. *Commun Biol*. (2020) 3:656. doi: 10.1038/s42003-020-01377-3

31. Mohandas N, Young ND, Jabbar A, Korhonen PK, Koehler AV, Hall RS, et al. The complement of family M1 aminopeptidases of *Haemonchus contortus* - Biotechnological implications. *Biotechnol Adv*. (2016) 34:65–76. doi: 10.1016/j.bioteChadv.2015.10.003

32. Zhou QJ, Zhang HL, Jiang XL, Du AF. The gene structure and promoter region of the vaccine target aminopeptidase H11 from the blood-sucking nematode parasite of ruminants, *Haemonchus contortus*. *Funct Integr Genomics*. (2010) 10:589–601. doi: 10.1007/s10142-010-0172-5

33. Ye L, Zhang Y, Wu S, Wang Z, Liu F, Wang C, et al. Immunoprotection efficacy of Con A-purified proteins against *Haemonchus contortus* in goats. *Vaccines*. (2022) 10:1891. doi: 10.3390/vaccines10111891

34. Knox D. Proteases in blood-feeding nematodes and their potential as vaccine candidates. *Adv Exp Med Biol*. (2011) 712:155–76. doi: 10.1007/978-1-4419-8414-2_10

35. Knox DP, Redmond DL, Newlands GF, Skuce PJ, Pettit D, Smith WD. The nature and prospects for gut membrane proteins as vaccine candidates for *Haemonchus contortus* and other ruminant trichostrongyloids. *Int J Parasitol*. (2003) 33:1129–37. doi: 10.1016/s0020-7519(03)00167-x

36. Nisbet AJ, McNeilly TN, Wildblood LA, Morrison AA, Bartley DJ, Bartley Y, et al. Successful immunization against a parasitic nematode by vaccination with recombinant proteins. *Vaccine*. (2013) 31:4017–23. doi: 10.1016/j.vaccine.2013.05.026

37. Mendez S, Zhan B, Goud G, Ghosh K, Dobardzic A, Wu W, et al. Effect of combining the larval antigens *Ancylostoma* secreted protein 2 (ASP-2) and metalloprotease 1 (MTP-1) in protecting hamsters against hookworm infection and disease caused by *Ancylostoma ceylanicum*. *Vaccine*. (2005) 23:3123–30. doi: 10.1016/j.vaccine.2004.12.022

38. van Die I, Gomord V, Kooyman FN, van den Berg TK, Cummings RD, Vervelde L. Core alpha1–>3-fucose is a common modification of N-glycans in parasitic helminths and constitutes an important epitope for IgE from *Haemonchus contortus* infected sheep. *FEBS Lett*. (1999) 463:189–93. doi: 10.1016/s0014-5793(99)01508-2

39. Jang-Lee J, Curwen RS, Ashton PD, Tissot B, Mathieson W, Panico M, et al. Glycomics analysis of *Schistosoma mansoni* egg and cercarial secretions. *Mol Cell Proteomics*. (2007) 6:1485–99. doi: 10.1074/mcp.M700004-MCP200

40. Faveeuw C, Mallevaey T, Paschinger K, Wilson IB, Fontaine J, Mollicone R, et al. *Schistosome* N-glycans containing core alpha 3-fucose and core beta 2-xylose epitopes are strong inducers of Th2 responses in mice. *Eur J Immunol*. (2003) 33:1271–81. doi: 10.1002/eji.200323717

41. van Diepen A, van der Velden NS, Smit CH, Meevissen MH, Hokke CH. Parasite glycans and antibody-mediated immune responses in *Schistosoma* infection. *Parasitology*. (2012) 139:1219–30. doi: 10.1017/s0031182012000273

42. Prasanphanich NS, Leon K, Secor WE, Shoemaker CB, Heimburg-Molinaro J, Cummings RD. Anti-schistosomal immunity to core xylose/fucose in N-glycans. *Front Mol Biosci*. (2023) 10:1142620. doi: 10.3389/fmolb.2023.1142620

43. Haslam SM, Coles GC, Munn EA, Smith TS, Smith HF, Morris HR, et al. *Haemonchus contortus* glycoproteins contain N-linked oligosaccharides with novel highly fucosylated core structures. *J Biol Chem*. (1996) 271:30561–70. doi: 10.1074/jbc.271.48.30561

44. Wang C, Gao W, Yan S, Zhu XQ, Suo X, Liu X, et al. N-glycome and N-glycoproteome of a hematophagous parasitic nematode *Haemonchus*. *Comput Struct Biotechnol J*. (2021) 19:2486–96. doi: 10.1016/j.csbj.2021.04.038

45. Paschinger K, Wilson IB. Two types of galactosylated fucose motifs are present on N-glycans of *Haemonchus contortus*. *Glycobiology*. (2015) 25:585–90. doi: 10.1093/glycob/cwv015

46. Tomiya N, Narang S, Lee YC, Betenbaugh MJ. Comparing N-glycan processing in mammalian cell lines to native and engineered *lepidopteran* insect cell lines. *Glycoconj J*. (2004) 21:343–60. doi: 10.1023/b:Glyc.0000046275.28315.87

47. Walski T, De Schutter K, Van Damme EJM, Smagghe G. Diversity and functions of protein glycosylation in insects. *Insect Biochem Mol Biol*. (2017) 83:21–34. doi: 10.1016/j.ibmb.2017.02.005

48. Toustou C, Walet-Balieu ML, Kiefer-Meyer MC, Houdou M, Lerouge P, Foulquier F, et al. Towards understanding the extensive diversity of protein N-glycan structures in eukaryotes. *Biol Rev Camb Philos Soc*. (2022) 97:732–48. doi: 10.1111/brv.12820

49. Geisler C, Jarvis DL. Identification of genes encoding N-glycan processing beta-N-acetylglucosaminidases in *Trichoplusia ni* and *Bombyx mori*: Implications for glycoengineering of baculovirus expression systems. *Biotechnol Prog*. (2010) 26:34–44. doi: 10.1002/btpr.298

50. Geisler C, Aumiller JJ, Jarvis DL. A fused lobes gene encodes the processing beta-N-acetylglucosaminidase in Sf9 cells. *J Biol Chem*. (2008) 283:11330–9. doi: 10.1074/jbc.M710279200

51. Altmann F, Schwihla H, Staudacher E, Glössl J, März L. Insect cells contain an unusual, membrane-bound beta-N-acetylglucosaminidase probably involved in the processing of protein N-glycans. *J Biol Chem*. (1995) 270:17344–9. doi: 10.1074/jbc.270.29.17344

52. Dicker M, Strasser R. Using glyco-engineering to produce therapeutic proteins. *Expert Opin Biol Ther*. (2015) 15:1501–16. doi: 10.1517/14712598.2015.1069271

53. Geisler C, Mabashi-Asazuma H, Jarvis DL. An overview and history of glyco-engineering in insect expression systems. *Methods Mol Biol*. (2015) 1321:131–52. doi: 10.1007/978-1-4939-2760-9_10

54. van der Kaaij A, van Noort K, Nibbering P, Wilbers RHP, Schots A. Glyco-engineering plants to produce helminth glycoproteins as prospective biopharmaceuticals: recent advances, challenges and future prospects. *Front Plant Sci*. (2022) 13:882835. doi: 10.3389/fpls.2022.882835

55. Mabashi-Asazuma H, Jarvis DL. CRISPR-Cas9 vectors for genome editing and host engineering in the baculovirus-insect cell system. *Proc Natl Acad Sci U.S.A*. (2017) 114:9068–73. doi: 10.1073/pnas.1705836114

56. Okada T, Ihara H, Ito R, Nakano M, Matsumoto K, Yamaguchi Y, et al. N-glycosylation engineering of lepidopteran insect cells by the introduction of the beta1,4-N-acetylglucosaminyltransferase III gene. *Glycobiology*. (2010) 20:1147–59. doi: 10.1093/glycob/cwq080

57. Hollister J, Grabenhorst E, Nimtz M, Conradt H, Jarvis DL. Engineering the protein N-glycosylation pathway in insect cells for production of biantennary, complex N-glycans. *Biochemistry*. (2002) 41:15093–104. doi: 10.1021/bi026455d

58. Hollister JR, Jarvis DL. Engineering lepidopteran insect cells for sialoglycoprotein production by genetic transformation with mammalian beta 1,4-galactosyltransferase and alpha 2,6-sialyltransferase genes. *Glycobiology*. (2001) 11:1–9. doi: 10.1093/glycob/11.1.1

59. Haslam SM, Dell A. Hallmarks of *Caenorhabditis elegans* N-glycosylation: complexity and controversy. *Biochimie*. (2003) 85:25–32. doi: 10.1016/s0300-9084(03)00041-5

60. Hanneman AJ, Rosa JC, Ashline D, Reinhold VN. Isomer and glycomer complexities of core GlcNAcs in *Caenorhabditis elegans*. *Glycobiology*. (2006) 16:874–90. doi: 10.1093/glycob/cwl011

61. Paschinger K, Gutternigg M, Rendić D, Wilson IB. The N-glycosylation pattern of *Caenorhabditis elegans*. *Carbohydr Res*. (2008) 343:2041–9. doi: 10.1016/j.carres.2007.12.018

62. Nguyen K, van Die I, Grundahl KM, Kawar ZS, Cummings RD. Molecular cloning and characterization of the *Caenorhabditis elegans* alpha1,3-fucosyltransferase family. *Glycobiology*. (2007) 17:586–99. doi: 10.1093/glycob/cwm023

63. Titz A, Butschi A, Henrissat B, Fan YY, Hennet T, Razzazi-Fazeli E, et al. Molecular basis for galactosylation of core fucose residues in invertebrates: identification of *Caenorhabditis elegans* N-glycan core alpha1,6-fucoside beta1,4-galactosyltransferase GALT-1 as a member of a novel glycosyltransferase family. *J Biol Chem*. (2009) 284:36223–33. doi: 10.1074/jbc.M109.058354

frontiers | Frontiers in Immunology

TYPE Original Research
PUBLISHED 28 February 2025
DOI 10.3389/fimmu.2025.1483274

OPEN ACCESS

EDITED BY
Md. Aminul Islam,
Bangladesh Agricultural University,
Bangladesh

REVIEWED BY
Raki Sudan,
Washington University in St. Louis,
United States
Rafael Freitas-Silva,
Medical University of Vienna, Austria

*CORRESPONDENCE
Sebastian Rausch
sebastian.rausch@fu-berlin.de

RECEIVED 19 August 2024
ACCEPTED 27 January 2025
PUBLISHED 28 February 2025

CITATION
Adjah J, D. Musimbi Z, Mugo RM, Midha A, Hartmann S and Rausch S (2025) Liver-draining portal lymph node responds to enteric nematode infection by generating highly parasite-specific follicular T helper and B cell responses. *Front. Immunol.* 16:1483274. doi: 10.3389/fimmu.2025.1483274

Liver-draining portal lymph node responds to enteric nematode infection by generating highly parasite-specific follicular T helper and B cell responses

Joshua Adjah, Zaneta D. Musimbi, Robert M. Mugo, Ankur Midha, Susanne Hartmann and Sebastian Rausch*

Department of Veterinary Medicine, Institute of Immunology, Freie Universität Berlin, Berlin, Germany

Introduction: While research on the gut-liver axis in non-communicable liver diseases has expanded exponentially, few studies have investigated the liver-gut relationship in the context of gastrointestinal nematode infections. This study aimed to determine whether liver-draining lymph nodes (LLNs) contribute to the immune response against a strictly enteric nematode infection.

Methods: We analyzed the cellular and functional immune responses in the portal (PLN) and celiac (CLN) liver-draining lymph nodes following infection with the small intestinal nematode *Heligmosomoides (polygyrus) bakeri (H. bakeri)*. The composition of dendritic cells and CD4+ T cell subsets in LLNs was compared to the mesenteric lymph nodes (MLN), the primary draining site of gut infections. Additionally, we examined Th2 effector cell expansion, plasmablast generation, and B cell activation across these lymphoid sites.

Results: Both PLN and CLN exhibited increased cellularity at d14 post-infection. The immune profile in CLN closely resembled that of MLN, characterized by a robust expansion of GATA-3+ Th2 effector cells at days 6 and 14 post-infection. This was accompanied by an early plasmablast response, producing low-affinity IgG1 antibodies targeting immune-dominant excretory-secretory (ES) products. In contrast, PLN showed weaker Th2 responses and lower early plasma cell responses compared to MLN and CLN. However, PLN displayed strong follicular T helper (TFH) activity, with a B cell profile biased toward germinal center reactions. This led to high-affinity IgG1 antibodies specifically binding VAL-1 and ACE-1.

Discussion: These findings demonstrate, for the first time, that liver-draining lymph nodes actively participate in the adaptive immune response to enteric nematode infections. While MLN and CLN function synergistically in generating early Th2 effector cells and rapid extrafollicular IgG1+ plasma cell responses, PLN specializes in TFH-driven germinal center reactions and affinity maturation.

KEYWORDS

liver lymph nodes, enteric nematode, *Heligmosomoides polygyrus bakeri*, Th2 cells, germinal center B cells, PLN, CLN

Introduction

Generally, lymph nodes (LNs) play critical roles in the development of immune responses during infection (1–3). The generation of tissue-specific immunity is enhanced as a result of the LNs which are strategically located throughout the body (4). This permits simultaneous antagonistic immune responses in different organs in a concerted manner, thus providing a more controlled immune response in different organs (5).

This niche-specific immunity is particularly pronounced in the gastrointestinal tract, in which different gut segments are drained by immunologically distinct LNs to meet the different needs of these gut segments (6, 7). Supporting the concept of LN 'sharing' and co-drainage, several studies showed that gut-associated LNs also drain the pancreas and liver to varying extents (8–10). Given the intricate gut-liver cross-talk (11, 12), there is a potential for mixed drainage between the gut and liver LNs which is poorly understood to date.

Two liver-draining lymph nodes (LLN) are present in mice, the celiac lymph node, CLN, and the portal lymph node, PLN (8, 13). These LLNs lie adjacent to each other, with the PLN more superficial and located to the right of the portal vein while the CLN is located slightly deeper in the peritoneal cavity (14). The human liver shares this anatomical arrangement where it also seems to be drained by two sets of LNs with similar localization as in mice (15, 16). Of note, the nomenclature of the two murine LLNs differed between studies, but one theme runs through these studies; the consistency in description of the co-draining and organogenesis of the CLN and PLN (8, 14). The CLN co-drains some parts of the small intestine and the peritoneal cavity whereas the PLN drains the liver to a greater extent (5, 14). Here, we follow the nomenclature of Brown and colleagues (5).

Using Evans blue dye, Mayer et al., revealed the involvement of these LLNs in gut-restricted infection to be dependent on the route (subserosal into the intestines or footpad injection of antigens) of infection (17), showing migration of dendritic cells (DCs) from the liver to the LLNs to prime and facilitate specific T cell responses. Interestingly, CLN and PLN appear to be independent liver-draining LNs, with different cellular compositions and modes of organogenesis (18). Hence, the two LN may act differently when comparing hepatic vs. enteric infections but also comparing the responses of CLN and PLN in the context of any given intestinal infection. While we are not aware of studies testing the latter, a study comparing the CLN and PLN responses to hepatic virus infection reported that they were predominantly involved in liver antiviral immune responses (13). Accordingly, lymphadenectomy of the PLN resulted in hepatitis B virus (HBV) persistence in immunocompetent mice (14). The CLN on the other hand was shown to be important in promoting liver-mediated adaptive immune tolerance via induction of regulatory T cells (Tregs) and scarcity of DCs (13).

We, therefore, asked whether and how the two lymphoid organs contributed to the immune response against intestinal nematode infections, taking advantage of the strictly enteric infection with *H. bakeri*, a natural parasite of mice. Similar to widespread and economically important gastrointestinal nematodes of cattle and small ruminants, this worm develops through a short histotrophic phase of about 8 days, spent by the growing larval stages in the small intestinal submucosa, before returning to the lumen of the upper small intestine where the adult worms mate and survive for up to 9 months. We also compared the responses in CLN and PLN to those in the mesenteric lymph nodes (MLN).

In line with earlier evidence for the CLN draining parts of the upper small intestine, it has also been shown that the CLN co-drain liver, duodenum, and peritoneum (5, 14), hence a mix of liver-derived soluble signals/DC with the signals and APC from small intestines. The PLN on the other hand was shown to more exclusively drain the liver to a greater extent (5, 14). Thus, the present work seeks to address whether the LLNs contribute to the instruction of classical Th2 cells in a strictly enteric gastrointestinal nematode infection and whether the co-drainage ongoing between the MLN and LLNs could impact the immune responses in these LLNs fostering Treg, Th2, or B cells specializations in them.

We explored two-time points of *H. bakeri* infection, days 6 (early phase) and 14 (peak phase), representing the phases of larval development in small intestinal tissue and the arrival of the mature larvae in the lumen of the intestine, respectively. We demonstrate a clear distinction between the two LLNs; CLN, like the MLN, are strong Th2 induction sites, while the PLN is biased towards TFH cells and, hence, generates high-quality B cell responses during the infection.

Results

The liver-draining lymph nodes contribute to T effector cell responses against *H. bakeri* infection

H. bakeri infects the small intestine of mice where the ingested infective larvae (L3) invade the submucosa of the duodenum and upper jejunum for development into the pre-adult stage, which returns to the small intestinal lumen at day 8 post-infection (19). The tissue damage provoked during the development of the histotropic larval stage results in a strong immune response reflected by the substantial increase in size and cellularity of the mesenteric lymph nodes (MLN) draining the duodenum and jejunum (Figures 1A, B). We further noticed that the size of the two lymph nodes draining the liver, namely celiac (CLN) and portal lymph nodes (PLN), were increased in mice infected with *H. bakeri* for 2 weeks (Figures 1A–C). Earlier studies demonstrated the multi-organ drainage by the CLN, comprising the liver and pancreas, but also the upper duodenum (5, 8, 13, 14), whereas the PLN solely drains the liver and pancreas (5). In accordance with the drainage of the upper SI shared between MLN and CLN, both sites comprised significantly elevated and similar frequencies of IL-4 and IL-13 competent Th2 cells during larval development (day 6 p.i.) and after transition to the patent stage of infection (day 14 p.i., Figure 1D). However, Th2 cells were also significantly increased in the PLN of infected mice at both timepoints, albeit at lower levels compared to MLN and CLN (Figure 1D). In parallel to the induction of Th2 cells, elevated IFN-g production by CD4+ T cells was seen in all LN samples at day 6, but the percentage of T-bet+ Th1 cells remained

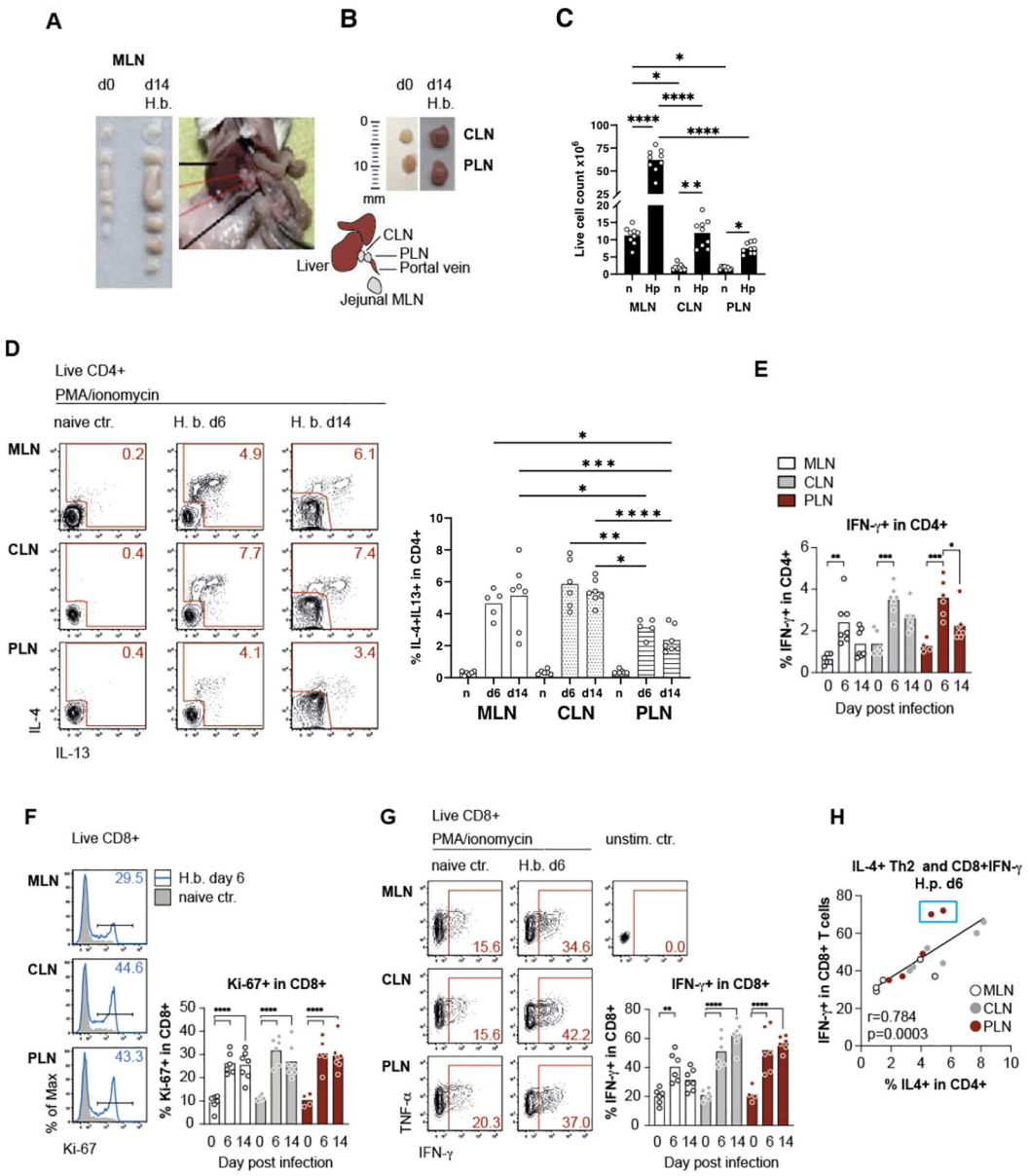

FIGURE 1
Mesenteric lymph nodes, in conjunction with liver-draining lymph nodes, contribute to T-cell effector responses against *H. bakeri* infection. **(A)** Mesenteric lymph nodes (MLN) at day 0 (d0) and day 14 (d14) post-infection with *H. b*, picture of BALB/c mouse dissected at day 14 to show the anatomical position of the two LLNs. **(B)** Image illustrating the jejunal MLN with the celiac (CLN) and portal lymph nodes (PLN), with a drawn scale for size comparison. Insets show the size of CLN and PLN on d0 and d14. **(C)** Quantification of live cell counts in MLN, CLN, and PLN on d0 and d14. Data are presented as mean ± SEM with statistical significance indicated. **(D)** Flow cytometry analysis of IL-4 and IL-13 expression in live $CD4^+$ T cells ($IL\text{-}4^+$ and $IL\text{-}13^+$ double-positive cells gated within $CD4^+IL\text{-}4^+$ population) from MLN, CLN, and PLN on d0, d6, and d14 post-infection. Representative plots (left) and cumulative data (right) demonstrate an increase in $IL\text{-}4^+$ and $IL\text{-}13^+$ $CD4^+$ T cells in infected mice. **(E)** Percentage of $IFN\text{-}\gamma^+$ $CD4^+$ T cells in MLN, CLN, and PLN on d0, d6, and d14 post-infection. Bars represent mean ± SEM, with statistical comparisons among time points. **(F)** Proliferation of live $CD8^+$ T cells in MLN, CLN, and PLN on d6 post-infection with *H. b.* Representative histograms show Ki-67 expression in $CD8^+$ T cells from naïve and infected mice (left). Bar graph (right) quantifying the percentage of $Ki\text{-}67^+$ $CD8^+$ T cells at different time points (d0, d6, and d14). **(G)** Cytokine production in live $CD8^+$ T cells from MLN, CLN, and PLN at d6 and d14 post-infection. Representative flow cytometry plots show IFN-γ and TNF-α expression (left), while the bar graph quantifies the percentage of $IFN\text{-}\gamma^+$ $CD8^+$ T cells at each time point (right). **(H)** Correlation between $IL\text{-}4^+$ Th2 cells and $IFN\text{-}\gamma^+$ $CD8^+$ T cells in MLN, CLN, and PLN at d6 post-infection. Each dot represents an individual mouse, with Pearson's correlation coefficient (r) and p-value shown. Statistical significance: *p < 0.05, **p < 0.01, ***p < 0.001, ****p < 0.0001.

unchanged, and the rate of IFN-g production leveled down in CD4+ T cells at day 14 post-infection (Figure 1E).

We further sought to compare the expression of Th2 effector functions in the different lymph nodes and therefore assessed the activity of CD8+ T cells, as earlier work reported the IL-4 dependent expansion of CD8+ memory-like T cells which was increased along the expansion of CD4+ Th2 cells in *H. bakeri*-infected mice (20, 21). Confirming these earlier studies, we determined a highly significant increase in the proliferation of CD8+ T cells in all active lymph nodes of infected mice (Figure 1F). Infection-derived CD8+ T cells

also displayed elevated T-bet expression, which translated to significantly stronger IFN-g responses upon *in vitro* stimulation compared to naïve controls (Figure 1G and data not shown). Interestingly, the comparable profiles observed across different lymph nodes suggest that Th2 cells are not only present but also actively induced in the PLN, where they contribute to the expansion of CD8+ VM cells as early as day 6 post-infection. This finding makes it unlikely that Th2 cells were initially induced in MLN or CLN and subsequently migrated to the PLN, as the PLN lacks a direct connection to the gut, a key site for Th2 induction.

Despite our claims that Th2 cell levels in the PLN are reduced by half compared to MLN and CLN (Figure 1D), the PLN exhibits a comparable magnitude of CD8+ T cell responses. This observation suggests that lower Th2 levels in the PLN, if present, do not negatively impact CD8+ T cell responses at day 6. Furthermore, IFN-g expression of CD8+ T cells was positively correlated with the extent of Th2 responses across the LNs.

Hence, while the majority of Th2 cells induced in response to a strictly enteric nematode infection derive from the larger MLN and CLN draining the site of infection, a more limited number of Th2 cells derive from the liver-draining PLN. Furthermore, the correlation between Th2 response and local expansion of memory-like CD8+ T cells indicates robust Th2 effector functions expressed in the active LNs. This included the liver-draining PLN which is activated during enteric nematode infection despite the lack of the lymphatics directly connecting the PLN to the site of infection.

CLN and PLN display different gut-homing characteristics of GATA-3+ T cells and ALDH enzyme activity

As we observed that the LLNs are a site of Th2 induction during *H. bakeri* infection, we next sought to determine if these T effector cells (Teff) contribute to anti-helminth immunity in the gut. Therefore, we assessed the expression of the gut-homing marker CCR9 (22) in Th2 cells in the different lymph nodes. CCR9-mediated gut homing of GATA-3+ cells is shown to correlate with high expression of aldehyde dehydrogenase (ALDH) in DCs isolated from the MLN of mice early during infection (22, 23). In addition, the early stage of infection drives the early recruitment of T cells to the infected gut and determines worm clearance (24). We, therefore, looked at the gut-homing marker CCR9 at day 6 to get an idea of how these cells behave in extra-lymphoid compartments and their contributions to controlling gut infection.

We observed that Th2 cells from the PLN express very low levels of CCR9 at days 6 and 14 compared to these cells in the CLN and MLN (Figures 2A, B). Higher RALDH activity (retinoic acid metabolism) in CD103+ MLN-DCs and an enhanced vitamin A metabolism during the early stage of infection resulted in higher CCR9+ T cells homing to the gut (25–27). Therefore, we assessed ALDH activity in CD103+ DCs at 6dpi using the Aldefluor kit. We found that low CCR9 expression in Th2 cells in the PLN was accompanied by low ALDH expression by CD103+ CD11c+ DCs.

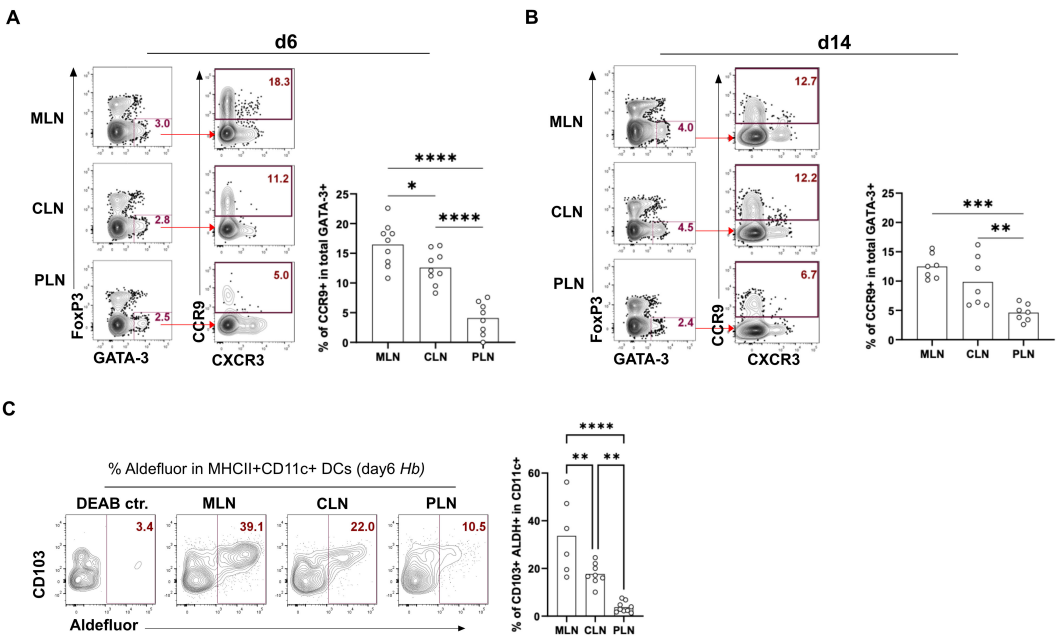

FIGURE 2
MLN, PLN, and CLN display differential expression of CD103+ ALDH+ DC along with differential gut homing of Th2. Frequencies of the gut homing marker CCR9 in total GATA-3+ Th2 cells in MLN, PLN, and CLN at **(A)** 6 days post-infection and **(B)** 14 days post-infection. Bar graphs report the mean percentages of CCR9+ in GATA-3+ Th2 (CD4+Foxp3- T helper cells) **(C)** Proportions of CD103+ ALDH+ DC in MLN, PLN, and CLN-derived cells on day 6 post-infection. Bar graphs report mean % of ALDH expression in MHCII+CD11c+CD103+ DCs. Cells were gated as CD8a- SiglecF- CD90- F4/80-. Cells were stained and analyzed by flow cytometry, representative FACS plots, and the data derived from at least two independent experiments performed with 3-4 mice per group shown. *p < 0.05, **p < 0.01, ***p < 0.001 and ****p < 0.0001 determined by Kruskal-Wallis test combined with Dunn's multiple comparison test or Mann-Whitney test.

In contrast, the higher expression of gut-homing markers by Th2 cells from the CLN and MLN was mirrored by the higher expression of ALDH by DCs (Figure 2C). Together, this data shows that MLN and CLN express higher proportions of the gut-homing marker CCR9 compared to PLN as a result of higher levels of ALDH activity in their DCs.

Differential B cell responses are associated with the magnitude of Th2 rather than TFH profiles

The quantification of IL-4 and GATA-3 expression in CD4+ T cells in the liver versus gut-draining lymph nodes indicated a trend for less extensive Th2 effector cell generation in PLN compared to the 'classical' gut-draining lymph nodes. However, the three sites displayed similar features associated with IL-4 signaling in worm infections, such as the strong outgrowth of B cells and the expansion of VM CD8+ T cells (Figure 1H). Furthermore, both B cell proliferation and IFN-g competence of CD8+ T cells strongly correlated with the individual levels of Th2 responses in a given organ rather than with the organ itself (Figure 1F). We, therefore, asked if qualitative differences in the B cell responses might be associated with the extent of Th2 differentiation and/or the balance of Th2 effector versus follicular T helper cell differentiation across the different lymphatic sites. We hence quantified IgG1-expressing cells by intracellular stains at day 6 and 14 post-infection and found a significant rise of IgG1+ cells in the three lymph nodes at day 14 post-infection (Figure 3A). As shown for CLN-derived cells in Figures 3B, C, IgG1+ cells were composed of B220+ cells which displayed a germinal center (GC) B cell phenotype by the expression of the canonical GC transcription factor Bcl6, the binding of peanut agglutinin (PNA) and the elevated expression of GL7. In contrast, a smaller subset of B220-IgG1+ cells lacked GC markers and expressed CD138 and Ly6C associated with plasma cells (28). Furthermore, the B220- subset had lost the CXCR5 expression required for positioning in the B cell follicles (Figures 3B, C) (29–31). IgG1+ PC accounted for a prominent part of the IgG1+ cells in both MLN and CLN of infected compared to control mice (Figure 3D). In contrast, only 2 out of 8 mice harbored a prominent IgG1+ PC population in the liver-draining PLN at day 14 p.i, and these individuals also displayed the highest IgG1+ PC responses in MLN and CLN (Figure 3D). Because earlier studies demonstrated the capability of Th2 cells for the instruction of extrafollicular B cell responses (32, 33), we tested for associations between the magnitude of Th2 and overall IgG1 responses as well as early IgG1+ PC differentiation across the LN at day 14 p.i. As shown in Figures 3E, F, the frequencies of Th2 cells were strongly correlated with the overall outgrowth of IgG1+ cells (Figure 3E) as well as with the subset of IgG1+ B220- PC cells (Figure 3F). In contrast, the more homogenous GC B cell responses were not linked with the extent of Th2 differentiation (Figures 3G, H). Furthermore, while the PLN of most of the infected mice comprised low proportions of IgG1+ PC, the B220+IgG1+ subset was the most enriched in GL7+ Bcl6^{high} GC B cells in the liver-draining LN (Figure 3I, Supplementary Figure 3). These data suggested that the liver-draining PLN provided an environment suited for the generation of germinal center reactions while being less prone to the rapid instruction of plasma cell differentiation in the context of enteric nematode infection (Supplementary Figure 3).

We complemented the investigation of B and Th2 cell responses by the quantification of follicular T helper (TFH) cell response at days 6 and 14 post-infection. TFH cells are required for efficient germinal center reactions, resulting in the generation of high-affinity IgG and the development of memory B cells (34), whereas Th2 cells providing IL-4 were shown to be sufficient for extrafollicular IgG1 class switching and the generation of short-lived PC (35–37). As shown in Figure 3J, particularly high frequencies of TFH cells identified by the expression of the chemokine receptor CXCR5 together with the inhibitory signaling molecule PD-1 were detectable in CLN at day 6 post-infection. However, CD4 cells isolated from the three LN at day 14 post-infection comprised similar frequencies of TFH cells (Figure 3J, Supplementary Figure 2), matching the homogenous proportions of B220+IgG1+ GC B cells (Figure 3G). TFH responses were not mirrored in the overall rate of IgG1 class switching but negatively correlated with the extent of early plasma cell responses (Figures 3K, L).

T cells in PLN are the only producers of parasite-specific IL-21 among the three LNs, driving efficient GC formation and high-quality antibody responses

IL-21 has been reported to be integral to protective humoral immunity, where it acts on B cells from the outset of an adaptive immune response to promote their expansion and contribution to germinal center reaction (38–40). Therefore, to assess the contribution of IL-21 to the observed B cell responses, single-cell suspensions from the MLN, CLN, and PLN were stimulated with *H. bakeri* excretory-secretory product (HES) or antibodies against CD3 and CD28 (strong T cell receptor stimulants), cultured for 72 hours, after which the supernatants were harvested and tested for IgG1 and IL-21. We found that all three LNs harbor B cells producing IgG1 at day 14. However, we detected IgG1 in the supernatants of PLN cells on day 6 (Figure 3A), suggesting an early and sustained IgG1 production by B cells in this lymph node. Interestingly, of all the LNs, we could only detect IL-21 in the supernatant of cultured PLN cells in response to T-cell receptor stimulation (Figures 3B, C). In summary, these data suggest that the PLN environment is conducive in terms of IL-21 response by TFH and could support GC and quality B cell responses.

B cells from PLN produce higher affinity IgG1 antibodies compared to MLN and CLN, which react to both VAL-1 and ACE-1

To confirm the assertion that the PLN environment supports higher quality B cell responses compared to the MLN and CLN, we run an SDS-PAGE of 'untouched' HES and de-glycosylated HES

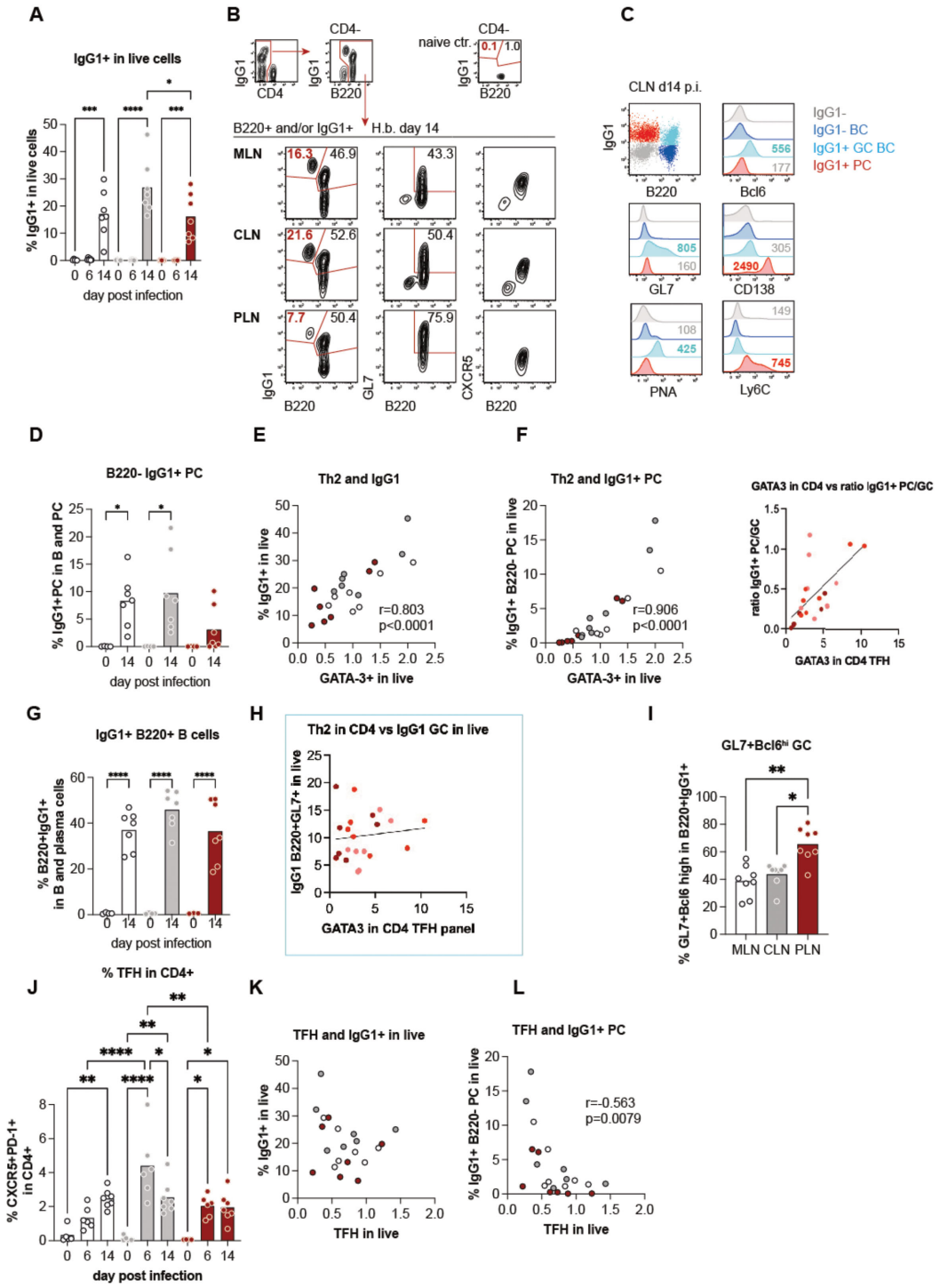

FIGURE 3
Differential B cell responses are associated with the magnitude of Th2 rather than TFH profiles. **(A)** Quantification of IgG1+ cells among live cells over the course of infection, showing a significant increase at day 14 post-infection. **(B)** Representative flow cytometry plots of B220+ and/or IgG1+ cells from mesenteric lymph nodes (MLN), cervical lymph nodes (CLN), and popliteal lymph nodes (PLN) at day 14 post-infection. Populations include germinal center(GC) B cells (B220+ GL7+ CXCR5+) and plasma cells (PCs; B220- IgG1+). **(C)** Flow cytometry analysis of IgG1+ subsets in CLN, highlighting markers associated with GC B cells (Bcl6, GL7) and PCs (CD138, Ly6C). **(D)** Percentage of B220- IgG1+ PCs across time points, showing significant expansion at day 14. **(E, F)** Correlation of Th2 marker GATA3+ in CD4+ T cells with IgG1+ cells **(E)** and B220- IgG1+ PCs **(F)** in live populations, with strong positive associations. **(G)** Proportions of B220+ IgG1+ GC B cells in B cell populations showing significant increases by day 14. **(H)** Correlation between GATA3 expression in CD4+ T follicular helper (TFH) cells and IgG1+ B220+ GC B cells, indicating a potential role of Th2 polarization. **(I)** Percentage of GL7+ Bcl6+ GC B cells within B220+ IgG1+ populations, showing a significantly higher proportion in the PLN compared to MLN and CLN. **(J)** Dynamics of CXCR5+ PD-1+ TFH cells in CD4+ T cell populations over time, peaking at day 14. **(K, L)** Negative correlation between TFH cell abundance and IgG1+ live cells **(K)** or B220- IgG1+ PCs **(L)**, suggesting TFH-independent regulation of PC responses.

using either PNGase F or O-glycosidase. The HES was de-glycosylated to remove carbohydrate moieties (present in adult ES) on antigenic epitope, the so-called Glycan A and B, which have been shown to induce non-protective antibodies and act as a decoy that generates ineffective humoral responses during primary *H. bakeri* infection (41). From the SDS-PAGE gel, 'untouched HES' as well as de-glycosylated HES show the two band sizes that correspond to Venom allergen/Ancylostoma secreted protein-Like-1 (VAL-1) and acetylcholinesterase-1 (ACE-1) proteins, depicted by the red and black boxes, respectively (Figure 4A). These proteins are suggested to represent two major vaccine targets that induce protective immunity against *H. bakeri* (42). Western blots were thereafter run using pooled sera from d14 *H. bakeri* infected BALB/c mice as well as the supernatant of MLN, CLN, and PLN cell suspensions after 72 hours of culture with HES. We found that the serum IgG1 reacted strongly to these two bands (red and black boxes – Figure 4B).

Next, we probed whether the supernatants from MLN, CLN, and PLN show similar binding patterns. We show that the supernatants from the MLN and CLN only reacted to the second band, ACE-1 (black box) while the supernatant from the PLN reacted to the two bands just like the pooled sera (red and black boxes and red arrows – Figure 4C). We also show that both the 'untouched' and de-glycosylated HES showed similar binding patterns when probed with pooled sera or supernatant (Figures 4B, C). Furthermore, we show that with the supernatants, the binding to the de-glycosylated HES was weaker shown in fainter bands than the 'untouched' HES. The binding intensities to the 'untouched' HES decreased in MLN, compared to CLN and PLN, with the PLN showing the highest intensity. The data together show that the PLN has a similar binding pattern to the pooled sera, reacting to the *H. bakeri* vaccine target proteins VAL-1 and ACE-1.

In summary, our data show that the PLN, even though it has restricted Th2 responses, compared to the MLN and CLN, possibly due to its high IFN-γ environment, is skewed towards TFH response. Even though the PLN shows lower PCs compared to the MLN and CLN at day 14, the PLN is able to form more GC, which enables it to produce more quality B cells and high-affinity antibody response (Figures 3D, I), evident in the binding of its supernatants to both VAL-1 and ACE-1 compared to the MLN and CLN (Figures 4A–C). Together, our data shows that the PLN is important for quality B cell responses during *H. bakeri* infection.

Discussion

Few studies of LNs in mice have identified cross-talks between gut-draining LNs and LNs at different anatomical locations (5, 8, 14). In mice, the LLNs have attracted attention only recently in the context of liver infections or gastrointestinal virus infections (5, 14). Not much work has been done on these LLNs in the context of

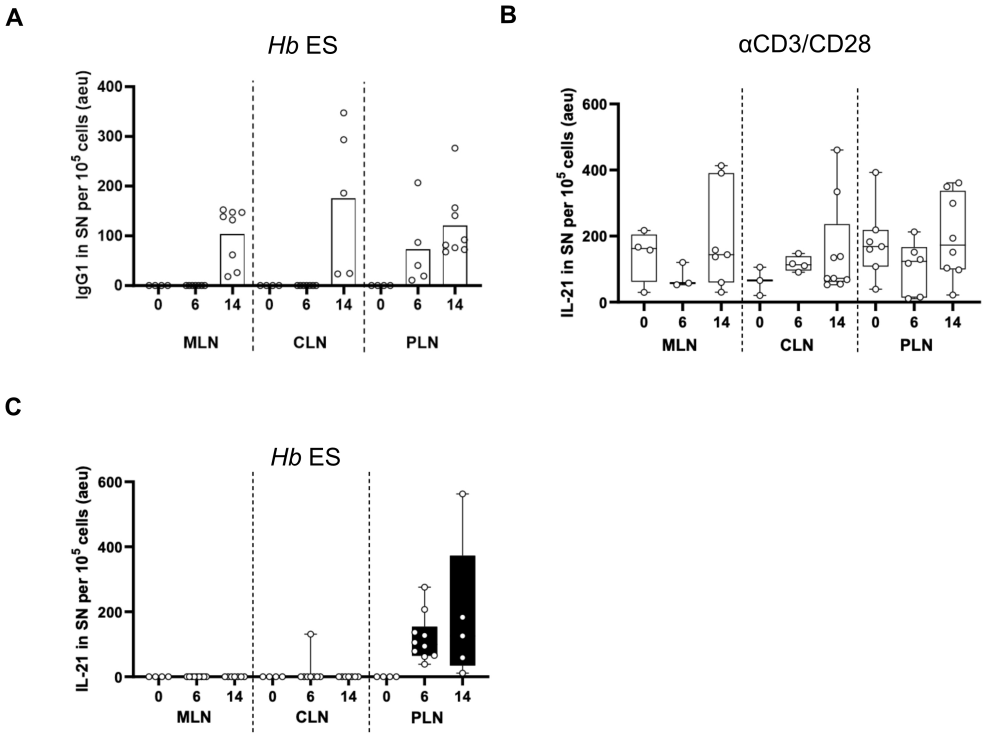

FIGURE 4
IgG1 and IL-21 profile in supernatants harvested after culturing cell suspensions of MLN, CLN, and PLN with *H. bakeri* excretory-secretory products (HES) **(A)** Arbitrary ELISA unit (EU) of IgG1 in the supernatant (SN) of cells cultured from MLN, PLN, and CLN at day 6 and 14 post-infection compared to steady state. **(B, C)** EU of IL-21 in supernatant (SN) of cells cultured from MLN, PLN, and CLN at day 6 and 14 post-infection compared to steady state. Data pooled from at least two independent experiments with 3-4 mice group is shown. Cells were stimulated with either anti-CD3/-CD28 **(B)** or *Hb* ES, *H. bakeri* excretory-secretory products **(C)**.

intestinal helminth infection, especially considering the gut-liver axis and antigen sharing between these organs (43, 44). In previous studies using nematode models, many Th2 cells have been shown to circulate to the liver, but the phenotype and impact on the infection were not addressed (45–47). In our model, we observed increased LLN size even though *H. bakeri* does not traverse the liver. Thus, we speculated that there could be induction of Th2 in the LLNs that may support the MLN during infection. Furthermore, our data suggest that there is indeed a dissemination of parasite antigens to the liver, evidenced by significant levels of parasite-specific CD40L+ Th2 cells in the liver (unpublished data), which could be the result of type 2 effector responses induced by the two LLN.

We also showed that the two LLNs behaved differently in terms of gut-homing marker expression on their Th2 cells. Cells from the CLN typically had similar phenotypes to those from the MLN whilst the PLN cells differed. We show a higher number of Th2 cells co-expressing the gut homing marker, CCR9 in the MLN and CLN (Figures 2A, B) compared to the PLN. This is likely due to different properties of migratory DC sharing between lymph nodes, especially lymph nodes draining the gut and related to the gut. Migratory DC sharing is important in fostering cross-talk and the imprinting of certain phenotypes (like gut-homing markers) on T cells in the different lymph nodes involved (5). The PLN is probably paramount in contributing to the high systemic Th2/1 hybrid cells, possibly due to their poor CCR9 expression (Figures 2A, B) (48). This we also confirmed by the ALDH levels and activity of CD103+ DC (Figure 2C), showing significantly fewer levels of these cells in the PLN compared to the CLN and MLN.

PLN has been shown to share migratory DC with the liver during a hepatotropic viral infection to a greater extent than CLN (5, 8, 13). This suggests an active role of the PLN in liver-specific infections. This phenomenon has also been reported by Brown and colleagues, who show that migratory DCs are shared to a greater extent between CLN and MLN than PLN (5). Alternatively, more antigen-primed migratory DC have access to the CLN compared to the PLN, perhaps due to its proximity to the intestine. The PLN might not be involved in tolerance but rather effector mechanisms and is probably the more important lymph node (in terms of draining the liver) for the liver during *H. bakeri* infection. This could also imply an extra role for the PLN's involvement in the mounting immune response to hepatic infections (8) aside from its somewhat involvement in intestinal infection. The PLN is probably involved in later T cell response or dealing with the excesses of the infection; for instance, gut translocated microbes (as a result of gut barrier dysfunction during the worm's life cycle) (49). We speculate this is due to the high IFN-γ competence of the Th2 PLN cells (Th2/1 hybrid cells) (50) compared to the other LNs (Supplementary Figure 1). This would have to be further investigated.

Our work and the work of others defined the MLN as the main site of Th2 generation and IgG1 class switching in *H. p. bakeri* infection (51–53). Here, we show that the two LLNs contribute to Th2 and TFH generation and the instruction of IgG1 responses. In accordance with the drainage of duodenal tissue by the CLN (5), the reaction of this LN largely phenocopied the MLN response according to the parameters investigated in this study. Despite potential additional cellular and soluble messenger input from the liver and peritoneal cavity, the CLN harbored about the same frequencies of GATA-3 high Th2 cell marked by the co-production of IL-4/-13 and a similar fraction of IL-4, -13, and -5 triple-competent cells as seen in MLN. In addition, both MLN and CLN displayed similar proportions of CXCR5+PD1+ TFH cells and comparable B cells IgG1 class switching (Figure 3J). As anticipated by the increase in size, also the PLN responded to the enteric infection. The frequencies of Th2 cells were only reduced by about 50% compared to MLN and CLN, which is remarkable as the PLN, to the best of our knowledge, lacks any afferent lymphatic connection to the intestine.

More striking, the TFH response expressed in PLN upon 6-14 days of *H. bakeri* infection mirrored those generated in MLN and CLN and the extent of IgG class switching was alike in the B cell populations of all three LNs. These responses were apparently generated with similar kinetics, as Th2 cells almost exclusively expressing high levels of Ki67 were prominent and in all investigated LN at d6 post-infection (Figure 1F). These data suggest that the strong Th2 responses dominating the MLN and CLN might interfere with optimal TFH and B cell interactions (54). However, the stratification of Th2 (IL4, GATA3 expression), TFH, and IgG1(EF/GC) and the associated gradual differences in Th2 effector cell counts did not reveal a dependence on EF/GC phenotypical composition of B cells. These data are, however, limited to MLN and spleen (not shown here), and similar investigations may result in different outcomes concerning the responses in CLN/PLN.

During an ongoing infection, lower affinity B cells express IgM and IgD but can re-enter GC and form new PC that produces high-affinity antibodies (55). There are a lot more B cells re-entering or forming GC in the PLN compared to the MLN and CLN. This is evident in the GC formation ability in PLN compared to the MLN and CLN (Figures 3I, 5C). IFN-γ signaling has also been reported to be very important in spontaneous GC formation (56). The PLN's highly IFN-γ competent environment (from Th2 cells, Supplementary Figure 1) during the infection could be driving the high GC formation in the PLN. Also, its lower IL-4 competence compared to the other LNs during infection could foster its GC-forming ability (54). These suggest that, even though earlier on in the infection, you have good PCs from MLN and CLN, these PC may not be providing high-affinity antibodies that are necessary for the infection. However, the PLN, which initially formed lower PCs, will later have their B cells re-entering the GC, where they are 'reprogrammed' to produce higher affinity and more quality antibody responses (Figures 5C, D). IL-21 production by TFH (57, 58) and calcium signaling via NFAT (59, 60) enable IL-21 to fine-tune B cell responses in relation to the immunological properties of the immunogen. This cytokine has also been shown to promote early B cell expansion by increasing cell cycle speed and cyclic re-entry, synergizing with BCR and CD40 to increase AKT and S6 phosphorylation (60–62). The consequence for B cell responses is that initially, a wide range of antigen affinities are promoted, increasing B cell response size and promotion of plasma cells (63, 64). PLN showed a sustained IgG1 response during the early and peak stages of *H. bakeri* infection. It was also the only LN, in whose cell suspension IL-21 was detected after culturing for 72

hours. This further confirms our earlier thought that the PLN is more biased towards TFH, due to its lower Th2 response (Supplementary Figure 2), which makes it a good site for the generation of more quality B cell responses later in the infection.

Furthermore, protective immunity against *H. bakeri* infection has been achieved by vaccination with adult HES (41). Analyses of serum from vaccinated mice identified two major antigens of the venom allergen and acetylcholinesterase families recognized by the protective immune response as VAL-1 and ACE-1, respectively. These two antigens have been thought to be a major vaccine target for *H. bakeri* infection (42). Our data shows that supernatants from MLN and CLN of day 14 *H. bakeri*-infected BALB/c mice could only react to ACE-1 (black box – Figure 5C), suggesting the absence of B cell clones that produce IgG1 against VAL-1. This phenomenon could be suggestive of the early PC expansion in the MLN and CLN (Figure 5A), which leads to the production of low-affinity IgG1 antibodies that do not recognize epitopes of the VAL-1 proteins (Figure 5C). The PLN, on the other hand, had a lower PC population at day 14 but formed more GC (Figure 3D), leading to the B cells churning out high-affinity IgG1 antibodies that are fully functional and reactive to both VAL-1 and ACE-1 (Figures 5B, C). The pooled sera also reacting to both VAL-1 and ACE-1 suggests that the VAL-1-specific IgG1 in the serum derives from the PLN and not the MLN and CLN (Figures 5B, C). Putting these together,

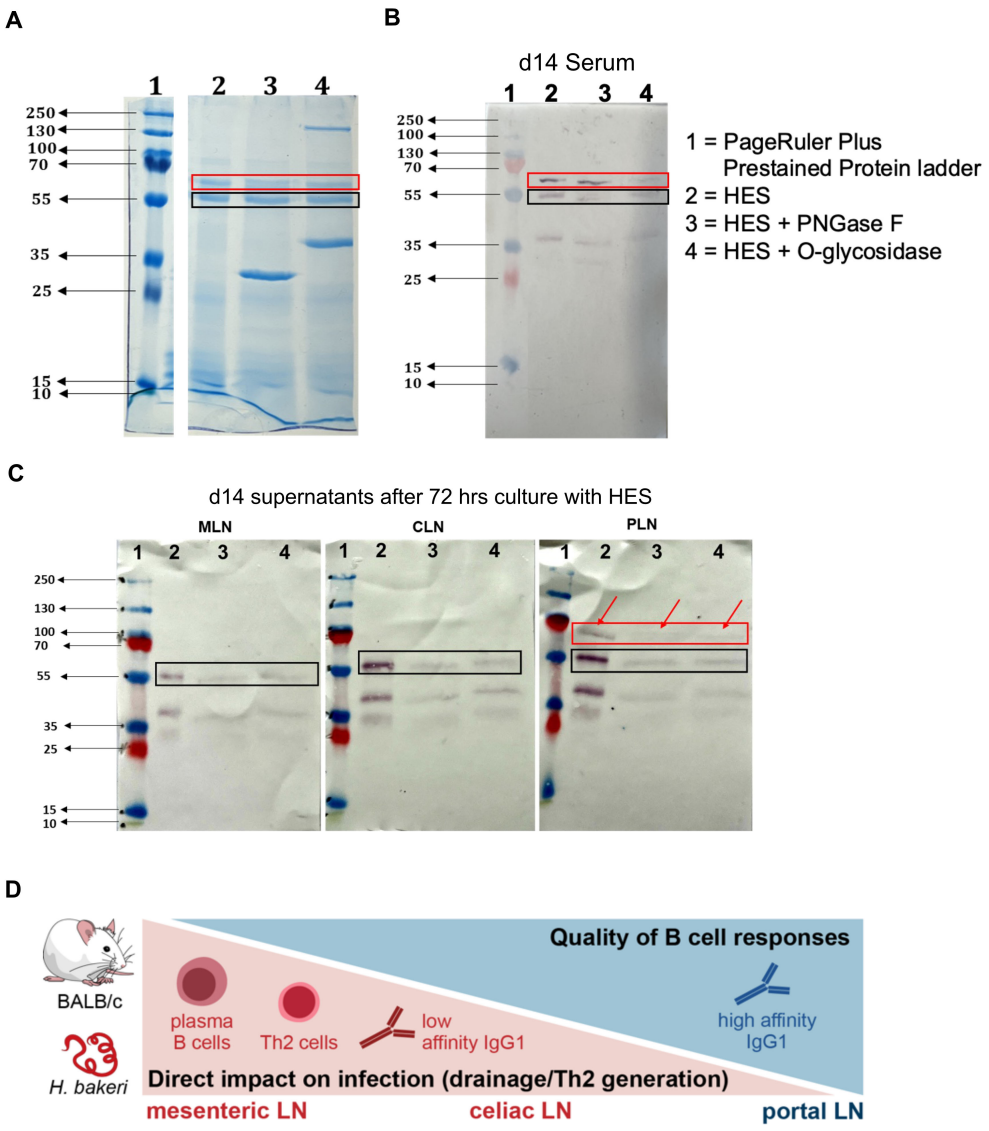

FIGURE 5
B cells from PLN produce higher affinity IgG1 antibodies compared to MLN and CLN, that react to both VAL-1 and ACE-1 of *H. bakeri* excretory-secretory product (HES) **(A)** SDS-PAGE of 'untouched' HES and de-glycosylated HES. Proteins were loaded at 10ug **(B)** Western blot of SDS-PAGE in **(A)** using pooled sera from day 14 of *H. bakeri* infected BALB/c mice **(C)** Western blot of SDS-PAGE in **(A)** using supernatants (1:2 dilution) from MLN, CLN and PLN cell suspensions cultures with HES for 72 hours from day 14 of *H. bakeri* infected BALB/c mice. Goat anti-mouse IgG1 conjugated to AP was used as a secondary antibody and BCIP/NBT as substrate. **(D)** A graphical summary of a suggested model for our findings. TFH and B cell response (and the lower Th2) are generated in PLN, which is not directly connected to the gut via lymphatics. But it may act as an overflow/2nd line of response to the gut infection as a result of a few DCs moving from the MLN to the PLN. This might provide the optimal conditions for a more appropriate/specific antibody response compared to the less specific B cell responses in MLN and CLN.

we report other lymphoid compartments that are important in the generation of B cell response during this infection. Our data suggest that the CLN and PLN are as important in mounting good B-cell responses just as the MLN. The PLN contributes to more sustained antibody responses by the formation of more GCs during the infection to enhance high-affinity antibody responses, which is necessary for protective immunity in *H. bakeri* infection.

In conclusion, GATA-3+ effector cells derive from the two LLNs in addition to the MLN during *H. bakeri* infection. The CLN behaves similarly to the MLN due to the fact that it also drains the gut and peritoneal cavity alongside the liver compared to the PLN which strictly drains the liver (5). The MLN and CLN are the more active LNs in generating T effector responses in *H. bakeri* infection. The PLN, on the other hand, is more important in generating quality B cell responses to enhance high-affinity antibody (IgG1) secretion, a consequence of it being a more TFH-skewed microenvironment. Further studies will be needed to demonstrate that the T and B cells induced in the LLNs are having a direct effect on *H. bakeri*, by either lymphodectomy or selective blocking of T and B cell egress from the LLNs. Also, the adoptive transfer of the cells from the LLNs could reveal other interesting findings of these LNs during *H. bakeri* infection.

Materials and methods

Mice and infections

The animal experiments were done in accordance with the National Animal Protection Guidelines with approval from the German Animal Ethics Committee for the Protection of Animals (G0176/17, G0113/15, H0438/17). Female BALB/c mice were ordered from Janvier (Saint-Berthevin, France) and were infected with 200 3rd-stage larvae of *H. bakeri* by oral gavage. Mice used in the experiments were anesthetized with xylazine and ketamine and sacrificed by cervical dislocation. All animal experiments were performed in accordance with the National Animal Protection Guidelines and approved by the German Animal Ethics Committee for the Protection of Animals (LAGeSo, G0176/20).

Cell isolation

MLN, CLN, and PLN were processed into single-cell suspensions using 70 µl cell strainers (BD Biosciences, San Jose, CA, USA). After washing in RPMI (1% FCS, 100U/ml penicillin, 100 mg/ml streptomycin (PAA, Wien, Austria), any residue red blood cells were removed with an erythrocyte lysis buffer, followed by two further washing steps.

Flow cytometry

For the detection of gut homing markers, cells isolated from lymphatic organs were stained for CCR9 (clone CW-1.2; PE-Cy7) and α4β7 (clone DATK32, biotin) at 37°C for 30 minutes, followed by incubation with a fixable viability dye (eFluor506 or eFluor780) on ice for 5 minutes. After labeling CD4 (clone RM4-5; Alexa 700, Brilliant Violet 510, or PerCP), cells were fixed using fix/perm buffer (Thermo Fisher) for 30 minutes at room temperature and stained intracellularly using the following reagents: FoxP3 (clone FJK-16s; PE-eFluor610, Alexa 488, or PerCP-Cy5.5), GATA-3 (clone TWAJ; eFluor 660), T-bet (clone 4B10; PE), and Ki-67 (SolA15, eFluor 450 or PE-Cy7). Streptavidin coupled with Brilliant Violet 605 was used as a secondary conjugate. Dendritic cells were analyzed using antibodies against MHCII (clone M5/114.15.2; APC), CD11c (clone N418; Brilliant Violet 421), and CD103 (clone 2E7, APC). Aldehyde dehydrogenase (ALDH) activity was determined using the Aldefluor kit (Stemcell Technologies). Non-specific binding of antibodies was prevented by adding FcγRII/III blocking antibody (clone 93). All antibodies and other reagents were from BioLegend, Thermo Fisher, or BD Biosciences. A catalog of the respective antibodies used in the multi-color flow cytometry can be seen in Supplementary Table 1.1 in the Supplementary Figures. Cells were acquired on FACSCantoTM II (BD Biosciences) or FACSAriaTM III (BD Biosciences), and data was analyzed using FlowJo (Tree Star Inc., Ashland, USA). The antibodies used for the detection of surface and intracellular markers are described in Supplementary Table S1. Dead cells were excluded using eFluor780 or eF560 fixable viability dye (Thermo Fisher, Waltham, USA). For intracellular staining of cytokines and transcription factors, cells were fixed and permeabilized using the Fixation/Permeabilization kit and Permeabilization buffer from ThermoFisher/eBioscience. Analyses of the samples were done using a Canto II flow cytometer and an Aria cell sorter (BD Biosciences, Heidelberg, Germany) and FlowJo software Version 10 (Tree Star Inc., Ashland, OR, USA) was used to analyze the data. The data for naïve and infected mice (days 6 and 14) presented in this study are pooled from at least two independent experiments with 3-4 mice per group in each experiment.

Cell culture *and in vitro* re-stimulation

For the analysis of cytokine production capacities of cells, MLN, CLN, and PLN cells were plated out per well in a round-bottom 96-well cell culture plate in a final volume of 200µL RPMI medium, containing 10% FCS, 100U/mL penicillin, and 100µg/mL streptomycin (all from PAA, Pasching, Austria). The cells were then stimulated with 1µg/mL of PMA/ionomycin and incubated for 3-4 hours at 37°C and 5% CO_2. The cells were further stained with a dead cell marker and other surface stains, fixed and permeabilized for intracellular staining, followed by acquisition via flow cytometry.

Parasite-specific IgG1 and IL-21 detection by ELISA

For the analysis of parasite-specific IgG1 and IL-21, $1x10^5$ of MLN, CLN, and PLN cells were plated out per well in a round-bottom 96-well cell culture plate in a final volume of 200µL RPMI medium containing 10% FCS, 100U/mL penicillin and 100µg/mL streptomycin (all from PAA, Pasching, Austria). The cells were

stimulated with either anti-HES (10µg/mL) or without. The cells were then incubated for 72 hours at 37°C and 5% CO_2. The cell suspensions were then spun down, and the supernatant was harvested and measured via sandwich. Absorbance was measured on a Biotek Synergy H1 Hybrid Reader at a 450nm wavelength.

HES preparations, SDS-PAGE, and Western blots

Adult *H. bakeri* excretory and secretory product (HES) were either deglycosylated with Peptide N-glycosidase F (PNGase F), which cleaves N-linked glycans from glycoproteins, or Endo-α-N-Acetylgalactosaminidase (O-glycosidase), that catalyzes the removal of O-disaccharides from glycoproteins. These enzymes are from New England Biolabs®. Glycosylated and deglycosylated HES were run on an SDS-PAGE, and Western blot was done on these using either serum from d14 *H. bakeri* infected BALB/c mice or supernatants from cell suspension from MLN, CLN, and PLN after culturing with HES for 72 hours according to the protocol published in (65). Briefly, the SDS-PAGE was blotted unto a nitrocellulose membrane, blots were blocked in 2% dry skim milk in TBS with 0.05% Tween 20 for 2 hours at room temperature and probed with either pooled sera (1:200 dilutions) or supernatants from cell suspensions of MLN, CLN, and PLN (1:2 dilutions) at 4 ^{0}C overnight. This was followed by 3 times washing in TBST, after which AP-conjugated secondary antibodies (anti-mouse IgG1 1:3000, antibodies-online.com) for 2 hours at room temperature. The blots were then washed 3 times in TBST and developed with SIGMAFAST™ BCIP®/NBT substrate (Sigma-Aldrich®).

Statistics

All statistical analyses were performed using GraphPad Prism Software (San Diego, CA, USA). Normality was tested with the Shapiro-Wilk test, followed by ordinary one-way-ANOVA or Kruskal-Wallis test and Tukey's or Dunn's multiple comparison test. Comparisons of the two groups were performed with an unpaired t-test or Mann-Whitney test.

Data availability statement

The original contributions presented in the study are included in the article/Supplementary Material. Further inquiries can be directed to the corresponding author.

Ethics statement

The animal study was approved by German Animal Ethics Committee for the Protection of Animals (LAGeSo, G0176/20). The study was conducted in accordance with the local legislation and institutional requirements.

Author contributions

JA: Conceptualization, Data curation, Formal analysis, Investigation, Methodology, Software, Validation, Visualization, Writing – original draft, Writing – review & editing. ZD: Methodology, Writing – review & editing. RM: Methodology, Writing – review & editing. AM: Validation, Writing – review & editing. SH: Conceptualization, Funding acquisition, Investigation, Project administration, Resources, Software, Supervision, Validation, Writing – original draft, Writing – review & editing. SR: Conceptualization, Formal analysis, Funding acquisition, Investigation, Methodology, Project administration, Resources, Software, Supervision, Validation, Writing – original draft, Writing – review & editing.

Funding

The author(s) declare financial support was received for the research, authorship, and/or publication of this article. We acknowledge funding by the German Research Foundation (DFG) to SH and SR within the DFG Research Training Group GRK 2046.

Acknowledgments

The authors acknowledge Yvonne Weber, Bettina Sonnenburg, Beate Anders, Marion Müller, Christiane Palissa, and Franziska Möbus for their excellent technical support and Anne Winkler for illustrative support.

Conflict of interest

The authors declare that the research was conducted in the absence of any commercial or financial relationships that could be construed as a potential conflict of interest.

The author(s) declared that they were an editorial board member of Frontiers, at the time of submission. This had no impact on the peer review process and the final decision.

Publisher's note

Supplementary material

The Supplementary Material for this article can be found online at: https://www.frontiersin.org/articles/10.3389/fimmu.2025.1483274/full#supplementary-material

References

1. Drayton DL, Liao S, Mounzer RH, Ruddle NH. Lymphoid organ development: From ontogeny to neogenesis. *Nat Immunol*. (2006) 7:344–53. doi: 10.1038/ni1330

2. Liao S, Padera TP. Lymphatic function and immune regulation in health and disease. *Lymphatic Res Biol*. (2013) 11:136–43. doi: 10.1089/lrb.2013.0012

3. Menzel L, Höpken UE, Rehm A. Angiogenesis in lymph nodes is a critical regulator of immune response and lymphoma growth. *Front Immunol*. (2020) 11:591741. doi: 10.3389/fimmu.2020.591741

4. Weisberg SP, Ural BB, Farber DL. Tissue-specific immunity for a changing world. *Cell*. (2021) 184:1517–29. doi: 10.1016/j.cell.2021.01.042

5. Brown H, Komnick MR, Brigleb PH, Dermody TS, Esterházy D. Lymph node sharing between pancreas, gut, and liver leads to immune crosstalk and regulation of pancreatic autoimmunity. *Immunity*. (2023) 56:2070–2085.e11. doi: 10.1016/j.immuni.2023.07.008

6. Houston SA, Cerovic V, Thomson C, Brewer J, Mowat AM, Milling S. The lymph nodes draining the small intestine and colon are anatomically separate and immunologically distinct. *Mucosal Immunol*. (2016) 9:468–78. doi: 10.1038/mi.2015.77

7. Pöysti S, Toivonen R, Takeda A, Silojärvi S, Yatkin E, Miyasaka M, et al. Infection with the enteric pathogen C. rodentium promotes islet-specific autoimmunity by activating a lymphatic route from the gut to pancreatic lymph node. *Mucosal Immunol*. (2022) 15:471–9. doi: 10.1038/s41385-022-00490-2

8. Barbier L, Tay SS, McGuffog C, Triccas JA, McCaughan GW, Bowen DG, et al. Two lymph nodes draining the mouse liver are the preferential site of DC migration and T cell activation. *J Hepatol*. (2012) 57:352–8. doi: 10.1016/j.jhep.2012.03.023

9. Shoda LKM, Young DL, Ramanujan S, Whiting CC, Atkinson MA, Bluestone JA, et al. A comprehensive review of interventions in the NOD mouse and implications for translation. *Immunity*. (2005) 23:115–26. doi: 10.1016/j.immuni.2005.08.002

10. Zaccone P, Cooke A. Helminth mediated modulation of Type 1 diabetes (T1D). *Int J Parasitol*. (2013) 43:311–8. doi: 10.1016/j.ijpara.2012.12.004

11. Mandato C, Delli Bovi AP, Vajro P. The gut-liver axis as a target of liver disease management. *Hepatobiliary Surg Nutr*. (2021) 10:100–2. doi: 10.21037/hbsn.2020.03.27

12. Rodrigues SG, van der Merwe S, Krag A, Wiest R. Gut-liver axis: Pathophysiological concepts and medical perspective in chronic liver diseases. *Semin Immunol*. (2024) 71:101859. doi: 10.1016/j.smim.2023.101859

13. Yu J, Chen Y, Wu Y, Ye L, Lian Z, Wei H, et al. The differential organogenesis and functionality of two liver-draining lymph nodes in mice. *J Autoimmun*. (2017) 84:109–21. doi: 10.1016/j.jaut.2017.08.005

14. Zheng M, Yu J, Tian Z. Characterization of the liver-draining lymph nodes in mice and their role in mounting regional immunity to HBV. *Cell Mol Immunol*. (2013) 10:143–50. doi: 10.1038/cmi.2012.59

15. Graham NJ, Libshitz HI. Cascade of metastatic colorectal carcinoma from the liver to the anterior diaphragmatic lymph nodes. *Acad Radiol*. (1995) 2:282–5. doi: 10.1016/S1076-6332(05)80185-0

16. Pupulim LF, Vilgrain V, Ronot M, Becker CD, Breguet R, Terraz S. Hepatic lymphatics: Anatomy and related diseases. *Abdominal Imaging*. (2015) 40:1997–2011. doi: 10.1007/s00261-015-0350-y

17. Mayer JU, Brown SL, MacDonald AS, Milling SW. Defined intestinal regions are drained by specific lymph nodes that mount distinct th1 and th2 responses against schistosoma mansoni eggs. *Front Immunol*. (2020) 11:592325. doi: 10.3389/fimmu.2020.592325

18. Zheng M, Tian Z. Liver-mediated adaptive immune tolerance. *Front Immunol*. (2019) 10:2525. doi: 10.3389/fimmu.2019.02525

19. Johnston CJC, Robertson E, Harcus Y, Grainger JR, Coakley G, Smyth DJ, et al. Cultivation of heligmosomoides polygyrus: an immunomodulatory nematode parasite and its secreted products. *J Visualized Experiments: JoVE*. (2015) 98:52412. doi: 10.3791/52412

20. Lin J, Mohrs K, Szaba F, Kummer L, Leadbetter E, Mohrs M. Virtual memory CD8 T cells expanded by helminth infection confer broad protection against bacterial infection. *Mucosal Immunol*. (2019) 12:258–64. doi: 10.1038/s41385-018-0100-x

21. Renkema KR, Lee J-Y, Lee YJ, Hamilton SE, Hogquist KA, Jameson SC. IL-4 sensitivity shapes the peripheral CD8+ T cell pool and response to infection. *J Exp Med*. (2016) 213:1319–29. doi: 10.1084/jem.20151359

22. Cassani B, Villablanca EJ, Quintana FJ, Love PE, Lacy–Hulbert A, Blaner WS, et al. Gut-tropic T cells that express integrin α4β7 and CCR9 are required for induction of oral immune tolerance in mice. *Gastroenterology*. (2011) 141:2109–18. doi: 10.1053/j.gastro.2011.09.015

23. Xu B, Deng C, Wu X, Ji T, Zhao L, Han Y, et al. CCR9 and CCL25: A review of their roles in tumor promotion. *J Cell Physiol*. (2020) 235:9121–32. doi: 10.1002/jcp.29782

24. Adjah J, Kapse B, Zhang H, Hartmann S, Rausch S. Differential resistance to nematode infection is associated with the genotype- and age- dependent pace of intestinal T cell homing. (2024). Preprint. doi: 10.21203/rs.3.rs-4850015/v1

25. Edele F, Molenaar R, Gütle D, Dudda JC, Jakob T, Homey B, et al. Cutting edge: instructive role of peripheral tissue cells in the imprinting of T cell homing receptor patterns. *J Immunol*. (2008) 181:3745–9. doi: 10.4049/jimmunol.181.6.3745

26. Frota-Ruchon A, Marcinkiewicz M, Bhat PV. Localization of retinal dehydrogenase type 1 in the stomach and intestine. *Cell Tissue Res*. (2000) 302:397–400. doi: 10.1007/s004410000281

27. Goverse G, Olivier BJ, Molenaar R, Knippenberg M, Greuter M, Konijn T, et al. Vitamin A metabolism and mucosal immune function are distinct between BALB/c and C57BL/6 mice: Cellular immune response. *Eur J Immunol*. (2015) 45:89–100. doi: 10.1002/eji.201343340

28. Lacotte S, Decossas M, Le Coz C, Brun S, Muller S, Dumortier H. Early differentiated CD138highMHCII+IgG+ Plasma cells express CXCR3 and localize into inflamed kidneys of lupus mice. *PloS One*. (2013) 8:e58140. doi: 10.1371/journal.pone.0058140

29. de Goër de Herve M-G, Abdoh M, Jaafoura S, Durali D, Taoufik Y. Follicular CD4 T cells tutor CD8 early memory precursors: an initiatory journey to the frontier of B cell territory. *iScience*. (2019) 20:100–9. doi: 10.1016/j.isci.2019.09.012

30. Hardtke S, Ohl L, Förster R. Balanced expression of CXCR5 and CCR7 on follicular T helper cells determines their transient positioning to lymph node follicles and is essential for efficient B-cell help. *Blood*. (2005) 106:1924–31. doi: 10.1182/blood-2004-11-4494

31. Haynes NM, Allen CDC, Lesley R, Ansel KM, Killeen N, Cyster JG. Role of CXCR5 and CCR7 in follicular th cell positioning and appearance of a programmed cell death gene-1High germinal center-associated subpopulation1. *J Immunol*. (2007) 179:5099–108. doi: 10.4049/jimmunol.179.8.5099

32. Corrado A, Ramonell RP, Woodruff MC, Tipton C, Wise S, Levy J, et al. Extrafollicular IgD+ B cells generate IgE antibody secreting cells in the nasal mucosa. *Mucosal Immunol*. (2021) 14:1144–59. doi: 10.1038/s41385-021-00410-w

33. Faliti CE, Mesina M, Choi J, Bélanger S, Marshall MA, Tipton CM, et al. Interleukin-2-secreting T helper cells promote extra-follicular B cell maturation via intrinsic regulation of a B cell mTOR-AKT-Blimp-1 axis. *Immunity*. (2024) 0:1317–9. doi: 10.1016/j.immuni.2024.11.006

34. Foster WS, Lee JL, Thakur N, Newman J, Spencer AJ, Davies S, et al. Tfh cells and the germinal center are required for memory B cell formation & humoral immunity after ChAdOx1 nCoV-19 vaccination. *Cell Rep Med*. (2022) 3:100845. doi: 10.1016/j.xcrm.2022.100845

35. Punnonen J, de Vries JE. IL-13 induces proliferation, Ig isotype switching, and Ig synthesis by immature human fetal B cells. *J Immunol (Baltimore Md: 1950)*. (1994) 152:1094–102. doi: 10.4049/jimmunol.152.3.1094

36. Aversa G, Punnonen J, Cocks BG, de Waal Malefyt R, Vega F, Zurawski SM, et al. An interleukin 4 (IL-4) mutant protein inhibits both IL-4 or IL-13-induced human immunoglobulin G4 (IgG4) and IgE synthesis and B cell proliferation: Support for a common component shared by IL-4 and IL-13 receptors. *J Exp Med*. (1993) 178:2213–8. doi: 10.1084/jem.178.6.2213. C.OMMAJ.R.X.X.X.

37. McKenzie AN, Culpepper JA, de Waal Malefyt R, Brière F, Punnonen J, Aversa G, et al. Interleukin 13, a T-cell-derived cytokine that regulates human monocyte and B-cell function. *Proc Natl Acad Sci*. (1993) 90:3735–9. doi: 10.1073/pnas.90.8.3735

38. Bouziat R, Biering SB, Kouame E, Sangani KA, Kang S, Ernest JD, et al. Murine norovirus infection induces TH1 inflammatory responses to dietary antigens. *Cell Host Microbe*. (2018) 24:677–688.e5. doi: 10.1016/j.chom.2018.10.004

39. Ettinger R, Sims GP, Fairhurst A-M, Robbins R, Da Silva YS, Spolski R, et al. IL-21 induces differentiation of human naive and memory B cells into antibody-secreting plasma cells. *J Immunol*. (2005) 175:7867–79. doi: 10.4049/jimmunol.175.12.7867

40. Wang S, Wang J, Kumar V, Karnell JL, Naiman B, Gross PS, et al. IL-21 drives expansion and plasma cell differentiation of autoreactive CD11chiT-bet+ B cells in SLE. *Nat Commun*. (2018) 9:1758. doi: 10.1038/s41467-018-03750-7

41. Hewitson JP, Filbey KJ, Grainger JR, Dowle AA, Pearson M, Murray J, et al. *Heligmosomoides polygyrus* Elicits a Dominant Nonprotective Antibody Response Directed against Restricted Glycan and Peptide Epitopes. *J Immunol*. (2011) 187:4764–77. doi: 10.4049/jimmunol.1004140

42. Hewitson JP, Ivens AC, Harcus Y, Filbey KJ, McSorley HJ, Murray J, et al. Secretion of protective antigens by tissue-stage nematode larvae revealed by proteomic analysis and vaccination-induced sterile immunity. *PloS Pathog*. (2013) 9:e1003492. doi: 10.1371/journal.ppat.1003492

43. Giannelli V. Microbiota and the gut-liver axis: Bacterial translocation, inflammation and infection in cirrhosis. *World J Gastroenterol*. (2014) 20:16795. doi: 10.3748/wjg.v20.i45.16795

44. Kouroumalis E, Tsomidis I, Voumvouraki A. Viral liver disease and intestinal gut–liver axis. *Gastrointestinal Disord*. (2024) 6:64–93. doi: 10.3390/gidisord6010005

45. Mohrs K, Harris DP, Lund FE, Mohrs M. Systemic Dissemination and Persistence of Th2 and Type 2 Cells in Response to Infection with a Strictly Enteric Nematode Parasite. *J Immunol*. (2005) 175:5306–13.

46. Mitre E, Klion AD. Eosinophils and helminth infection: protective or pathogenic? *Semin Immunopathol*. (2021) 43:363–81.

47. Min B, Prout M, Hu-Li J, Zhu J, Jankovic D, Morgan ES, et al. Basophils Produce IL-4 and Accumulate in Tissues after Infection with a Th2-inducing Parasite. *J Exp Med*. (2004) 200:507–17. doi: 10.1084/jem.20040590

48. Kapse B, Zhang H, Affinass N, Ebner F, Hartmann S, Rausch S. Age-dependent rise in IFN-γ competence undermines effective type 2 responses to nematode infection. *Mucosal Immunol.* (2022) 15:1270–82. doi: 10.1038/s41385-022-00519-6

49. Classon CH, Li M, Clavero AL, Ma J, Feng X, Tibbitt CA, et al. Intestinal helminth infection transforms the CD4+ T cell composition of the skin. *Mucosal Immunol.* (2022) 15:257–67. doi: 10.1038/s41385-021-00473-9

50. Affinass N, Zhang H, Löhning M, Hartmann S, Rausch S. Manipulation of the balance between Th2 and Th2/1 hybrid cells affects parasite nematode fitness in mice. *Eur J Immunol.* (2018) 48:Article 12. doi: 10.1002/eji.201847639

51. Strandmark J, Rausch S, Hartmann S. Eosinophils are required to suppress Th2 responses in Peyer's patches during intestinal infection by nematodes. *Mucosal Immunol.* (2017) 10:661–72. doi: 10.1615/CritRevImmunol.2016018726

52. Ekkens MJ, Liu Z, Liu Q, Whitmire J, Xiao S, Foster A, et al. The Role of OX40 Ligand Interactions in the Development of the Th2 Response to the Gastrointestinal Nematode Parasite Heligmosomoides polygyrus. *J Immunol.* (2003) 170:384–93. doi: 10.4049/jimmunol.170.1.384

53. King IL, Mohrs K, Mohrs M. A Nonredundant Role for IL-21 Receptor Signaling in Plasma Cell Differentiation and Protective Type 2 Immunity against Gastrointestinal Helminth Infection. *J Immunol.* (2010) 185:6138–45.

54. Han Y, Yao R, Yang Z, Li S, Meng W, Zhang Y, et al. Interleukin-4 activates the PI3K/AKT signaling to promote apoptosis and inhibit the proliferation of granulosa cells. *Exp Cell Res.* (2022) 412:113002. doi: 10.1016/j.yexcr.2021.113002

55. Haase P, Schäfer S, Gerlach RG, Winkler TH, Voehringer D. B cell fate mapping reveals their contribution to the memory immune response against helminths. *Front Immunol.* (2022) 13:1016142. doi: 10.3389/fimmu.2022.1016142

56. Domeier PP, Chodisetti SB, Soni C, Schell SL, Elias MJ, Wong EB, et al. IFN-γ receptor and STAT1 signaling in B cells are central to spontaneous germinal center formation and autoimmunity. *J Exp Med.* (2016) 213:715–32. doi: 10.1084/jem.20151722

57. Dienz O, Eaton SM, Bond JP, Neveu W, Moquin D, Noubade R, et al. The induction of antibody production by IL-6 is indirectly mediated by IL-21 produced by CD4+ T cells. *J Exp Med.* (2009) 206:69–78. doi: 10.1084/jem.20081571

58. Suto A, Kashiwakuma D, Kagami S, Hirose K, Watanabe N, Yokote K, et al. Development and characterization of IL-21–producing CD4+ T cells. *J Exp Med.* (2008) 205:1369–79. doi: 10.1084/jem.20072057

59. Kim Y-M, Pan JY-J, Korbel GA, Peperzak V, Boes M, Ploegh HL. Monovalent ligation of the B cell receptor induces receptor activation but fails to promote antigen presentation. *Proc Natl Acad Sci.* (2006) 103:3327–32. doi: 10.1073/pnas.0511315103

60. Mehta DS, Wurster AL, Weinmann AS, Grusby MJ. NFATc2 and T-bet contribute to T-helper-cell-subset-specific regulation of IL-21 expression. *Proc Natl Acad Sci.* (2005) 102:2016–21. doi: 10.1073/pnas.0409512102

61. Luo W, Weisel F, Shlomchik MJ. B cell receptor and CD40 signaling are rewired for synergistic induction of the c-myc transcription factor in germinal center B cells. *Immunity.* (2018) 48:313–326.e5. doi: 10.1016/j.immuni.2018.01.008

62. Zeng R, Spolski R, Casas E, Zhu W, Levy DE, Leonard WJ. The molecular basis of IL-21–mediated proliferation. *Blood.* (2007) 109:4135–42. doi: 10.1182/blood-2006-10-054973

63. Dvorscek AR, McKenzie CI, Robinson MJ, Ding Z, Pitt C, O'Donnell K, et al. IL-21 has a critical role in establishing germinal centers by amplifying early B cell proliferation. *EMBO Rep.* (2022) 23:e54677. doi: 10.15252/embr.202254677

64. Paus D, Phan TG, Chan TD, Gardam S, Basten A, Brink R. Antigen recognition strength regulates the choice between extrafollicular plasma cell and germinal center B cell differentiation. *J Exp Med.* (2006) 203:1081–91. doi: 10.1084/jem.20060087

65. Yang P-C, Mahmood T. Western blot: Technique, theory, and trouble shooting. *North Am J Med Sci.* (2012) 4:429. doi: 10.4103/1947-2714.100998

frontiers | Frontiers in Immunology

TYPE Original Research
PUBLISHED 01 May 2025
DOI 10.3389/fimmu.2025.1527129

OPEN ACCESS

EDITED BY
Joydeep Paul,
Adamas University, India

REVIEWED BY
Jayaraman Tharmalingam,
University of Wisconsin-Madison,
United States
Neetu Singh,
University of Texas MD Anderson Cancer
Center, United States

*CORRESPONDENCE
Paul H. Davis
pdavis@unomaha.edu

†PRESENT ADDRESS
Evie G. Ehrhorn,
Department of Cancer Research, University of
Nebraska Medical Center, Omaha, NE,
United States

‡These authors have contributed equally to
this work

RECEIVED 12 November 2024
ACCEPTED 18 March 2025
PUBLISHED 01 May 2025

CITATION
Schulze TT, Neville AJ, Ehrhorn EG,
Alsuleiman SA, Vennerstrom JL and Davis PH
(2025) Spleen and peripheral blood
immunopathology in an outbred model of
adult-stage murine schistosomiasis.
Front. Immunol. 16:1527129.
doi: 10.3389/fimmu.2025.1527129

Spleen and peripheral blood immunopathology in an outbred model of adult-stage murine schistosomiasis

Thomas T. Schulze[1,2‡], Andrew J. Neville[1‡], Evie G. Ehrhorn[1†], Sarah A. Alsuleiman[1], Jonathan L. Vennerstrom[3] and Paul H. Davis[1*]

[1]Department of Biology, University of Nebraska at Omaha, Omaha, NE, United States, [2]Department of Pathology, Microbiology, and Immunology, University of Nebraska Medical Center, Omaha, NE, United States, [3]Department of Pharmaceutical Sciences, University of Nebraska Medical Center, Omaha, NE, United States

Schistosomiasis, a parasitic disease caused by flatworms of genus *Schistosoma*, is a neglected tropical disease that causes significant morbidity in the developing world. Despite numerous efforts to eradicate the disease, the parasite remains a significant global burden, particularly within Sub-Saharan Africa. *Schistosoma* species possess an arsenal of potent mechanisms to defend against direct attack from host immune cells and a remarkable ability to modulate the host immune system through proximal and systemic modes that facilitate its stage-specific development, survival, and reproduction. Standardized animal models have been developed that serve as an important resource for dissecting parasite and host immunobiology and for drug and vaccine efficacy studies. However, a comprehensive understanding of the immune responses to *Schistosoma mansoni* in the standard outbred Swiss Webster mouse model is still lacking, particularly with the granulocyte composition of the spleen and the associated blood cytokine responses that occur during chronic infections. To continue characterization of this important secondary lymphoid tissue and the peripheral blood, we examined infected mouse spleens and additionally performed a detailed flow cytometric analysis of the splenic compartment from infected mice with specific attention to granulocytes and Th2-associated leukocytes. Peripheral blood from infected animals was used to evaluate a panel of Th1- and Th2-associated cytokines for comparison. Lastly, an analytical blood count and differential was also reported to provide a case study of late-stage chronic schistosomiasis. In mice infected with *S. mansoni*, we identified granulocytosis within the spleen including increased eosinophils, neutrophils, basophils, and mast cells. Additionally, ILC2s and dendritic cells were increased. The cytokine data suggests an IL33-independent mixed Th1/Th2 response with upregulation of granulocyte proliferative and recruitment factors. The late-stage chronic schistosomiasis case study identified blood neutrophilia and eosinophilia but with absent basophils. These data enhance our understanding of the complex immune response that occurs with schistosomiasis and may offer new insights to support therapeutic strategies against this important disease.

KEYWORDS

schistosomiasis, helminth, trematode, *Schistosoma mansoni*, cytokine profile, hematology, granulocytosis

Introduction

Schistosomiasis is a significant human disease caused by helminths of the genus *Schistosoma*. The disease is highly debilitating and typically associated with impoverished regions (1). To date, six *Schistosoma* species capable of infecting humans have been identified with most cases caused by *S. mansoni*, *S. haematobium*, and *S. japonicum* (1–3). Currently, schistosomiasis is thought to infect at least 200 million people with sub-Saharan Africa carrying the highest incidence (4, 5). Schistosomiasis is rarely fatal; however, the infected may suffer from chronic disease-associated morbidities (6). Recent efforts to estimate the global burden of disease highlight the challenges associated with estimating the true impacts of chronic diseases such as schistosomiasis (7). Likely contributors that hinder the control of human schistosomiasis include poor infrastructure development, less than ideal treatment options, and a lack of a vaccine (3, 8). Moreover, reliance on a limited range of and extended treatment timeframes of chemotherapies (i.e. praziquantel) has led to suspected drug resistance in some species (9). Consequently, there is a renewed interest in single-dose therapies, particularly those that clear the juvenile and adult stages of infection, such as those reported in Gardner et al. (10), and the recently optimized aryl hydantoin compound series (11).

Helminth parasites have developed an impressive persistence strategy that includes both immune evasion and remodeling, enabling them to parasitize the host for years and to facilitate egg release (12). Accordingly, the immunobiology of schistosomiasis is complex and includes a temporal lifecycle-associated immune profile that shifts during the transition from initial infection to mature egg-producing worm pairs (13). Additionally, the immune environment is multifactorial where the worms, eggs, and host immune response are all known to participate in unique and competing immune-modulating behaviors. An incomplete understanding of schistosomiasis immunology and pathogenesis has been a barrier to breakthroughs that are urgently needed to design more effective treatments and to identify new opportunities to exploit the parasite's immune modulation strategies. During the initial acute infection (typically 4-5 weeks post-infection with cercariae), the developing juvenile worms trigger a mixed immune response composed of Th1- and Th2-associated factors (13). At approximately 5-6 weeks of development, egg production begins, and the host immune response is pushed further toward a Th2-dominant environment (13, 14). The Th2 environment is characterized by elevated IL-4, IL-5, and IL-13, and is accompanied by elevated granulocytes such as eosinophils (15, 16). Notably, many granulocyte effector molecules (e.g. eosinophil peroxidase, neutrophil elastase) have shown potent effects on adult worms and schistosomula *in vitro* (17–19), yet worms successfully persist inside hosts for years despite continual infection-associated granulocytosis (16). As the disease progresses to the chronic stage, the Th2 environment can diminish as IL-10 is secreted by regulatory lymphocytes which are thought to control disease severity (15). Notably, the tug-and-pull between Th1 and Th2 during infection must be balanced as hyperpolarization (in either direction) was demonstrated to be lethal in animal models (15). Indeed, understanding the immunology and pathogenesis of schistosomiasis may be key as many treatments, including praziquantel, show an immune requirement, where host immune components appear to be necessary for effective worm burden reduction (20–23).

Murine schistosomiasis has become the preferred animal model for human schistosomiasis and has been used for various studies, particularly for immunology and therapeutic development (24, 25). However, maintenance of the intermediate parasite life stages and optimization of animal infection methods remain challenging and require training and specialty facilities (26). To address these challenges, the NIH-supported Schistosomiasis Resource Center maintains the parasite life cycle for multiple *Schistosoma* species (e.g. *mansoni*, *japonicum*, and *haematobium*) and provides standardized infected rodent models for end-users to utilize for studies. While these animal models have been used to dissect many aspects of immunobiology, we still lack a full understanding of innate immune and tissue-specific granulocyte populations, particularly within secondary lymphoid tissues (e.g. spleen) which contribute to the collective immune response and may participate in antigen presentation (27). The objective of this study was to utilize this rodent model to characterize how the splenic compartment and peripheral blood cytokine environment change in response to chronic *S. mansoni* infection with a focus on Th2 effector granulocytes and the associated innate lymphoid cells (i.e. ILC2) which are thought to participate in the immune response.

Here we investigated the outbred Swiss Webster (CFW) *S. mansoni* mouse model, performing a detailed evaluation of the infected spleen, including flow cytometric analysis of granulocyte composition among splenocytes. We observed elevated granulocyte populations and increased Th2-associated innate cells, including eosinophils, neutrophils, basophils, mast cells, and type 2 innate lymphoid cells (ILC2s). Cytokine analysis of infected animal peripheral blood suggests an IL33-independent mixed Th1/Th2 cytokine response with hallmarks of inflammation and immune regulation, in agreement with previous observations (28–30). Lastly, in a single mouse case study that survived and presented a very late-stage chronic schistosomiasis infection (19 weeks post-infection), blood hematology parameters, and a complete leukocyte differential indicated neutrophilia and eosinophilia, but absent of basophils.

Materials and methods

Establishing adult-stage and chronic schistosomiasis in mice

S. mansoni infected Swiss Webster CFW female mice were obtained from the Schistosomiasis Resource Center (Rockville, MD). Mice were purchased from either Taconic or Charles River Laboratories. Infections were performed percutaneously by tail exposures to freshly hatched cercariae (approximately 200 per mouse: average 190, range 182-192 cercariae) when mice were 5-6 weeks old. All infections were performed with *S. mansoni* strain NMRI (BEI Resources, NR-21963).

Isolation of spleen for phenotypic analysis

Three uninfected and infected mice were asphyxiated with CO_2 prior to tissue collection. Spleens were harvested immediately and maintained in 1X HBSS without calcium, magnesium, and phenol red (Corning, cat# 21022CV) at 4°C until images were taken and masses measured using an analytical balance. Spleen samples were stored <4 h before inspection. Statistical analysis (unpaired t-test) and graphing were performed with GraphPad PRISM ver. 10.2.3. The bar graphs presents the mean and standard error of the means (SEM) (error bars) for each group (n=3 mice per group). The infected animals used in these studies were 13 weeks old and 7 weeks post-infection (PI), and uninfected mice were age-matched.

Flow cytometric analysis of splenocytes during adult-stage schistosomiasis

The infected mice used in these studies were 13 weeks old and 7 weeks post-infection. Uninfected mice were age-matched to infected mice. The method and precise protocol used for preparation of splenocytes was previously optimized and published by our lab (31). Briefly, three outbred Swiss Webster female mouse spleens were pooled for both the uninfected and infected samples that were used for the flow cytometry studies. Splenocytes from either infected or uninfected mice were used for each group's FMOs and unstained controls to account for potential differences in cell autofluorescence and other possible variations between the infected and uninfected splenocyte samples. Bead compensation controls (MACS® Comp Bead Kit, anti-REA, Miltenyi Biotec, cat.# 130-104-693) were run in parallel for each flow cytometry acquisition run sample to account for instrument drift and to construct the spectral matrices. An LSRFortessa™ X-50 (BD Biosciences) flow cytometer instrument was used for data acquisition and the analyses and plots were executed with FlowJo™ v10.10.0 Software (BD Life Sciences). Annotated figures were prepared with Adobe Illustrator ver. 28.7.0 (Beta). Each marker evaluated had its own associated fluorescent minus one (FMO) control which was used for strict gating of positive/negative populations. The gating strategy is illustrated in the respective figures.

Peripheral blood cytokine analysis

Uninfected and infected Swiss Webster CFW females (n=8 per group) were age-matched within 1 week (approximately 7 weeks post-infection, approximately 200 cercariae percutaneously) at the time of sample collection. 24 hours before cardiac blood collection, mice received a common drug solvent (90/3/7% of water, ethanol, and Tween®80, respectively). The solvent was filter-sterilized using a 0.22 µm PES membrane (MilliporeSigma™, cat# SCGP00525), and orally (PO) administered volume of 4.0 µL/gram of mouse weight via an 18G oral gavage (SAI Infusion Technologies, cat# FN18-38M). This solvent was used as a vehicle comparator, commonly used as a drug vehicle solvent in drug discovery efforts using the *S. mansoni* outbred mouse model. 24 hours post-administration of solvent, mice were euthanized by CO_2 asphyxiation and peripheral blood was isolated via cardiac puncture using a 1 mL syringe (Easy Glide Sterile Syringe Luer Lock; EGLL1ML-100) with attached 23-gauge needles (BD, catalog # 305143). Blood was immediately transferred to MiniCollect® TUBE 0.8 ml CAT Serum Separator (Greiner, catalog # 450472) tubes and allowed to clot at room temperature for 30 minutes. Samples were spun at 2,000 x g for 10 minutes at room temperature and the supernatant containing serum was aliquoted in 1.5 mL low-retention microcentrifuge tubes (Thermo Scientific, cat# 3451) and stored at -20 °C until analysis. Serum samples were diluted 1:4 in Diluent 41 reagent (Meso Scale Diagnostic Services, cat# R50AH-1) and assayed using a 10 analyte Meso Scale U-PLEX Custom Biomarker Group 1 (mouse) Multiplex Assay Kit (Meso Scale Diagnostics, cat# K15069L-1) following the manufacturer's instructions. A Meso Scale QuickPlex SQ 120 model 1300 instrument was used to measure electrochemiluminescene (ECL) signals and the raw data was initially prepared with the Meso Scale WorkBench 4 Software version 4.0.13 (Meso Scale Diagnostics). Data was transformed in Microsoft Excel version 2.411 (Microsoft, USA) and was analyzed and graphed with GraphPad Prism ver. 10.2.3 and statistical significance was determined by a two-tailed unpaired t-test. Cytokine concentrations (pg/mL) are presented as the mean ± standard error of the mean (SEM).

Analytical complete blood count and differential

Reference uninfected Swiss Webster CFW female mice (n=7) were solvent-treated as above and euthanized with CO_2 asphyxiation prior to immediate blood collection. Peripheral blood was obtained through cardiac punctures with 23-gauge needles (BD, catalog # 305143) attached to S-Monovette® K_3EDTA tubes (Sarstedt, catalog # 06.1664.100) and immediately inverted 8-10 times and stored at 4 °C. Samples were shipped to IDEXX facilities after preparation (same day) for processing the following morning. IDEXX test code 63160: Comprehensive CBC with MPV, RDW and Retic Hgb was performed. The infected mouse (n=1) was approx. 6 months old at time of sampling, and 19 weeks post-infection.

Results

Spleens from mice with schistosomiasis show splenomegaly and malformations

Spleens obtained from infected animals were first examined macroscopically for phenotypic differences compared to normal, uninfected reference spleens. The spleens from infected animals showed increases in both length and mass and obvious discolorations consistent with splenomegaly (Figure 1). The increased

spleen masses were statistically significant (n=3; p=0.009) whereas increases in length were near significance (n=3; p=0.060). Notably, discoloration and a spotted phenotype was observed in the infected spleens (Figure 1C) with one organ showing severe discoloration resembling a large granuloma or tissue fibrosis (32). In comparison to organs obtained from mice infected with *S. japonicum*, the spleen malformations appear less heterogenous or more evenly distributed (32).

Flow cytometric characterization of splenocytes from adult-stage schistosomiasis

To dissect the cellular composition of the infected spleens vs. uninfected controls, an optimized flow cytometry panel was utilized with modifications (31) to examine the granulocyte compartment of total mouse splenocytes. Splenocyte samples were prepared by pooling whole spleen from multiple donors (n=3 spleens per condition) prior to generating splenocyte suspensions, to obtain a representative sample. Notably, the protocol used for preparation of cell suspensions was previously optimized in our lab to maximize granulocyte recovery and reduce cellular activation during preparation (31). Granulocytes are known to be sensitive, short-lived and easily activated during preparation based on the isolation methods used (e.g. density gradients (33); moreover, the composition of processing buffers (e.g. BSA or fetal serum) can significantly affect cell recovery (31, 34, 35).

For relative quantification of the cell subsets, the results are calculated with FlowJo™ software and reported using both percent of intact single-cells and as a percent of $CD45^+$ cells (Table 1), where CD45 serves as a general marker of leukocytes. The gating strategies and resulting cell populations are shown in for the uninfected reference (Figure 2) and infected (Figure 3) samples. A large increase in the $CD45^-$ subset, relative to the overall sample/cell population, was seen in the infected (14.31%) versus uninfected (2.23%) which is shown in Figures 2, 3 (panel SSC-A vs. CD45). This may be due in part to altered hematopoiesis that is associated with murine schistosomiasis and can cause increased events that are $CD45^-$ and are likely $Ter119^+$ (e.g. erythrocytes from altered splenic erythropoiesis) (36, 37). Essentially, this might indicate expansion of the erythroid lineage in the spleen that reduces the proportion of cells that are $CD45^+$.

Further analysis of the infected mouse splenocytes shows expanded populations of granulocytes including neutrophils, basophils, eosinophils, and mast cells (Table 1; Figure 4). Spleen-derived eosinophils showed the largest increase (20.9x) in this dataset followed by putative ILC2s (14.6x increase). Neutrophils, basophils and eosinophils all showed a marked increase ranging between 4-5x (% of $CD45^+$). Additionally, the granulocyte populations isolated in the infected mice (Figure 3) showed increased SSC-A profiles, indicating increased granularity and likely signifying an activated or stimulated phenotype that is differentiated from uninfected mice (Figure 2) (38, 39). Dendritic cells have previously been shown to play a role in the induction of the Th2 response in response to eggs (40). Pan-dendritic cells (Lin^- $CD45^+CD11c^+$) showed an approximate 1.36x increase in their abundance and showed variable CD11b expression that was present in both the uninfected reference (Figure 2) and infected samples (Figure 3). Notably, the gating strategies utilized here can be tissue specific. For example, spleen derived eosinophils are Lin^- $CD45^+CD11b^+CD11c^-Ly6G^-SiglecF^+$; however, this can differ by tissue and mouse strain (41). Bone marrow and lung derived eosinophils have been shown to contain a $CD11c^{low}$ population which might render this gating strategy ineffective in those tissues (42).

Innate lymphoid cells (ILCs) lack surface markers commonly found on T and B cells and are known to be tissue-resident and immune regulatory (43). ILCs are now understood to sustain immune responses, react early compared to adaptive immune counterparts, and contain subgroups such as ILC1, 2, and 3 corresponding to Th1, Th2, and Th17 associated cells (43). The

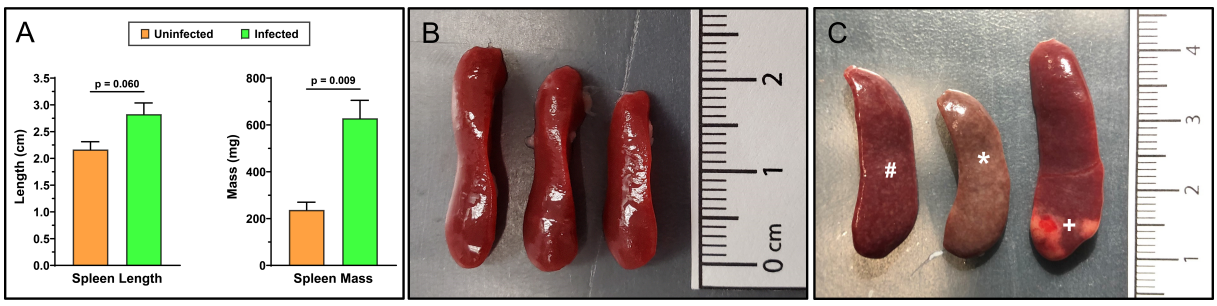

FIGURE 1
Spleens of adult-stage *S. mansoni* infected mice have pronounced splenomegaly, discoloration, and malformations. Mean spleen masses and lengths **(A)** were obtained from female Swiss Webster mice that were either uninfected **(B)** or 7 weeks post-infected percutaneously with ~200 *Schistosoma mansoni* cercariae **(C)**. Spleens were visually inspected and measured for masses and lengths to detect splenomegaly (n=3 mice/group). Mean infected masses and lengths show clear and significant splenomegaly that is associated with chronic schistosomiasis. Annotated discolorations (*), varied malformations, and some larger regions resembling granulomas or fibrotic tissue (+) are noticeable in the infected spleens **(C)**. Additionally, a consistent spotted phenotype (#) was observed across all infected spleens but absent from uninfected spleens. Infected and uninfected mice were age-matched. Data was analyzed and graphed with GraphPad Prism ver. 10.2.3 and statistical significance was determined with a two-tailed unpaired t-test. Data is presented as the group mean ± standard error of the mean (SEM).

10.3389/fimmu.2025.1527129

TABLE 1 Flow cytometry analysis of splenocytes in uninfected reference vs. adult-stage schistosomiasis mice.

Cell Population	Gating Strategy	Reference Uninfected (% of CD45+)	Infected (% of CD45+), Change vs. Reference	Reference Uninfected (% of Single Cells)	Infected (% of Single Cells), Change vs. Reference
Neutrophil	$CD11c^-CD11b^+Ly6G^+$	1.34	5.63, 4.20x	1.16	4.12, 3.55x
Pan-Dendritic/ Macrophage	$CD11c^+$	0.33	0.45, 1.36x	0.29	0.33, 1.14x
Basophil	$CD11c^-$ $Ly6G^-FcεR1α^+CD117^-$	0.11	0.48, 4.36x	0.091	0.35, 2.95x
Eosinophil	$CD11c^-$ $CD11b^+Ly6G^-SiglecF^+$	0.18	3.77, 20.9x	0.16	2.76, 17.3x
Mast	$CD11c^-CD11b^-$ $Ly6G^-$ $FcεR1α^+CD117^+$	4.38E-3	0.025, 5.71x	3.78E-3	0.019, 5.03x
ILC2, putative	$CD11c^-CD11b^-Ly6G^-$ $SiglecF^-CD117^+$	0.27	3.95, 14.6x	0.23	2.89, 12.6x

The splenocyte samples visualized in the representative flow cytometry panels are from a single experiment (n=1) and were generated from pooled spleen samples (n=3 animals for uninfected and infected) to generate a representative sample for the outbred background (female Swiss Webster CFW) and infected condition. The preparation procedure was adapted from (31). Splenocytes were analyzed via multicolor (9-color) flow cytometry to measure changes to relevant granulocytes and innate lymphocytes to profile the splenic composition during murine chronic schistosomiasis *mansoni*. Cell populations shown here are reported as either a percentage of single intact cells or a percentage of $CD45^+$ for comparison and were calculated in FlowJo software version 10.10.0. All populations included here are Lin^-CD45^+; $Lin=Ter119^+CD3^+CD19^+CD335^+$. The ILC2 population is putative and may contain additional subtypes. The pan-dendritic/ macrophage gate may also contain monocytes, which can express both CD11c and CD11b at varying levels.

ILC2 subset has been previously identified in mouse bone marrow, lung, fat, gut, and skin tissues with an apparent tissue-specific transcriptome (44). ILC2s are thought to be tissue-resident and long-lived but may move between tissues (45) and are typically associated with the production of IL-5, IL-9, and IL-13 (46). As ILC2s are thought to be principally associated with Th2 immune responses that are induced during schistosomiasis (45, 47), they were assessed in the infected spleen. Notably, as the ILC cell surface markers often vary by tissue of residence, and have yet to be fully characterized, these should be considered putative ILC2s which may contain other subtypes and may have migrated from other tissues. We identified a minor population in the spleen (<1% in the reference; identified as $Lin^-CD45^+CD11b^-CD11c^-Ly6G^-SiglecF^-$ $FcERIα^-CD117^+$) that expanded 14.6x (% of $CD45^+$) during chronic schistosomiasis (Table 1; Figure 4).

Cytokine profiling during adult-stage schistosomiasis indicates a mixed Th1/Th2 phenotype

It is now understood that cytokine profiles differ by stage of infection (i.e. weeks post-infection), the species/strain of *Schistosoma*, magnitude of infection, and the background strain of mice (48). During initial infections, *Schistosoma* species trigger a Th1 immune response that transitions over time to a Th2 environment (49). These environments typically include elevated IL-4, IL-5 and IL-13 (50, 51). To continue the cytokine characterization for this standardized model of *S. mansoni*, we generated a blood cytokine profile to compare to the splenocyte datasets. A custom U-plex MesoScale plate was designed with a panel of Th1 and Th2 cytokines/ chemokines, including those with known responses, and a subset of less characterized cytokines that are granulocyte-associated (e.g. Eotaxin-1, GM-CSF, KC/GRO). CFW female mice (n=8) were utilized for each group to compare uninfected vs. adult-stage schistosomiasis (approximately 7 weeks post-infection). The means and standard error of the means (SEM) for each analyte are displayed in Figure 5. Notably, and with the exception of IL-33, all cytokines/ chemokines measured were significantly increased ($p<0.05$) indicating a mixed proinflammatory phenotype including both Th1 and Th2-associated cytokines. IL-33 is considered an alarmin associated with cell damage that can function as a driver of Th2 responses by stimulating the release of IL-5 and IL-13 (52). However, it has been shown in *S. mansoni*-infected animals that IL-33 and its associated ST2 pathway are not essential for the Th2 polarization that occurs during disease, which is supported by this dataset (28).

Late-stage chronic schistosomiasis hematology and comprehensive differential case study

A single mouse (Swiss Webster CFW female) with late-stage chronic schistosomiasis (19 weeks post-infection) was included in an expanded complete blood count and differential to examine how the blood compartment is altered, and to compare to the changes measured within the spleen (approximately 7 weeks post-infection). The blood data results are available in Table 2 and the leukocyte differential is included in Table 3. Consistent with the splenic data, granulocytes in the blood compartment were increased including neutrophils and eosinophils, with eosinophils showing the largest increases (31x vs. reference, Table 3). Interestingly, while basophils

10.3389/fimmu.2025.1527129

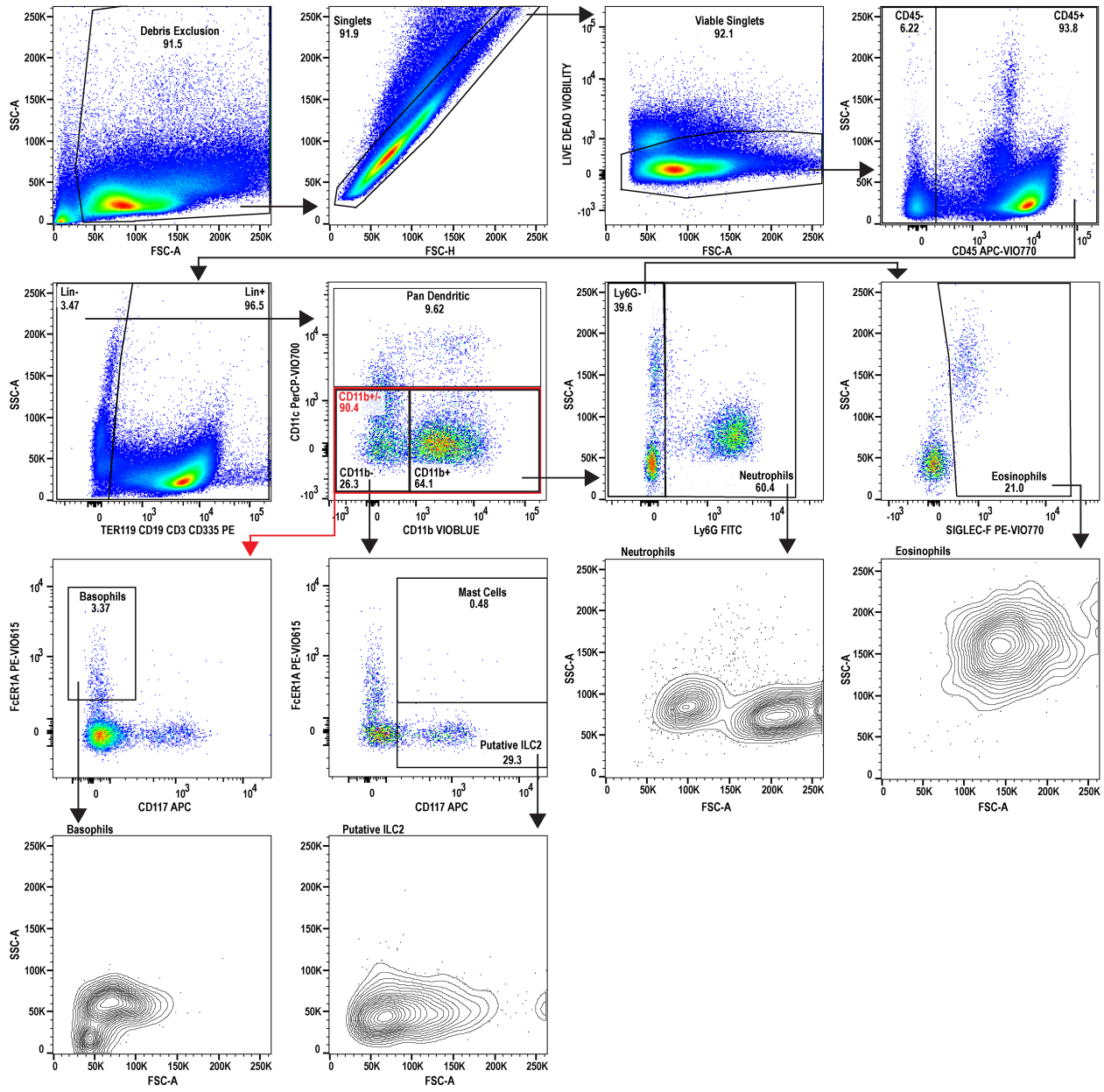

FIGURE 2
Flow cytometric analysis of uninfected reference splenocytes. A 9-color flow cytometry panel was utilized to profile the splenic immune cells and to specifically inspect the granulocyte lineage. A dump gate is included to filter out abundant lymphocytes ($CD3^+$, $CD19^+$, $CD335^+$) and $Ter119^+$ cells which are denoted as Lin^+. Gating was performed to isolate eosinophils, neutrophils, basophils, and mast cells. Additionally, type 2 innate lymphocytes (ILC2) and dendritic cells were also inspected. FSC-A and SSC-A plots are also provided for the granulocytes for phenotyping activation state and to examine heterogeneity. This uninfected sample serves as the reference for comparing to the infected sample (see Figure 3). The splenocytes used for analysis were prepared by pooling spleens from three individual donor mice (n=3, Swiss Webster CFW females). Data analysis was performed with FlowJo™ v10.10.0 Software (BD Life Sciences).

showed increased splenic residence (Table 1), they were undetectable in the peripheral blood of the infected animal, yet the reference animals showed a small population in circulation (11/μL on average, Table 3). The blood analysis (Table 2) similarly showed elevated absolute counts of WBCs in the chronically infected mouse (25.3 K/μL) versus uninfected mice (7.2 K/μL) and slight changes to parameters such as HGB, HCT were detected, in addition to others.

Discussion

Schistosomiasis remains a significant challenge in the developing world and a better understanding of the complex immune pathology may lead to the design of more effective therapeutics and vaccines. Despite documented susceptibilities to host granulocytes, which increase during infections and display activated or primed cellular phenotypes, *Schistosoma* species persist

10.3389/fimmu.2025.1527129

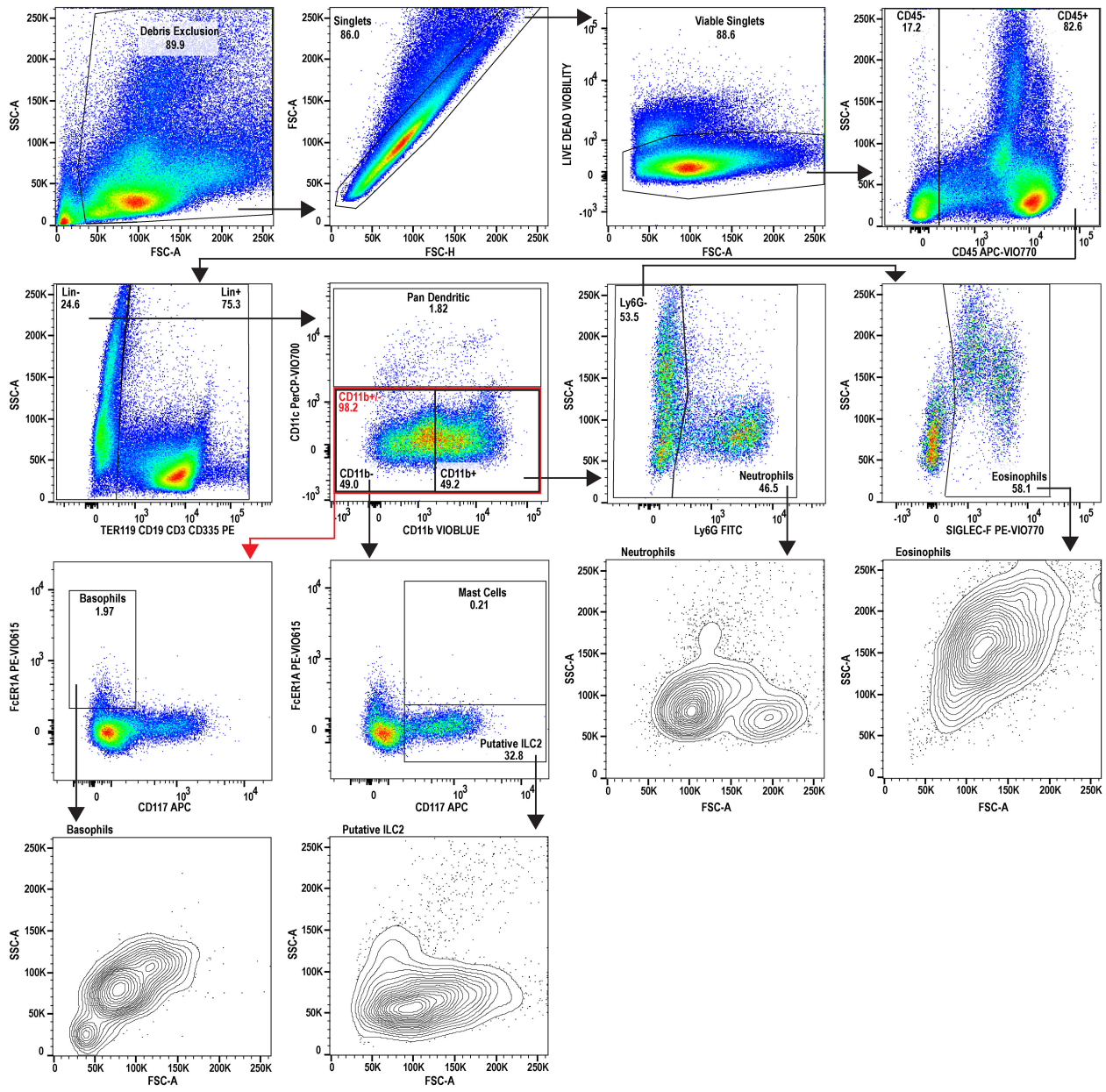

FIGURE 3
Flow cytometric analysis of splenocytes during adult-stage schistosomiasis. A 9-color flow cytometry panel was utilized to profile the splenic immune cells from infected animals, to specifically inspect the granulocyte lineage, and gated identically to Figure 2. FSC-A and SSC-A plots for the granulocytes examined suggest a stimulated or activated cellular phenotype supported by increases to SSC-A and increased heterogeneity in neutrophils. The putative splenic ILC2 population additionally appears to be expanded during schistosomiasis. The splenocytes used for analysis were prepared by pooling spleens from three individual donor mice infected with *Schistosoma mansoni* (n=3, Swiss Webster CFW females, 7 weeks post-infection with approx. 200 cercariae percutaneous). Data analysis was performed with FlowJo™ v10.10.0 Software (BD Life Sciences).

inside hosts for years in humans (53). In this work we provide a brief phenotypic analysis of infected mice spleens, a detailed inspection of the granulocyte and innate lymphocyte content of the mouse splenic compartment and assess a panel of Th1- and Th2-associated cytokines in the peripheral blood during adult-stage schistosomiasis, which can vary widely by tissues and infection stage (13). Lastly, we present a case study that includes an analytical blood count and leukocyte differential comparing uninfected mice to a late-stage chronically infected mouse. In the context of schistosomiasis, host tissues such as the liver are relatively well studied where secondary lymphoid tissues, such as the spleen, have been neglected. Immunophenotyping and characterization studies such as these are useful for building a comprehensive understanding of the infected host immune environments and response to disease that can vary by *Schistosoma* species and the host/strain utilized (48).

The gross pathology observed in the spleen (Figure 1) are consistent with those that has been published in the literature to

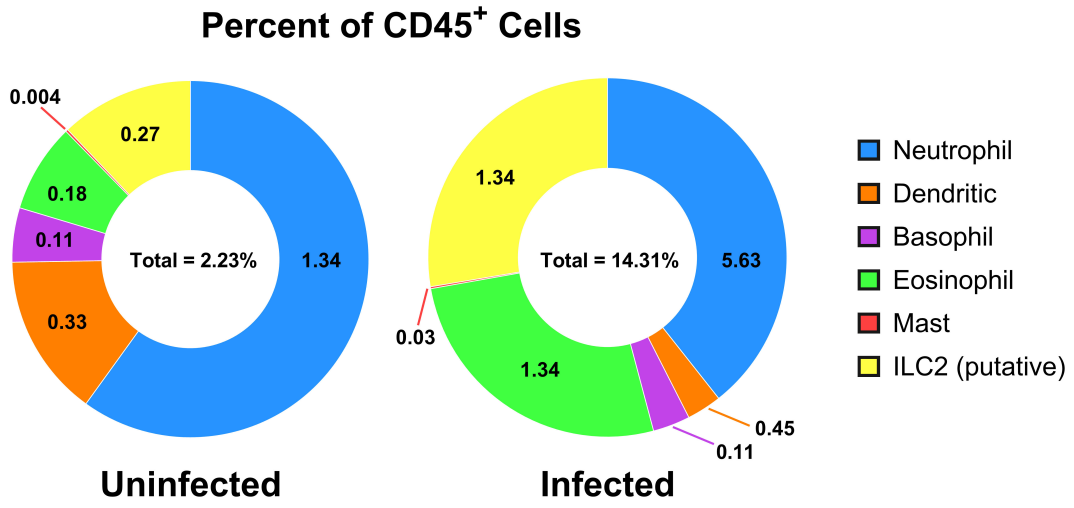

FIGURE 4
Cell populations of $CD45^+$ cells in uninfected versus adult-stage schistosomiasis-infected spleens. Presented is a summary figure of the spleen flow cytometry data presented in Table 1, corresponding to the flow cytometry analyses of the uninfected (Figure 2) and infected (Figure 3) mouse spleens. The donut figure displays each cell type as the percentage of all $CD45^+$ cells. Data analysis was performed with FlowJo™ v10.10.0 Software (BD Life Sciences) and the figure was generated using GraphPad Prism version 10.2.3.

date (32). Egg deposition within spleens is uncommon with *Schistosoma* species but has been observed with species such as *S. japonicum* in C57BL/6 mice where deposition was observed to be common, but granulomas were less frequent (32). Notably, mice that did present with granulomas appeared to have changes to lymphoid follicles and enhanced humoral responses, indicated by increased IL-4, IL-5, and IL-10 in splenocyte supernatants (32). Case studies of eggs deposits in human spleens with *S. mansoni* have emerged more recently and it remains unclear if these are representative (54). These findings are relevant to human medicine as atypical egg deposits can present with symptoms that are misdiagnosed as different conditions, confusing medical practitioners, and resulting in contraindicated procedures or treatments (54, 55). In future studies, it would be useful to systematically evaluate egg burden with this model of Swiss Webster (CFW) mice, using similar methods that are used to harvest eggs from infected mice livers (i.e. homogenization followed by sieves), described in (56) to comprehensively investigate the frequency of egg deposition in mouse spleens, specifically for *S. mansoni*. It remains possible that these deposits are present but less obvious as they are typically not evaluated in the spleen.

The analysis of splenocytes and peripheral blood identified marked eosinophilia which is characteristic of *S. mansoni* (57). This coincides with (and is likely maintained by) elevated serum IL-5 measured in the cytokine data [Figure 5; (58)]. The splenic eosinophils and neutrophils in infected mice show an activated and/or differentiated phenotype indicated by an increased SSC-A, and an increase in the apparent neutrophil heterogeneity (Figure 3, neutrophil and eosinophil SSC-A vs. FSC-A) that are known to occur in a Th1/Th2 cytokine environment, in addition to density changes (59).

Mast cells have been shown to recruit to liver granulomas and schistosomula in primates; however, they remain understudied in the context of murine and human schistosomiasis (60, 61). Moreover, mast cell effectors may be necessary for cytotoxic responses to schistosomula (62). Previous studies with schistosomiasis identified increased colony-forming cells for mast cells and granulocyte-macrophages from bone marrow and splenic origin that correlated with increased transcription of IL-3 and IL-9 (63). We build upon these findings (comparing C57BL/6 to Swiss Webster CFW) and demonstrate the spleens of infected mice do appear to show an increased mast cell population (+5.71x as a $\%CD45^+$) that remains quite small in both the uninfected and infected spleens. However, it is gated with relatively high resolution as $Lin^-CD45^+CD11b^-CD11c^-Ly6G^-SiglecF^-Fc\varepsilon R1\alpha^+CD117^+$ supporting the population as mast cells (64–66).

There is an interesting link between chronic schistosomiasis and basophils where egg antigen exposure has been shown to trigger release of IL-4 and IL-13 (67) and basophils appear to be necessary for parasite egg-associated granuloma formation (68). However, some debate remains on which granulocyte is the dominant source of IL-4 (59). The *Schistosoma* egg antigen (SEA) was previously shown to be a principal driver of the Th2 immune response and is likely a key modulator driving these cytokine responses observed in blood (69). Indeed, Th2 polarization is well documented with murine and human schistosomiasis and appears to occur at the onset of egg production from adult worms (70). Our results support increased splenic basophils ($Lin^-CD45^+CD11b^+CD11c^-Ly6G^-SiglecF^-Fc\varepsilon R1\alpha^+CD117^-$) that appear to be absent in the peripheral blood of a case study with late-stage chronic schistosomiasis. Notably, the granulocytes gated here are gated on $CD11b^+$. However, there exists a $Lin^-CD45^+SiglecF^+$ cell population that is $CD11b^{-/low}$ which appears to also expand during schistosomiasis (data not shown), possibly encompassing a progenitor population within the eosinophil or myeloid lineage. The neutrophil populations quantified here (Table 1) had no significant $CD11b^-$ population (not shown).

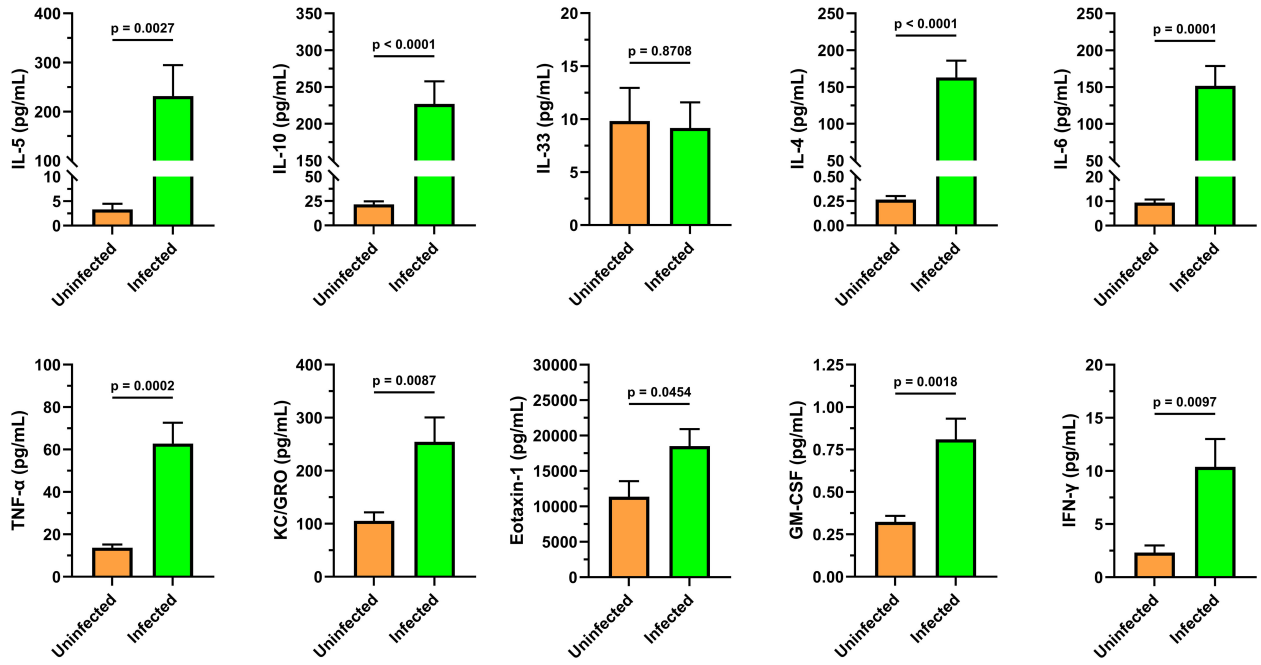

FIGURE 5
Cytokine analysis of infected animal cardiac blood identifies mixed Th1/Th2 immune response. A custom MesoScale U-PLEX assay was designed to assay a panel of 10 cytokines including markers that associate with Th1 and Th2 immunity to characterize the immune environment to compare to the spleen flow cytometry (Figures 3, 4) and blood analytical datasets (Tables 2, 3). The cytokine signals indicate a complex immune response characterized by Th1 and Th2 cytokines that appear to be independent of IL33/St2 signaling. Granulocyte-associated factors such as GM-CSF, Eotaxin-1, and KC/GRO all showed significant upregulation. These serum samples were collected from uninfected (n=8) and infected (n=8) female CFW Swiss Webster mice that were approximately 7 weeks post-infection with *S. mansoni* (approx. 200 cercariae percutaneous). All samples were within their respective lower (LLOD) and upper (ULOD) limits of detection, except for the IL-4 levels in the uninfected group were slightly lower than the 0.56 pg/mL LLOD of IL-4. Data was analyzed and graphed with GraphPad Prism ver. 10.2.3 and statistical significance was determined with a two-tailed unpaired t-test. Data is presented as the group mean ± standard error of the mean (SEM).

In addition to the Th2-associated granulocytes, type-2 innate lymphoid cells (ILC2s) were also considered. It has been well established that the ILC2 subset is defined by GATA3 transcription factor dependence and produces type 2 cytokines (71). Moreover, IL-33, IL-25, and TSLP appear to be key activators of ILC2s in both mice and humans and are thought to be epithelial derived (72, 73). Based on the cytokine dataset from peripheral blood (Figure 5), we have identified a convincing expansion of a putative ILC2 population in the spleen that appears to be independent of IL-33. The data presented here supports previous reports that link schistosomiasis with induction of ILC2s (47). Notably, the measurement of innate lymphoid cells via flow cytometry is continually developing and markers can vary by mouse strain and tissue of analysis, and splenic ILC2s are less characterized versus those of lung and liver (74). Based on the gating strategy used here, this putative ILC2 population may also contain LTi cells that can be $Lin^{-}CD45^{+}CD11b^{-}CD11c^{-}Ly6G^{-}SiglecF^{-}Fc\varepsilon R1\alpha^{-}CD117^{+}$; yet this is not fully understood (71, 73). To further refine these subsets, the ILC2 population could additionally be gated for $CD5^{+}$ to remove any residual T cells (75). Furthermore, to increase confidence in this population, ST2/IL-33R (73) or transcription factors $GATA3_{+}$ and/or $ROR\gamma t^{-}$ can be included (74).

The lack of significant change in IL-33 levels, despite a robust Th2 cytokine and cellular response, provides an interesting avenue that can be explored further; previous reports have shown that IL-33 appears to be dispensable for *S. mansoni* maturation and causes insignificant effects on egg abundance (29, 76). However, IL-33's importance may differ by *Schistosoma* species, where *S. japonicum* infection reports identified increased serum IL-33 which corresponds to egg production suggesting it may be induced by eggs (77, 78). Indeed, parasite eggs are thought to be a primary driver of the Th2 immune responses observed across *Schistosoma* species, as oviposition timing correlates with cytokine production (79). Reports examining this effect in *S. mansoni* identified negligible IL-33 but did identify increased intestinal IL-25 and TSLP (thymic stromal lymphopoietin) that similarly correspond with oviposition timing (29). As IL-33, IL-25, and TSLP have been suggested to provide functional redundancy (80), the differences between *Schistosoma* species may be solely due to evolutionary preferences. The same trends with cytokines in this dataset appear to be consistent with cases of *S. mansoni* infections in humans where blood IL-33 and ST2 showed reduced mRNA in peripheral blood cells yet elevated IL-4, IL-6, and IL-10 measured via cytometric beads (81). Additionally, the cytokine responses are temporal and trend together; previously, it was demonstrated that GM-CSF, TNF-α, IL-13, IL-2, IL-4, IL-17, IFN-γ, IL-5, were all increased in the serum of C57BL/6J (relatively less IL-4 vs. other studies) that all corresponded to the timing of adult pairing and oviposition (82). In terms of the trend, these data agree with the cytokine profile identified here (Figure 5).

10.3389/fimmu.2025.1527129

TABLE 2 Schistosomiasis hematology case study, late-stage chronic infection.

CBC Parameters	Reference Uninfected, n=7, mean (SD)	Chronically Infected, n=1, 19 Weeks Post-Infection
WBC (K/μL)	7.2 (1.8)	25.3
RBC (M/μL)	10.06 (0.41)	9.21
HGB (g/dL)	15.2 (0.4)	13.8
HCT (%)	47.2 (1.6)	44.7
MCV (fL)	47 (2)	49
Red Cell Distribution Width (%)	23.3 (0.8)	22.4
MCH (pg)	15.1 (0.4)	15
MCHC (g/dL)	32.2 (0.4)	30.9
Platelet estimate	adequate	adequate
Platelet count (K/μL)	891 (61)	775
MPV (fL)	7.0 (0.2)	7.5
RBC Morphology		
Manual Retic (%)	5.5 (1.0)	7.2
Reticulocyte (%)	4.3 (0.7)	3.7
Absolute Retic based on Manual Retic (%)	547 (92)	663
Absolute Reticulocyte (K/μL)	436 (70)	341
Reticulocyte Hemoglobin Content (pg)	18.3 (0.5)	18
Nucleated RBC (/100 WBC)	none seen	none seen
Polychromasia	moderate[a]	moderate
Anisocytosis	slight	slight
Poikilocytosis	none seen	none seen
Heinz bodies	none seen	none seen

[a]For the inspection of samples for polychromasia in the uninfected mice, 1 animal from an n=7 showed "slight" and the remaining 6 showed "moderate".

A single animal case study (Swiss Webster CFW female) with late-stage chronic schistosomiasis (19 weeks PI) was used to isolate peripheral blood via the cardiac route and was analyzed and provided by IDEXX BioAnalytics with the Comprehensive CBC with MPV, RDW, and Retic Hgb; test code 63160. The general CBC, hematological parameters, and detailed investigations into the erythroid lineage and cell examinations are presented. Late-stage schistosomiasis shows alterations to WBCs, platelets, RBCs, and reticulocytes.

TABLE 3 Schistosomiasis comprehensive leukocyte differential case study, late-stage chronic infection.

Relative Leukocyte Counts	Reference Uninfected, n=7, mean (SD)	Chronically Infected, n=1, 19 Weeks Post-Infection
Neutrophil (%)	8.3 (1.5)	10
Lymphocytes (%)	86.2 (2.6)	69
Band (%)	none seen	none seen
Eosinophil (%)	1.5 (0.8)	13
Monocyte (%)	3.9 (1.3)	8
Basophil (%)	0.2 (0.1)	0
Metamyelocyte (%)	none seen	none seen
Myelocyte (%)	none seen	none seen
Promyelocyte (%)	none seen	none seen
Unclassified (%)	none seen	none seen
Absolute Counts		
Unclassified (/μL)	none seen	none seen
Neutrophil (/μL)	580 (133)	2530
Band (/μL)	none seen	none seen
Eosinophil (/μL)	106 (67)	3289
Basophil (/μL)	11 (4)	0
Monocyte (/μL)	286 (132)	2024
Lymphocyte (/μL)	6174 (1600)	17457
Metamyelocyte (/μL)	none seen	none seen
Myelocyte (/μL)	none seen	none seen
Promyelocyte (/μL)	none seen	none seen

A single animal case study (Swiss Webster CFW female) with late-stage chronic schistosomiasis (19 weeks PI) was used to isolate peripheral blood via the cardiac route and was analyzed and provided by IDEXX BioAnalytics with the Comprehensive CBC with MPV, RDW and Retic Hgb; test code 63160. The panel includes a comprehensive leukocyte differential with relative (%) and absolute counts. Leukocyte subtypes and progenitors are also included. Marked increases in most blood leukocytes were identified, however basophils were absent from circulation.

The complete blood count and leukocyte differential obtained from IDEXX BioAnalytics (Tables 2, 3) has limitations in the that it includes a single chronically infected animal; however, the reference dataset is robust (n=7). Notably, the panel includes expanded hematology parameters such as reticulocytes that may be of interest to the field. The case study of the 19 week post-infection mouse can be insightful as it may provide a snapshot of a late-stage chronic infection, whereas many studies (e.g. worm burden reduction) are typically performed within 10 weeks post-infection. However, one possibility which cannot be eliminated is that this particular mouse may have achieved a reduced worm burden, through natural means or otherwise, despite displaying notably unwell behavior and appearance. Of note, the previously mentioned absence of basophils in circulation (Table 3), yet increased abundance in the splenocytes breaks the trend compared to neutrophils and eosinophils which were increased in both the the adult-stage infected spleen (7 weeks PI; Table 1) and in the circulation of a late-stage chronic infection (19 weeks PI; Table 3). This discrepancy between elevated basophils in the infected spleen (Table 1) but absence in the peripheral blood (Table 3) could indicate migration patterns or tissue-specific roles that would require further studies to delineate. Additionally, it remains possible that this change could be due to differences between infection durations, the limited sample size of the study, or instrument limits of detection; thus, these findings will need to be validated for reproducibility.

More broadly, relatively less is known about the role of granuolytes in late-stage infection, although eosinophils (predominantly), neutrophils, and macrophages are consistently found in tissue granulomas (83). The role eosinophils play in the late-stage of granulomatous infection is under reconsideration, with these cells possibly serving in an immune modulatory role, as opposed to a solely worm- or egg-targeting purpose (84). Similarly, the basophil contribution to schistosomiasis is poorly understood; however, it has been demonstrated previously that basophil depletion decreases the size of both lung and liver granulomatous lesions, providing a possible link to pathogenesis (68). These data confirm previous findings of splenic basophilia, which was similarly observed in *S. mansoni*-infected female BALB/c mice (68). Over time, the outer perimeter of granulomas appears to become infused with B lymphocytes, possibly in support of antibody production against the highly antigenic eggs, which generate a Th2 response in the host; however, these may also play a regulatory role (57). Altogether, the immune system appears to carefully balance inflammation and prevention of disease progression in *S. mansoni* infections, possibly leveraging granulocytes in this effort, although more work is needed to evaluate this (85).

Our current findings advance our understanding of an outbred *S. mansoni* mouse model frequently used for therapeutic and vaccine development. Advancing our understanding of the unique and complex immune response facilitated by human-relevant *Schistosoma* species may lead to novel therapeutic targets and vaccine opportunities that would enable us to reduce the global health burden caused by schistosomiasis which remains a top neglected infectious disease in the developing world (86).

Data availability statement

The original contributions presented in the study are included in the article/supplementary material. Further inquiries can be directed to the corresponding author.

Ethics statement

The animal study was approved by University of Nebraska at Omaha IACUC. The study was conducted in accordance with the local legislation and institutional requirements.

Author contributions

TS: Conceptualization, Data curation, Formal analysis, Investigation, Methodology, Validation, Visualization, Writing – original draft, Writing – review & editing. AN: Conceptualization, Data curation, Formal analysis, Investigation, Methodology, Validation, Visualization, Writing – original draft, Writing – review & editing. EE: Investigation, Writing – review & editing. SA: Investigation, Writing – review & editing. JV: Funding acquisition, Resources, Writing – review & editing. PD: Funding acquisition, Project administration, Resources, Supervision, Writing – review & editing.

Funding

The author(s) declare that financial support was received for the research and/or publication of this article. Funding was provided by NIH NIGMS 5P20GM103427, NIH NIAID 2R01AI116723, and Nebraska NASA fellowship.

Acknowledgments

The following reagent was provided by the NIAID Schistosomiasis Resource Center for distribution through BEI Resources, NIAID, NIH: Schistosoma mansoni, Strain NMRI, Newly Exposed Swiss Webster Mice, NR-21963. We thank Dr. Paul Denton (University of Nebraska at Omaha) for technical assistance. Additionally, we thank the University of Nebraska Medical Center (UNMC) Flow Cytometry Research Facility and its staff for data acquisition. The UNMC Flow Cytometry Core Research Facility is administrated through the Office of the Vice Chancellor for Research and supported by state funds from the Nebraska Research Initiative (NRI) and The Fred and Pamela Buffett Cancer Center's National Cancer Institute Cancer Support Grant. Major instrumentation has been provided by the Office of the Vice Chancellor for Research, The University of Nebraska Foundation, the Nebraska Banker's Fund, and by the NIH-NCRR Shared Instrument Program. This work constituted a portion of the dissertation of TS.

Conflict of interest

The authors declare that the research was conducted in the absence of any commercial or financial relationships that could be construed as a potential conflict of interest.

Generative AI statement

The author(s) declare that no Generative AI was used in the creation of this manuscript.

Publisher's note

References

1. McManus DP, Dunne DW, Sacko M, Utzinger J, Vennervald BJ, Zhou X-N. Schistosomiasis. *Nat Rev Dis Primer*. (2018) 4:13. doi: 10.1038/s41572-018-0013-8

2. Gryseels B, Polman K, Clerinx J, Kestens L. Human schistosomiasis. *Lancet Lond Engl*. (2006) 368:1106–18. doi: 10.1016/S0140-6736(06)69440-3

3. Inobaya MT, Olveda RM, Chau TN, Olveda DU, Ross AG. Prevention and control of schistosomiasis: a current perspective. *Res Rep Trop Med*. (2014) 2014:65–75. doi: 10.2147/RRTM.S44274

4. GBD 2016 Disease and Injury Incidence and Prevalence Collaborators. Global, regional, and national incidence, prevalence, and years lived with disability for 328 diseases and injuries for 195 countries, 1990-2016: a systematic analysis for the Global Burden of Disease Study 2016. *Lancet Lond Engl*. (2017) 390:1211–59. doi: 10.1016/S0140-6736(17)32154-2

5. van der Werf MJ, de Vlas SJ, Brooker S, Looman CWN, Nagelkerke NJD, Habbema JDF, et al. Quantification of clinical morbidity associated with schistosome infection in sub-Saharan Africa. *Acta Trop*. (2003) 86:125–39. doi: 10.1016/s0001-706x(03)00029-9

6. Adenowo AF, Oyinloye BE, Ogunyinka BI, Kappo AP. Impact of human schistosomiasis in sub-Saharan Africa. *Braz J Infect Dis Off Publ Braz Soc Infect Dis*. (2015) 19:196–205. doi: 10.1016/j.bjid.2014.11.004

7. Hotez PJ, Alvarado M, Basáñez M-G, Bolliger I, Bourne R, Boussinesq M, et al. The global burden of disease study 2010: interpretation and implications for the neglected tropical diseases. *PloS Negl Trop Dis*. (2014) 8:e2865. doi: 10.1371/journal.pntd.0002865

8. Perera DJ, Ndao M. Promising technologies in the field of helminth vaccines. *Front Immunol*. (2021) 12:711650. doi: 10.3389/fimmu.2021.711650

9. Vale N, Gouveia MJ, Rinaldi G, Brindley PJ, Gärtner F, Correia da Costa JM. Praziquantel for Schistosomiasis: Single-Drug Metabolism Revisited, Mode of Action, and Resistance. *Antimicrob Agents Chemother*. (2017) 61(5):e02582-16. doi: 10.1128/AAC.02582-16

10. Gardner JMF, Mansour NR, Bell AS, Helmby H, Bickle Q. The discovery of a novel series of compounds with single-dose efficacy against juvenile and adult Schistosoma species. *PLoS Negl Trop Dis*. (2021) 15(7):e0009490. doi: 10.1371/journal.pntd.0009490

11. Leas DA, Keiser J, Charman SA, Shackleford DM, Jones JO, Campbell M, et al. Single-Dose Drug Development Candidate for Schistosomiasis. *ACS Infect Dis*. (2024) 10(11):3963–72. doi: 10.1021/acsinfecdis.4c00677

12. Zarowiecki M, Berriman M. What helminth genomes have taught us about parasite evolution. *Parasitology*. (2015) 142 Suppl 1:S85–97. doi: 10.1017/S0031182014001449

13. Costain AH, Phythian-Adams AT, Colombo SAP, Marley AK, Owusu C, Cook PC, et al. Dynamics of host immune response development during schistosoma mansoni infection. *Front Immunol*. (2022) 13:906338. doi: 10.3389/fimmu.2022.906338

14. Grzych JM, Pearce E, Cheever A, Caulada ZA, Caspar P, Heiny S, et al. Egg deposition is the major stimulus for the production of Th2 cytokines in murine schistosomiasis mansoni. *J Immunol Baltim Md 1950*. (1991) 146:1322–7. doi: 10.4049/jimmunol.146.4.1322

15. Hoffmann KF, Cheever AW, Wynn TA. IL-10 and the dangers of immune polarization: excessive type 1 and type 2 cytokine responses induce distinct forms of lethal immunopathology in murine schistosomiasis. *J Immunol Baltim Md*. (2000) 1950:164. doi: 10.4049/jimmunol.164.12.6406

16. Makepeace BL, Martin C, Turner JD, Specht S. Granulocytes in helminth infection – who is calling the shots? *Curr Med Chem*. (2012) 19:1567–86. doi: 10.2174/092986712799828337

17. Freudenstein-Dan A, Gold D, Fishelson Z. Killing of schistosomes by elastase and hydrogen peroxide: implications for leukocyte-mediated schistosome killing. *J Parasitol*. (2003) 89:1129–35. doi: 10.1645/GE-96R

18. Incani RN, McLaren DJ. Neutrophil-mediated cytotoxicity to schistosomula of Schistosoma mansoni *in vitro*: studies on the kinetics of complement and/or antibody-dependent adherence and killing. *Parasite Immunol*. (1981) 3:107–26. doi: 10.1111/j.1365-3024.1981.tb00389.x

19. Moser G, Sher A. Studies of the antibody-dependent killing of schistosomula of Schistosoma mansoni employing haptenic target antigens. II. *In vitro* killing of TNP-schistosomula by human eosinophils and neutrophils. *J Immunol Baltim Md 1950*. (1981) 126:1025–9. doi: 10.4049/jimmunol.126.3.1025

20. Brindley PJ, Strand M, Norden AP, Sher A. Role of host antibody in the chemotherapeutic action of praziquantel against Schistosoma mansoni: identification of target antigens. *Mol Biochem Parasitol*. (1989) 34:99–108. doi: 10.1016/0166-6851(89)90001-7

21. Brindley PJ, Sher A. The chemotherapeutic effect of praziquantel against Schistosoma mansoni is dependent on host antibody response. *J Immunol Baltim Md 1950*. (1987) 139:215–20. doi: 10.4049/jimmunol.139.1.215

22. Doenhoff MJ. The immune-dependence of chemotherapy in experimental schistosomiasis. *Mem Inst Oswaldo Cruz*. (1989) 84 Suppl 1:31–7. doi: 10.1590/s0074-02761989000500004

23. Fallon PG, Cooper RO, Probert AJ, Doenhoff MJ. Immune-dependent chemotherapy of schistosomiasis. *Parasitology*. (1992) 105 Suppl:S41–48. doi: 10.1017/s003118200007534x

24. Abdul-Ghani RA, Hassan AA. Murine schistosomiasis as a model for human schistosomiasis mansoni: similarities and discrepancies. *Parasitol Res*. (2010) 107:1–8. doi: 10.1007/s00436-010-1855-5

25. Cheever AW, Lenzi JA, Lenzi HL, Andrade ZA. Experimental models of Schistosoma mansoni infection. *Mem Inst Oswaldo Cruz*. (2002) 97:917–40. doi: 10.1590/s0074-02762002000700002

26. Lombardo FC, Pasche V, Panic G, Endriss Y, Keiser J. Life cycle maintenance and drug-sensitivity assays for early drug discovery in Schistosoma mansoni. *Nat Protoc*. (2019) 14:461–81. doi: 10.1038/s41596-018-0101-y

27. Cosenza-Contreras M, de Oliveira E Castro RA, Mattei B, Campos JM, Gonçalves Silva G, de Paiva NCN, et al. The schistosomiasis spleenOME: unveiling the proteomic landscape of splenomegaly using label-free mass spectrometry. *Front Immunol*. (2018) 9:3137. doi: 10.3389/fimmu.2018.03137

28. Maggi L, Rocha IC, Camelo GMA, Fernandes VR, Negrão-Corrêa D. The IL-33/ST2 pathway is not essential to Th2 stimulation but is key for modulation and survival during chronic infection with Schistosoma mansoni in mice. *Cytokine*. (2021) 138:155390. doi: 10.1016/j.cyto.2020.155390

29. Mukendi JPK, Nakamura R, Uematsu S, Hamano S. Interleukin (IL)-33 is dispensable for Schistosoma mansoni worm maturation and the maintenance of egg-induced pathology in intestines of infected mice. *Parasit Vectors*. (2021) 14:70. doi: 10.1186/s13071-020-04561-w

30. Wynn TA, Cheever AW, Williams ME, Hieny S, Caspar P, Kühn R, et al. IL-10 regulates liver pathology in acute murine schistosomiasis mansoni but is not required for immune down-modulation of chronic disease. *J Immunol*. (1998) 160:4473–80. doi: 10.4049/jimmunol.160.9.4473

31. Schulze TT, Neville AJ, Chapman RC, Davis PH. Mouse splenocyte enrichment strategies via negative selection for broadened single-cell transcriptomics. *STAR Protoc*. (2022) 3:101402. doi: 10.1016/j.xpro.2022.101402

32. Wang Y, Zhang J, Yin J, Shen Y, Wang Y, Xu Y, et al. The formation of egg granulomas in the spleens of mice with late Schistosoma japonicum infection alters splenic morphology. *Parasit Vectors*. (2015) 8:375. doi: 10.1186/s13071-015-0988-x

33. Son K, Mukherjee M, McIntyre BAS, Eguez JC, Radford K, LaVigne N, et al. Improved recovery of functionally active eosinophils and neutrophils using novel immunomagnetic technology. *J Immunol Methods*. (2017) 449:44–55. doi: 10.1016/j.jim.2017.06.005

34. Bedner E, Burfeind P, Gorczyca W, Melamed MR, Darzynkiewicz Z. Laser scanning cytometry distinguishes lymphocytes, monocytes, and granulocytes by differences in their chromatin structure. *Cytometry*. (1997) 29:191–6. doi: 10.1002/(SICI)1097-0320(19971101)29:3<191::AID-CYTO1>3.0.CO;2-F

35. Sedgwick JB, Shikama Y, Nagata M, Brener K, Busse WW. Effect of isolation protocol on eosinophil function: Percoll gradients versus immunomagnetic beads. *J Immunol Methods*. (1996) 198:15–24. doi: 10.1016/0022-1759(96)00139-1

36. Wijshake T, Rose J, Wang J, Zielke J, Marlar-Pavey M, Chen W, et al. Schistosome infection impacts hematopoiesis. *J Immunol Baltim Md 1950*. (2024) 212:607–16. doi: 10.4049/jimmunol.2300195

37. Yang X, Chen D, Long H, Zhu B. The mechanisms of pathological extramedullary hematopoiesis in diseases. *Cell Mol Life Sci CMLS*. (2020) 77:2723–38. doi: 10.1007/s00018-020-03450-w

38. Piasecka J, Thornton CA, Rees P, Summers HD. Diffusion mapping of eosinophil-activation state. *Cytom Part J Int Soc Anal Cytol*. (2020) 97:253–8. doi: 10.1002/cyto.a.23884

39. Thurau AM, Schylz U, Wolf V, Krug N, Schauer U. Identification of eosinophils by flow cytometry. *Cytometry*. (1996) 23:150–8. doi: 10.1002/(SICI)1097-0320(19960201)23:2<150::AID-CYTO8>3.0.CO;2-O

40. Phythian-Adams AT, Cook PC, Lundie RJ, Jones LH, Smith KA, Barr TA, et al. CD11c depletion severely disrupts Th2 induction and development *in vivo*. *J Exp Med*. (2010) 207:2089–96. doi: 10.1084/jem.20100734

41. Hey Y-Y, Tan JKH, O'Neill HC. Redefining myeloid cell subsets in murine spleen. *Front Immunol*. (2015) 6:652. doi: 10.3389/fimmu.2015.00652

42. Dyer KD, Garcia-Crespo KE, Killoran KE, Rosenberg HF. Antigen profiles for the quantitative assessment of eosinophils in mouse tissues by flow cytometry. *J Immunol Methods*. (2011) 369:91–7. doi: 10.1016/j.jim.2011.04.009

43. Vivier E, Artis D, Colonna M, Diefenbach A, Di Santo JP, Eberl G, et al. Innate lymphoid cells: 10 years on. *Cell*. (2018) 174:1054–66. doi: 10.1016/j.cell.2018.07.017

44. Ricardo-Gonzalez RR, Van Dyken SJ, Schneider C, Lee J, Nussbaum JC, Liang H-E, et al. Tissue signals imprint ILC2 identity with anticipatory function. *Nat Immunol*. (2018) 19:1093–9. doi: 10.1038/s41590-018-0201-4

45. Mathä L, Takei F, Martinez-Gonzalez I. Tissue resident and migratory group 2 innate lymphoid cells. *Front Immunol*. (2022) 13:877005. doi: 10.3389/fimmu.2022.877005

46. Tait Wojno ED, Beamer CA. Isolation and identification of innate lymphoid cells (ILCs) for immunotoxicity testing. *Methods Mol Biol Clifton NJ*. (2018) 1803:353–70. doi: 10.1007/978-1-4939-8549-4_21

47. Nausch N, Mutapi F. Group 2 ILCs: A way of enhancing immune protection against human helminths? *Parasite Immunol*. (2018) 40:e12450. doi: 10.1111/pim.12450

48. Jutzeler KS, Le Clec'h W, Chevalier FD, Anderson TJC. Contribution of parasite and host genotype to immunopathology of schistosome infections. *Parasit Vectors*. (2024) 17:203. doi: 10.1186/s13071-024-06286-6

49. Stadecker MJ, Asahi H, Finger E, Hernandez HJ, Rutitzky LI, Sun J. The immunobiology of Th1 polarization in high-pathology schistosomiasis. *Immunol Rev*. (2004) 201:168–79. doi: 10.1111/j.0105-2896.2004.00197.x

50. Burke ML, Jones MK, Gobert GN, Li YS, Ellis MK, McManus DP. Immunopathogenesis of human schistosomiasis. *Parasite Immunol*. (2009) 31:163–76. doi: 10.1111/j.1365-3024.2009.01098.x

51. Kumar R, Mickael C, Chabon J, Gebreab L, Rutebemberwa A, Garcia AR, et al. The causal role of IL-4 and IL-13 in schistosoma mansoni pulmonary hypertension. *Am J Respir Crit Care Med*. (2015) 192:998–1008. doi: 10.1164/rccm.201410-1820OC

52. Matta BM, Lott JM, Mathews LR, Liu Q, Rosborough BR, Blazar BR, et al. IL-33 is an unconventional Alarmin that stimulates IL-2 secretion by dendritic cells to selectively expand IL-33R/ST2+ regulatory T cells. *J Immunol Baltim Md*. (2014) 1950:193. doi: 10.4049/jimmunol.1400481

53. Collins JJ, Wendt GR, Iyer H, Newmark PA. Stem cell progeny contribute to the schistosome host-parasite interface. *eLife*. (2016) 5:e12473. doi: 10.7554/eLife.12473

54. Gobbi F, Martelli G, Attard L, Buonfrate D, Angheben A, Marchese V, et al. Schistosoma mansoni eggs in spleen and lungs, mimicking other diseases. *PloS Negl Trop Dis*. (2015) 9:e0003860. doi: 10.1371/journal.pntd.0003860

55. Grunstein P, Broquie G, Gayet AM, Bazelly B, Fouret P. Pulmonary bilharziasis due to Schistosoma mansoni simulating Carrington's disease. *Rev Pneumol Clin*. (1988) 44:36–8.

56. Tucker MS, Karunaratne LB, Lewis FA, Freitas TC, Liang Y-S. Schistosomiasis. *Curr Protoc Immunol*. (2013) 103:19.1.1–19.1.58. doi: 10.1002/0471142735.im1901s103

57. Malta KK, Palazzi C, Neves VH, Aguiar Y, Silva TP, Melo RCN. Schistosomiasis mansoni-recruited eosinophils: an overview in the granuloma context. *Microorganisms*. (2022) 10:2022. doi: 10.3390/microorganisms10102022

58. Sher A, Coffman RL, Hieny S, Scott P, Cheever AW. Interleukin 5 is required for the blood and tissue eosinophilia but not granuloma formation induced by infection with Schistosoma mansoni. *Proc Natl Acad Sci U.S.A*. (1990) 87:61–5. doi: 10.1073/pnas.87.1.61

59. Rumbley CA, Sugaya H, Zekavat SA, El Refaei M, Perrin PJ, Phillips SM. Activated eosinophils are the major source of Th2-associated cytokines in the schistosome granuloma. *J Immunol Baltim Md*. (1999) 1950:162. doi: 10.4049/jimmunol.162.2.1003

60. Epstein WL, Fukuyama K, Danno K, Kwan-Wong E. Granulomatous inflammation in normal and athymic mice infected with schistosoma mansoni: an ultrastructural study. *J Pathol*. (1979) 127:207–15. doi: 10.1002/path.1711270408

61. Hsü SY, Hsü HF, Penick GD, Hanson HO, Schiller HJ, Cheng HF. Immunoglobulin E, mast cells, and eosinophils in the skin of rhesus monkeys immunized with x-irradiated cercariae of Schistosoma japonicum. *Int Arch Allergy Appl Immunol*. (1979) 59:383–93. doi: 10.1159/000232285

62. Capron M, Rousseaux J, Mazingue C, Bazin H, Capron A. Rat mast cell-eosinophil interaction in antibody-dependent eosinophil cytotoxicity to Schistosoma mansoni schistosomula. *J Immunol Baltim Md 1950*. (1978) 121:2518–25. doi: 10.4049/jimmunol.121.6.2518

63. Khalil RM, Luz A, Mailhammer R, Moeller J, Mohamed AA, Omran S, et al. Schistosoma mansoni infection in mice augments the capacity for interleukin 3 (IL-3) and IL-9 production and concurrently enlarges progenitor pools for mast cells and granulocytes-macrophages. *Infect Immun*. (1996) 64:4960–6. doi: 10.1128/iai.64.12.4960-4966.1996

64. Kritikou E, Depuydt MAC, de Vries MR, Mulder KE, Govaert AM, Smit MD, et al. Flow cytometry-based characterization of mast cells in human atherosclerosis. *Cells*. (2019) 8:334. doi: 10.3390/cells8040334

65. Lilla JN, Chen C-C, Mukai K, BenBarak MJ, Franco CB, Kalesnikoff J, et al. Reduced mast cell and basophil numbers and function in Cpa3-Cre; Mcl-1fl/fl mice. *Blood*. (2011) 118:6930–8. doi: 10.1182/blood-2011-03-343962

66. Obata K, Mukai K, Tsujimura Y, Ishiwata K, Kawano Y, Minegishi Y, et al. Basophils are essential initiators of a novel type of chronic allergic inflammation. *Blood*. (2007) 110:913–20. doi: 10.1182/blood-2007-01-068718

67. Knuhr K, Langhans K, Nyenhuis S, Viertmann K, Kildemoes AMO, Doenhoff MJ, et al. Schistosoma mansoni Egg-Released IPSE/alpha-1 Dampens Inflammatory Cytokine Responses via Basophil Interleukin (IL)-4 and IL-13. *Front Immunol*. (2018) 9:2293. doi: 10.3389/fimmu.2018.02293

68. Anyan WK, Seki T, Kumagai T, Obata-Ninomiya K, Furushima-Shimogawara R, Kwansa-Bentum B, et al. Basophil depletion downregulates Schistosoma mansoni egg-induced granuloma formation. *Parasitol Int*. (2013) 62:508–13. doi: 10.1016/j.parint.2013.07.003

69. Everts B, Perona-Wright G, Smits HH, Hokke CH, van der Ham AJ, Fitzsimmons CM, et al. Omega-1, a glycoprotein secreted by Schistosoma mansoni eggs, drives Th2 responses. *J Exp Med*. (2009) 206:1673–80. doi: 10.1084/jem.20082460

70. Pearce EJ. Priming of the immune response by schistosome eggs. *Parasite Immunol*. (2005) 27:265–70. doi: 10.1111/j.1365-3024.2005.00765.x

71. Bar-Ephraïm YE, Mebius RE. Innate lymphoid cells in secondary lymphoid organs. *Immunol Rev*. (2016) 271:185–99. doi: 10.1111/imr.12407

72. Huang Y, Guo L, Qiu J, Chen X, Hu-Li J, Siebenlist U, et al. IL-25-responsive, lineage-negative KLRG1(hi) cells are multipotential "inflammatory" type 2 innate lymphoid cells. *Nat Immunol*. (2015) 16:161–9. doi: 10.1038/ni.3078

73. Zeng B, Shi S, Ashworth G, Dong C, Liu J, Xing F. ILC3 function as a double-edged sword in inflammatory bowel diseases. *Cell Death Dis*. (2019) 10:315. doi: 10.1038/s41419-019-1540-2

74. Sadeghalvad M, Khijakadze D, Orangi M, Takei F. Flow cytometric analysis of innate lymphoid cells: challenges and solutions. *Front Immunol*. (2023) 14:1198310. doi: 10.3389/fimmu.2023.1198310

75. Burkhard SH, Mair F, Nussbaum K, Hasler S, Becher B. T cell contamination in flow cytometry gating approaches for analysis of innate lymphoid cells. *PloS One*. (2014) 9:e94196. doi: 10.1371/journal.pone.0094196

76. Kamdem SD, Konhawa F, Kuemkon EM, Meyo Kamguia L, Tchanana GK, Nche F, et al. Negative association of interleukin-33 plasma levels and schistosomiasis infection in a site of polyparasitism in rural Cameroon. *Front Immunol*. (2019) 10:2827. doi: 10.3389/fimmu.2019.02827

77. Peng H, Zhang Q, Li X, Liu Z, Shen J, Sun R, et al. IL-33 Contributes to Schistosoma japonicum-induced Hepatic Pathology through Induction of M2 Macrophages. *Sci Rep*. (2016) 6:29844. doi: 10.1038/srep29844

78. Yu Y, Deng W, Lei J. Interleukin-33 promotes Th2 immune responses in infected mice with Schistosoma japonicum. *Parasitol Res*. (2015) 114:2911–8. doi: 10.1007/s00436-015-4492-1

79. Pearce EJ, Kane C M, Sun J J, Taylor J, McKee AS, Cervi L. Th2 response polarization during infection with the helminth parasite Schistosoma mansoni. *Immunol Rev*. (2004) 201:117–26. doi: 10.1111/j.0105-2896.2004.00187.x

80. Vannella KM, Ramalingam TR, Borthwick LA, Barron L, Hart KM, Thompson RW, et al. Combinatorial targeting of TSLP, IL-25, and IL-33 in type 2 cytokine-driven inflammation and fibrosis. *Sci Transl Med*. (2016) 8:337ra65. doi: 10.1126/scitranslmed.aaf1938

81. do Nascimento WRC, Nóbrega Cg de O, Fernandes E de S, Santos P d'Emery A, Melo FL, Albuquerque Mcp de A, et al. Schistosoma mansoni infection decreases IL-33-mRNA expression and increases CXCL9 and CXCL10 production by peripheral blood cells. *Med Microbiol Immunol (Berl)*. (2022) 211:211–8. doi: 10.1007/s00430-022-00745-6

82. Scheer S, Krempl C, Kallfass C, Frey S, Jakob T, Mouahid G, et al. mansoni bolsters anti-viral immunity in the murine respiratory tract. *PloS One*. (2014) 9:e112469. doi: 10.1371/journal.pone.0112469

83. Llanwarne F, Helmby H. Granuloma formation and tissue pathology in *Schistosoma japonicum* versus *Schistosoma mansoni* infections. *Parasite Immunol*. (2021) 43:e12778. doi: 10.1111/pim.12778

84. Amaral KB, Silva TP, Dias FF, Malta KK, Rosa FM, Costa-Neto SF, et al. Histological assessment of granulomas in natural and experimental Schistosoma mansoni infections using whole slide imaging. *PloS One*. (2017) 12:e0184696. doi: 10.1371/journal.pone.0184696

85. Schwartz C, Fallon PG. Schistosoma "Eggs-iting" the host: granuloma formation and egg excretion. *Front Immunol*. (2018) 9:2492. doi: 10.3389/fimmu.2018.02492

86. King CH, Galvani AP. Underestimation of the global burden of schistosomiasis. *Lancet Lond Engl*. (2018) 391:307–8. doi: 10.1016/S0140-6736(18)30098-9

frontiers | Frontiers in Immunology

TYPE Original Research
PUBLISHED 05 May 2025
DOI 10.3389/fimmu.2025.1600838

OPEN ACCESS

EDITED BY
Joydeep Paul,
Adamas University, India

REVIEWED BY
Arunkumar Subramanian,
SRM Institute of Science and Technology, India
Sejuti Ray Chowdhury,
Adamas University, India

*CORRESPONDENCE
Yang Dai
daiyang@jipd.com
Hongxia Bai
bhx19830204@163.com

†These authors have contributed equally to this work

RECEIVED 27 March 2025
ACCEPTED 09 April 2025
PUBLISHED 05 May 2025

CITATION
Yuan C, Wang Q, Chen Y, Ding X, Zhang Q, Yao J, Zhang B, Dai Y and Bai H (2025) Protective effects of *Nippostrongylus brasiliensis*-derived uridine via the apical sodium-dependent bile acid transporter in a mouse model of TNBS-induced inflammatory bowel disease. *Front. Immunol.* 16:1600838. doi: 10.3389/fimmu.2025.1600838

Protective effects of *Nippostrongylus brasiliensis*-derived uridine via the apical sodium-dependent bile acid transporter in a mouse model of TNBS-induced inflammatory bowel disease

Caiyi Yuan[1†], Qiang Wang[2†], Yuying Chen[1,3†], Xin Ding[2], Qiang Zhang[2], Jiakai Yao[2], Bei Zhang[2], Yang Dai[1,2*] and Hongxia Bai[4*]

[1]School of Public Health, Nanjing Medical University, Nanjing, China, [2]National Health Commission Key Laboratory of Parasitic Disease Control and Prevention, Jiangsu Provincial Key Laboratory on Parasitic and Vector Control Technology, Jiangsu Provincial Medical Key Laboratory, Jiangsu Institute of Parasitic Diseases, Wuxi, China, [3]Department of Parasitic Disease Prevention and Control, Guangzhou Tianhe District Center for Disease Control and Prevention, Guangzhou, China, [4]Department of Science and Education, Xishan People's Hospital of Wuxi City, Wuxi, China

Introduction: Inflammatory bowel disease (IBD), a chronic immune-mediated gastrointestinal disorder mainly covering Crohn's Disease and Ulcerative Colitis, has an unclear etiology. The exploration of novel intervention strategies remains a key scientific issue that is urgently needed for IBD treatment. The hygiene hypothesis has led researchers to notice that worm infections can regulate the immune system, which might help treat inflammatory diseases. *Nippostrongylus brasiliensis (Nb)*, similar to human hookworms in life cycle and symptoms, is often used in hookworm research. Our previous study also demonstrated that Nb-derived uridine screened from ES could exert anti-inflammatory and anti-atherosclerotic effects.

Methods: In this study, we established the protective and anti-inflammation effect of Nb infection and ES intervention in TNBS-induced IBD model in mice and further validated the efficiency of uridine screened from ES. Moreover, we conducted an RNA sequencing (RNA-Seq) analysis to elucidate the relevant possible functional mechanisms responsible for the protective and anti-inflammation effects of ES or uridine administration.

Results: Current results have demonstrated that uridine can exhibit a protective effect on TNBS-induced IBD in mice. Moreover, it was identified that *slc10a2* exhibited high expression after uridine intervention. By specific inhibition of the encoding protein (ASBT), its impact on the protective efficacy has been interrupted.

Discussion: The current study has illustrated that uridine is capable of exerting potential therapeutic and anti-inflammatory effects on Inflammatory Bowel Disease (IBD) by modulating *slc10a2*. These findings could offer a novel therapeutic target for the intervention of IBD.

KEYWORDS

Nippostrongylus brasiliensis, uridine, apical sodium-dependent bile acid transporter, inflammatory bowel disease, RNA sequencing

1 Introduction

Inflammatory bowel disease (IBD) is a chronic immune-mediated disorder of the gastrointestinal tract, mainly consisting of Crohn's Disease and Ulcerative Colitis. From 1990 to 2017, the incidence rate of IBD rose from 3.7 million to nearly 6.8 million worldwide, causing a global burden of diseases (1). The incidence rate of IBD is still rising in the newly industrialized and developing countries and maintains a high stability in western countries (2). Currently, factors such as genetic susceptibility, host immune dysfunction, changes in gut microbiota, and environmental influences are considered to be the main pathogenesis of IBD (3). Benefit from the availability of multiple deep sequencing platforms, genetic research on IBD has also made significant progress that more than 200 genetic polymorphisms were identified to be linked with the increased risk of IBD such as adaptive immunity, mucosal immunity, and immune tolerance, and autophagy (4). The changes in the structure and function of gut microbiota could trigger host immune and metabolic responses which alter gut immune responses and ecosystems, exacerbating the symptoms of IBD (5). However, its exact etiology and specific drug are still need to be confirmed (6). The existing drug therapies only alleviate a few symptoms and are often accompanied by certain side effects, making it difficult to achieve a complete cure. Moreover, the recurrence of IBD seriously impairs patients' quality of life and is highly correlated with the risk of colorectal cancer (7). Therefore, exploring novel intervention strategies is a crucial scientific issue urgently needed for IBD treatment.

In recent years, the "hygiene hypothesis" has provided new perspectives for pharmacological strategies in treating inflammatory diseases. This hypothesis posits that the development of immune system depends on its co-evolution with microorganisms. Excessively clean environments during childhood may lead to reduced exposure to microorganisms, affecting the normal development of the immune system and ultimately increasing the risk of autoimmune diseases in adulthood (8). Based on the hygiene hypothesis, the immune-regulatory functions of worms have been found to inhibit the progression of inflammation. This has been demonstrated in studies on worms therapies such as using schistosome and hookworm interventions to treat IBD, arthritis, celiac disease and other inflammatory conditions (9–11). Thus, the phenomenon of worm infection regulating the immune system has gradually attracted the attention of researchers in the search for treatment for certain inflammatory diseases.

Hookworms are common soil-transmitted nematode. The species that mainly infect humans include *Ancylostoma duodenale*, *Necator Americanus*, and *Ancylostoma ceylanicum*. Hookworm infections affect the health of approximately 500 million people in tropical regions worldwide, resulting in an annual loss of 3.2 million Disability Adjusted Life Years (DALYs), making it one of the most significant neglected tropical disease globally (12). Hookworms parasitize the human body, causing chronic infections and eliciting a type II immune response in the host. This response promotes B cells to secret IgE antibodies via the secretion of IL-4 and IL-13, initiating an anti-parasitic immune response that suppress the type I immune-related inflammatory response, minimizing host damage and facilitating tissue repair (12). Previous research has shown that experimental infection of *Necator Americanus* in humans can induce a Th2 immune response and inhibit the expression of IFN-γ and IL-17A, thereby alleviating inflammation in patients with celiac disease (13). A variety of worm-derived molecules, including proteins, lipids, and enzymes, have been identified as potentially exerting multiple immune-regulatory functions in different inflammatory disease models (14). Consequently, the iatrogenic "worm therapy" holds promise for treating diseases caused by immune system disorders, including IBD (15, 16), and opens up new avenues for the development of intervention methods for inflammatory diseases.

Nippotrongylus brasiliensis (*N. brasiliensis*, Nb) has a life cycle and pathogenic symptoms similar to those of human hookworms and is often used as an ideal model for hookworm research (17). Previous studies have found that Nb infection can trigger an immune response resembling the characteristics of type II response in human hookworm infections, including enhanced CD4+T cell dependent IgE production, eosinophilia, and mastocytosis (18). Relevant research has determined that NB-DNase II, a small molecule derived from Nb, could modulate

innate immune responses and the development of dendritic cells, thereby activating regulatory T cells (Tregs) (19). Therefore, screening and analyzing molecules from Nb-derived products could be a novel strategy for devising therapeutic methods for inflammatory diseases. Our previous studies have screened out 10 active molecules with anti-inflammatory effects from 45 metabolites of ES (excretory and secretory products) (20). ES, being the main product of adult Nb parasitism in the host intestine, has been found to inhibit ovalbumin-induced mouse asthma (21). In our previous study, we used ultra-performance liquid chromatography-mass spectrometry (UHPLC-MS) to perform untargeted metabolomics analysis on the intestinal contents of mice infected with Nb and ES from Nb-derived products. We found that the content of uridine increased significantly compared to the normal control (20). Uridine is an essential pyrimidine nucleoside for RNA synthesis and participates in several crucial metabolic processes (22). According to relevant research reports, uridine has shown certain protective effects in multiple animal models of inflammatory diseases (23, 24). Additionally, our previous study also demonstrated that Nb-derived uridine screened from ES can exert anti-inflammatory and anti-atherosclerotic effects *in vitro* and *in vivo* against atherosclerosis (25). Therefore, hookworm infection can regulate the host's immune response to effectively mitigate the progression of autoimmune diseases, presenting a new approach for the development of IBD interventions based on hookworms.However, it is still necessary to verify whether IBD, as a classic inflammatory disease, can be intervened by ES or uridine.

In this study, we established the protective and anti-inflammation effect of Nb infection and ES intervention in a TNBS-induced IBD mouse model and further validated the efficacy of uridine screened from ES. We also conducted an RNA sequencing (RNA-Seq) analysis to identify differentially expressed genes in mice intervened with ES or uridine. Based on these findings, we elucidated the possible functional mechanisms responsible for the protective and anti-inflammation effects of ES or uridine administration in IBD mice, aiming to provide therapeutic targets for the immunotherapy of IBD.

2 Materials and methods

2.1 Animals, parasites and ethical statement

Sprague Dawley rats (male, 300 g) and C57BL/6 mice (8 weeks old, female) were provided by the Animal Center of Jiangsu Institute of Parasitic Diseases (JIPD, Wuxi, China). The Nb was donated by Professor Alex Loukas at James Cook University and has been stored and maintained in our laboratory for approximately seven years. All rats and mice were acclimated to the feeding environment for one week before being used in the experiment. Normal feeding was maintained during the experiment to ensure a favorable living environment for the animals. The Ethical Committee of the JIPD approved all experimental work involving animals (accession numbers: JIPD-2020-007 and JIPD-2021-001). All animals used in this study were housed in a standard environment with a temperature ranging from 21°C to 25°C, a humidity level of 60% to 65%, a 10 to 14-hour light–dark cycle, and unrestricted access to food and water.

2.2 Nb culture and ES preparation

Approximately 3500 L3 stage larvae were subcutaneously injected into rats. Rat feces were collected after infection until the 9th day. A mixture of 5 μg/mL amphotericin solution, carbon powder, and corn cob padding was added to the feces, which was then transferred to the absorbent paper in a culture dish for cultivation at 26°C. After 1 week, larvae were observed migrating to the edge of the culture dish. These larvae were collected and washed in PBS. The infection process was repeated. On day 7 post-infection, adult worms were collected from the small intestines of infected rats and used for ES production according to our previous method (20, 25). The suspension was transferred to a sterile 50-mL centrifuge tube and washed twice with Dulbecco's phosphate-buffered saline (DPBS) containing antibiotic antimycotic (Gibco-Thermo Fisher, Waltham, MA, USA) and then transferred into a flat bottom 24-well plate and cultured for 7 days in RPMI-1640 medium (Gibco-Thermo Fisher) at 37°C and 5% CO_2. The culture supernatant was collected and replaced with fresh medium every 24 hours. After centrifugation at 2,000 g and filtration through a 0.22 mm filter to remove eggs, parasite fragments and remaining solution, the final excretory-secretory products (ES) were obtained and stored at −80 °C for later use.

2.3 IBD modeling and protective efficacy evaluation by Nb and its derived products

Due to its advantages of easy induction and good reproducibility, 2, 4, 6-Trinito-benzene-sulfonic acid (TNBS) is widely used in the study of the pathogenesis of IBD and the screening of potential therapeutic drugs, as it possesses similar immunological and histopathological features to human IBD (26). A total of 24 C57BL/6 mice were randomly divided into four groups, including normal control group (NC group), TNBS modeling group (TNBS group), Nb infection in TNBS model (Nb + TNBS group), and ES intervention in TNBS model (ES + TNBS group), with 6 mice in each group for validating Nb and ES in IBD. Mice in the ES group were orally administered 200 μL of ES daily for 7 days before modeling, while mice in the Nb group were subcutaneously injected with 500 Nb L3 stage larvae on day 5 before modeling. Except for the NC group, mice in other groups were perfused with a 40 mg/mL TNBS (Sigma-Aldrich, MO, USA) solution through the rectum (100 μL per mouse) for IBD modeling on day 0. Body weight was recorded daily, and the

mice were euthanized on the other 5th day. The colon was separated and removed for subsequent measurement (Figure 1A).

For Nb derived uridine assessment experiment, an additional 18 C57BL/6 mice were randomly allocated into three groups (with 6 mice in each group), including the NC group, TNBS group, and uridine intervention in TNBS model (U + TNBS group). Mice in U + TNBS group were orally gavaged with 10 mg/kg of uridine on a daily basis for 7 days prior to the modeling process. On day 0, mice in both the TNBS group and Uridine group underwent colitis induction with 100 μL of a 40 mg/mL TNBS solution by rectal enema. The body weight and activity of each mouse were monitored daily starting from the commencement of the experiment. On the 5th day after TNBS administration, all mice were euthanized and the colon was removed for subsequent measurement (Figure 2A).

2.4 Inflammatory-related cytokines detection

For the detection of cytokine levels detection, approximately 1 cm from the bottom of the colon was excised, washed with PBS and homogenized in PBS on ice. Then, an equal volume of RIPA buffer containing protease inhibitors was added, and the tissue was lysed at room temperature for 30 minutes with gently agitated throughout the lysis process. After centrifugation to remove sediment, the total protein concentration of supernatant from colonic tissue was quantified by BCA assay (Absin, Shanghai, China). The detection of cytokines in the mouse colon was carried out using TNF-α/IL-1β/IL-6 (Absin, Shangai, China) and IL-10 ((Solarbio, Beijing, China) ELISA kits according to the instructions (intra- and inter-assay CVs were less than 10%).

2.5 Histological analysis

After euthanizing all the mice, the colon was dissected and washed with PBS to remove the feces. Approximately 1 cm of the distal colon was collected and then immersed in 4% paraformaldehyde overnight for fixation. The colon tissue was sectioned using a semiautomatic microtome (RM2235, Leica, Wetzlar, Germany) and stained with hematoxylin-eosin (HE) solution after being embedded in paraffin. The tissue sections were observed under a microscope (BX63, Olympus, Tokyo, Japan) and scored according to the following grading criteria: 0, no inflammatory; 1, slight leukocyte infiltration, with visible infiltration less than 10% under high magnification and no structural changes; 2, moderate leukocyte infiltration, with the infiltration area being 10% to 25%, crypt elongation, and the

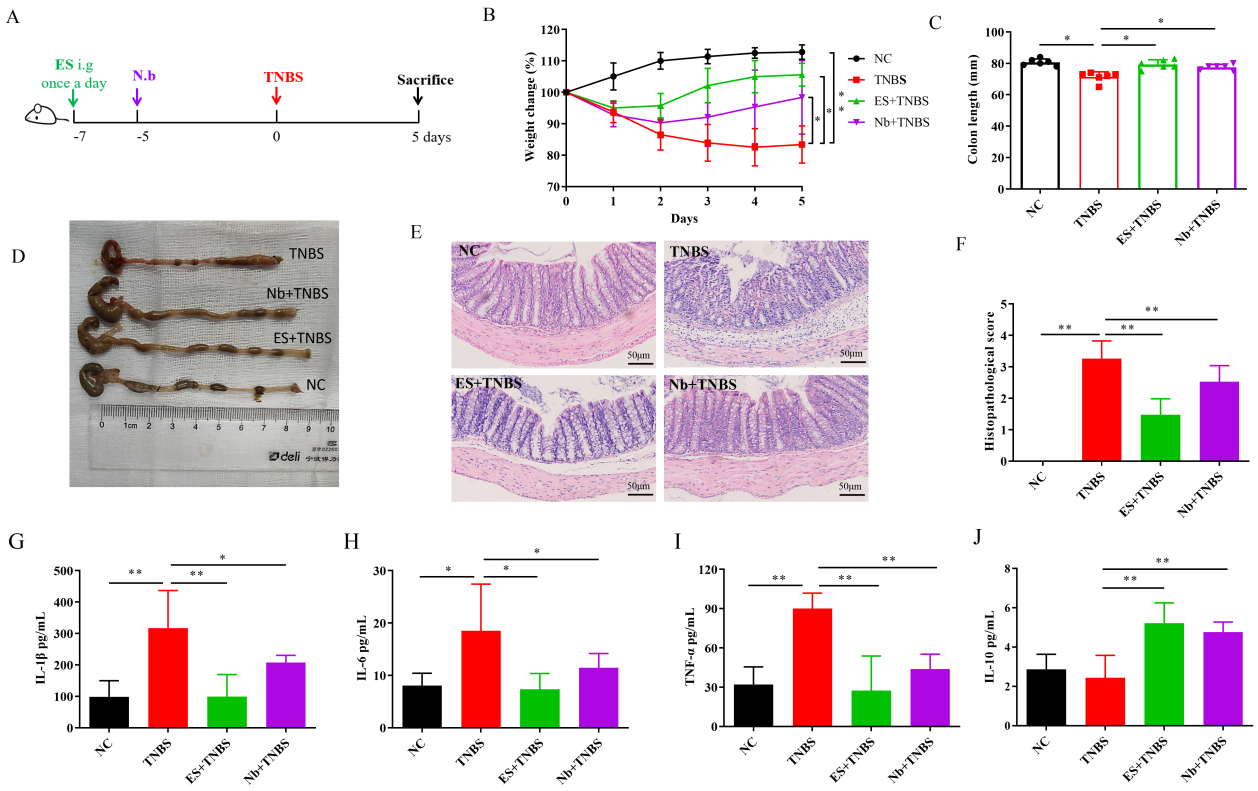

FIGURE 1
Nb infection and ES intervention confer protection against TNBS-induced IBD in mice (n=6). **(A)** Schematic illustration of the experimental design of Nb and ES administration in IBD model. **(B)** Changes in body weight over 5 days in comparison with the modeling day. **(C, D)** Comparative and statistical analysis of colon length. **(E)** Transverse section of the mouse colon stained with HE (under 400× magnification). **(F)** Histological score of colon. **(G–J)** Levels of inflammatory-related cytokines in the colon following Nb infection and ES intervention in mice including IL-1β, IL-6, TNF-α and IL-10 (n = 6). * and ** means $p < 0.05$ and 0.01, respectively.

thickening of the intestinal wall not exceeding the mucosal layer and no ulcers; 3, high leukocyte infiltration, with the infiltration area being 25% to 50%, crypt elongation, thickening of intestinal wall, and appearance of superficial ulcers; 4, diffuse leukocyte infiltration, with the infiltration area exceed 50%, crypt elongation and curvature, thickening of intestinal wall, and occurrence of extensive ulcers.

2.6 RNA sequencing and RT-qPCR analysis for colon tissues

Colon samples of mice were randomly selected from the TNBS group, ES+TNBS group and Uridine +TNBS group for RNA sequencing (RNA-Seq) analysis. Firstly, RNA was extracted and then subjected to agarose gel electrophoresis and a microplate reader for quantitative quality inspection to determine the purity and integrity of RNA samples. Secondly, mRNA was enriched using magnetic beads with Oligo dT (Thermo Fisher Scientific, MA, USA) and then randomly fragmented by fragmentation buffer (Agilent Technologies, CA, USA). Using the above mRNA as a template, the first strand of cDNA was synthesized by random hexamers primers (Thermo Fisher), followed by the addition of buffer, dNTPs, and DNA polymerase I (Qiagen, Germany) to synthesize the second strand of cDNA. Finally, the double stranded cDNA was purified via AMPure XP beads (Beckman Coulter, CA, USA). The purified double stranded cDNA was subjected to terminal repair, followed by the addition of an A tail and ligation of sequencing adapters. Then, fragment size selection was performed using AMPure XP beads, and finally PCR enrichment was performed to construct a cDNA library. The constructed library was sequenced using the Illumina HiSeq™ platform (Illumina, CA, USA) to obtain raw reads, and subsequent bioinformatics analysis was based on clean reads, which were obtained by removing reads containing adapters, low-quality, and uncertain base from raw reads. Clean reads were aligned with the reference genome through HISAT2 software, and the FPKM values of gene expression in each sample were calculated via feature Counts software. Finally, differentially expressed genes from ES+TNBS group and Uridine +TNBS group were screened based on the corrected p value (< 0.05) and log2foldchange (> 1) when compared to that in the TNBS group. Additionally, a comparative analysis between the differentially expression genes

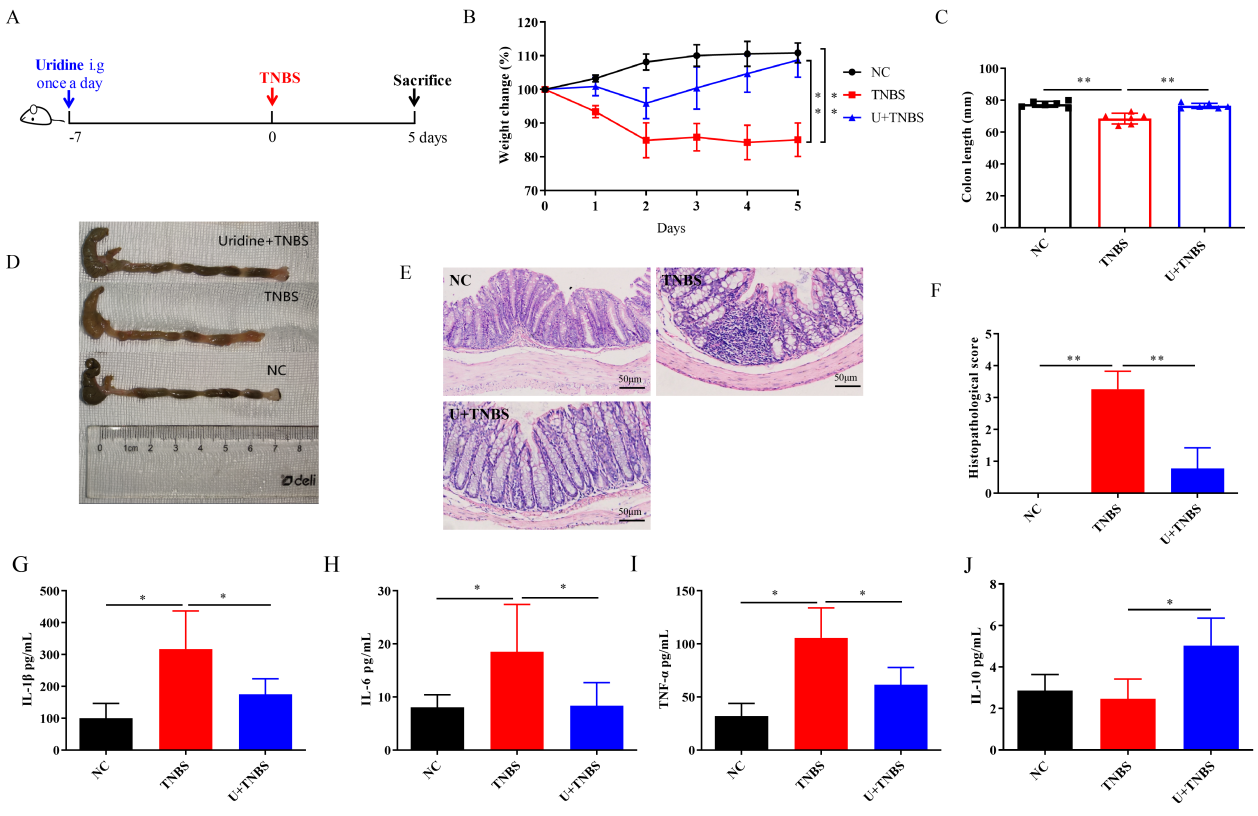

FIGURE 2
Uridine intervention confers protection against TNBS-induced IBD in mice (n=6). **(A)** Schematic illustration of the experimental design of uridine administration in IBD model. **(B)** Changes in body weight over 5 days in comparison with the modeling day. **(C, D)** Comparative and statistical analysis of colon length. **(E)** Transverse section of the mouse colon stained with HE (under 400× magnification). **(F)** Histological score of colon. **(G–J)** Levels of inflammatory-related cytokines in the colon following uridine intervention in mice including IL-1β, IL-6, TNF-α and IL-10 (n = 6). * and ** means p < 0.05 and 0.01, respectively.

from ES+TNBS group and Uridine+TNBS group was conducted. Further, the overlapping genes were selected for KEGG signaling pathway enrichment analysis to determine the most significantly top 20 among them.

For further confirmation of the potential target genes (obtained above) for uridine, another 1 cm colon samples from all groups were collected and stored at −80°C for further mRNA expression levels detection by reverse transcription-PCR (RT-PCR) using Applied Biosystems QuantStudio7 Pro (Thermo Fisher). Primers are shown in Table 1. RNA was extracted by the FastPure Complex Tissue/Cell Total RNA Isolation Kit (Vazyme, Nanjing, China), and its concentration was measured via NanoDrop2000 (Gibco-Thermo Fisher). Reverse transcription was performed according to the HiScript IV All-in-One Ultra RT SuperMix for qPCR (Vazyme, Nanjing, China) and the reaction system was operated by HiScript IV All-in-One Ultra RT SuperMix for qPCR (Vazyme, Nanjing, China). The reaction conditions contained pre-denaturation (95°C for 300 s) and 40 denaturation cycles (95°C for 10 s, 60°C for 30 s) and dissolution curve (95°C 15 s, 60°C 60 s, 95°C 15 s).

2.7 Mechanism exploration for uridine in alleviating IBD

As observed in the RNA sequencing and RT-qPCR analysis above, the gene, *slc10a*, was selected as a potential target of uridine, which encodes Apical Sodium-Dependent Bile Acid Transporter (ASBT) and can be inhibited by Linerixibat (GSK2330672). To explore the *in vivo* mechanism of uridine's action, the group intervened with both uridine and GSK2330672 in TNBS model (U + TNBS + GSK group) was added in this part. Mice in this group were orally gavaged with 100 μL of GSK2330672 at a concentration of 10 mg/kg twice a day for 7 days (27). The experimental procedures for the other groups remained unchanged (Figure 4A). Cytokine detection and histological analysis were also conducted following the methods described above in sections 2.4 and 2.5.

2.8 Statistically analysis

The statistical analysis was performed using IBM SPSS 22 Statistics (IBM Corporation, Armonk, NY, USA). One-way ANOVA and independence *t*-test were employed to compare means and determine statistical differences between different conditions. *p* values were denoted as * $p < 0.05$ and ** $p < 0.01$ to indicate significant differences.

TABLE 1 Primers used in present study.

Genes	Primers (5′-3′)
slc10a2-F	TAGATGGCGACATGGACCTCA
slc10a2-R	CCCGAGTCAACCCACATCTTG
β-actin-F	TGACGTTGACATCCGTAAAGACC
β-actin-R	CTCAGGAGGAGCAATGATCTTGA

3 Results

3.1 Protective effects of Nb infection and ES intervention against TNBS-induced IBD

Compared with the NC group, mice in the TNBS group exhibited a significant reduction in body weight after modeling. Both Nb infection and ES intervention effectively mitigate the weight loss induced by TNBS in the IBD model (Figure 1B, $p < 0.05$). The colon length in the TNBS group was significantly shorter than that in the NC group, however, the shortening was less pronounced in both the Nb + TNBS and ES + TNBS group (Figures 1C, D, $p < 0.05$). In contrast to the NC group, TNBS treatment caused severe pathological damage, including structural destruction of colonic crypts, loss of goblet cells, and significant inflammatory infiltration. In the Nb + TNBS group and ES + TNBS group, the epithelial layer and crypt structure were clearly visible, with reduced infiltration (Figure 1E) resulting in a significant increase in the pathological score (Figure 1F, $p < 0.01$).

The levels of pro-inflammatory cytokines, such as IL-1β, IL-6, and TNF-α, in the colon tissue of the TNBS group, were significantly higher than those in the NC group (Figures 1G, I, $p < 0.05$ or < 0.01). After Nb infection or ES intervention, the levels of those pro-inflammatory cytokines were significantly reduced compared to the TNBS group (Figures 1G, I, $p < 0.05$ or < 0.01). The level of anti-inflammatory cytokine IL-10 was significantly increased in the Nb + TNBS and ES + TNBS group compared to the TNBS group, while no significant changes were observed in the TNBS group compared to the NC group (Figure 1J, $p < 0.01$). These results indicated that Nb infection and ES intervention could alleviate the progression of IBD by inhibiting the inflammatory responses in TNBS-induced IBD mouse model.

3.2 Protective effects of Nb-derived uridine against TNBS-induced IBD

As previously reported, uridine, a metabolite from adult Nb, is the major component of ES products and has demonstrated good anti-inflammatory activity both *in vitro* and *in vivo* (21). However, it protective effect on TNBS-induced IBD remains to be further explored. As shown in Figure 2, uridine intervention effectively alleviate the weight loss caused by TNBS-induced IBD in mice (Figure 2B, $p < 0.01$). The colon length of the TNBS group was significantly shorter than that in the NC group, and severe edema and bleeding were observed in the colon tissue (Figures 3C, D, $p < 0.01$). The degree of colon injury in the U + TNBS group was significantly improved compared to that in the TNBS group (Figures 2C, D, $p < 0.01$). Compared with the TNBS group, the U + TNBS group exhibited less pathological damage with a more intact colonic epithelial layer and crypt structure (Figures 2E, F, $p < 0.01$).

Regarding the levels of inflammatory-related cytokines in colon tissues, uridine intervention reduce the upregulation of pro-inflammatory cytokine levels caused by TNBS induced IBD, including IL-1β, IL-6, and TNF-α (Figures 2G, I, $p < 0.05$), and

promoted the expression of IL-10 in mice colon (Figure 2J, $p < 0.05$). These results indicated that uridine could also exert a protective effect against TNBS induced IBD in mice by reducing the pro-inflammatory response and enhancing anti-inflammatory efficiency.

3.3 Association between slc10a2 expression and uridine's protective effect against TNBS-induced IBD

To explore the possible mechanism underlying uridine's protective effect against IBD, RNA-Seq technology was used to screen and identify downstream target genes. In this study, four colon samples from the TNBS group, ES+TNBS group and U+TNBS group were selected for RNA-Seq analysis. Compared with the TNBS group, the distribution of differentially expressed genes in U + TNBS group was visualized using a heat map and a volcano plot. A total of 15 differentially expressed genes were identified, among which *slc10a2*, *zc3h6*, *gapdh*, *edn3*, and *iglv2* were significantly upregulated (Figures 3A, B).

Based on the analysis of differentially expressed genes, KEGG signaling pathway enrichment analysis was performed to determine the top 20 most significantly enriched signaling pathways. The results showed that the differentially expressed genes in the U + TNBS group were mainly enriched in antigen processing and presentation, protein processing in the endoplasmic reticulum, MAPK signaling pathway, bile secretion, estrogen signaling pathway, and IL-17 signaling pathway (Figure 3C). Furthermore, a comparative analysis between the differentially expression genes from ES+TNBS group and U+TNBS group was conducted, only two genes, *slc10a* and *edn3*, were upregulated in the both sets of comparisons (Figure 3A; Supplementary Figures S1, S2). A more in-depth investigation showed that *slc10a2* encodes the Apical Sodium-dependent Bile Acid Transporter (ASBT), which is closely associated with the bile acids transportation (28). The bile acid signaling pathway plays a pivotal role in regulating intestinal immunity and the microbial flora, making it a promising therapeutic target for IBD (29). The gene expression level of *slc10a2* was further verified by using RT-qPCR. It was significantly upregulated after ES and uridine interventions

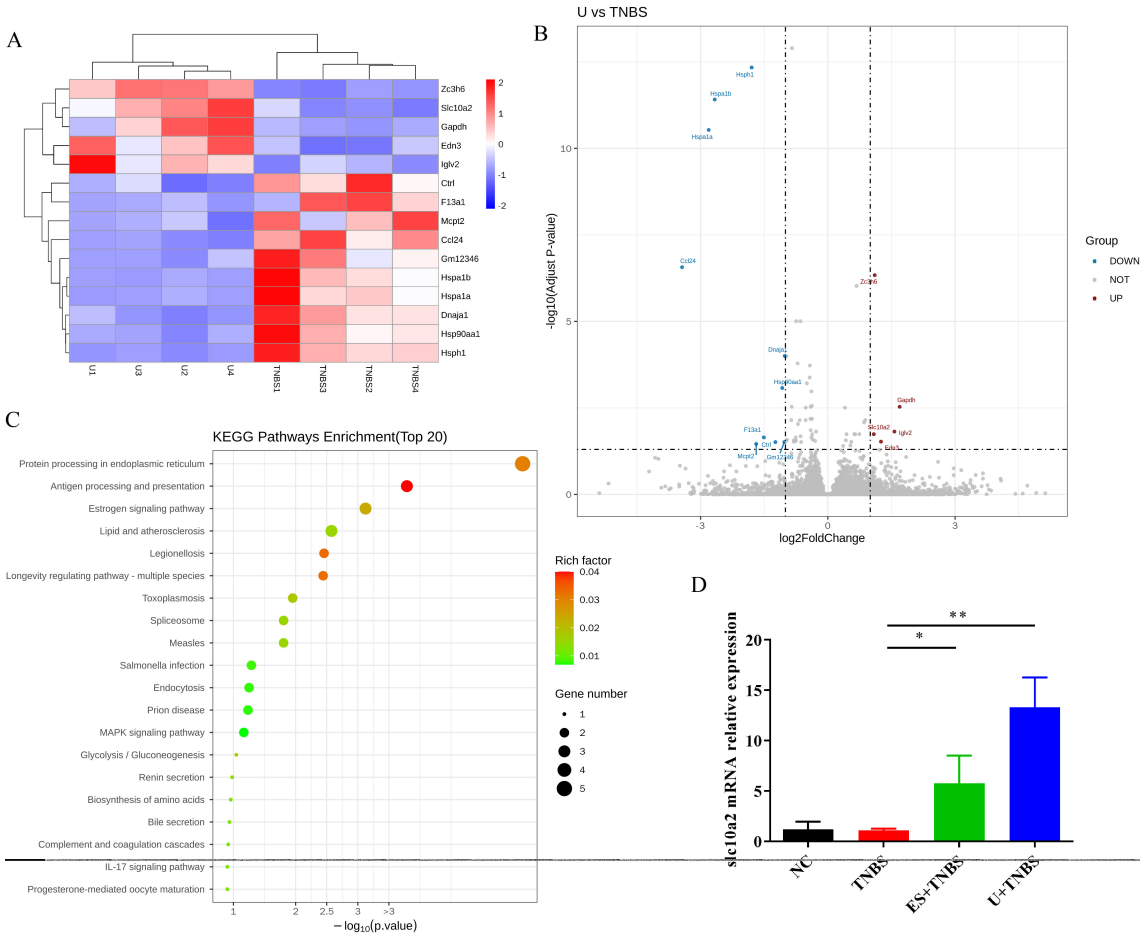

FIGURE 3
RNA-Seq analysis of colon tissue between TNBS and uridine group. **(A)** Cluster diagram of differentially expressed genes between TNBS and uridine group ($n \geq 3$). **(B)** Volcanic map of differential gene expression distribution. **(C)** KEGG enrichment bubble plot of differentially expressed genes. **(D)** Colon mRNA relative expression of *slc10a2* by RT-qPCR ($n \geq 6$).

compared to the TNBS group (Figure 3D, $p < 0.05$ and < 0.01, respectively). Based on this evidence, it was speculated that the expression of *slc10a2* might be associated with the protective effect of uridine against TNBS-induced IBD.

3.4 Importance of apical sodium dependent bile acid transporter in uridine's protective effect against TNBS-induced IBD

As mentioned above, *slc10a2* encodes ASBT, which can be inhibited by Linerixibat (GSK2330672). To further investigate the role of *slc10a2* expression in uridine's protective effect against TNBS-induced IBD, an animal experiment was conducted. The results showed that, compared with the Uridine + TNBS group, the addition of inhibitor intervention failed to alleviate intestinal damage and weight loss (Figures 4B, C, $p < 0.05$). Moreover, that addition of inhibitor intervention maintained the intestinal impair caused by TNBS (Figure 4D, $p < 0.05$). Histological findings indicate that, compared to the Uridine + TNBS group, the addition of the inhibitor intervention did not reduce histological damage; instead, it led to a higher pathological score (Figures 4E, F, $p < 0.01$). Additionally, the addition of inhibitor intervention to the Uridine + TNBS group upregulated the levels of IL-1β and TNF-α (Figures 4G, I, $p < 0.05$), while no significant changes were observed in levels of IL-6 and IL-10 (Figures 4H, J). Collectively, these results suggest that specific inhibition of ASBT can counteract the anti-inflammatory effect and the protective effect of uridine against TNBS-induced IBD.

4 Discussion

The small molecules present in the excrement and secretions of adult hookworms parasitizing in the host's small intestine play a crucial role in the host-pathogen interaction. Previous metabolomics studies have revealed that non-protein small molecule metabolites derived from Nb possess anti-inflammatory bioactivity, which makes them worthy of further exploration as a novel strategic approach for treating inflammatory diseases (30, 31). This study demonstrated that uridine, a highly expressed metabolite screened from ES products, can protect against TNBS-induced IBD in mice (21). Through RNA sequencing analysis of the colons, it was found that *slc10a2* was highly expression after uridine intervention. By specifically inhibiting the encoded protein, ASBT, and observing its impact on the protective efficacy, the underlying mechanism of uridine's protection in IBD was further investigated. We speculated

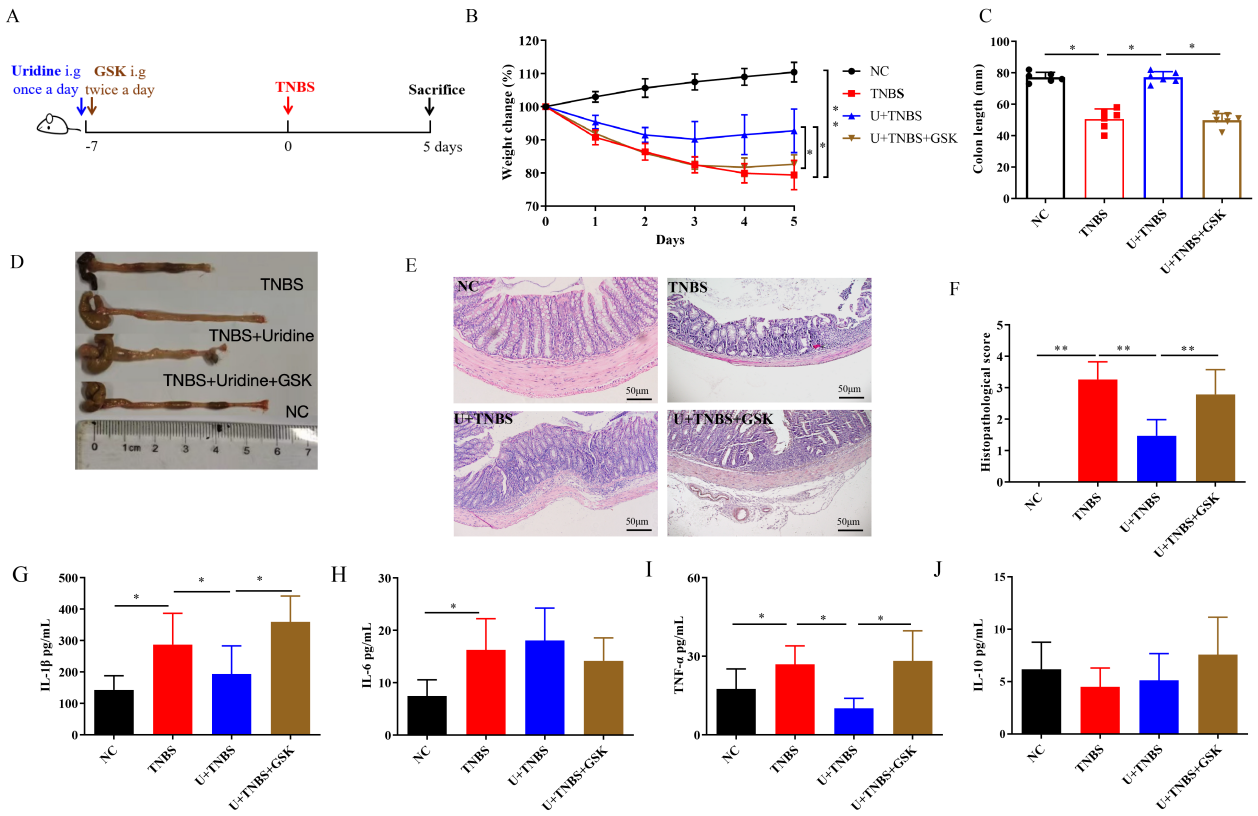

FIGURE 4
The inhibition of *slc10a2* attenuated the protective effect of uridine against TNBS-induced IBD in mice (n=6). **(A)** Schematic illustration of the experimental design in IBD model. **(B)** Changes in body weight over 5 days in comparison with the modeling day. **(C, D)** Comparative and statistical analysis of colon length. **(E)** Transverse section of the mouse colon stained with HE (under 400× magnification). **(F)** Histological score of colon. **(G–J)** Levels of inflammatory-related cytokines in the colon following uridine and GSK intervention in mice including IL-1β, IL-6, TNF-α and IL-10 (n=6). * and ** means $p < 0.05$ and 0.01, respectively.

that ASBT could be an effective therapeutic target for uridine to achieve anti-inflammatory and protective functions in TNBS-induced IBD. However, further experimental verification is needed in the future.

The TNBS-induced colitis model exhibits classic immunological and histopathological characteristics reminiscent of human IBD, and is widely used of IBD pathogenesis and the screening of potential therapeutic agents (26). This model typically causes symptoms such as diarrhea, reduced food intake, and weight loss in mice (26). Inflammatory bowel disease (IBD) and many other inflammatory disorders are characterized by elevated expression of pro-inflammatory cytokines, such as TNF-α, IL-6 and IL-1β (32). The increased secretion of those pro-inflammatory cytokines can disrupt the tight junction barrier in the intestinal epithelium, leading to increase epithelial permeability and exacerbating the inflammatory cascade. Conversely, IL-10 plays a crucial role in suppressing intestinal mucosal damage and inflammation (33, 34). In this study, both Nb infection and ES intervention effectively mitigated the histopathological lesions, body weight decline, and reduction in pro-inflammatory cytokines levels induced by IBD in mice. Given the metabolomic analysis of uridine in ES, we further evaluated the protective efficacy of ES intervention and the correlation between its component uridine in the subsequent experiments.

Uridine is essential for maintaining cellular function and energy metabolism, and has been widely used to alleviate cell toxicity and enhance neurophysiological function (35, 36). It has been shown to have anti-inflammatory effects in various experimental animal models, such as those of asthma, pneumonia, and arthritis. These effects are achieved by inhibiting the secretion of pro-inflammatory cytokines and relieving related symptoms (23, 24, 37). Our previous research screened uridine from the excretory and secreted products of Nb and further investigated its therapeutic effects on inflammatory diseases like atherosclerosis (25). Uridine was found to have anti-inflammatory and anti-atherosclerotic effects both *in vitro* and *in vivo*, making it a key metabolite in ES products (25). In this study, we found that the prophylactic administration of uridine, screened from ES, in the IBD mouse model significantly ameliorate the progression of IBD and reduced damage to the colon tissue. The uridine-treated group showed a decrease in the expression of pro-inflammatory factors and an increase in anti-inflammatory factors. These results were consistent with those from another dextran sulfate sodium (DSS)-induced colitis model, in which colonic instillation of uridine effectively protected against inflammation by regulating inflammatory cytokines in local tissues and circulation (38). Collectively, these studies suggest that uridine, as a small molecule selected from ES products, can be considered the main active molecule in ES for the treatment of IBD in mice.

High-throughput RNA sequencing can comprehensively obtain the complete information of all mRNA in the required tissues and organs under specific conditions, and is a novel technique for studying gene transcription and regulatory characteristics. In this study, based on a portion of the RNA-seq data, it was hypothesized that the therapeutic effect of uridine on Inflammatory Bowel Disease (IBD) might be related to several upregulated genes. Among them, *slc10a2* was identified, which is closely related to bile acid transport (28). Through the bile acid signaling pathway, the Apical Sodium-Dependent Bile Acid Transporter (ASBT) encoded by *slc10a2* can inhibit inflammation, stimulate the production of anti-inflammatory factors, and promote the regeneration of the epithelial barrier, making it a potential therapeutic target for IBD (29). Some other studies have also shown that the therapeutic effect of glucocorticoids in IBD can be partially attributed to the increased expression of ASBT (39). To verify the potential molecular mechanism of uridine's therapeutic effect on IBD, specific and irreversible blockade of ASBT was carried out. With the addition of the inhibitor, uridine intervention failed to alleviate the pathological damage in enteritis, and no significant difference was detected in the expression of pro-inflammatory cytokines compared with the TNBS group. These results indicated that blocking ASBT could lead to the failure of uridine to protect against the pathological damage of enteritis and control inflammation.

There were some limitations in this study. ES, as the main product from Nb, is a complex composed of soluble proteins, small molecules, and extracellular vesicles (20). Although uridine could exert similar anti-inflammatory and protective effects in this study, it cannot fully represent the full efficacy of ES that further research is still needed on other components. Meanwhile, uridine itself has certain pharmacological effects that further verification is also necessary to determine the probable synergistic effects of other components together in ES.

5 Conclusion

In conclusion, this study demonstrated that uridine exerts potential therapeutic and anti-inflammatory effects on Inflammatory Bowel Disease (IBD) through the modulation of *slc10a2*. These findings not only deepen our understanding of IBD pathogenesis but also provide a novel therapeutic target for future IBD interventions. However, further studies are warranted to elucidate the detailed molecular mechanisms of uridine-mediated *slc10a2* regulation and to evaluate its therapeutic efficacy and safety in clinical settings.

Data availability statement

The datasets presented in this study can be found in online repositories. The names of the repository/repositories and accession number(s) can be found in the article/Supplementary Material.

Ethics statement

The animal studies were approved by The Ethical Committee of the Jiangsu Institute of Parasitic Diseases. The studies were

conducted in accordance with the local legislation and institutional requirements. Written informed consent was obtained from the owners for the participation of their animals in this study.

Author contributions

CY: Methodology, Validation, Writing – original draft. QW: Validation, Writing – original draft. YC: Writing – original draft, Validation. XD: Writing – original draft, Writing – review & editing. QZ: Formal Analysis, Writing – original draft. JY: Investigation, Writing – original draft. BZ: Writing – original draft, Data curation. YD: Writing – review & editing, Supervision, Writing – original draft, Conceptualization, Funding acquisition, Project administration. HB: Visualization, Writing – original draft, Conceptualization.

Funding

The author(s) declare that financial support was received for the research and/or publication of this article. This research was funded by the Jiangsu Province Capability Improvement Project through Science, Technology and Education (No. ZDXYS202207). It is a plan formulated to further improve the innovation of health science and technology during the 14th Five Year Plan period, comprehensively enhance the level and innovation capability of health science and technology in Jiangsu Province, and better support the high-quality development of the province's health industry and biopharmaceutical industry. This research was simultaneously funded by the Scientific Research Program of Wuxi Health Commission (M202221, M202302).

Conflict of interest

The authors declare that the research was conducted in the absence of any commercial or financial relationships that could be construed as a potential conflict of interest.

Generative AI statement

The author(s) declare that no Generative AI was used in the creation of this manuscript.

Publisher's note

Supplementary material

The Supplementary Material for this article can be found online at: https://www.frontiersin.org/articles/10.3389/fimmu.2025.1600838/full#supplementary-material

SUPPLEMENTARY FIGURE S1
Cluster diagram of differentially expressed genes between TNBS and ES group ($n \geq 3$).

SUPPLEMENTARY FIGURE S2
RNA-Seq analysis of colon tissue between TNBS and ES group. **(A)** Volcanic map of differential gene expression distribution. **(B)** KEGG enrichment bubble plot of differentially expressed genes. ($n \geq 3$).

References

1. Collaborators, G.I.B.D. The global, regional, and national burden of inflammatory ibowel disease in 195 countries and territories, 1990–2017: a systematic analysis for the Global Burden of Disease Study 2017. *Lancet Gastroenterol Hepatol.* (2019) 5:17–30. doi: 10.1016/S2468-1253(19)30333-4

2. Ng SC, Shi HY, Hamidi N, Underwood FE, Tang W, Benchimol EI, et al. Worldwide incidence and prevalence of inflammatory bowel disease in the 21st century: a systematic review of population-based studies. *Lancet.* (2017) 390:2769–78. doi: 10.1016/S0140-6736(17)32448-0

3. Luo H, Cao G, Luo C, Tan D, Vong CT, Xu Y, et al. Emerging pharmacotherapy for inflammatory bowel diseases. *Pharmacol Res.* (2022) 178:106146. doi: 10.1016/j.phrs.2022.106146

4. Lal S, Kandiyal B, Ahuja V, Takeda K, Das B. Gut microbiome dysbiosis in inflammatory bowel disease. *Prog Mol Biol Transl Sci.* (2022) 192:179–204. doi: 10.1016/bs.pmbts.2022.09.003

5. Subramanian A, Jahabardeen A, Thamaraikani T. Vellapandian, Chitra. More on the interplay between gut microbiota, autophagy, and inflammatory bowel disease is needed. *World J Gastroenterol.* (2024) 30:3356–60. doi: 10.3748/wjg.v30.i27.3356

6. AnandB P, Sunita J. Treatment of inflammatory bowel disease BID. *Pharmacol Rep.* (2011) 63:629–42. doi: 10.1016/s1734-1140(11)70575-8

7. Nadeem MS, Kumar V, Al-Abbasi FA, Kamal MA, Anwar F. Risk of colorectal cancer in inflammatory bowel diseases. *Semin Cancer Biol.* (2020) 64:51–60. doi: 10.1016/j.semcancer.2019.05.001

8. Sanya RE, Nkurunungi G, Andia Biraro I, Mpairwe H, Elliott AM. A life without worms. *Trans R Soc Trop Med Hygiene.* (2017) 111:3–11. doi: 10.1093/trstmh/trx010

9. Osada Y, Shimizu S, Kumagai T, Yamada S, Kanazawa T. Schistosoma mansoni infection reduces severity of collagen-induced arthritis via down-regulation of pro-inflammatory mediators. *Int J Parasitology.* (2009) 39:457–64. doi: 10.1016/j.ijpara.2008.08.007

10. Croese J, Giacomin P, Navarro S, Clouston A, McCann L, Dougall A, et al. Experimental hookworm infection and gluten microchallenge promote tolerance in celiac disease. *J Allergy Clin Immunol.* (2015) 135:508–516.e505. doi: 10.1016/j.jaci.2014.07.022

11. TG M, Nieuwendijk R, De Man J, De Winter B, Herman A, Van Marck E, et al. Concurrent infection with Schistosoma mansoni attenuates inflammation induced changes in colonic morphology, cytokine levels, and smooth muscle contractility of trinitrobenzene sulphonic acid induced colitis in rats. *Gut.* (2004) 53:99–107. doi: 10.1136/gut.53.1.99

12. Loukas A, Hotez PJ, Diemert D, Yazdanbakhsh M, McCarthy JS, Correa-Oliveira R, et al. Hookworm infection. *Nat Rev Dis Primers.* (2016) 2:16088. doi: 10.1038/nrdp.2016.88

13. Sestak K, McSorley HJ, Gaze S, Daveson J, Jones D, Anderson RP, et al. Suppression of inflammatory immune responses in celiac disease by experimental hookworm infection. *PloS One.* (2011) 6:e24092. doi: 10.1371/journal.pone.0024092

14. Lothstein KE, Gause WC. Mining helminths for novel therapeutics. *Trends Mol Med.* (2021) 27:345–64. doi: 10.1016/j.molmed.2020.12.010

15. Zhao Y, Zhang S, Jiang L, Jiang J, Liu H. Preventive effects of Schistosoma japonicum ova on trinitrobenzenesulfonic acid-induced colitis and bacterial

translocation in mice. *J Gastroenterology Hepatology*. (2009) 24:1775–80. doi: 10.1111/j.1440-1746.2009.05986.x

16. Summers RW, Elliott D, Urban J Jr., Thompson R, Weinstock J. Trichuris suis therapy in Crohn's disease. *Gut*. (2005) 54:87–90. doi: 10.1136/gut.2004.041749

17. Camberis M, Le Gros G, Urban J. Animal Model of Nippostrongylus brasiliensis and Heligmosomoides polygyrus. *Curr Protoc Immunol*. (2003) 19:Unit19.12. doi: 10.1002/0471142735.2003.55.issue-1

18. Bouchery T, Volpe B, Shah K, Lebon L, Filbey K, LeGros G, et al. The Study of Host Immune Responses Elicited by the Model Murine Hookworms Nippostrongylus brasiliensis and Heligmosomoides polygyrus. *Curr Protoc Mouse Biol*. (2018) 7:236–86. doi: 10.1002/cpmo.34

19. Bouchery T, Moyat M, Sotillo J, Silverstein S, Volpe B, Coakley G, et al. Hookworms evade host immunity by secreting a deoxyribonuclease to degrade neutrophil extracellular traps. *Cell Host Microbe*. (2020) 27:277–289.e276. doi: 10.1016/j.chom.2020.01.011

20. Chen Y, Zhang M, Ding X, Yang Y, Chen Y, Zhang Q, et al. Mining anti-inflammation molecules from nippostrongylus brasiliensis-derived products through the metabolomics approach. *Front Cell Infection Microbiol*. (2021) 11:781132. doi: 10.3389/fcimb.2021.781132

21. Trujillo-Vargas CM, Werner-Klein M, Wohlleben G, Polte T, Hansen G, Ehlers S, et al. Helminth-derived products inhibit the development of allergic responses in mice. *Am J Respiratory Crit Care Med*. (2007) 175:336–44. doi: 10.1164/rccm.200601-054OC

22. Guijas C, Montenegro-Burke JR, Warth B, Spilker ME, Siuzdak G. Metabolomics activity screening for identifying metabolites that modulate phenotype. *Nat Biotechnol*. (2018) 36:316–20. doi: 10.1038/nbt.4101

23. Evaldsson C, Rydén I, Uppugunduri S. Anti-inflammatory effects of exogenous uridine in an animal model of lung inflammation. *Int Immunopharmacol*. (2007) 7:1025–32. doi: 10.1016/j.intimp.2007.03.008

24. Luo Y, Chen H, Huang R, Wu Q, Li Y, He Y. Guanosine and uridine alleviate airway inflammation via inhibition of the MAPK and NF-κB signals in OVA-induced asthmatic mice. *Pulmonary Pharmacol Ther*. (2021) 69:102049. doi: 10.1016/j.pupt.2021.102049

25. Zhang Y, Ding X, Yuan C, Yang Y, Zhang Q, Yao J, et al. Anti-Inflammatory Responses Produced with Nippostrongylus brasiliensis-Derived Uridine via the Mitochondrial ATP-Sensitive Potassium Channel and Its Anti-Atherosclerosis Effect in an Apolipoprotein E Gene Knockout Mouse Model. *Biomolecules*. (2024) 14:672. doi: 10.3390/biom14060672

26. Wirtz S, Popp V, Kindermann M, Gerlach K, Weigmann B, Fichtner-Feigl S, et al. Chemically induced mouse models of acute and chronic intestinal inflammation. *Nat Protoc*. (2017) 12:1295–309. doi: 10.1038/nprot.2017.044

27. Wang Y, Matye D, Nguyen N, Zhang Y, Li T. HNF4α Regulates CSAD to couple hepatic taurine production to bile acid synthesis in mice. *Gene Expression*. (2018) 18:187–96. doi: 10.3727/105221618x15277685544442

28. Dawson PA, Haywood J, Craddock AL, Wilson M, Tietjen M, Kluckman K, et al. Targeted deletion of the ileal bile acid transporter eliminates enterohepatic cycling of bile acids in mice. *J Biol Chem*. (2003) 278:33920–7. doi: 10.1074/jbc.M306370200

29. Bromke MA, Krzystek-Korpacka M. Bile acid signaling in inflammatory bowel disease. *Int J Mol Sci*. (2021) 22:9096. doi: 10.3390/ijms22169096

30. Yeshi K, Creek DJ, Anderson D, Ritmejerytė E, Becker L, Loukas A, et al. Metabolomes and Lipidomes of the Infective Stages of the Gastrointestinal nematodes, Nippostrongylus brasiliensis and Trichuris muris. *Metabolites*. (2020) 10:446. doi: 10.3390/metabo10110446

31. Wangchuk P, Shepherd C, Constantinoiu C, Ryan RYM, Kouremenos KA, Becker L, et al. Hookworm-derived metabolites suppress pathology in a mouse model of colitis and inhibit secretion of key inflammatory cytokines in primary human leukocytes. *Infection Immun*. (2019) 87:e00851-18. doi: 10.1128/iai.00851-18

32. Műzes G. Changes of the cytokine profile in inflammatory bowel diseases. *World J Gastroenterology*. (2012) 18:5848–61. doi: 10.3748/wjg.v18.i41.5848

33. Nusrat A, Turner J, Madara J. Molecular physiology and pathophysiology of tight junctions. IV. Regulation of tight junctions by extracellular stimuli: nutrients, cytokines, and immune cells. *Am J Physiol Gastrointest Liver Physiol*. (2000) 279:851–7. doi: 10.1152/ajpgi.2000.279.5.G851

34. Al-Sadi R, Boivin M, Ma T. Mechanism of cytokine modulation of epithelial tight junction barrier. *Front Bioscience*. (2009) 14:2765–78. doi: 10.2741/3413

35. McEvilly M, Popelas C, Tremmel B. Use of uridine triacetate for the management of fluorouracil overdose. *Am J Health-System Pharm*. (2011) 68:1806–9. doi: 10.2146/ajhp100434

36. Mironova GD, Khrenov MO, Talanov EY, Glushkova OV, Parfenyuk SB, Novoselova TV, et al. The role of mitochondrial KATP channel in anti-inflammatory effects of uridine in endotoxemic mice. *Arch Biochem Biophysics*. (2018) 654:70–6. doi: 10.1016/j.abb.2018.07.006

37. d'Acquisto F, Chenna Narendra S, Chalise JP, Magnusson M, Uppugunduri S. Local but not systemic administration of uridine prevents development of antigen-induced arthritis. *PloS One*. (2015) 10:e0141863. doi: 10.1371/journal.pone.0141863

38. Jeengar MK, Thummuri D, Magnusson M, Naidu VGM, Uppugunduri S. Uridine ameliorates dextran sulfate sodium (DSS)-induced colitis in mice. *Sci Rep*. (2017) 7:3924. doi: 10.1038/s41598-017-04041-9

39. Jung D, Fanti A C, Scheurer U, Fried M. Human ileal bile acid transporter gene ASBT (SLC10A2) is transactivated by the glucocorticoid receptor. *GUT*. (2004) 53:78–84. A, K.-U.G. doi: 10.1136/gut.53.1.78

frontiers | Frontiers in Immunology

TYPE Original Research
PUBLISHED 25 September 2025
DOI 10.3389/fimmu.2025.1603385

OPEN ACCESS

EDITED BY
Muhammad Tofazzal Hossain,
Bangladesh Agricultural University, Bangladesh

REVIEWED BY
Katherine Figarella,
University of Texas Health Science Center at Houston, United States
Nataša Radulović,
University of Belgrade, Serbia

*CORRESPONDENCE
Clarissa Prazeres da Costa
Clarissa.dacosta@tum.de

†These authors have contributed equally to this work

RECEIVED 31 March 2025
ACCEPTED 11 September 2025
PUBLISHED 25 September 2025

CITATION
Sternkopf LE, Prodjinotho UF, Gres V, Repgen N, Steiger K, Schluckebier J, Sikasunge CS, Stelzle D, Makasi C, Winkler AS, Ngowi BJ, Villalobos N, Ebner F, Häcker G, Henneke P and Prazeres da Costa C (2025) Helminthic larval stage induces cellular apoptosis via caspase 9-mediated mitochondrial dysfunction.
Front. Immunol. 16:1603385.
doi: 10.3389/fimmu.2025.1603385

Helminthic larval stage induces cellular apoptosis via caspase 9-mediated mitochondrial dysfunction

Leonardo Elias Sternkopf[1,2†], Ulrich Fabien Prodjinotho[1,2†], Vitka Gres[3], Nikolaus Repgen[4], Katja Steiger[5], Julia Schluckebier[1,2], Chummy S. Sikasunge[6], Dominik Stelzle[2], Charles Makasi[7,8], Andrea Sylvia Winkler[2,9,10], Bernard J. Ngowi[8,11], Nelly Villalobos[12], Friederike Ebner[4], Georg Häcker[13], Philipp Henneke[3,14] and Clarissa Prazeres da Costa[1,2,15*]

[1]Institute for Medical Microbiology, Immunology and Hygiene, TUM School of Medicine and Health, Technical University of Munich (TUM), Munich, Germany, [2]Center for Global Health, TUM School of Medicine, Technical University of Munich (TUM), Munich, Germany, [3]Institute for Infection Prevention and Control and Center for Chronic Immunodeficiency (CCI), Medical Center and Faculty of Medicine, University of Freiburg, Freiburg, Germany, [4]Infection Pathogenesis, School of Life Sciences, Technical University of Munich (TUM), Freising, Germany, [5]Institute of Pathology, Technical University of Munich (TUM), Munich, Germany, [6]Department of Paraclinical Studies, School of Veterinary Medicine, University of Zambia, Lusaka, Zambia, [7]Department of Neurology, Kilimanjaro Christian Medical University College, Moshi, Tanzania, [8]National Institute for Medical Research, Muhimbili Research Centre, Dar es Salaam, Tanzania, [9]Department of Neurology, TUM School of Medicine, Technical University of Munich (TUM), Munich, Germany, [10]Department of Community Medicine and Global Health, Institute of Health and Society, Faculty of Medicine, University of Oslo, Oslo, Norway, [11]Mbeya College of Health and Allied Sciences, University of Dar es Salaam, Mbeya, Tanzania, [12]Departamento de Patología, Facultad de Medicina Veterinaria y Zootecnia, Universidad Nacional Autónoma de México (UNAM), Mexico City, Mexico, [13]Institute of Medical Microbiology and Hygiene, Medical Center - University of Freiburg, Faculty of Medicine, University of Freiburg, Freiburg, Germany, [14]Centre for Integrative Biological Signalling Studies, University of Freiburg, Freiburg, Germany, [15]German Center for Infection and Research (DZIF), Munich, Germany

Introduction: In human neurocysticercosis (NCC), the cellular and molecular mechanisms of host-parasite interactions triggering brain inflammation and epileptic seizures in Sub-Saharan Africa are poorly understood. Emerging evidence indicates that the viability of the cyst of the pork tapeworm *Taenia solium* determines brain inflammation and, thus, symptom development and disease severity. We have previously shown that while viable cyst-released molecules promote immune regulation and often asymptomatic disease, the fluid from degenerating cysts causes inflammation in microglia and peripheral immune cells, potentially driving immune-mediated pathology. This study aims to elucidate the apoptotic signaling pathways underlying this process and their relevance for symptomatic disease in NCC patients.

Materials and methods: Human and porcine peripheral immune cells, as well as murine microglia, were exposed to *T. solium* cyst vesicular fluid (CVF). Apoptosis signaling pathways were analysed using flow cytometric FLICA (fluorochrome-labeled inhibitors of caspases) caspase 8 and 9 assays, while mitochondrial dysfunction was assessed via TMRE and MitoTracker Deep Red and Green fluorescent probes. Apoptosis-inducing CVF molecules were identified by differential mass spectrometry and functionally tested using specific inhibitors.

Caspase activity and soluble mediators (FasL, ROS, TNFα) were measured in NCC asymptomatic and symptomatic patients' sera, and inflammatory T cell infiltrates expressing caspases near viable and degenerating cysts in naturally infected pig brain slices were examined via immunohistology.

Results: We found that vesicular fluid derived from cysts primarily induced apoptosis and caspase 3 and 9 activity, and only minimal necrosis, in a dose-dependent manner across central and peripheral immune cells. This effect was prominent in $CD16^+$ monocytes, microglia, and in $CD3^+$ T cell-expressing caspase 3 near degenerating brain cysts. Apoptotic signaling was predominantly mediated by a dynamic remodeling of caspase 9 pathway, accompanied by a significant loss of mitochondrial potential and a sharp decrease in Bid and Bcl2 transcription, favoring the intrinsic over the FasL-dependent extrinsic pathway and mechanisms. This process is primarily mediated by small molecules (< 30 kDa), and remained unaffected by heat and proteinase treatment. Notably, symptomatic NCC patients exhibited elevated FasL levels correlating with increased caspase activity, underscoring the potential contribution of apoptosis to disease pathogenesis.

Conclusions: This study identifies caspase 9-mediated apoptosis as a mechanism of helminth-induced brain inflammation and implicates FasL in symptomatic disease progression. These insights enhance our understanding of NCC immunopathogenesis and may inform future therapeutic strategies targeting apoptotic pathways.

KEYWORDS

T. solium cyst vesicular fluid, neurocysticercosis, inflammation, apoptosis pathways, caspase 9 activity

Introduction

Neurocysticercosis (NCC), a human parasitic disease caused by larval cyst stages of the pork tapeworm *Taenia solium*, remains a major public health concern in endemic regions, particularly in low- and middle-income countries (LMICs) of Sub-Saharan Africa, Latin America, and Southeast Asia (1). NCC is the leading cause of acquired epilepsy worldwide, disproportionately affecting rural populations with limited access to healthcare (2). The pathogenesis of NCC is closely linked to the viability and degenerative state of *T. solium* cysts in the central nervous system (CNS) (3, 4). While viable cysts typically sustain a state of immune tolerance via regulatory T cells (Tregs), leading mainly to asymptomatic or mild disease, cyst degeneration and death are believed to trigger a pronounced inflammatory response, often culminating in symptomatic NCC. This is characterized by epileptic seizures, chronic headaches, and neuroinflammation (4–7). However, the precise cellular and molecular mechanisms by which degenerating cysts modulate immune responses and contribute to neuroinflammation remain incompletely understood. In this study, we explored the implication of apoptosis pathways in regulating these processes.

The host immune response to NCC involves a complex interplay between resident brain cells, including microglia and astrocytes, and activated and infiltrating peripheral immune cells such as monocytes and their macrophage progeny, and T cells (3, 8–10). Recent studies indicate that microglia, the most frequent mononuclear cells of the resting CNS (11), play a central role in recognizing and responding to degenerating cyst materials by secreting pro-inflammatory mediators (TNFα, IFNγ, IL-1ß, IL-18, IL-12) (8, 10, 12) and phagocytosing damaged neurons and neurotoxic aggregates. Thus, they potentially shape the neuroimmune microenvironment and preserve nervous tissue homeostasis (3, 12, 13). Additionally, systemic immune dysregulation, including monocyte and lymphocyte recruitment, activation, and apoptosis, has been observed in NCC (5, 14–19). This suggests that parasite-derived factors may influence immune cell survival and function. While previous work has highlighted the main role of cytokine storms, cyst-associated mechanical and synaptic obstruction in NCC-related neuroinflammation, the contribution of apoptotic pathways, particularly caspase-dependent signaling, to disease progression has not been fully clarified.

Apoptosis, the best understood form of regulated cell death, is essential for many important biological processes, such as in embryonic development, maintenance of cellular homeostasis, and negative selection of T lymphocytes (20–22). Thus, it is a

fundamental mechanism governing immune homeostasis and pathogen clearance. It is orchestrated by two major pathways, both of which are found in parasitic helminth infections: the extrinsic and the intrinsic pathways. The extrinsic pathway is mediated by the activation of death receptors such as Fas and TNF receptor superfamily members. The intrinsic mitochondrial pathway, on the other hand, is induced through cellular stressors, like hypoxia or heat shock, and is tightly regulated by the balance of pro- and anti-apoptotic Bcl-2 family proteins (20, 23–25). The intrinsic pathway is particularly critical for CNS pathology, as mitochondrial dysfunction, caspase 9 activation, and increased systemic immune cell apoptosis have been implicated in neurodegenerative diseases and inflammatory responses of the CNS (26, 27). Thus, it seems imperative to thoroughly characterize cyst-regulated central and peripheral cell apoptosis and dissect their molecular signatures, particularly in relation to caspase-driven mitochondrial dysfunction.

Our previous research demonstrated that degenerating cysts promote microglial and macrophage activation and apoptosis, yet the effect on peripheral immune cells and the precise molecular triggers remained unidentified. Here, we sought to define the apoptotic signaling pathways involved in NCC pathogenesis, focusing on the role of caspase-mediated mitochondrial dysfunction. Using a combination of *in vitro* cellular assays, caspase activity profiling, mass spectrometry-based proteomics, and animal infection and patient serum analyses, we characterized the differential immune responses and apoptosis elicited in the presence of viable versus degenerating cysts. We further examined apoptotic gene (e.g. Bid, Bcl2) regulation by cyst molecules and provided insights into the relative contributions of intrinsic versus extrinsic apoptotic pathways during NCC pathogenesis through caspase 3, 8, 9 activity, and association with FasL levels in symptomatic and asymptomatic NCC patients.

Materials and methods

Animals and *T. solium* cyst products

C57BL/6 mice were purchased from Envigo (Germany) or bred in-house and maintained under specific pathogen-free conditions at the Institute of Medical Microbiology, Immunology, and Hygiene (MIH), Animal facility, TU Munich. All experiments were performed in accordance with and approved by local government authorities of Regierung von Oberbayern (Az. 55.2-1-54-2532-145-17). Cyst vesicular fluid (CVF) was prepared as described previously (3). *T. solium* cysts were collected from the muscle tissue of a heavily infected pig at the University of Zambia School of Veterinary Medicine (ethical approval Ref. 2018-Mar-002/0005948). Following collection, the cysts were washed with phosphate-buffered saline (PBS) (Merck, Cat. No. D8662). For CVF preparation, the cysts were transferred to a sterile dish, cut open with a scalpel, and the released fluid was collected. The collected fluid was sterile filtered through 0.45 µm size filters, centrifuged at 15.000 g for 60 min at 4 °C. Then, materials were immediately treated with Phenylmethylsulphonyl fluoride (PMSF, final concentration 5 mM) and leupeptin (final concentration 2.5 µM), and aliquoted at a concentration of 1 mg/ml in PBS. All prepared materials were tested for endotoxin (levels < 0.05 EU/ml) and stored at -80 °C until use.

Human PBMC and plasma from patients with NCC and controls

Human plasma from healthy controls and persons with NCC was examined for soluble apoptosis-inducing mediators. The patients were recruited within the TOPANA study, a prospective cohort study implemented in rural Tanzania. The study received ethical approval by the Klinikum Rechts der Isar (Technical University of Munich, Germany) Ethical Committee (Reference 33/19S) and by the National Ethics Health Research Committee (NatREC) of Tanzania (Reference NIMR/HQ/R.8c/Vol.I/1808 for TOPANA and NIMR/HQ/R.8a/Vol.IX/2597 for SOLID). The protocol and study design of the study have been published elsewhere (28, 29). In brief, patients were recruited at three district hospitals (Tosamaganga, Chunya, Vwawa). NCC diagnosis was done in July 2021 according to the latest Del Brutto criteria, using computer tomography (CT) scan and laboratory testing (LDBio cysticercosis Western Blot IgG, apDia Cysticercosis Ag-ELISA) (30, 31). Patients with NCC were classified as symptomatic through the presence or history of severe progressive headaches and/or epileptic seizures and having parenchymal and extraparenchymal NCC with active lesions and mostly degenerating/calcified cysts (28). Asymptomatic NCC patients had no history of epileptic seizures and/or severe progressive headaches but had a mix of viable and degenerating cysts, with most being viable. Participants were tested for HIV by serology, *Mycobacterium tuberculosis* in the sputum, *Strongyloides* spp. in the feces, and underwent fundoscopy for the exclusion of ocular NCC according to the IDSA/ASTMH recommendations (32). Blood samples were taken from the study participants and after giving informed consent. Peripheral blood mononuclear cells (PBMC) were isolated as previously described (33). Plasma was separated from the cellular components of the blood using density gradient centrifugation (700 x g, 25 min, 20 °C), and stored at -80 °C until usage. The cohort included NCC non-infected Tanzanian individuals as controls (group 1), NCC asymptomatic individuals (group 2) and symptomatic NCC patients with epilepsy and/or severe progressive headaches (group 3). The participants included in this study were age and sex-matched (see detail in Table 1).

Human cell isolation from healthy volunteers, stimulation, and analysis

The study was approved by the local ethical committee of the Technical University of Munich (Reference: 215/18S), and all individuals included in the study consented to enrollment. Human PBMC were isolated from whole blood samples of

TABLE 1 Study participant groups.

Parameter	Controls	NCC asymptomatic	NCC symptomatic
Total number	6	6	6
Sex (male/female)	3/3	3/3	3/3
Age (range(median))	28 – 60 (40)	27 – 61 (43)	24 – 56 (38)
Symptoms	No	No	Epileptic seizures and/or severe progressive headaches

healthy volunteers from mixed genders using density gradient centrifugation and stored in liquid nitrogen as described in (33). Human unlabeled monocytes were purified from freshly isolated human PBMCs using the Miltenyi Pan Monocyte Isolation Kit, human (Miltenyi, Germany, Cat. No. 130-096-537), according to the manufacturer's protocol. The purity of monocytes was routinely ≥ 80%. $2.5x10^5$ cells per well were plated in 96 U-bottom well plates and stimulated with CVF (0.01 – 5 µg/ml) and incubated for 0–72 h at 37 °C, 5% CO_2. Staurosporine (TOCRIS, Bio-techne, Cat. No. 1285) (100 nM or 500 nM) was used to induce apoptosis. After incubation period, surface markers (CD3, CD4, CD8, CD14, CD16 (all antibodies from Biolegend: Cat. No. 317331, 317433, 344723, 325607, 302025), were analyzed by flow cytometry on a CytoFLEX S (Beckman Coulter). Early apoptotic (Annexin V^+/PI^-, late apoptotic (Annexin V^+/PI^+), and necrotic (Annexin V^-/PI^+) cell populations were determined by Annexin V/PI kit (Biolegend, Cat. No. 640914). For intracellular staining, cells were fixed and permeabilized with BD Cytofix/Cytoperm (BD Biosciences, Cat. No. 554714) for detection of active caspase 3 (BD Pharmingen, Cat. No. 570332). FAM FLICA™ Caspase-8 and Caspase-9 Kits (Bio-Rad, Cat. No. ICT099, ICT912) were used for detection of active caspases 8 and 9.

Column fractionation and CVF-fragment induction of apoptosis

To determine the role of proteins in the CVF in the induction of apoptosis on PBMCs, active proteins in the CVF were inactivated by heat-inactivation using 56 °C for 1h, 56 °C for 3h, 99 °C for 1h, and 99 °C for 3h and 10µg/ml Proteinase K (Sigma-Aldrich, Cat. No. P2308) digestion overnight at 37 °C, 5% CO_2. SDS page and Coomassie staining were performed to confirm effective protein inactivation. CVF was additionally treated with the cysteine protease inhibitor E-64 (Sigma-Aldrich, Cat. No. E3132) 10µM for 1 hour to inhibit cysteine proteases (e.g. Cathepsins). After protein inactivation and protease inhibition, PBMCs were stimulated with 2.5 µg/ml pretreated CVF for 72 h, and apoptosis induction was evaluated using Annexin V/PI. Furthermore, CVF was separated according to molecular size using 30 kDa column fractionation (GE Healthcare, Cat. No. 17VS50039A). Flow through and retarded CVF fractions (< 30 kDa, > 30 kDa) were used for stimulation of PBMCs and apoptosis was detected.

Mitochondrial function and membrane potential evaluation

To measure mitochondrial damage, PBMCs were stained with Tetramethylrhodamine, ethyl ester, perchlorate (TMRE) (ThermoFisher Scientific, Cat. No. T669) and MitoTracker following CVF stimulation. For TMRE staining, TMRE was diluted to 10nM in RPMI (Merck, Cat. No. R0883) (10% FCS (Merck, Cat. No. S0615) and 1% Penicillin/Streptomycin (Merck, Cat. No. P4333) and cyclosporin H (Enzo, Cat. No. 83602-39-5) (final concentration 0.5 µM), and incubated with CVF-treated PBMCs for 30 minutes at 37 °C to assess the loss of mitochondrial transmembrane potential. For MitoTracker staining, PBMC were incubated with MitoTracker Deep Red FM (ThermoFisher Scientific, Cat. No. M46753) and MitoTracker Green FM (ThermoFisher Scientific, Cat. No. M7514) in PBS for 60 minutes at 37 °C to evaluate the mitochondrial potential and mass loss, respectively (34).

TABLE 2 The oligonucleotide sequences used for the qRT-PCR.

Gene	Forward primer (5′-3′)	Reverse primer (5′-3′)
Gapdh	ACTCCACTCACGGCAAATTC	TCTCCATGGTGGTGAAGACA
TNFα	TCGTAGCAAACCACCAAGTG	CCTTGTCCCTTGAAGAGAACC
Caspase 3	CTCGCTCTGGTACGGATGTG	TCCCATAAATGACCCCTTCATCA
Caspase 8	TGCTTGGACTACATCCCACAC	GTTGCAGTCTAGGAAGTTGACC
Caspase 9	GGCTGTTAAACCCCTAGACCA	TGACGGGTCCAGCTTCACTA
FasL	TCCGTGAGTTCACCAACCAAA	GGGGGTTCCCTGTTAAATGGG
Bid	GCCGAGCACATCACAGACC	TGGCAATGTTGTGGATGATTTCT
Bcl-2	GCTACCGTCGTGACTTCGC	CCCCACCGAACTCAAAGAAGG

Porcine cell isolation, stimulation, and analysis

Porcine blood samples were obtained from freshly slaughtered pigs at a local slaughterhouse. The blood was collected in 500 ml bottles containing 1g EDTA (Ethylenediaminetetraacetic acid) anticoagulant. Samples were stored at 4 °C within an hour of collection and processed within 24 hours.

Porcine PBMCs were isolated using SepMate™ isolation tubes (Stemcell Technologies, Cat. No. 85460) and Histopaque®-1077 (Merck, Cat. No. 10771). The blood was first diluted 1:1 with sterile PBS/2% fetal calf serum (FCS) (Merck, Cat. No. S0615), and then layered onto Histopaque within centrifugation tubes. PBMCs were separated using a density gradient. Centrifugation was performed at 700xg for 25 min with the lowest acceleration and break. The PBMC layer was collected using a single-use pipette. PBCMs were washed twice with PBS + 2% FCS. Remaining erythrocytes were lysed using 0.5 ml erythrocyte lysis buffer (0.01 M $KHCO_3$, 0.155 M NH_4Cl, 0.1 mM EDTA) per 10 ml blood for 4 min at RT.

PBMCs were resuspended in RPMI (Merck, Cat. No. R8758) supplemented with 10% FCS (Merck, Cat. No. S0615), 100 U/ml penicillin, 100 µg/ml streptomycin (Merck, Cat. No. P4333). Porcine monocytes were separated from freshly isolated PBMCs using the autoMACS separator (Miltenyi Biotec). PBMCs from each animal were rebuffered in autoMACS running buffer (Miltenyi Biotec, Cat. No. 130-091-221). Cells were labeled with CD14 MicroBeads (Miltenyi Biotec, clone Tük4, Cat. No. 130-050-201) and separated according to the manufacturer's instructions. $CD14^+$ monocytes were pelleted and resuspended in RPMI. Trypan blue staining and automated cell counting were used to determine the number of viable monocytes and PBMCs.

2.5–5 x 10^5 cells of porcine PBMCs and 3 x10^5 cells of porcine monocytes were plated per well and stimulated with 2.5 µg/ml CVF for 0–72 h at 37 °C and 5% CO_2. After incubation, porcine-specific anti-CD4α (clone 74-12-4, mouse IgG2b, inhouse + anti-mouse IgG2b, clone R12-3, BD Biosciences, Cat. No. 743177), anti-CD8α (clone 11/295/33, mouse IgG2a, inhouse + anti-mouse IgG2a, clone RMG2 A-62, BioLegend, Cat. No. 407117), anti-CD3e (clone BB-23-8E6-8C8, BD Biosciences, Cat. No. 743177), anti-CD172a (clone 74-22-15, mouse IgG1, inhouse + anti-mouse IgG1, clone X-56, Miltenyi, Cat. No. 130-096-593) and CD14 (clone Tük4, Bio-Rad, Cat. No. MCA1568P647) antibodies were used to characterize cell populations on an Attune NxT Flow cytometer (Thermo Fisher Scientific). Induction of apoptosis was detected with Annexin V/PI kit (Invitrogen, Cat. No. 13242) and Staurosporine (500 nM) (Sigma-Aldrich, Cat. No. S6942) served as a positive control.

Immunohistology of naturally infected pig brain slices

Ten 2 - 4-year-old pigs (6 females and 4 males, 4 uninfected and 6 naturally infected with *T. solium* cysticercosis, were purchased from rural rearers. The animals were diagnosed for cysticercosis by tongue examination. Pigs were humanely euthanized at the Faculty of Veterinary Medicine and Zootechnics in accordance with Mexican official standard NOM-033-SAG/ZOO-2014. Blood samples were collected immediately after euthanasia, and brain tissue was dissected. Brain samples were fixed in neutral buffered 10% formalin for 48 hours. After dehydration, brain tissue was embedded in paraffin blocks.

Serial sections of 2µm slices were mounted on Superfrost (HE) or Superfrost Plus (IHC) slides using a rotary microtome (ThermoFisher Scientific, Cat. No. HM355S). The sections were stained with Hematoxylin-Eosin to evaluate general pathological changes using standard protocols. In brief, the wax was removed with xylene and then passed through different changes of alcohol to remove the xylene. After rehydration with distilled water, the sections were stained with hematoxylin for 8 minutes. Following rinsing with tab water, counterstaining with 1% alcoholic eosin was performed for 4 minutes. Slides were dehydrated by passing through different changes of alcohol and cleared with xylene.

To visualize and localize cell populations in the granulomatous regions surrounding *T. solium* cysts in the pig brains, immunohistochemical (IHC) staining was performed using an autostainer (Bond RXm system, Leica). In brief, the sections were deparaffinized with the Leica Kit de-wax (Leica, Cat. No. AR9222) and rehydrated by washing with decreasing alcohol concentrations. Epitope retrieval was done with heat induction using citrate buffer (pH=6) for 20 minutes (40 minutes for anti-CD79a). Endogenous peroxidase activity was blocked by incubating the sections with 3% hydrogen peroxidase (Leica) for 5 minutes, and non-specific binding sites were blocked with normal goat serum (Abcam, Cat. No. ab138478). Primary antibodies were then added to the sections for 15 minutes at room temperature (anti-CD3 (Cellmarque, Cat. No. MRQ39), anti-CD79a (ThermoFisher, Cat. No. HM57), anti-Iba1 (poly, Wako, Cat. No. 019-19741), and anti-Caspase 3 (Cell Signaling, Cat. No. 5A1E)). Antibody detection was done with a polymer refine detection kit (Leica, Cat. No. DS9800) and Diaminobenzidine (DAB) (Merck, Cat. No. D12384) was used for visualization. The sections were counterstained with hematoxylin for 10 minutes and dehydrated with increasing alcohol concentrations and xylene. Pertex mounting medium (Histolab, Cat. No. SEA-0100-00A) was used to mount the sections. All antibodies were tested for cross-reactivity in pigs and adequate positive controls were used in each staining run.

Analysis of histological pig brain slides

Histology was evaluated under the supervision of a board-certified veterinary Pathologist (K.S.). For digital image analysis, the software QuPath [v0.5.1] was used. To quantify $CD3^+$ and $CD79a^+$ cells, 8–10 rectangles (1,25 mm x 0,875 mm) covering the area around the cysts were drawn for automated cell counting, and positive and negative cells were counted automatically with QuPath software.

Mouse microglia isolation, culture, and stimulation

Newborn mice (P1-P4) were decapitated, and the olfactory bulbs and the cerebellum were removed, as well as the meninges and choroid plexus. Tissue was dissociated and filtered through 100 µl cell strainer. Cells were centrifuged for 5 min at 1500 RPM at 4 °C. The cell pellet was resuspended in 5 ml of DMEM (Dulbecco's Modified Eagle Medium) high glucose (Gibco, Cat. No. 11965092) (10% FCS, 0.5% Ciprofloxacin) and plated on a T25 culture flask, which was previously coated overnight with 5 ug/ml Poly-L-Lysine (Merck, Cat. No. P8920). The T25 culture flasks were incubated for 12 days with repeated medium exchange at 37 °C in a 5% CO_2 humidified incubator. 48h before further analysis, 20ng/ml of M-CSF (Macrophage colony-stimulating factor) (Pepro-Tech, Cat. No. 315-02) was added to the cultures. The cultures were trypsinized in 0.05% Trypsin-EDTA for 15 minutes at 37 °C, washed with medium, scraped, and seeded to 96-well flat-bottom plate (Thermo Fisher Scientific), with a density of 1 x 10^5 cells per well. After resting overnight, cells were stimulated with CVF (2.5 µg/ml) for 0 - 72h, and, either lysed for qPCR (quantitative polymerase chain reaction), or proceeded for active caspases detection with intracellular staining for cleaved caspase 3 (Bio-techne, R&D Systems, Cat. No. IC835G) and with FLICA caspase assays for active caspase 8 (Bio-Rad, Cat. No. ICT099) and 9 (Bio-Rad, Cat. No. ICT960) using flow cytometry.

ELISA

Commercially available ELISA kits were used according to the manufacturer's instructions. Human TNFα ELISA (R&D Systems, Cat. No. DTA00D) and FasL (R&D Systems, Cat. No. DFL00B) were used to evaluate the levels of both apoptosis mediators in the culture supernatants of CVF-stimulated PBMCs from healthy individuals and in plasma samples from NCC patients and controls from Tanzania.

Intracellular ROS detection

An intracellular fluorometric reactive oxygen species (ROS) assay (Cell Biolabs, Cat. No. STA-342) was used according to the manufacturer's instructions to measure the intracellular ROS activity within the CVF-stimulated PBMCs. Briefly, human PBMCs were stimulated with CVF 2.5 µg/ml. After 72 h, cells were washed twice with PBS, and 100 µl of 1X cell-permeable fluorogenic probe Dichlorodihydrofluorescin diacetate (DCFH-DA) were added to the wells and incubated at 37 °C, 5% CO_2. After 45 min, cells were washed twice with PBS, and the fluorescence intensity, proportional to intracellular ROS activity to the DCF, was measured with a CLARIOstar Plus plate reader (BMG LABTECH) at 480 nm/530 nm. 100 µM and 1000 µM H_2O_2 were added to the cells as positive controls.

RNA extraction and qPCR

For microglia RNA extraction, cells were treated with RLysis buffer containing 1% β-mercaptoethanol, and RNA was extracted using the Extractme Total RNA Micro Spin kit (BLIRT, Cat. No. EM31.1-050) according to manufacturer's information. RNA was reversely transcribed to cDNA with the SuperScript™ IV VILO mix (ThermoFisher Scientific). qRT-PCR was performed with ABsolute qPCR SYBR Green (Thermo Fisher Scientific) at the LightCycler 480 (Roche). ΔΔCt was used to calculate relative gene expression and differences. The oligonucleotide sequences used for the qRT-PCR are detailed in Table 2.

Mass spectrometry analysis of CVF

The mass spectrometry analysis of *T. solium* CVF was performed as previously described (3). The retrieved data were analyzed using the WormBase Parasite database for *T. solium* (Version: WS282, October 2022) to identify apoptosis-related molecules in the CVF.

Statistical analysis

For statistical analysis, the Prism software (Version 10.1.2) (GraphPad Software, LLC, San Diego, CA, USA) was used. For direct comparisons between two groups, a Mann-Whitney test was employed. For more than two groups, we applied a Kruskal-Wallis test followed by Dunn's multiple comparison test and a two-way ANOVA test followed by Tukey's multiple comparison test if more time points were observed. P values < 0.05 were considered statistically significant.

Results

The vesicular fluid from degenerated *T. solium* cyst (CVF) causes apoptosis but not necrosis in human T cells and monocytes

Our previous findings indicated that cyst-derived vesicular fluid (CVF) from *T. solium* cysts promotes apoptosis in alveolar macrophages (3). Here, we extended our investigation to assess the pro-apoptotic effects of CVF on various peripheral immune cell populations. To evaluate the impact of CVF on PBMCs, we analyzed both early apoptotic (Annexin V^+/PI^-) and late apoptotic (Annexin V^+/PI^+) cell populations by Annexin V/PI staining. Our data revealed that CVF induced significant apoptosis in PBMCs (Figure 1A; Supplementary Figure S1). This effect was concentration-dependent and predominantly restricted to apoptosis rather than necrosis, affecting both $CD3^+$ T cells (Figure 1B) and $CD3^-$ cells (non-T cells) (Figure 1C) in a dose-dependent manner (Supplementary Figure S2). Notably, $CD3^-$ immune cells exhibited a more

pronounced apoptotic response compared to $CD3^+$ T cells (Figure 1D). Furthermore, the apoptotic effect intensified over time, particularly in the late apoptotic $CD3^+$ and $CD3^-$ cell populations (Figure 1E) as well as in $CD3^+CD4^+$ and $CD3^+CD8^+$ T cell subsets (Figure 1F). Interestingly, while $CD3^-$ and $CD8^+$ early apoptotic cells decreased over time, late apoptotic populations increased, suggesting a dynamic progression from early to late apoptosis upon CVF exposure (Figures 1E, F). Given that $CD3^-$ cells were significantly affected by CVF-induced apoptosis, we further investigated monocyte subpopulations to determine their susceptibility, since monocytes are also the second largest cell population in PBMCs after lymphocytes (35). Monocytes were purified from PBMCs using magnetic-activated cell sorting (MACS) and categorized into classical ($CD14^+CD16^-$) and non-classical ($CD14^{dim}CD16^+$) monocytes. Our findings confirmed the pro-apoptotic potential of CVF, demonstrating a time-dependent shift from early to late apoptosis in both monocyte subsets (Figure 1G). Of note, monocytes were very sensitive to spontaneous cell apoptosis, especially in the first 24 h of culture as reported elsewhere (36, 37).

In summary, our findings demonstrate that degenerating *T. solium* cysts actively drive apoptosis, rather than non-apoptotic death (necrosis), in peripheral immune cell populations. This effect was particularly pronounced in $CD8^+$ T cells and monocytes. These results underscore the selective targeting of immune cells by degenerating cyst-derived molecules, further implicating their role in NCC-associated systemic immune inflammation and dysregulation.

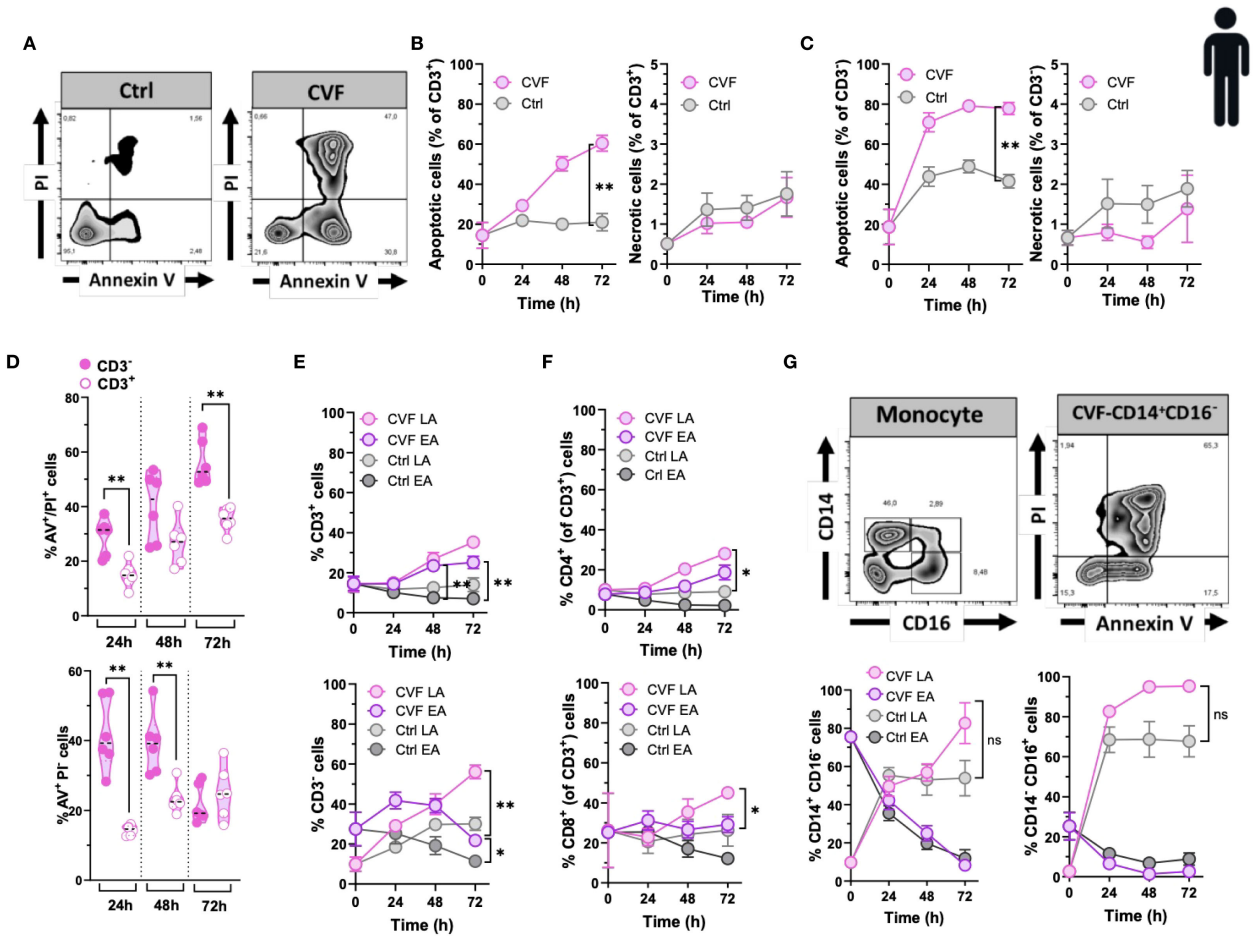

FIGURE 1
The vesicular fluid of *T. solium* cyst (CVF) causes apoptosis but not necrosis in human T cells and monocytes. **(A)** FACS plots of 72h CVF-stimulated (right panel) and non-stimulated (control, left panel) PBMCs for detecting early (Annexin V^+/PI^-) and late (Annexin V^+/PI^+) apoptotic and necrotic (Annexin V^-/PI^+) cell populations using Annexin V/PI-gating. **(B, C)** CVF-induced apoptosis and necrosis in $CD3^+$ **(B)** and $CD3^-$ **(C)** cell populations. **(D)** A direct comparison between $CD3^-$ and $CD3^+$ cells for late (upper panel) and early (lower panel) apoptosis induced by CVF as compared to control. **(E, F)** Time-dependent induction of early and late apoptosis in $CD3^+$ **(E)** (upper panel) and $CD3^-$ **(E)** (lower panel), and in $CD4^+$ **(F)** (upper panel) and $CD8^+$ **(F)** (lower panel) cell populations. **(G)** CVF-induced apoptosis in human monocytes in a time-dependent manner. **(G)** (upper panels) FACS plots of the characterization of monocyte subpopulations (upper left) and apoptosis in $CD14^+CD16^-$ monocytes (upper right). **(G)** (lower panels) Early and late apoptosis induced by CVF in classical ($CD14^+CD16^-$) (lower left) and non-classical ($CD14^-CD16^+$) (lower right) monocyte subpopulations after 72h culture. Data information: Graphs show data from 6–8 different samples. Statistical analysis was performed using a Two-way ANOVA followed by Tukey's multiple comparison tests **(B, C, E–G)** and a Mann-Whitney test **(D)**. Data are represented as means ± SEM. $^*P < 0.05$; $^{**}P < 0.01$.

Cyst degeneration drives T and B cell infiltration and microglia/macrophage activation in brains of naturally infected pigs

Pigs serve as natural hosts for *T. solium* cysts and their infection mirrors in many ways human NCC in terms of immunopathological responses (9, 15, 38). To extend our findings on CVF-induced apoptosis in host immune cells, we examined the effects of CVF on porcine peripheral immune cells and assessed its relevance to the CNS by analyzing immune responses in naturally infected pigs harboring granulomas with intact and degenerating *T. solium* cysts in the brain. Porcine PBMCs were treated with CVF under the same conditions as human PBMCs, and apoptosis was assessed in $CD3^+$ T cells, including major subsets ($CD4^+CD8\alpha^-$, $CD4^-CD8\alpha^+$, $CD4^+CD8\alpha^+$), as well as in $CD172a^+$ monocytes (Figures 2A-C). Unlike humans, pigs possess a unique population of $CD4^+CD8\alpha^+$ double-positive T cells, which are thought to originate from $CD4^+$ helper T cells that acquire CD8α expression following antigen recognition (39, 40). Similar to human cells, early apoptosis in porcine PBMCs declined over time, promoting late stages of apoptosis, which peaked at 24 h post-CVF treatment, with a delayed response in $CD4^-CD8\alpha^+$ T cells (Figure 2A). However, in contrast to human T lymphocytes, CVF-dependent necrosis increased significantly over time in all porcine lymphocyte populations (Figure 2B). In addition, late apoptotic cells steadily increased in the $CD3^-$ compartment over time, while $CD3^+$ lymphocytes displayed a reduction in late apoptosis after 48 h of treatment (Figures 2A–B). Porcine monocyte subsets are primarily identified by CD172a, CD14, and CD163 expression (41). Given that all porcine monocytes express CD172a (41), we focused on $CD172a^+$ monocytes for better comparability with human monocytes. Similar to porcine T lymphocytes, $CD172a^+$ monocytes showed a peak in late apoptosis at 24 h post-CVF treatment, which declined at later time points (Figure 2C). Necrosis also increased over time in monocytes, although this change was not statistically significant (Figure 2C). These results suggest that while CVF predominantly induces apoptosis in human immune cells, it promotes a substantial degree of necrosis in porcine immune cells. This indicates a species-specific variation in the mechanisms of degenerated cyst-induced cell death.

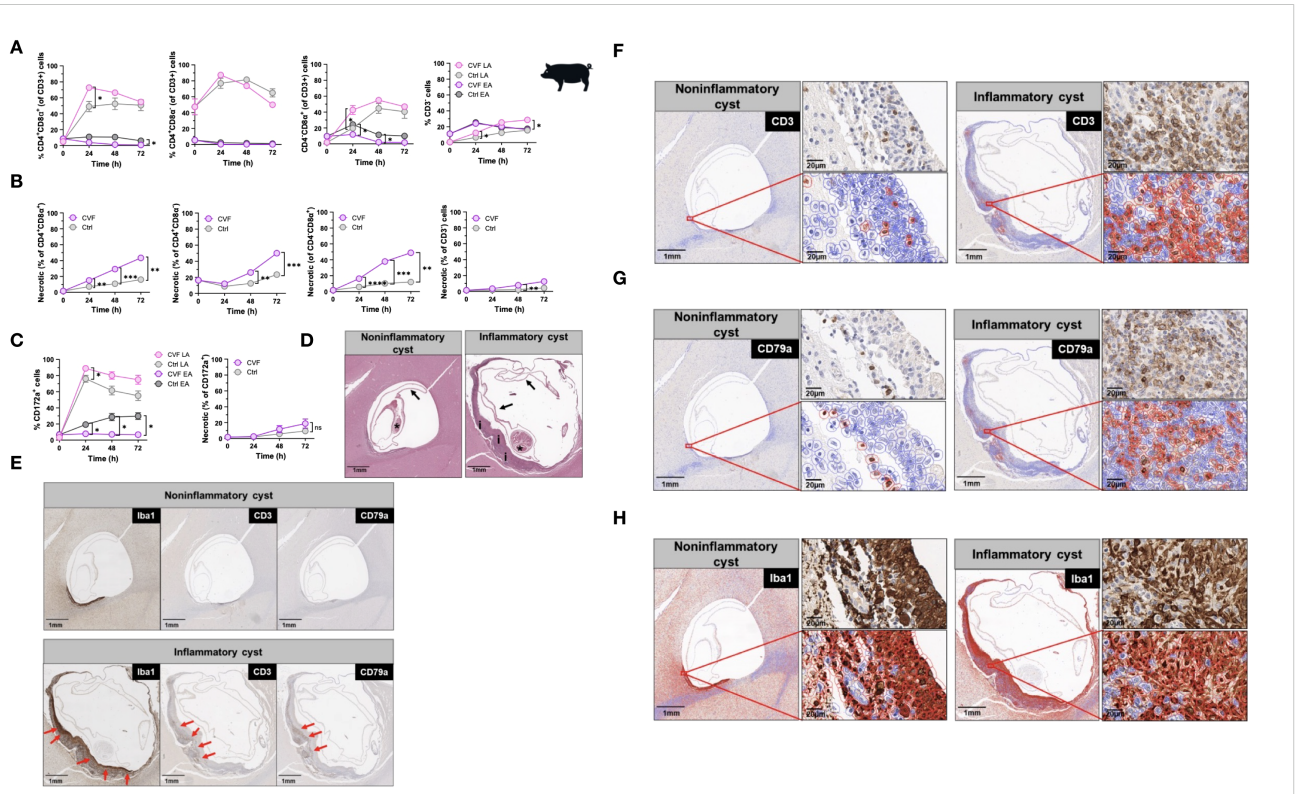

FIGURE 2
Cyst degeneration drives T and B cell infiltration and microglia/macrophage activation in brains of naturally infected pigs. **(A, B)** Time-dependent induction of early and late apoptosis **(A)** and necrosis **(B)** by CVF in porcine $CD4^+CD8\alpha^+$, $CD4^+CD8\alpha^-$, $CD4^-CD8\alpha^+$, and $CD3^-$ cell populations. **(C)** Time-dependent induction of early and late apoptosis (left panel) and necrosis (right panel) in porcine $CD172a^+$ monocytes. **(D, H)** Paraffin-embedded naturally infected pig brain slices were stained for characterization of T. solium cyst stage and inflammatory cell infiltrates. **(D)** Staining of viable/noninflammatory (left panel) and degenerating/inflammatory (right panel) cysts according to (42) and (38). Arrows indicate the collapsed bladder wall, the asterisks display the scolex of the parasite, and "i" shows the inflammatory infiltrate around the degenerating cyst. **(E)** Localization of the macrophage/microglia (Iba^+), T ($CD3^+$), B ($CD79^+$) cell infiltrates (red arrows) surrounding the cyst in infected pig brain. **(F, H)** Quantification of $CD3^+$ T **(F)**, $CD79a^+$ B **(G)** cells and $Iba1^+$ macrophage/microglia **(H)** (red-bordered cells) in cyst surrounding tissue assessed by QuPath Software. Original image sections shown on upper right panels for each cyst stage. Data information: **(A–C)** Graphs show data from 8 different samples. Statistical analysis was performed using a Two-way ANOVA followed by Tukey's multiple comparison test. Data are represented as means ± SEM. **(D, H)** Images were analyzed using the Software QuPath [v0.5.1]. *P < 0.05; **P < 0.01; ***P < 0.001; ****P < 0.0001.

In humans, the most severe clinical manifestations of NCC, including recurrent seizures and progressive headaches, are often associated with degenerating cysts encased within granulomatous structures in the brain (8). To investigate the immunopathological relevance of CVF-induced apoptosis *in vivo*, we first analyzed immune cell infiltrates in brain sections from five NCC-infected pigs, comparing regions surrounding degenerating "inflammatory" *T. solium* cysts to those surrounding viable "non-inflammatory" cysts (38, 42). Employing a combination of HE staining with spatial analysis of $CD3^+$ T and $CD79^+$ B lymphocytes and the $Iba1^+$ activated macrophages/microglia, we identified 18 cysts classified into three stages according to the classification used by Gutierrez and Singh (38, 42). In brief, viable cysts (noninflammatory) were classified as cysts with a well-stainable parasite with intact scolex and bladder wall and no edema or inflammation in the surrounding tissue. Degenerating cysts (inflammatory) had an intact bladder wall and scolex, but nuclear disintegration and a mixed inflammatory or granulomatous reaction around the cysts were observed. Although calcified cysts were also detected, no defined structure was found in these cysts. Of the 18 cysts, 1 was a viable cyst (noninflammatory), 11 were degenerating (inflammatory), and 6 were calcified or unclassifiable cysts. Out of the 11 inflammatory cysts, 6 had clearly visible parasites with scolex and are thus included in the present investigation. Representative images of a noninflammatory and an inflammatory cyst from the same pig are shown in Figure 2D. Immunohistochemical staining for CD3, CD79a, and Iba1 revealed a distinctive localization of immune cells within granulomatous structures. $Iba1^+$ activated macrophages/microglia were predominantly located on the inner side of the granuloma, adjacent to degenerating cysts (Figures 2E, H). In contrast, $CD3^+$ T cells and $CD79a^+$ B cells were primarily found in the outer layers of the granuloma (Figures 2E, G). Quantitative analysis indicated an approximately three-fold increase in $CD3^+$ T cell infiltration (Figures 2E, F) and a ten-fold increase in $CD79a^+$ B cell infiltration (Figures 2E, G) around inflammatory cysts compared to non-inflammatory cysts (Figures 2E, G; Supplementary Figures S3A, B).

These findings provide compelling evidence that cyst-derived vesicular fluid products contribute to peripheral immune cell apoptosis and inflammation. Moreover, cyst degeneration is associated with significant immune cell infiltration in the CNS, highlighting its potential role in NCC immunopathogenesis.

CVF-induced cell apoptosis is modulated preferentially through the caspase 9 pathway

Several signaling pathways contribute to apoptosis, with the extrinsic pathway initiated by death receptors, and the intrinsic pathway that occurs through the mitochondria, being the main ones (43). To determine which apoptotic pathways are activated by CVF, we assessed caspase activity, given that caspase 3 serves as a key effector in both apoptotic mechanism pathways (44). CVF treatment led to a significant increase in $CD3^+$ T cell-expressing active caspase 3, including both $CD4^+$ and $CD8^+$ subsets, compared to untreated and staurosporine-treated positive controls (Figure 3A). To distinguish between the extrinsic and intrinsic apoptosis pathways, we evaluated the activation of initiator caspases for both pathways: caspase 8 (extrinsic) and caspase 9 (intrinsic) (44). Using fluorochrome-labeled inhibitor of caspase (FLICA) assays, we observed significant activation of both caspase 8 and caspase 9 in $CD3^+$, $CD4^+$, and $CD8^+$ T cells, as well as in $CD3^-$ non-T cells (Figure 3B). However, in monocytes, only caspase 9 was activated, with no detectable caspase 8 activity (Figure 3B). Of note, CVF treatment shifted the entire monocyte compartment toward $CD16^+$-expressing monocytes. Despite the involvement of both pathways in lymphocytes, caspase 9 activation was significantly higher than caspase 8, suggesting a predominant role of the intrinsic mitochondrial pathway in CVF-induced apoptosis. An analogous pattern was found in microglia, where CVF-induced caspase 3 activation (Figure 3C) correlated with a progressive increase in cleaved caspase 9 levels, whereas cleaved caspase 8 decreased sharply over time (Figure 3D).

To determine whether CVF stimulation modulated gene expression of caspases, we performed qRT-PCR analysis (Figure 3E). Caspase 9 expression increased over time, although not statistically significant, while caspase 3 and caspase 8 expression declined. Additionally, we analyzed key mediators influencing caspase 8 and caspase 9 activation. TNFα and FasL, two primary inducers of the extrinsic apoptotic pathway (23), showed no significant changes in mRNA levels. Similarly, the expression of Bcl-2, an anti-apoptotic protein (45), remained unchanged. In contrast, Bid exhibited a marked decline. Of note, Bid is a pro-apoptotic protein and active inducer of mitochondrial outer membrane permeabilization that bridges caspase 8 activation to the extrinsic pathway (45). This suggests that the caspase 8 - Bid axis is not a major contributor to CVF-induced apoptosis. To explore the relevance of these findings *in vivo*, we stained brain tissue sections from NCC-infected pigs for caspase 3. Apoptotic caspase 3^+ cells were detected exclusively in areas surrounding degenerating inflammatory cysts (Figure 3F).

Taken together, these findings indicate that CVF predominantly activates the mitochondrial apoptosis pathway via caspase 9, leading to caspase 3 activation and immune cell death. Furthermore, the presence of apoptotic cells in the CNS near degenerating cysts underscores the potential role of CVF-induced apoptosis in NCC immunopathogenesis.

CVF treatment causes loss of mitochondrial membrane potential and dysfunction

Our data demonstrate that *T. solium* CVF preferentially activates the intrinsic apoptosis pathway to promote cell death. A hallmark of this pathway is mitochondrial dysfunction, characterized by the release of cytochrome C from the mitochondria and a loss of mitochondrial transmembrane potential (44, 46). We thus next assessed the mitochondrial integrity following CVF exposure using the TMRE and MitoTracker assays in human PBMC. As depicted in Figure 4A,

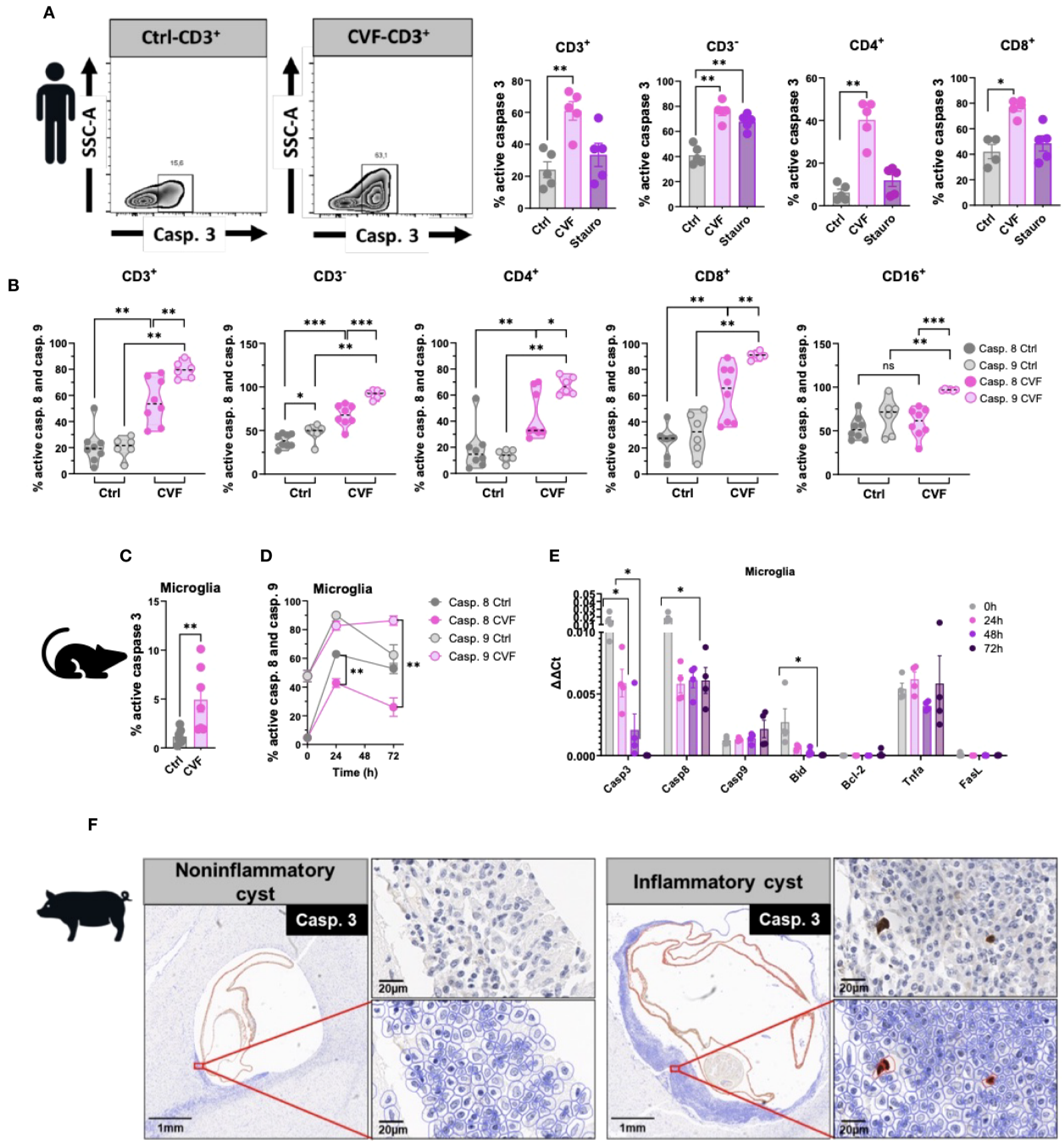

FIGURE 3
CVF-induced cell apoptosis is modulated preferentially through the caspase 9 pathway. **(A)** Active caspase 3 induction in $CD3^+$ and $CD3^-$ and in $CD4^+$ and $CD8^+$ cell populations by 72h stimulation of human PBMC by CVF as compared to the positive control staurosporine. **(B)** Activity of cleaved caspases 8 and 9 in $CD3^+$, $CD3^-$, $CD4^+$, $CD8^+$ T cells and $CD16^+$ monocytes as detected by FLICA assays following 72h stimulation with CVF. **(C)** Active caspase 3 induction in murine microglia at 72h. **(D)** FACS analysis of time-dependent modulation of cleaved caspase 8 and 9 activity in murine microglia by CVF. **(E)** Time-dependent expression of apoptosis related genes in microglia modulated by CVF. **(F)** Naturally infected pig brain slices stained for caspase 3-expressing cells surrounding inflammatory and non-inflammatory cysts assessed by QuPath Software. Original image sections shown on upper right panels for each cyst stage. Data information: Graphs show data from 4–8 different samples. Statistical analysis was performed using a Mann-Whitney test **(A–C)**, a Two-way ANOVA followed by Tukey's multiple comparison test **(D, E)**. Data are represented as means ± SEM. Images were analyzed using the Software QuPath [v0.5.1]. *P < 0.05; **P < 0.01; ***P < 0.001.

CVF-treated cells exhibited a significant reduction in TMRE fluorescence and signal, indicating mitochondrial transmembrane potential loss and depolarization across $CD3^+$ T cell and $CD3^-$ non-T cell compartments, as well as $CD4^+$ and $CD8^+$ T cells (Figure 4B), and $CD16^+$ monocytes (Figure 4C). MitoTrackers are cationic fluorescent probes that accumulate inside mitochondria due to the high mitochondrial transmembrane potential and are useful tools to visualize mitochondrial mass, integrity, and morphology

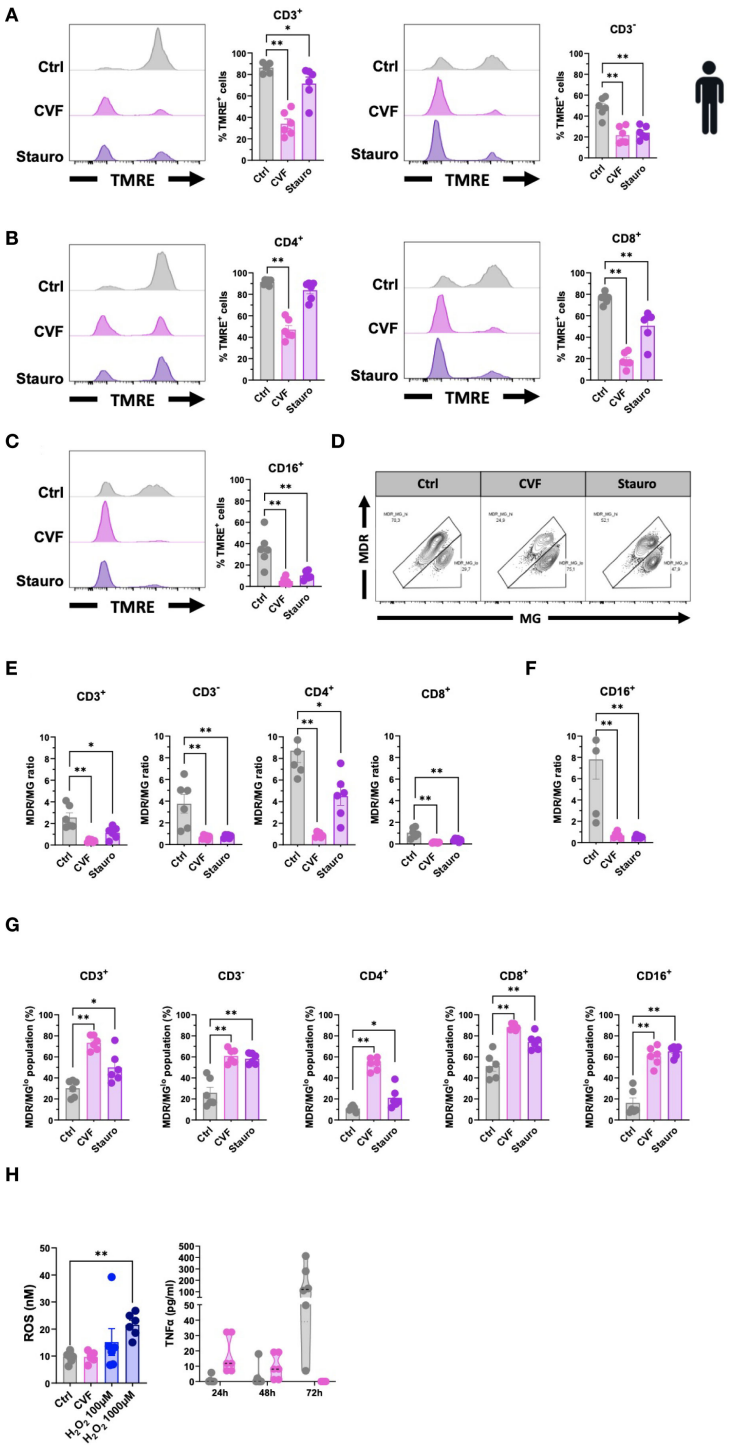

FIGURE 4
CVF treatment causes loss of mitochondrial membrane potential and dysfunction. **(A–C)** Assessment of mitochondrial damage and dysfunctionality in $CD3^+$ and $CD3^-$ T cells **(A)**, $CD4^+$ and $CD8^+$ T cells **(B)**, and $CD16^+$ monocytes **(C)** following 72h CVF treatment of human PBMC. **(D–F)** Evaluation of the mitochondrial activity per mass (MDR/MG ratio) in T cells and monocytes. **(D)** FACS plots characterizing MDR/MG ratio in $CD3^+$ T cells. **(E, F)** MDR/MG ratio in $CD3^+$, $CD3^-$, $CD4^+$, and $CD8^+$ T cells **(E)**, and in $CD16^+$ monocytes **(F)**. **(G)** MDR/MG^{lo} cell populations with increased mitochondrial mass but reduced transmembrane potential following CVF stimulation in T cell populations and monocytes. **(H)** Evaluation of intracellular ROS activity in human PBMC following 72h stimulation with CVF (left panel). H_2O_2 is used as a positive control. Culture supernatants were collected at different time points, and levels of TNFα (right panel) were analyzed. Data information: Graphs show data from 6 different samples. Statistical analysis was performed using a Mann-Whitney test and a Kruskal-Wallis test followed by a Dunn's multiple comparison test. Data are represented as means ± SEM. *$P < 0.05$; **$P < 0.01$.

(47). We used MitoTracker Deep Red (MDR) and MitoTracker Green (MG) to assess mitochondrial membrane potential and mitochondrial mass, respectively (34). The MDR/MG ratio is considered a parameter for mitochondrial activity per mass (34). As Figures 4D, F show, we observed a marked decrease in the MDR/MG ratio, suggesting an impairment of mitochondrial activity relative to mass for the lymphocyte (Figures 4D, E) and $CD16^+$ monocyte (Figure 4F) populations treated with CVF and Staurosporine as compared to the untreated controls. This was accompanied by an increase in MDR/MG^{lo} populations (Figure 4G), further supporting mitochondrial dysfunction.

Mitochondrial impairment involves many upstream mediators and cellular stress signals in the induction of the intrinsic apoptosis pathway such as mitochondrial DNA damage, heat shock, hypoxia, ER stress, and reactive oxygen species (ROS) (23, 45, 48–51). We tested the involvement of intracellular ROS activity using a fluorometric ROS assay in human PBMC as compared to TNFα, a marker of the extrinsic pathway (Figure 4H), and to provide further mechanistic insights. We detected no difference in intracellular ROS levels between the CVF-treated and control cells, while TNFα decreased over time in CVF-stimulated PBMCs. Thus, treatment with CVF led to cellular mitochondrial damage and depolarization, associated with impaired mitochondrial function.

Symptom development in NCC patients increases cellular apoptosis sensitivity and soluble FasL mediator in the periphery

To investigate whether markers for apoptosis such as FasL or TNFα would be detectable in symptomatic NCC patients, we made use of samples from our previous study (28). In this study, we had recruited a cohort of Tanzanian participants, including healthy controls and NCC-infected asymptomatic and symptomatic patients harboring active lesions with degenerating cysts in the brain (28) (Figure 5A). To assess the involvement of apoptosis-associated soluble mediators in NCC, we measured plasma levels of TNFα and FasL in the different patient groups (Figure 5B). TNFα levels did not significantly differ across the cohort groups. However,

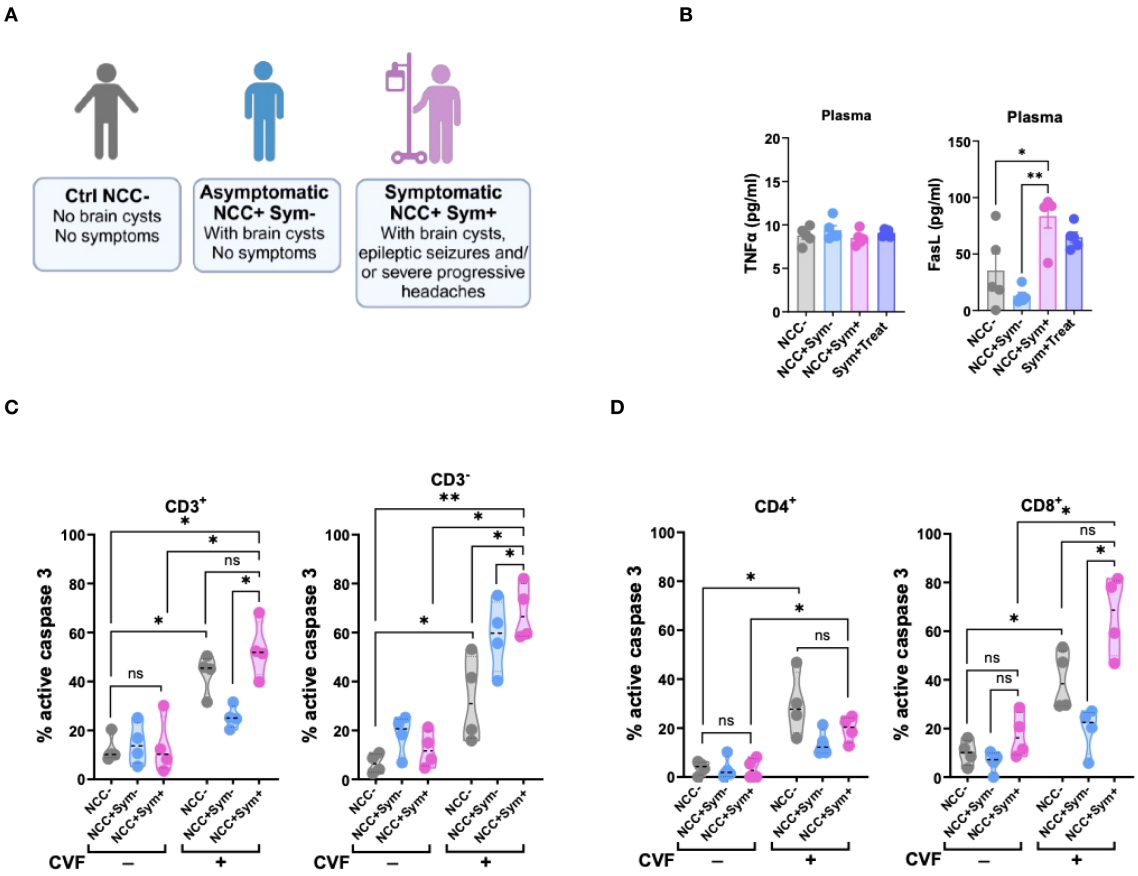

FIGURE 5
Symptomatic NCC patients show elevated signs of T cell apoptosis and soluble FasL mediator in the periphery. **(A)** Illustration of NCC patient groups and controls. **(B)** Evaluation of TNFα (left panel) and FasL (right panel) levels in the plasma of NCC patients and controls. **(C, D)** Caspase 3 activity in $CD3^+$ and $CD3^-$ **(C)**, and in $CD4^+$ and $CD8^+$ **(D)** T cell populations following 72h CVF stimulation of PBMC from uninfected (NCC-) and infected asymptomatic (NCC^+Sym^-) and symptomatic (NCC^+Sym^+) NCC patients as compared to unstimulated controls. Data information: Graphs show data from 4–6 different samples. Patients were age-matched. Statistical analysis was performed using a Mann-Whitney test and Kruskal–Wallis one-way ANOVA followed by a Dunn's multiple comparison test **(B–D)**. Data are represented as means ± SEM. *P < 0.05; **P < 0.01.

symptomatic NCC patients exhibited significantly higher plasma levels of FasL compared to asymptomatic patients and healthy controls (Figure 5B). Notably, asymptomatic patients had a trend of lower FasL levels than healthy controls. These findings suggested that degenerating cysts may contribute to the elevated levels of the pro-apoptotic mediator FasL.

To further explore the relevance of caspase 3-driven apoptosis in symptomatic NCC, we assessed caspase 3 activity in PBMCs from patients after stimulation with CVF *ex vivo* (Figures 5C, D). In the absence of stimulation, caspase 3 activity was similar between the different groups. However, upon CVF exposure, PBMCs from symptomatic NCC patients exhibited a marked increase in caspase 3 activity across all cell populations, except $CD4^+$ T cells, when compared to healthy controls. In contrast, PBMCs from asymptomatic NCC patients demonstrated a relatively weaker response to CVF, except for $CD3^-$ cells, when compared to the controls (Figures 5C, D).

Taken together, these results indicate a strong association between elevated levels of the soluble inflammatory mediator FasL and caspase-driven apoptosis with symptomatic disease in NCC.

Early and late stages of apoptosis are not induced by cysteine proteases but distinct factors enriched in CVF

Having demonstrated that *T. solium* CVF induced apoptosis preferentially through the caspase 9-mediated mitochondrial pathway in various immune cell populations, we next sought to identify specific CVF molecules responsible for this pro-apoptotic effect. To achieve this, we conducted a differential mass spectrometry analysis of CVF components. Among the identified CVF molecules (3), we detected 12 proteins, namely cysteine proteases, known to be associated with apoptotic pathways, including the caspases (2, 3, 6, and 7), cathepsins (B, D, L, O, and W), and calpains (1, 2, and 3) (52, 53) (Figure 6A). To determine the role of cysteine proteases in CVF-induced apoptosis, we pretreated PBMCs with E-64, an irreversible cysteine protease inhibitor (54), and assessed apoptosis levels. Surprisingly, E-64 pretreatment did not prevent CVF-induced early or late apoptosis in $CD3^+$ and $CD3^-$ cells (Figure 6B), nor in $CD4^+$ and $CD8^+$ T cells (Figure 6C), indicating that cysteine proteases may not be essential mediators of CVF-driven apoptosis.

We next evaluated the biochemical properties of the active pro-apoptotic molecules in CVF by subjecting CVF to heat treatment (56 °C and 99 °C), as well as proteinase K digestion, to assess the involvement of protein-based factors (Figure 6D; Supplementary Figure S4). While heat treatment at 99 °C for 3 hours mildly reduced early apoptosis induction in $CD3^+$, $CD4^+$ (Figure 6D), and $CD8^+$ T cells (Supplementary Figure S4), overall, treatment at lower temperature and with proteinase K did not significantly alter CVF-induced apoptosis. Accordingly, cysteine proteases and heat- or proteinase K-sensitive proteins did not appear to be the primary drivers of CVF-mediated late-stage apoptosis.

Next, we investigated the molecular size of the active pro-apoptotic factors. We fractionated CVF into molecules smaller or larger than 30 kDa and assessed the pro-apoptotic potency. We found that molecular size with the chosen cut-off did not significantly impact the apoptotic potency of CVF. However, we observed a trend to stronger pro-apoptotic effects, mostly late apoptosis, by molecules < 30 kDa, as compared to molecules > 30 kDa in $CD3^+$, $CD3^-$ cells (Figure 6E), and $CD4^+$ and $CD8^+$ T cells (Figure 6F).

These results indicated that CVF-mediated apoptosis was driven by small or a combination of small molecular weight components rather than heat- and proteinase-sensitive proteins. The identification of these pro-apoptotic molecules may provide insights into immune-mediated inflammation and disease exacerbation during NCC. A proposed model of CVF-induced apoptosis mechanisms and implications during NCC is presented in Figure 7.

Discussion

This study highlights the pivotal role of caspase 9-mediated apoptosis in *T. solium* CVF-induced cell death at peripheral and central nervous system levels, underscoring its relevance in NCC-associated inflammation. This pathway, potentially initiated by small molecules rather than proteins or enzymes, drives significant loss of mitochondrial membrane potential, increased mitochondrial mass and dysfunction, ultimately leading to cellular apoptosis. Clinically, CVF, used in this study as a surrogate to mimic degenerating cysts, promoted caspase activation associated with higher serum levels of pro-apoptotic FasL during symptom development in patients with NCC. These findings, supported by the detection of caspase 3^+ cells around degenerating cysts in the brain of NCC-infected pigs, highlight a link between parasite-driven apoptosis, disease pathogenesis, and severity.

Previous investigations have demonstrated the apoptosis of $CD3^+$ lymphocytes in the inflammatory infiltrate around *T. solium* cysts in infected pig brains (19, 55), with a potential role of caspase 3 (55). Further studies revealed that the cysts release Annexin B1, which binds to eosinophils and neutrophils and induces apoptosis through the induction of Ca^{2+} influx. Interestingly, Annexin B1 had no proapoptotic effect on lymphocytes (56). Our discovery of the intrinsic apoptotic pathway activation involving caspase 9 is particularly important in the context of neuroinflammatory diseases, where mitochondrial dysfunction and programmed cell death contribute to disease pathology and progression (20, 44, 50). Our data support the idea that mitochondrial integrity is severely compromised upon CVF exposure, leading to a significant loss of mitochondrial transmembrane potential across multiple immune cell subsets, including $CD4^+$ and $CD8^+$ T cells and monocytes. Importantly, these findings reinforce the central role of mitochondrial damage in CVF-induced immune cell death, aligning with previous reports on helminth-derived molecules (e.g. *S. mansoni*-derived apoptosis-inducing factor, *B. pahangi* antigen (BpA), excretory/secretory-

A

Molecule	Molecular weight (kDa)	Theoretical pI
Caspase 2	50.7	6.35
Caspase 3	31.6	6.09
Caspase 6	33.3	6.46
Caspase 7	34.3	5.72
Cathepsin D	44.6	6.10
Cathepsin L	37.6	5.31
Cathepsin B	37.8	6.40
Cathepsin W	42.1	7.14
Cathepsin O	36.0	7.06
Calpain 1	81.9	5.49
Calpain 2	80.0	4.87
Calpain 3	94.3	5.77

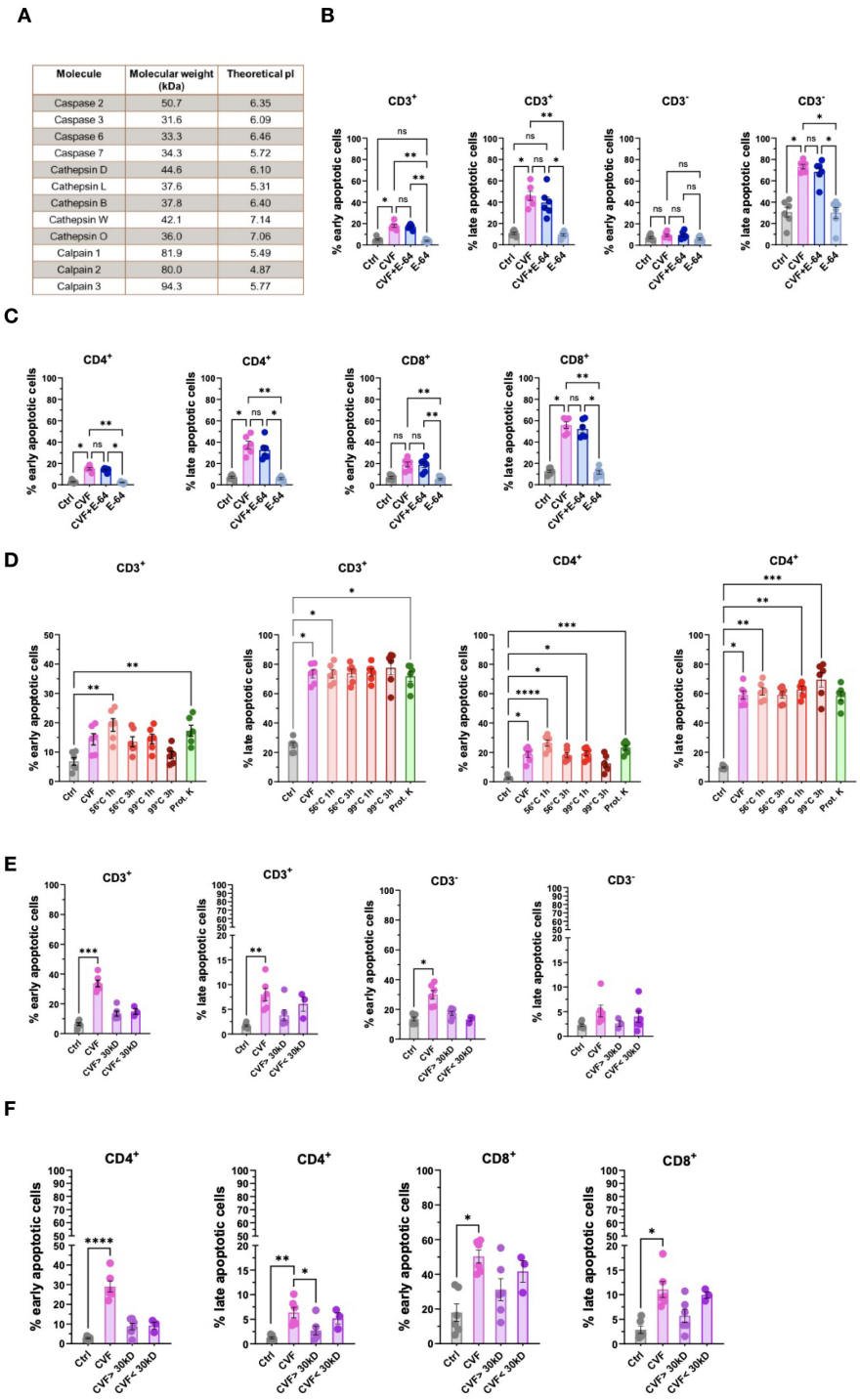

FIGURE 6
Early and late stages of apoptosis are not induced by cysteine proteases but distinct factors enriched in the CVF. **(A)** Identification of cysteine proteases and apoptosis signaling pathway-related molecules present in CVF by differential mass spectrometry. **(B, C)** Effect of cysteine protease inhibitor E-64 on CVF-induced early and late apoptosis in $CD3^+$ and $CD3^-$ **(B)**, and in $CD4^+$ and $CD8^+$ **(C)** T cells in PBMC after 72h. **(D)** Effect of heat treatment and proteinase K digestion of CVF on the induction of early and late apoptosis stages in $CD3^+$ and $CD4^+$ T cells. **(E, F)** Column fractionation of CVF and induction of early and late apoptosis stages in $CD3^+$ and $CD3^-$ **(E)** and $CD4^+$ and $CD8^+$ **(F)** T cell populations. Data information: The mass spectrometry data was analyzed using WormBase Parasite database for *T. solium* (Version WS282, October 2022). Graphs show data from 6 different samples. Statistical analysis was performed using Kruskal-Wallis test followed by a Dunn's multiple comparison test. Data are represented as means ± SEM. *P < 0.05; **P < 0.01; ***P < 0.001; ****P < 0.0001. ns, non-significant.

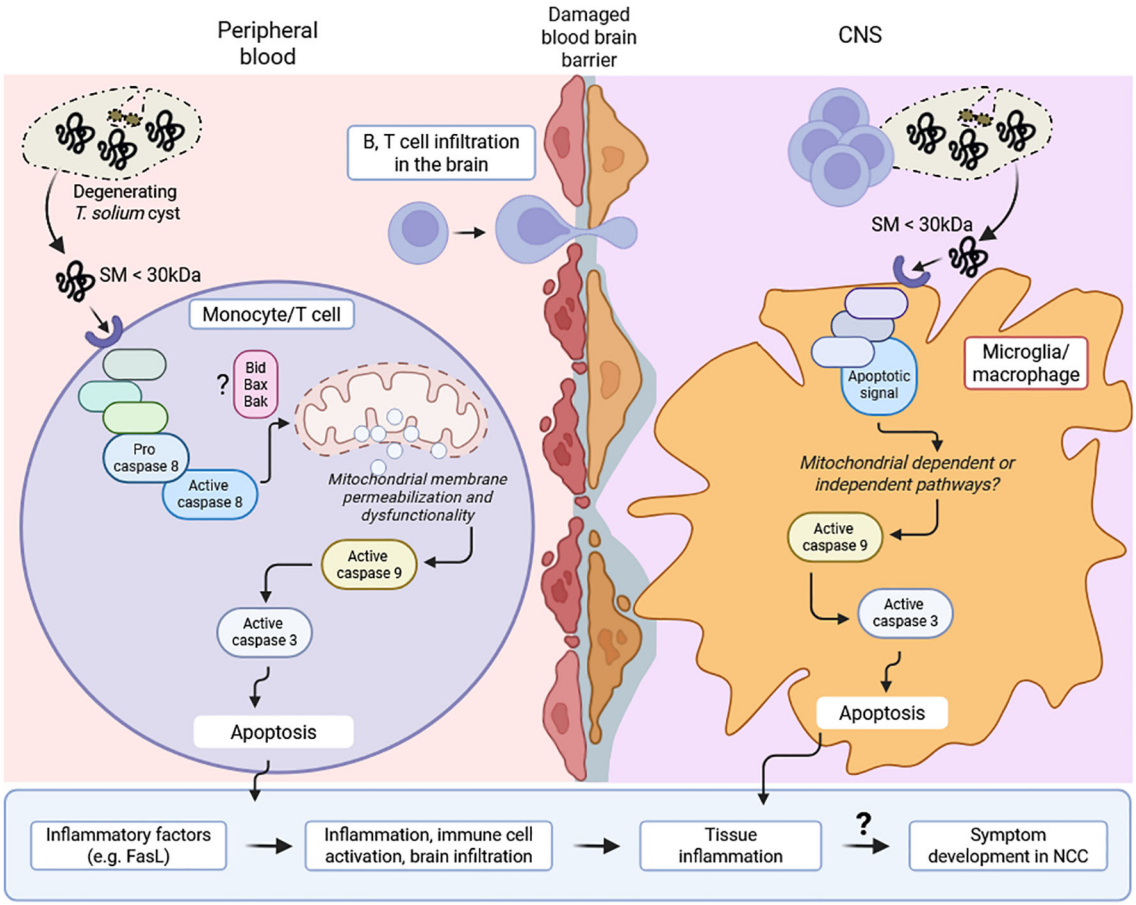

FIGURE 7
Proposed model of CVF-induced apoptosis mechanisms and implications during NCC. Cyst degeneration releases small molecules (SM) (< 30 kDa), which induce apoptotic signal within peripheral cells (monocyte, T cell) and microglia/macrophage in the central nervous system (CNS). This signal activates caspase 8 cascade and mitochondrial membrane permeabilization leading to caspase 9 accumulation. This initiates caspase 3-associated apoptosis, immune cell activation and inflammatory factors such as FasL. Similarly, CNS inflammation following mitochondrial-dependent or independent-caspase 9-induced apoptosis in microglia/macrophage drives immune cell (B, T cell) infiltration in the brain. The increasing cell death and ongoing inflammation may eventually drive a disruption in the structure and function of neuronal synapse and excitability, leading to the development and progression of symptoms (e.g. epilepsy) in NCC patients.

products of *E. multilocularis* larvae), interfering with host cell viability, activation, and metabolism (57–62). Our data reveal a notable species-specific difference in the type of cell death induced by *T. solium* CVF, with porcine immune cells exhibiting a higher degree of necrosis compared to predominantly apoptosis in human cells. Several factors could explain this divergence. First, pigs possess a distinct composition of peripheral immune cell subsets, including a high frequency of double-positive ($CD4^+CD8^+$) T cells, absent in humans, which may have differential sensitivity to parasitic antigens or stress-induced cell death pathways (63, 64). Second, interspecies differences in the expression or density of pattern recognition receptors (e.g., TLRs, CLRs), cytokine receptors, and death receptors (e.g., Fas, TNFR) could alter cellular susceptibility to CVF components. Third, metabolic profiles and redox homeostasis differ between human and pig and may affect mitochondrial integrity and cellular stress responses, thereby influencing the threshold for apoptosis versus necrosis (65). Moreover, species-specific differences in protease expression and stability (e.g., cathepsins) may also modulate downstream death pathways. Importantly, naturally infected pigs often harbor cysts at various developmental stages, and the presence of both viable and degenerating cysts in the brain reflects a chronic infection state. This chronicity could influence the cellular microenvironment, including immune cell composition, activation status, and susceptibility to apoptosis, as compared to acute infection. For example, chronic cyst fluid antigenic stimulation may prime resident immune cells such as microglia and infiltrating monocytes toward a more apoptosis-susceptible phenotype, particularly via mitochondrial stress and caspase 9 activation, as observed in our data. These findings highlight the complexity of modeling human NCC in animal systems when translating immune responses across species. Future comparative studies employing transcriptomic or receptor profiling approaches may provide better mechanistic insight into these interspecies variations and help refining porcine models for human-relevant translational research and neurological diseases.

Inflammatory conditions such as multiple sclerosis, Alzheimer's disease, and other neurodegenerative disorders have been linked to activation of caspase 9 and mitochondrial apoptosis pathways (27, 66). Given that mitochondrial damage leads to the release of Cytochrome c and subsequent caspase 9 activation, our data thus suggests furthermore that the mitochondrial pathway may be crucial in immune-mediated neuroinflammation. Notably, following CVF exposure, we observed a progressive increase of caspase 9 activity in microglia, which reside in granulomas around degenerating cysts. We have previously shown that CVF abrogates phagocytic function in microglia, resulting in the release of the pro-epileptic mediator TGF-β (3). In this study, we show now that this may result from prolonged apoptosis. Importantly, the loss of microglia in inflammatory infiltrates through apoptosis and the reduced phagocytosis of dying cells and dead cell debris due to the CVF impacting microglia, may potentially contribute to epileptogenesis. Indeed, effective microglial phagocytosis of apoptotic cells and degenerated neuronal remnants is essential for minimizing CNS inflammation and related symptoms by preserving healthy neuronal networks (24, 67).

Epileptic seizures are the most common symptom of NCC, with 70-90% of symptomatic NCC patients being affected (6). The mechanisms driving epileptic manifestations in NCC are, to date, not fully understood. In line with our findings, the conditional knockout of apoptosis-signaling-kinase 1 (ASK-1) in microglia led to decreased seizure severity and histological damage in a kainic acid-induced mouse seizure model (68). ASK-1 is activated under stress conditions, driving the activation of the mitochondrial apoptosis pathway through phosphorylation of c-Jun N-terminal kinase (JNK) and p38 MAPK (23, 69). Furthermore, in a mouse model of NCC, doxycycline treatment-dependent inhibition of mitochondrial apoptosis and subsequent Cytochrome c release (70) resulted in reduced mortality and diminished levels of neuronal apoptosis and inflammatory infiltrates in the CNS (71). CNS inflammation driven by the pro-apoptotic effect of CVF may not only contribute to epileptogenesis, but further instigate the breakdown of the blood-brain barrier (72, 73). As a consequence, increased exposure of the brain to inflammatory soluble mediators from the periphery, such as serum albumin, has been shown to induce inflammatory TGF-β-signaling in astrocytes, leading to excitatory synaptogenesis and reduced glutamate uptake capacity (72, 73).

A key aspect of our study is the identification of peripheral host soluble mediators associated with apoptosis in NCC patients. Symptomatic NCC patients exhibited significantly elevated FasL levels in the plasma and increased caspase 3-dependent apoptosis susceptibility of peripheral blood cells, thus potentially also contributing to NCC symptom development. Binding of FasL to Fas receptor (CD95) results in the recruitment of the Fas-associated death domain (FADD), leading to autoactivation of procaspases 8 and 10, causing the activation of the effector caspases 3 and 7 (23, 74). In line with our findings, Chen et al. found significantly elevated FasL levels in the cerebrospinal fluid of NCC patients, with NCC patients with calcified active lesions in the brain displaying higher serum levels of FasL levels compared to uninfected controls (75). Indeed, elevated FasL levels have been found in various neuroinflammatory conditions (76, 77). This could have important implications for understanding disease severity (e.g. neurological symptom development) and therapeutic interventions in symptomatic NCC patients. Nonetheless, the observed discrepancy between the dominant caspase 9-mediated intrinsic apoptosis pathway *in vitro* and the elevated levels of the extrinsic pathway mediator FasL detected in the plasma of symptomatic NCC patients likely reflects the interconnected, dynamic and complex nature of the regulation of apoptotic mechanisms *in vivo*. Indeed, following cyst degeneration and CVF leaking, it is plausible that FasL can be upregulated by activated T cells, macrophages, and microglia in response to chronic antigenic stimulation, proinflammatory cytokines (such as TNFα, IFNγ), or cell stress, all of which are features of active NCC lesions (4, 10, 30). Furthermore, crosstalk between the extrinsic and intrinsic pathways is well-established. FasL-induced caspase 8 activation can amplify mitochondrial dysfunction via Bid cleavage and truncation, while caspase 9-mediated intrinsic apoptosis may, in turn, promote FasL expression through feedback signaling (45, 78). Therefore, FasL elevation in symptomatic patients may not be the primary trigger of apoptosis but rather reflect a downstream consequence of ongoing tissue inflammation and immune activation. Thus, the clinical setting introduces additional inflammatory factors that can upregulate FasL and engage the extrinsic apoptosis pathway. Furthermore, different immune cell populations may exhibit varying apoptotic sensitivities, with some relying more on Fas-FasL interactions during chronic infection. Also, the lower FasL levels in asymptomatic patients could reflect a reduced engagement of Fas–FasL–mediated apoptotic pathways in the peripheral circulation of individuals harboring latent infection. This may contribute to the maintenance of immune homeostasis and protection from overt inflammatory responses, which aligns with the clinically silent status of these patients associated with immunosuppression and higher Treg levels (3, 4, 14, 79). In addition, in our study, we did not detect statistically significant differences in TNF-α levels between symptomatic, asymptomatic NCC patients, and uninfected controls. Indeed, TNF-α is a highly dynamic cytokine with a short half-life in circulation, and its levels are influenced by the timing of sample collection relative to disease progression and stimulating antigen load in circulation. It is possible that in our cross-sectional sampling design, peak TNF-α levels had already declined or fluctuated. Moreover, TNF-α exerts much of its pathological function in NCC locally within the CNS, rather than in the periphery (18, 30, 80, 81). Thus, systemic levels may not fully reflect the localized inflammatory milieu within the CNS. While TNF-α plays a role in NCC-associated inflammation, our data suggest that peripheral TNF-α levels alone may not serve as a reliable surrogate marker of disease severity or for apoptotic activity. Increasing the group sample size would provide further biological relevance for this immune aspect. This suggests that apoptosis in NCC is context-dependent, with the intrinsic pathway being potentially more relevant during early parasite-host interactions, while the extrinsic pathway may become prominent as neuroinflammation progresses with distinct cyst stages and interacting molecules.

To elucidate the molecular determinants of CVF-mediated apoptosis, we employed mass spectrometry analysis and functional inhibition assays. While CVF contains cysteine proteases such as caspases, cathepsins, and calpains, their inhibition via E-64 did not prevent apoptosis, indicating that alternative non-protease factors contribute to the observed effects or suggesting that the pro-apoptotic activity is not solely dependent on classical cysteine protease activity. This contrasts with previous reports, suspecting cysteine proteases being the cause of the proapoptotic effect of *T. solium* metacestode excretory-secretory (E/S) products (82, 83). These differences may be explained by the use in our setting of CVF products and not E/S products, which may contain different levels and groups of cysteine proteases. Furthermore, our biochemical fractionation experiments revealed that the active pro-apoptotic molecules in CVF are likely to be small (< 30 kDa) and resistant to proteinase K digestion. Annexin B1 from *T. solium* metacestodes has been postulated to have proapoptotic effects on innate immune cells (e.g. eosinophils) activating the intrinsic apoptosis pathway through induction of calcium influx (56). Although we identified annexin B2 from our mass spectrometry analysis, its molecular weight (MW) is > 30 kDa. Also, tetraspanins, protease inhibitors, and other non-identified small peptides in the hydatid cyst fluid released from *E. granulosus* can interfere with host immune signaling, contributing to apoptosis in certain immune and cancer cells (84, 85). This raises intriguing possibilities regarding parasite-derived metabolites or other small molecules that could be modulating host cell apoptosis. Notably, several of the identified pro-apoptotic molecules in CVF, including cathepsin L, cathepsin S, and caspases, have known functional subunit fragments ranging between 10–30 kDa (86, 87). It remains plausible that small active forms or degradation products of these proteases contribute to apoptosis through non-canonical mechanisms, or that other bioactive metabolites, peptides, or post-translationally modified fragments below 30 kDa may be involved. The heat- and protease-resistant nature of the apoptogenic activity suggests a role for non-pure protein or highly stable small molecules, possibly of metabolic origin (88). Thus, non-protein molecules, including lipids, small peptides, and potentially parasite-derived extracellular vesicles (EVs) containing miRNAs (e.g., miR-71, miR-146) may modulate host signaling pathways related to apoptosis and mitochondrial function (89, 90). However, conventional mass spectrometry may not fully resolve these candidates, especially if they are low-abundance, chemically modified, or highly hydrophobic. Future investigations integrating untargeted metabolomics, peptidomics, and high-resolution small molecule profiling, potentially through LC-MS/MS, NMR, or ultrasound probe and size and activity-guided fractionation, are needed to definitively identify the active components. Given the established role of mitochondrial apoptosis in neuroinflammatory diseases, future studies should aim to characterize these CVF-derived apoptogenic molecules and their potential as therapeutic targets.

In conclusion, our study provides novel mechanistic insights into how *T. solium* cyst fluid molecules manipulate host cell apoptosis, particularly through caspase 9 activation, and its role in mitochondrial dysfunction and immune-driven neuroinflammation in NCC. Our findings contribute to a better understanding of NCC progression and pathogenesis. This offers avenues to develop strategies for identification of symptomatic NCC patients via peripheral biomarkers such as FasL, and to mitigate parasite-induced immune dysregulation to eventually improve clinical outcomes in NCC patients.

Data availability statement

The original contributions presented in the study are included in the article/Supplementary Material. Further inquiries can be directed to the corresponding author.

Ethics statement

The studies involving humans were approved by the Klinikum Rechts der Isar (Technical University of Munich, Germany) Ethical Committee (Reference 33/19S) and the National Ethics Health Research Committee (NatREC) of Tanzania (Reference NIMR/HQ/R.8c/Vol.I/1808 for TOPANA and NIMR/HQ/R.8a/Vol.IX/2597 for SOLID). The studies were conducted in accordance with the local legislation and institutional requirements. The participants provided their written informed consent to participate in this study. The animal study was approved by Local government authorities of Regierung von Oberbayern (Az. 55.2-1-54-2532-145-17) and the University of Zambia School of Veterinary Medicine (ethical approval Ref. 2018-Mar-002/0005948). The study was conducted in accordance with the local legislation and institutional requirements.

Author contributions

LS: Data curation, Formal Analysis, Investigation, Methodology, Validation, Visualization, Writing – original draft, Writing – review & editing. UP: Conceptualization, Data curation, Formal Analysis, Funding acquisition, Investigation, Methodology, Project administration, Supervision, Validation, Visualization, Writing – original draft, Writing – review & editing. VG: Data curation, Formal Analysis, Investigation, Methodology, Validation, Visualization, Writing – review & editing. NR: Data curation, Formal Analysis, Investigation, Methodology, Validation, Visualization, Writing – review & editing. KS: Data curation, Formal Analysis, Investigation, Methodology, Software, Validation, Visualization, Writing – review & editing. JS: Investigation, Methodology, Writing – review & editing. CS: Funding acquisition, Methodology, Resources, Validation, Visualization, Writing – review & editing. DS: Methodology, Validation, Visualization, Writing – review & editing. CM: Validation, Visualization, Writing – review & editing. AW: Funding acquisition, Resources, Validation, Visualization, Writing – review & editing. BN: Funding acquisition, Resources, Validation, Visualization, Writing – review & editing. NV: Investigation, Methodology, Resources, Validation, Visualization, Writing – review & editing. FE: Data curation, Formal Analysis, Investigation, Methodology, Validation, Visualization, Writing – review & editing. GH: Methodology, Validation, Visualization, Writing – review & editing. PH: Validation, Visualization, Writing

– review & editing. CP: Conceptualization, Data curation, Formal Analysis, Funding acquisition, Investigation, Methodology, Project administration, Supervision, Validation, Visualization, Writing – review & editing, Resources.

Funding

The authors declare financial support was received for the research, authorship, and/or publication of this article. This work was supported by the German Federal Ministry of Education and Research (BMBF) through the project CYSTINET-Africa under the funding code 01KA1610. LES was supported by the doctoral program in Translational Medicine by the TUM Graduate School of the TUM School of Medicine and Health.

Acknowledgments

We want to thank Bettina Bernard and Cora Mibus for their excellent technical help and valuable consulting. We are grateful to all patients and matched controls who participated in the study. We thank the Comparative Experimental Pathology (CEP), School of Medicine and Health, TUM for excellent technical support.

Conflict of interest

The authors declare that the research was conducted in the absence of any commercial or financial relationships that could be construed as a potential conflict of interest.

The author(s) declared that they were an editorial board member of Frontiers, at the time of submission. This had no impact on the peer review process and the final decision.

Generative AI statement

The author(s) declare that no Generative AI was used in the creation of this manuscript.

Any alternative text (alt text) provided alongside figures in this article has been generated by Frontiers with the support of artificial intelligence and reasonable efforts have been made to ensure accuracy, including review by the authors wherever possible. If you identify any issues, please contact us.

Publisher's note

Supplementary material

The Supplementary Material for this article can be found online at: https://www.frontiersin.org/articles/10.3389/fimmu.2025.1603385/full#supplementary-material

References

1. WHO. Taeniasis/cysticercosis (2022). Available online at: https://www.who.int/news-room/fact-sheets/detail/taeniasis-cysticercosis. (Accessed March 20, 2025).

2. Jewell PD, Abraham A, Schmidt V, Buell KG, Bustos JA, Garcia HH, et al. Neurocysticercosis and HIV/AIDS co-infection: A scoping review. *Trop Med Int Health*. (2021) 26:1140–52. doi: 10.1111/tmi.13652

3. Prodjinotho UF, Gres V, Henkel F, Lacorcia M, Dandl R, Haslbeck M, et al. Helminthic dehydrogenase drives PGE(2) and IL-10 production in monocytes to potentiate Treg induction. *EMBO Rep*. (2022) 23:e54096. doi: 10.15252/embr.202154096

4. Prodjinotho UF, Lema J, Lacorcia M, Schmidt V, Vejzagic N, Sikasunge C, et al. Host immune responses during Taenia solium Neurocysticercosis infection and treatment. *PloS Negl Trop Dis*. (2020) 14:e0008005. doi: 10.1371/journal.pntd.0008005

5. Fleury A, Cardenas G, Adalid-Peralta L, Fragoso G, Sciutto E. Immunopathology in Taenia solium neurocysticercosis. *Parasite Immunol*. (2016) 38:147–57. doi: 10.1111/pim.12299

6. Steyn TJS, Awala AN, de Lange A, Raimondo JV. What causes seizures in neurocysticercosis? *Epilepsy Curr*. (2023) 23:105–12. doi: 10.1177/15357597221137418

7. Winkler AS. Neurocysticercosis in sub-Saharan Africa: a review of prevalence, clinical characteristics, diagnosis, and management. *Pathog Glob Health*. (2012) 106:261–74. doi: 10.1179/2047773212Y.0000000047

8. Dametto E. Histopathology of the human brain in neurocysticercosis. *J Mol Histol Med Physiol*. (2016) 106:5–7.

9. Fleury A, Trejo A, Cisneros H, García-Navarrete R, Villalobos N, Hernández M, et al. Taenia solium: development of an experimental model of porcine neurocysticercosis. *PloS Negl Trop Dis*. (2015) 9:e0003980. doi: 10.1371/journal.pntd.0003980

10. Restrepo BI, Alvarez JI, Castaño JA, Arias LF, Restrepo M, Trujillo J, et al. Brain granulomas in neurocysticercosis patients are associated with a Th1 and Th2 profile. *Infect Immun*. (2001) 69:4554–60. doi: 10.1128/IAI.69.7.4554-4560.2001

11. Colonna M, Butovsky O. Microglia function in the central nervous system during health and neurodegeneration. *Annu Rev Immunol*. (2017) 35:441–68. doi: 10.1146/annurev-immunol-051116-052358

12. Alloo J, Leleu I, Grangette C, Pied S. Parasite infections, neuroinflammation, and potential contributions of gut microbiota. *Front Immunol*. (2022) 13:1024998. doi: 10.3389/fimmu.2022.1024998

13. Rodríguez-Gómez JA, Kavanagh E, Engskog-Vlachos P, Engskog MKR, Herrera AJ, Espinosa-Oliva AM, et al. Microglia: agents of the CNS pro-inflammatory response. *Cells*. (2020) 9. doi: 10.3390/cells9071717

14. Adalid-Peralta L, Arce-Sillas A, Fragoso G, Cárdenas G, Rosetti M, Casanova-Hernández D, et al. Cysticerci drive dendritic cells to promote *in vitro* and *in vivo* Tregs differentiation. *Clin Dev Immunol*. (2013) 2013:981468. doi: 10.1155/2013/981468

15. de Lange A, Mahanty S, Raimondo JV. Model systems for investigating disease processes in neurocysticercosis. *Parasitology*. (2019) 146:553–62. doi: 10.1017/S0031182018001932

16. Pérez-Torres A, Ustarroz M, Constantino F, Villalobos N, de AA. Taenia solium cysticercosis: lymphocytes in the inflammatory reaction in naturally infected pigs. *Parasitol Res*. (2002) 88:150–2. doi: 10.1007/s00436-001-0510-6

17. Presas AM, Robert L, Jiménez JA, Willms K. Apoptosis patterns in experimental Taenia solium and Taenia crassiceps strobilae from golden hamsters. *Parasitol Res*. (2005) 96:1–5. doi: 10.1007/s00436-005-1316-8

18. Sáenz B, Fleury A, Chavarría A, Hernández M, Crispin JC, Vargas-Rojas MI, et al. Neurocysticercosis: local and systemic immune-inflammatory features related to severity. *Med Microbiol Immunol*. (2012) 201:73–80. doi: 10.1007/s00430-011-0207-0

19. Sikasunge CS, Phiri IK, Johansen MV, Willingham AL3rd, Leifsson PS. Host-cell apoptosis in Taenia solium-induced brain granulomas in naturally infected pigs. *Parasitology*. (2008) 135:1237–42. doi: 10.1017/S0031182008004678

20. Häcker G. Apoptosis in infection. *Microbes Infect*. (2018) 20:552–9. doi: 10.1016/j.micinf.2017.10.006

21. Opferman JT. Apoptosis in the development of the immune system. *Cell Death Differ*. (2008) 15:234–42. doi: 10.1038/sj.cdd.4402182

22. Zhang N, Hartig H, Dzhagalov I, Draper D, He YW. The role of apoptosis in the development and function of T lymphocytes. *Cell Res*. (2005) 15:749–69. doi: 10.1038/sj.cr.7290345

23. Redza-Dutordoir M, Averill-Bates DA. Activation of apoptosis signalling pathways by reactive oxygen species. *Biochim Biophys Acta*. (2016) 1863:2977–92. doi: 10.1016/j.bbamcr.2016.09.012

24. Tsuchiya K. Inflammasome-associated cell death: Pyroptosis, apoptosis, and physiological implications. *Microbiol Immunol*. (2020) 64:252–69. doi: 10.1111/1348-0421.12771

25. Waguia Kontchou C, Tzivelekidis T, Gentle IE, Hacker G. Infection of epithelial cells with Chlamydia trachomatis inhibits TNF-induced apoptosis at the level of receptor internalization while leaving non-apoptotic TNF-signalling intact. *Cell Microbiol*. (2016) 18:1583–95. doi: 10.1111/cmi.12598

26. Norat P, Soldozy S, Sokolowski JD, Gorick CM, Kumar JS, Chae Y, et al. Mitochondrial dysfunction in neurological disorders: Exploring mitochondrial transplantation. *NPJ Regener Med*. (2020) 5:22. doi: 10.1038/s41536-020-00107-x

27. Rohn TT, Rissman RA, Davis MC, Kim YE, Cotman CW, Head E. Caspase-9 activation and caspase cleavage of tau in the Alzheimer's disease brain. *Neurobiol Dis*. (2002) 11:341–54. doi: 10.1006/nbdi.2002.0549

28. Stelzle D, Makasi C, Schmidt V, Trevisan C, Van Damme I, Ruether C, et al. Efficacy and safety of antiparasitic therapy for neurocysticercosis in rural Tanzania: a prospective cohort study. *Infection*. (2023) 51:1127–39. doi: 10.1007/s15010-023-02021-y

29. Trevisan C, Damme IV, Ngowi B, Schmidt V, Stelzle D, Møller KS, et al. Trial design of a prospective multicenter diagnostic accuracy study of a point-of-care test for the detection of taenia solium taeniosis and neurocysticercosis in hospital-based settings in Tanzania. *Diagnostics (Basel)*. (2021) 11. doi: 10.3390/diagnostics11091528

30. Lema YL, Prodjinotho UF, Makasi C, Nanyaro MA, Kilale AM, Mfinanga S, et al. Evaluating the modulation of peripheral immune profile in people living with HIV and (Neuro)cysticercosis. *PloS Negl Trop Dis*. (2024) 18:e0012345. doi: 10.1371/journal.pntd.0012345

31. Del Brutto OH, Nash TE, White ACJr., Rajshekhar V, Wilkins PP, Singh G, et al. Revised diagnostic criteria for neurocysticercosis. *J Neurol Sci*. (2017) 372:202–10. doi: 10.1016/j.jns.2016.11.045

32. White ACJr., Coyle CM, Rajshekhar V, Singh G, Hauser WA, Mohanty A, et al. Diagnosis and treatment of neurocysticercosis: 2017 clinical practice guidelines by the infectious diseases society of america (IDSA) and the american society of tropical medicine and hygiene (ASTMH). *Am J Trop Med Hyg*. (2018) 98:945–66. doi: 10.4269/ajtmh.18-88751

33. Schlott F, Steubl D, Ameres S, Moosmann A, Dreher S, Heemann U, et al. Characterization and clinical enrichment of HLA-C*07:02-restricted Cytomegalovirus-specific CD8+ T cells. *PloS One*. (2018) 13:e0193554. doi: 10.1371/journal.pone.0193554

34. Yu YR, Imrichova H, Wang H, Chao T, Xiao Z, Gao M, et al. Disturbed mitochondrial dynamics in CD8(+) TILs reinforce T cell exhaustion. *Nat Immunol*. (2020) 21:1540–51. doi: 10.1038/s41590-020-0793-3

35. Kleiveland CR, Verhoeckx K, Cotter Pl, López-Expósito I, Kleiveland C, Tor L, et al. Peripheral blood mononuclear cells. In: Verhoeckx K, Cotter P, López-Expósito I, Kleiveland C, Lea T, Mackie A, editors. *The Impact of Food Bioactives on Health:* in vitro *and* ex vivo *models*. Springer Copyright, Cham (CH (2015). p. 161–7.

36. Lund PK, Namork E, Brorson SH, Westvik AB, Joø GB, Øvstebø R, et al. The fate of monocytes during 24 h of culture as revealed by flow cytometry and electron microscopy. *J Immunol Methods*. (2002) 270:63–76. doi: 10.1016/S0022-1759(02)00272-7

37. Zhao C, Tan YC, Wong WC, Sem X, Zhang H, Han H, et al. The CD14(+/low) CD16(+) monocyte subset is more susceptible to spontaneous and oxidant-induced apoptosis than the CD14(+)CD16(-) subset. *Cell Death Dis*. (2010) 1:e95. doi: 10.1038cddis.2010.69

38. Singh AK, Prasad KN, Prasad A, Tripathi M, Gupta RK, Husain N. Immune responses to viable and degenerative metacestodes of Taenia solium in naturally infected swine. *Int J Parasitol*. (2013) 43:1101–7. doi: 10.1016/j.ijpara.2013.07.009

39. Pescovitz MD, Sakopoulos AG, Gaddy JA, Husmann RJ, Zuckermann FA. Porcine peripheral blood CD4+/CD8+ dual expressing T-cells. *Vet Immunol Immunopathol*. (1994) 43:53–62. doi: 10.1016/0165-2427(94)90120-1

40. Zuckermann FA. Extrathymic CD4/CD8 double positive T cells. *Vet Immunol Immunopathol*. (1999) 72:55–66. doi: 10.1016/S0165-2427(99)00118-X

41. Fairbairn L, Kapetanovic R, Beraldi D, Sester DP, Tuggle CK, Archibald AL, et al. Comparative analysis of monocyte subsets in the pig. *J Immunol*. (2013) 190:6389–96. doi: 10.4049/jimmunol.1300365

42. Gutierrez Y. The cestode. In: *Diagnostic pathology of parasitic infections with clinical correlation*. Oxford University Press, USA (2002).

43. Xu G, Shi Y. Apoptosis signaling pathways and lymphocyte homeostasis. *Cell Res*. (2007) 17:759–71. doi: 10.1038/cr.2007.52

44. Kesavardhana S, Malireddi RKS, Kanneganti TD. Caspases in cell death, inflammation, and pyroptosis. *Annu Rev Immunol*. (2020) 38:567–95. doi: 10.1146/annurev-immunol-073119-095439

45. Kantari C, Walczak H. Caspase-8 and bid: caught in the act between death receptors and mitochondria. *Biochim Biophys Acta*. (2011) 1813:558–63. doi: 10.1016/j.bbamcr.2011.01.026

46. Crowley LC, Christensen ME, Waterhouse NJ. Measuring mitochondrial transmembrane potential by TMRE staining. *Cold Spring Harb Protoc*. (2016) 2016. doi: 10.1101/pdb.prot087361

47. Neikirk K, Marshall AG, Kula B, Smith N, LeBlanc S, Hinton A Jr. MitoTracker: A useful tool in need of better alternatives. *Eur J Cell Biol*. (2023) 102:151371. doi: 10.1016/j.ejcb.2023.151371

48. Circu ML, Aw TY. Reactive oxygen species, cellular redox systems, and apoptosis. *Free Radic Biol Med*. (2010) 48:749–62. doi: 10.1016/j.freeradbiomed.2009.12.022

49. Circu ML, Aw TY. Glutathione and modulation of cell apoptosis. *Biochim Biophys Acta*. (2012) 1823:1767–77. doi: 10.1016/j.bbamcr.2012.06.019

50. Madesh M, Hajnóczky G. VDAC-dependent permeabilization of the outer mitochondrial membrane by superoxide induces rapid and massive cytochrome c release. *J Cell Biol*. (2001) 155:1003–15. doi: 10.1083/jcb.200105057

51. Orrenius S, Gogvadze V, Zhivotovsky B. Calcium and mitochondria in the regulation of cell death. *Biochem Biophys Res Commun*. (2015) 460:72–81. doi: 10.1016/j.bbrc.2015.01.137

52. Khan H, Garg N, Singh TG, Kaur A, Thapa K. Calpain inhibitors as potential therapeutic modulators in neurodegenerative diseases. *Neurochem Res*. (2022) 47:1125–49. doi: 10.1007/s11064-021-03521-9

53. Shen X, Zhao YF, Xu SQ, Wang L, Cao HM, Cao Y, et al. Cathepsin L induced PC-12 cell apoptosis via activation of B-Myb and regulation of cell cycle proteins. *Acta Pharmacol Sin*. (2019) 40:1394–403. doi: 10.1038/s41401-019-0286-9

54. Sigma-Aldrich. *E-64 protease inhibitor (E3132)*. Merck KGaA (2024). Available online at: https://www.sigmaaldrich.com/DE/de/product/sigma/e3132?gclid=CjwKCAjwxY-3BhAuEiwAu7Y6s2BVPD-pa80FI19TE5PT00opMdUEsEfB3wuYFl9pFki5E1rGmSN49hoC4wIQAvD_BwE&adfcd=1726243768.xbOczpTnI0OnF4fTfgKdAQ.Mjg2MTEzMywyMDg4NTAx.

55. Mkupasi EM, Sikasunge CS, Ngowi HA, Leifsson PS, Johansen MV. Detection of cysteine protease in Taenia solium-induced brain granulomas in naturally infected pigs. *Vet Parasitol*. (2013) 197:360–3. doi: 10.1016/j.vetpar.2013.05.004

56. Yan HL, Xue G, Mei Q, Ding FX, Wang YZ, Sun SH. Calcium-dependent proapoptotic effect of Taenia solium metacestodes annexin B1 on human eosinophils: a novel strategy to prevent host immune response. *Int J Biochem Cell Biol*. (2008) 40:2151–63. doi: 10.1016/j.biocel.2008.02.018

57. Babal P, Milcheva R, Petkova S, Janega P, Hurnikova Z. Apoptosis as the adaptation mechanism in survival of Trichinella spiralis in the host. *Parasitol Res*. (2011) 109:997–1002. doi: 10.1007/s00436-011-2343-2

58. Bienvenu AL, Gonzalez-Rey E, Picot S. Apoptosis induced by parasitic diseases. *Parasit Vectors*. (2010) 3:106. doi: 10.1186/1756-3305-3-106

59. Chen L, Rao KV, He YX, Ramaswamy K. Skin-stage schistosomula of Schistosoma mansoni produce an apoptosis-inducing factor that can cause apoptosis of T cells. *J Biol Chem*. (2002) 277:34329–35. doi: 10.1074/jbc.M201344200

60. Das Mohapatra A, Panda SK, Pradhan AK, Prusty BK, Satapathy AK, Ravindran B. Filarial antigens mediate apoptosis of human monocytes through Toll-like receptor 4. *J Infect Dis*. (2014) 210:1133–44. doi: 10.1093/infdis/jiu208

61. Friedrich A, Pechstein J, Berens C, Lührmann A. Modulation of host cell apoptotic pathways by intracellular pathogens. *Curr Opin Microbiol*. (2017) 35:88–99. doi: 10.1016/j.mib.2017.03.001

62. Nono JK, Pletinckx K, Lutz MB, Brehm K. Excretory/secretory-products of Echinococcus multilocularis larvae induce apoptosis and tolerogenic properties in dendritic cells *in vitro*. *PloS Negl Trop Dis*. (2012) 6:e1516. doi: 10.1371/journal.pntd.0001516

63. Charerntantanakul W, Roth JA. Biology of porcine T lymphocytes. *Anim Health Res Rev*. (2006) 7:81–96. doi: 10.1017/S1466252307001235

64. Wang N, Bai X, Tang B, Yang Y, Wang X, Zhu H, et al. Primary characterization of the immune response in pigs infected with Trichinella spiralis. *Vet Res*. (2020) 51:17. doi: 10.1186/s13567-020-0741-0

65. Abass K, Reponen P, Anyanwu B, Pelkonen O. Inter-species differences between humans and other mammals in the *in vitro* metabolism of carbofuran and the role of human CYP enzymes. *Environ Toxicol Pharmacol*. (2023) 102:104243. doi: 10.1016/j.etap.2023.104243

66. Wojcik P, Jastrzebski MK, Zieba A, Matosiuk D, Kaczor AA. Caspases in alzheimer's disease: mechanism of activation, role, and potential treatment. *Mol Neurobiol*. (2024) 61:4834–53. doi: 10.1007/s12035-023-03847-1

67. Diaz-Aparicio I, Paris I, Sierra-Torre V, Plaza-Zabala A, Rodríguez-Iglesias N, Márquez-Ropero M, et al. Microglia actively remodel adult hippocampal neurogenesis through the phagocytosis secretome. *J Neurosci*. (2020) 40:1453–82. doi: 10.1523/JNEUROSCI.0993-19.2019

68. Zhang Y, Wang Z, Wang R, Xia L, Cai Y, Tong F, et al. Conditional knockout of ASK1 in microglia/macrophages attenuates epileptic seizures and long-term neurobehavioural comorbidities by modulating the inflammatory responses of microglia/macrophages. *J Neuroinflammation*. (2022) 19:202. doi: 10.1186/s12974-022-02560-5

69. Hatai T, Matsuzawa A, Inoshita S, Mochida Y, Kuroda T, Sakamaki K, et al. Execution of apoptosis signal-regulating kinase 1 (ASK1)-induced apoptosis by the mitochondria-dependent caspase activation. *J Biol Chem*. (2000) 275:26576–81. doi: 10.1074/jbc.M003412200

70. Davies JE, Wang L, Garcia-Oroz L, Cook LJ, Vacher C, O'Donovan DG, et al. Doxycycline attenuates and delays toxicity of the oculopharyngeal muscular dystrophy mutation in transgenic mice. *Nat Med*. (2005) 11:672–7. doi: 10.1038/nm1242

71. Alvarez JI, Krishnamurthy J, Teale JM. Doxycycline treatment decreases morbidity and mortality of murine neurocysticercosis: evidence for reduction of apoptosis and matrix metalloproteinase activity. *Am J Pathol*. (2009) 175:685–95. doi: 10.2353/ajpath.2009.081073

72. David Y, Cacheaux LP, Ivens S, Lapilover E, Heinemann U, Kaufer D, et al. Astrocytic dysfunction in epileptogenesis: consequence of altered potassium and glutamate homeostasis? *J Neurosci*. (2009) 29:10588–99. doi: 10.1523/JNEUROSCI.2323-09.2009

73. Weissberg I, Wood L, Kamintsky L, Vazquez O, Milikovsky DZ, Alexander A, et al. Albumin induces excitatory synaptogenesis through astrocytic TGF-β/ALK5 signaling in a model of acquired epilepsy following blood-brain barrier dysfunction. *Neurobiol Dis*. (2015) 78:115–25. doi: 10.1016/j.nbd.2015.02.029

74. Mahmood Z, Shukla Y. Death receptors: targets for cancer therapy. *Exp Cell Res*. (2010) 316:887–99. doi: 10.1016/j.yexcr.2009.12.011

75. Chen X, Yu X, Wang Y, Zhu J, Gu J. Soluble Fas/FasLare elevated in the serum and cerebrospinal fluid of patients with neurocysticercosis. *Parasitol Res*. (2017) 116:3027–36. doi: 10.1007/s00436-017-5613-9

76. Krzyzowska M, Kowalczyk A, Skulska K, Thorn K, Eriksson K. Fas/fasL contributes to HSV-1 brain infection and neuroinflammation. *Front Immunol*. (2021) 12:714821. doi: 10.3389/fimmu.2021.714821

77. Lenzlinger PM, Marx A, Trentz O, Kossmann T, Morganti-Kossmann MC. Prolonged intrathecal release of soluble Fas following severe traumatic brain injury in humans. *J Neuroimmunol*. (2002) 122:167–74. doi: 10.1016/S0165-5728(01)00466-0

78. Beaudouin J, Liesche C, Aschenbrenner S, Horner M, Eils R. Caspase-8 cleaves its substrates from the plasma membrane upon CD95-induced apoptosis. *Cell Death Differ*. (2013) 20:599–610. doi: 10.1038/cdd.2012.156

79. Adalid-Peralta L, Fleury A, García-Ibarra TM, Hernández M, Parkhouse M, Crispín JC, et al. Human neurocysticercosis: *in vivo* expansion of peripheral regulatory T cells and their recruitment in the central nervous system. *J Parasitol*. (2012) 98:142–8. doi: 10.1645/GE-2839.1

80. Aguilar-Rebolledo F, Cedillo-Rivera R, Llaguno-Violante P, Torres-Lopez J, Munoz-Hernandez O, Enciso-Moreno JA. Interleukin levels in cerebrospinal fluid from children with neurocysticercosis. *Am J Trop Med Hyg*. (2001) 64:35–40. doi: 10.4269/ajtmh.2001.64.35

81. Evans CA, Garcia HH, Hartnell A, Gilman RH, Jose PJ, Martinez M, et al. Elevated concentrations of eotaxin and interleukin-5 in human neurocysticercosis. *Infect Immun*. (1998) 66:4522–5. doi: 10.1128/IAI.66.9.4522-4525.1998

82. Molinari JL, Mejia H, White ACJr., Garrido E, Borgonio VM, Baig S, et al. Taenia solium: a cysteine protease secreted by metacestodes depletes human CD4 lymphocytes *in vitro*. *Exp Parasitol*. (2000) 94:133–42. doi: 10.1006/expr.2000.4490

83. Tato P, Fernández AM, Solano S, Borgonio V, Garrido E, Sepúlveda J, et al. A cysteine protease from Taenia solium metacestodes induce apoptosis in human CD4+ T-cells. *Parasitol Res*. (2004) 92:197–204. doi: 10.1007/s00436-003-1008-1

84. Ranasinghe SL, Boyle GM, Fischer K, Potriquet J, Mulvenna JP, McManus DP. Kunitz type protease inhibitor EgKI-1 from the canine tapeworm Echinococcus granulosus as a promising therapeutic against breast cancer. *PloS One*. (2018) 13: e0200433. doi: 10.1371/journal.pone.0200433

85. Xian J, Zhao P, Wang N, Wang W, Zhang Y, Meng J, et al. Molecular characterization of a tetraspanin TSP11 gene in echinococcus granulosus and evaluation its immunoprotection in model dogs. *Front Vet Sci*. (2021) 8:759283. doi: 10.3389/fvets.2021.759283

86. Lavrik IN, Golks A, Krammer PH. Caspases: pharmacological manipulation of cell death. *J Clin Invest*. (2005) 115:2665–72. doi: 10.1172/JCI26252

87. Ponder KG, Boise LH. The prodomain of caspase-3 regulates its own removal and caspase activation. *Cell Death Discov*. (2019) 5:56. doi: 10.1038/s41420-019-0142-1

88. Gatsios A, Kim CS, Crawford JM. Escherichia coli small molecule metabolism at the host-microorganism interface. *Nat Chem Biol*. (2021) 17:1016–26. doi: 10.1038/s41589-021-00807-5

89. Bosurgi L, Rothlin CV. Management of cell death in parasitic infections. *Semin Immunopathol*. (2021) 43:481–92. doi: 10.1007/s00281-021-00875-8

90. Gutierrez-Loli R, Orrego MA, Sevillano-Quispe OG, Herrera-Arrasco L, Guerra-Giraldez C. MicroRNAs in taenia solium neurocysticercosis: insights as promising agents in host-parasite interaction and their potential as biomarkers. *Front Microbiol*. (2017) 8:1905. doi: 10.3389/fmicb.2017.01905

Frontiers in Immunology

Explores novel approaches and diagnoses to treat immune disorders.

The official journal of the International Union of Immunological Societies (IUIS) and the most cited in its field, leading the way for research across basic, translational and clinical immunology.

Discover the latest Research Topics

See more →

Frontiers

Avenue du Tribunal-Fédéral 34
1005 Lausanne, Switzerland
frontiersin.org

Contact us

+41 (0)21 510 17 00
frontiersin.org/about/contact